

Nitrile-Directed C–H Functionalization and Lewis Acid-Catalyzed Oligosaccharide Synthesis

by

Annabel Quinlivan Ansel

A dissertation submitted in partial fulfillment
of the requirements for the degree of
Doctor of Philosophy
(Chemistry)
in the University of Michigan
2020

Doctoral Committee:

Professor John Montgomery, Chair
Professor Joerg Lahann
Professor Anne J. McNeil
Associate Professor Pavel Nagorny

Annabel Quinlivan Ansel

aqansel@umich.edu

ORCID iD: [0000-0002-7456-5827](https://orcid.org/0000-0002-7456-5827)

© Annabel Q. Ansel 2020

Dedication

This dissertation is dedicated to Ann Quinlivan. Your selflessness, resilience, and endless pursuit of knowledge are inspiring.

Acknowledgements

First, I would like to thank my advisor, Professor John Montgomery, for his guidance over the last five years. I appreciate the opportunity to join your lab, and the freedom that you have given to me to explore a wide array of chemistry during my time in graduate school. I am grateful for your encouragement and constructive criticism, which have made me the scientist I am today.

I am thankful for my amazing colleagues in the Montgomery lab. The positive energy and endless laughter made working in lab a joy. I am grateful for my early mentors and good friends Michael Gilbert, Jessica Stachowski, David Todd, Eric Wiensch, Alex Nett, and Hilary Kerchner. Thank you also to Kirk Shimkin, Girish Sati, and Cole Cruz. Your friendship, advice, and guidance later in my graduate career were invaluable. To Alex Rand, Daniel Nasrallah, Rosa Vasquez, Sara Alektiar, Josh Martin, Yishu Xu, and Mo Chen, thank you for the scientific insight, companionship, and cheerful memories. I especially want to thank Amie Frank and Wesley Pein for their support and comradery. Thank you for the helpful edits, countless rides home, and lively nights at HOMES. Graduate school would not have been the great experience it was without you.

I would also like to thank Janelle Kirsch and Becky Watson. I value your loyal friendship through the good times, and bad. The tailgates, Saturday-night shenanigans, and floats down the Huron River have made graduate school a true delight. Janelle, thank you for the climbing sessions, sushi outings, and companionship since day one. Becky, thank you for being a mentor,

especially during my job search, and a great friend. I will always look back on the last five years fondly, and I look forward to continuing our friendship in the years ahead.

I am thankful for friends outside of the department, in Ann Arbor and elsewhere, who have made my time at the University of Michigan unforgettable. Thank you to Brandon Lee, Caleb Frank, Lauren Willigan, Tim Trippel, Annie Shapiro, Hayley Nasrallah, Shurjo Banerjee, Ben Wachs, Shadrach Hepner, and Tim Lycurgus. I am grateful for my friends from college and high school who made time to see me when I was home, providing welcomed breaks from the struggles of graduate school. Special thanks to Allie and Colby Kubat, Ellie Dusheck, Eesha Katarya, Greta Aarsvold, Hannah Bundrick, and Caroline Maliske.

Thank you to my family near, and far, for their love and encouragement. I am blessed to have so many fun-loving and supportive aunts, uncles, cousins, and other extended family members. I am especially indebted to my grandparents. Through their examples, I have learned the value of family and hard work. To Ann Quinlivan thank you for your generosity, optimism, kindness, love and wise words. Thank you to Darrell and Loni Ansel, for your unwavering love and encouragement. I treasure the memories of your weekend in Ann Arbor.

I would not be where I am today without my parents Beth and Jeff, and my sisters, Mimi and Lily. Your love and support have been critical to my success. Mimi and Lily, thank you for the encouraging texts, lighthearted snapchats, and fun-filled visits to Michigan over the years.

Most importantly, thank you to my parents. Your sacrifices and hard work have made it possible for me to focus on my studies. Thank you for teaching me to never give up, be kind above all else, and always look on the bright-side. I am grateful for the endless phone calls, countless laughs, and family vacations that have made the last five years so memorable.

Table of Contents

Dedication	ii
Acknowledgements	iii
List of Tables	x
List of Figures	xii
List of Abbreviations	xviii
Abstract	xxiv
Chapter 1 Introduction to Nitrile-Directed C–H Activation and Reductive Decyanation	1
1.1 Introduction to C–H Functionalization	1
1.2 Directed C–H Functionalization via Palladium Catalysis	4
1.2.1 Nitrogen-Directed C–H Functionalization	6
1.3 Nitrile-Directed C–H Functionalization	8
1.3.1 Nitrile C–H Activation via σ -donation	9
1.3.2 Distal-Directed C–H Functionalization	12
1.3.3 Nitrile C–H Activation via π -coordination	16
1.4 Introduction to Catalytic Reductive Decyanation	20
1.5 Conclusion	23
1.6 References	25
Chapter 2 Development of Methods for Nitrile-Directed C–H Functionalization and Reductive Decyanation	30
2.1 Motivation and Project Goals	30
2.2 Development of a Distal Nitrile-Directed C–H Acetoxylation	31

2.2.1	Optimization Studies.....	32
2.3	Substrate Scope for the Distal Nitrile-Directed C–H Acetoxylation.....	38
2.3.1	Additional Studies and Discussion Regarding Substrate Scope.....	40
2.4	Development of a Distal Nitrile-Directed C–H Pivalation.....	44
2.5	Control Studies for the Distal Nitrile-Directed C–H Activation.....	46
2.5.1	Mechanistic Hypothesis.....	49
2.6	Development of a Proximal Nitrile-Directed C–H Methoxylation.....	50
2.6.1	Optimization Studies.....	50
2.6.2	Control Studies and Scope Investigation.....	56
2.6.3	Mechanistic Hypothesis.....	59
2.7	Development of a Nickel-Catalyzed Reductive Decyanation.....	60
2.7.1	Motivation and Inspiration.....	60
2.7.2	Optimization of the Nickel-Catalyzed Reductive Decyanation.....	61
2.7.3	Substrate Scope for the Nickel-Catalyzed Reductive Decyanation.....	65
2.8	Synthetic Demonstrations and Conclusions.....	66
2.9	References.....	68
Chapter 3 Introduction to Glycosylation and Polysaccharide Synthesis.....		71
3.1	Introduction to Carbohydrates and Glycosylation.....	71
3.1.1	Introduction to Glycosylation.....	73
3.1.2	Glycosyl Fluorides as Glycosyl Donors.....	76
3.2	Montgomery Group Contributions to the Glycosylation Literature.....	78
3.2.1	Fluoride Migration Catalysis for Iterative Glycosylation.....	78
3.3	Introduction to Polysaccharides and Glycoconjugates.....	80
3.3.1	Introduction to Polysaccharides and Glycobiology.....	81
3.3.2	Strategies for the Synthesis of Polysaccharides.....	84

3.3.3	Strategies for the Synthesis of Dendrimers.....	90
3.4	Conclusion	92
3.5	References.....	92
Chapter 4 Progress Towards the Synthesis of Complex Polysaccharides via Triarylborane Catalysis.....		
		96
4.1	Motivation and Project Goals	96
4.2	Initial Strategy for Polysaccharide Synthesis	97
4.2.1	Synthesis of the C6 Monomer.....	98
4.2.2	Initial Polymerization Results.....	99
4.3	Progress Towards Strategic Polysaccharide Synthesis.....	101
4.3.1	Modified Strategy and C4 Monomer Synthesis.....	101
4.3.2	Polymerization Results with a C4 Monomer	103
4.3.3	Polymerization Results with a C2 Monomer	111
4.3.4	Assessment of Modified Boranes in Polysaccharide Synthesis.....	113
4.3.5	Synthesis of Additional Monosaccharide Monomers	116
4.4	Progress towards the Synthesis of Glyco-Dendrimers.....	118
4.4.1	Motivation for Dendrimer Synthesis	118
4.4.2	Attempts Towards Dendrimer Synthesis via Polymerization.....	119
4.4.3	Progress Towards the Iterative Synthesis of Dendrimers	121
4.5	Conclusion and Future Directions	126
4.6	References.....	128
Chapter 5 Conclusion.....		
		130
5.1	Conclusion	130
Chapter 6 Experimental Details		
		133
6.1	General Considerations.....	133
6.2	Chapter 2 Experimental	134

6.2.1	Additional Experiments and Optimization Tables.....	134
6.2.1.1	Norbornene Experiments	135
6.2.1.2	Anhydride and Hypervalent Iodine Experiments	136
6.2.1.3	C–O Amination Optimization.....	137
6.2.1.4	Additional Methoxylation Experiments.....	137
6.2.2	General Procedures for Chapter 2 (A-G).....	138
6.2.2.1	General Procedure (A) for the Synthesis of Biaryl Substrates (via cyanoborylation/Suzuki).....	138
6.2.2.2	General Procedure (B) for the Synthesis of Biaryl Substrates (via Wittig/hydrogenation).....	139
6.2.2.3	General Procedure (C) for the Distal <i>meta</i> -Acetoxylation of Biaryl Substrates	140
6.2.2.4	General Procedure (D) for the Distal <i>meta</i> -Pivalation of Biaryl Substrates...	140
6.2.2.5	General Procedure (E) for the Proximal <i>ortho</i> -Methoxylation of Biaryl Substrates	141
6.2.2.6	General Procedure (F) for the Decyanation of Bibenzyl Benzonitriles	141
6.2.2.7	General Procedure (G) for the Decyanation of Biphenyl Benzonitriles	142
6.2.3	Starting Material Synthesis for Chapter 2.....	142
6.2.4	Spectral Characterization of Acetoxylation Products	155
6.2.5	Spectral Characterization of Miscellaneous Transformations	168
6.2.6	Spectral Characterization of Decyanation Compounds	172
6.2.7	General Procedure for Authentic Standard Synthesis (and Characterization).....	176
6.2.8	Calibration Curve for <i>meta</i> -Acetoxylation GC-FID Analysis	178
6.2.9	General Explanation for Regioselectivity Determination and Sample Characterization.....	179
6.3	Chapter 4 Experimental	182
6.3.1	General Procedures for Chapter 4 (A-H).....	182

6.3.1.1	General Procedure (A) for the Fluorination of Monosaccharides	182
6.3.1.2	General Procedure (B) for the Trimethylsilyl Protection of Acceptors	182
6.3.1.3	General Procedure (C) for the Tributylsilyl Protection of Acceptors	183
6.3.1.4	General Procedure (D) for the Triethylsilyl Protection of Acceptors	183
6.3.1.5	General Procedure (E) for the Tris(pentafluoropenyl) Borane-Catalyzed Polysaccharide Synthesis (Cap included, No Slow Addition)	184
6.3.1.6	General Procedure (F) for the Tris(pentafluoropenyl) Borane-Catalyzed Polysaccharide Synthesis (Cap Included, Slow Addition)	185
6.3.1.7	General Procedure (G) for the Triarylborane-Catalyzed Polysaccharide Synthesis (No Cap Included, No Slow Addition)	186
6.3.2	Spectral Characterization of Compounds in Chapter 4	186
6.3.3	Spectral Data for Polysaccharide Optimization	213
6.3.4	Sample MALDI Analysis of Polysaccharide Products	227
6.4	References	227
6.6	NMR Spectra of New Compounds	231

List of Tables

Table 2-1 Temperature and time screen for distal <i>meta</i> C–H acetoxylation.	33
Table 2-2 Oxidant screen for distal <i>meta</i> C–H acetoxylation.....	34
Table 2-3 Palladium and ligand screen for distal <i>meta</i> C–H acetoxylation.....	35
Table 2-4 Additive screen for distal <i>meta</i> C–H acetoxylation.....	36
Table 2-5 Select control screens for distal <i>meta</i> C–H acetoxylation.....	37
Table 2-6 Brief solvent screen for distal <i>meta</i> C–H acetoxylation.....	37
Table 2-7 Substrate scope of nitrile-directed <i>meta</i> C–H acetoxylation.	38
Table 2-8 Optimization of nitrile-directed distal <i>meta</i> C–H pivalation.....	45
Table 2-9 Initial temperature and time screen for nitrile-directed <i>ortho</i> C–H methoxylation.....	51
Table 2-10 Oxidant screen for nitrile-directed <i>ortho</i> C–H methoxylation.	52
Table 2-11 Additive screens for nitrile-directed <i>ortho</i> C–H methoxylation.....	53
Table 2-12 Further screens for nitrile-directed <i>ortho</i> C–H methoxylation.....	54
Table 2-13 Final time and temperature screens for nitrile-directed <i>ortho</i> C–H methoxylation. ..	55
Table 2-14 Methoxylation optimization on pivalated substrate 2-7.	57
Table 2-15 Methoxylation attempts on naphthalene substrate 2-2g.	58
Table 2-16 Initial optimization of nickel-catalyzed reductive decyanation.....	61
Table 2-17 Ligand screen for nickel-catalyzed reductive decyanation.	62
Table 2-18 Optimization of nickel-catalyzed reductive decyanation on 4-phenylbenzotrile....	63
Table 2-19 Final optimization of nickel-catalyzed reductive decyanation.....	64
Table 4-1 Initial screen of C4 monomers in triarylborane catalyzed polysaccharide synthesis.	104

Table 4-2 Preliminary solvent and temperature screen of C4 monomers in triarylborane catalyzed polysaccharide synthesis.....	105
Table 4-3 Preliminary screen of monomer 4-19 in triarylborane catalyzed polysaccharide synthesis.....	106
Table 4-4 Screen of C2 monomer 4-22 in triarylborane catalyzed polysaccharide synthesis....	112
Table 4-5 Preliminary screen of modified boranes in triarylborane-catalyzed polysaccharide synthesis.....	114
Table 6-1 Acetoxylation selectivity with norbornene additives.....	135
Table 6-2 Brief optimization for C–O activation of distal pivalate.....	137
Table 6-3 Acetoxylation ¹ H NMR analysis.....	180

List of Figures

Figure 1-1 Transition metal-catalyzed C–H activation.....	1
Figure 1-2 Classic challenges and strategies used in modern C–H activation.	2
Figure 1-3 Early C–H functionalization work by Shulpin, Shilov, and Fujiwara.	3
Figure 1-4 First Pd(OAc) ₂ catalyzed aromatic acetoxylation with PhI(OAc) ₂ as a terminal oxidant.....	4
Figure 1-5 Non-selective Pd(OAc) ₂ catalyzed aromatic acetoxylation by Crabtree and coworkers.	4
Figure 1-6 Distortion-interaction analysis for palladium-catalyzed arene CMD C–H activation. .	5
Figure 1-7 Sanford’s seminal directed C–H acetoxylation.....	6
Figure 1-8 Representative examples of palladium-catalyzed directed C–H activation of arenes. .	7
Figure 1-9 Dual directing capability of the nitrile functional group in C–H activation.	8
Figure 1-10 Computational analysis of palladium-catalyzed C–H activation with a nitrile-containing templates.	10
Figure 1-11 N-protected amino acid ligand has dual impact on reactivity and selectivity, when DG = CN.....	11
Figure 1-12 Yu’s model for selective meta-C–H activation methodology by use of a removable template.....	12
Figure 1-13 Yu’s seminal template-directed C–H activation.	13
Figure 1-14 Yu’s template induced <i>meta</i> -C–H acetoxylation of anilines (I) and subsequent hydrolysis for template removal (II).....	14
Figure 1-15 Yu’s remote site-selective arylation of benzoazines.....	15
Figure 1-16 Selective ruthenium-catalyzed C–H activation of benzonitriles.....	16
Figure 1-17 Sun’s palladium-catalyzed C–H alkoxylation of benzonitriles.....	17

Figure 1-18 Jeganmohan's ruthenium-catalyzed C–H olefination of benzonitriles.	18
Figure 1-19 Distal <i>ortho</i> -olefination of biased substrate (I), requiring <i>in situ</i> generation of imidamide (II) to direct functionalization.	19
Figure 1-20 Conversion of the nitrile functional group via standard organic transformations. ...	20
Figure 1-21 Standard pathways for transition-metal-catalyzed decyanative functionalizations. .	21
Figure 1-22 Chatani's rhodium-catalyzed reductive decyanation.	22
Figure 1-23 Maiti's catalytic nickel-catalyzed reductive-decyanation and proposed catalytic cycle.	23
Figure 2-1 Model substrate synthesis, project goals, and biological relevance.	30
Figure 2-2 Lead result for distal <i>meta</i> -C–H acetoxylation.	32
Figure 2-3 Regioisomer authentic standard synthesis.	33
Figure 2-4 Regioselective olefination at <i>ortho</i> position due to secondary directing effect of proximal nitrogen.	40
Figure 2-5 Control reactions for ether substrate 2-3j.	41
Figure 2-6 Effect of conformational rigidity of a template on C–H activation selectivity.	42
Figure 2-7 Indole substrate 2-2p acetoxylation by palladium-catalyzed (A) and metal-free (B) methods.	42
Figure 2-8 Representative heterocyclic substrate synthesis.	44
Figure 2-9 Nitrile-directed distal meta C–H pivalation of substrate 2-2g.	45
Figure 2-10 Optimized C–O amination of distal pivalation product.	46
Figure 2-11 Control studies for distal nitrile-directed transformations.	47
Figure 2-12 Experiments to probe the role of the anhydride in distal nitrile-directed C–H functionalization.	48
Figure 2-13 Mechanistic proposal for <i>meta</i> nitrile-directed C–H functionalization.	49
Figure 2-14 Lead results for <i>ortho</i> - nitrile-directed C–H functionalization.	50
Figure 2-15 Regiodivergent nitrile-directed C–H functionalization.	55
Figure 2-16 Methoxylation attempts on acetoxyated model substrate 2-3a.	56

Figure 2-17 Mechanistic proposal for nitrile-directed <i>ortho</i> C–H methoxylation.....	59
Figure 2-18 Montgomery nickel-NHC-catalyzed reduction of silyloxyarenes.	60
Figure 2-19 Reductive decyanation using Montgomery triethylsilane conditions.	61
Figure 2-20 Substrate scope examined for the nickel-catalyzed reductive decyanation.	66
Figure 2-21 Rapid molecular diversification via traceless nitrile-directed C–H functionalization.	67
Figure 3-1 Common mono- and polysaccharides found in nature.....	72
Figure 3-2 Standard glycosylation mechanism with neighboring group participation for setereoselectivity.....	73
Figure 3-3 Seminal glycosylation methods by Fischer, Koenigs, and Knorr.	74
Figure 3-4 Commonly employed glycosyl donor leaving groups for chemical glycosylation.	74
Figure 3-5 Seminal glycosylation method using glycosyl fluoride donors.	76
Figure 3-6 Glycosylation of silyl ethers using glycosyl fluorides and boron trifluoride etherate.	77
Figure 3-7 Stereoselective glycosylation of using glycosyl fluoride donors and catalytic boron trifluoride etherate.....	77
Figure 3-8 Montgomery fluoride migration catalysis for iterative glycosylation.....	79
Figure 3-9 Mechanism for BFC-catalyzed glycosylation.	79
Figure 3-10 Synthesis of chitosan from chitin.	81
Figure 3-11 Glycoconjugate example: tumor-associated <i>globo H antigen</i>	82
Figure 3-12 Dendrimer structure and propensity to engage in multivalent intercellular interactions.....	83
Figure 3-13 Stepwise synthesis of oligosaccharides.....	84
Figure 3-14 Block synthesis of oligosaccharides.....	85
Figure 3-15 Armed-disarmed glycosylation for the synthesis of oligosaccharides.....	86
Figure 3-16 Active-latent glycosylation (with alkenyl glycosides) for the synthesis of oligosaccharides.....	87
Figure 3-17 One-pot synthesis of ciclamycin trisaccharide.....	87

Figure 3-18 Early catalytic glycosylations in oligosaccharide synthesis.....	88
Figure 3-19 Lanthanum perchlorate promoted oligomerization of glycosyl fluorides.....	89
Figure 3-20 Representative glycol-dendrimer synthesis.....	91
Figure 4-1 Project goals for a triarylborane-catalyzed polysaccharide synthesis.....	96
Figure 4-2 Initial hypothesis and bifunctional C6 monomer.....	97
Figure 4-3 Synthesis of bifunctional C6 monomer.....	98
Figure 4-4 Initial C6 monomer polymerization results.....	99
Figure 4-5 Initial C6 monomer polymerization with slow addition.....	100
Figure 4-6 Modified hypothesis and bifunctional C4 monomer.....	101
Figure 4-7 Synthesis of bifunctional C4 monomer.....	102
Figure 4-8 Initial C4 monomers examined.....	103
Figure 4-9 Syringe-pump polymerization setup.....	103
Figure 4-10 Iterative addition polymerization experiment.....	107
Figure 4-11 Follow up iterative addition polymerization experiment.....	108
Figure 4-12 Polymerization experiment with adamantol acceptor: slow addition, extended stir.	108
Figure 4-13 Polymerization experiment with adamantol acceptor: no slow addition, two hour stir.	109
Figure 4-14 Polymerization experiment with adamantol acceptor: slow addition, one hour stir.	109
Figure 4-15 Adamantol oligosaccharides: deglycosylation experiment.....	110
Figure 4-16 Potential silyl migration occurring with C4 bifunctional monosaccharide.....	111
Figure 4-17 C2 monomer and cap examined.....	111
Figure 4-18 Isolation of deglycosylation/hydrolyzed products in Montgomery fluoride migration catalysis.....	113
Figure 4-19 Modified boranes synthesized for Montgomery fluoride migration catalysis.....	114
Figure 4-20 Synthesis of maltose-derived bifunctional C4 monomer.....	116

Figure 4-21 Synthesis of bifunctional C2 monomer and cap.	117
Figure 4-22 Project goals for triarylborane catalyzed dendrimer synthesis.	118
Figure 4-23 Silyl-protection of benzyl alcohol dendrimer core.....	119
Figure 4-24 Poly-glycosylation of silyl-protected dendrimer core with a bifunctional monosaccharide.....	119
Figure 4-25 Mono-glycosylation of silyl-protected dendrimer core with a bifunctional monosaccharide.....	120
Figure 4-26 Mono-glycosylation of silyl-protected dendrimer core.....	121
Figure 4-27 Deacetylation optimization for dendrimer synthesis.....	122
Figure 4-28 TMS-protection optimization for dendrimer synthesis.	123
Figure 4-29 Secondary glycosylation for dendrimer synthesis.....	123
Figure 4-30 Iterative glyco-dendrimer synthesis.	124
Figure 4-31 Alternative glycosyl fluoride for branched dendrimer synthesis.	124
Figure 4-32 Alternative glycosyl fluoride glycosylation and attempted deprotection for branched dendrimer synthesis.	125
Figure 4-33 Dendrimer synthesis with alternate core.	125
Figure 4-34 Glycoconjugate project summary and outlook.....	126
Figure 4-35 Potential monosaccharide and core structures for dendrimer synthesis.....	127
Figure 5-1 Development of divergent methods for traceless nitrile-directed C–H functionalization.	130
Figure 5-2 Progress towards triarylborane-catalyzed polysaccharide and glycoconjugate synthesis.....	132
Figure 6-1 Yu’s ligand-enabled C–H functionalization using modified norbornenes.....	135
Figure 6-2 Additional anhydride/hypervalent iodine studies.....	136
Figure 6-3 Attempted scope expansion for nitrile-directed ortho C–H methoxylation.	137
Figure 6-4 General procedure (A) for the synthesis of biaryl substrates (via cyanoborylation/Suzuki).....	138

Figure 6-5 General procedure (B) for the synthesis of biaryl substrates (via Wittig/hydrogenation).....	139
Figure 6-6 Acetoxylation standard synthesis.....	176
Figure 6-7 Calibration curve for <i>meta</i> -acetoxylation GC-FID analysis.	179
Figure 6-8 Sample COSY analysis for C–H acetoxylation.	181
Figure 6-9 Polymerization slow addition setup.	185
Figure 6-10 Sample MALDI-TOF analysis for polymerization results.....	227

List of Abbreviations

α : alpha

Å: angstrom

Ac: acetate

Acac: acetylacetone

Ar: aryl

β : beta

9-BBN: 9-borabicyclo[3.3.1]nonane

BCF: tris(pentafluorophenyl)borane catalyst ($\text{B}(\text{C}_6\text{F}_5)_3$)

BDE: bond dissociation energy

Bn: benzyl

bpy: 2,2'-bipyridine

Bpin: pinacolboron

Boc: *tert*-butyloxycarbonyl protecting group

Bu: butyl

Bz: benzoyl

dba: dibenzylideneacetone

c: cyclo

C: Celsius, carbon position on hexose

cat: catalytic

cm: centimeters

CMD: concerted metalation-deprotonation

COD: cyclcooctadiene

Cp: cyclopentadienyl

d: doublet

DAST: diethylaminosulfur trifluoride

dba: dibenzylideneacetone

DBU: 1,8-diazabicyclo[5.4.0]undec-7-ene

DCE: 1,2-dichloroethane

DCM: dichloromethane

DDQ: 2,3-dichloro-5,6-dicyano-1,4-benzoquinone

DG: directing group

DMAP: 4-(dimethylamino)pyridine

DFT: density functional theory

DME: dimethoxyethane

DMF: dimethylformamide

DMSO: dimethyl sulfoxide

DMTST: dimethyl(methylthio)sulfonium tetrafluoroborate

dr: diastereomeric ratio

dtbbpy: 4,4'-di-*tert*-butyl-2,2'-bipyridine

DTBMP: di-*tert*-butyl methyl pyridine **ee:** enantiomeric excess

E: energy

e.g.: for example

EI: electrospray ionization

er: enantiomeric ratio

Et: ethyl

EtOAc: ethyl acetate

Equiv: equivalent

G: gibbs free energy

GC-FID: gas chromatography-flame ionization detector

GCMS: gas chromatography-mass spectrometry

Gly: glycoside

h: hour

HMDS: hexamethyldisilazane

HRMS: high resolution mass spectroscopy

HTIB: hydroxy(tosyloxy)iodobenzene

i: iso, same

***i*-Bu:** isobutyl

***i*-Pr:** isopropyl

i. e.: that is

IDCP: iodonium di-*sym*-collidine trifluoromethanesulfonate

IMes: 1,3-bis(2,4,6-trimethylphenyl)-1,3-dihydro-2*H*-imidazol-2-ylidene

IPr: 1,3-bis(2,6-diisopropylphenyl)-1,3-dihydro-2*H*-imidazol-2-ylidene

IPr^{Me}: 4,5-dimethyl-1,3-bis(2,4,6-triisopropylphenyl)-4,5-dihydro-imidazolium

IPr^{*OMe}: N,N'-Bis(2,6-bis(diphenylmethyl)-4-methoxyphenyl)imidazole-2-ylidene

IR: infrared spectroscopy

***J*:** coupling constant

L: ligand

L_n: ligands

LG: leaving group

μ: micro

M: molarity, transition metal

m: multiplet

MALDI-TOF: matrix-assisted laser desorption/ionization- time-of-flight

Me: methyl

mg: milligram

MHz: mega hertz

mL: milliliter

mmol: millimole

mol: mole

MPAA: Monoprotected amino acid

MS: molecular sieves, mass spectroscopy

n: number of units

***n*-Bu:** butyl

***n*-Hex:** hexyl

***n*-Pent:** pentyl

***n*-Pr:** propyl

NBE: norbornene

NBS: *N*-bromosuccinimide

NCS: *N*-chlorosuccinimide

NIS: *N*-iodosuccinimide

NCTS: *N*-Cyano-*N*-phenyl-*p*-toluenesulfonamide

NHC: *N*-heterocyclic carbene

NIS: *N*-iodosuccinimide

NMR: nuclear magnetic resonance

P: permanent protecting group

Pd/C: palladium on carbon

PG: protecting group

Ph: phenyl

Piv: pivalate

ppm: parts per million

Pr: propyl

R: generic group

r.t.: room temperature

RuPhos: 2-Dicyclohexylphosphino-2',6'-diisopropoxybiphenyl

s: singlet

SET: single electron transfer

T: template, auxiliary, temporary protecting group

TS: transition state

t: tertiary

***t*-Bu:** *tert*-butyl

***t*-Amyl:** *tert*-amyl

t: triplet

TBAB: tetrabutylammonium bromide
TBAF: tetrabutylammonium fluoride
TBAI: tetrabutylammonium iodide
TBS: *tert*-butyldimethyl silyl
TBDPS: *tert*-butyldiphenylsilyl
TES: triethylsilyl
Temp: temperature
Tf: trifluoromethanesulfonyl, triflate
TFA: trifluoroacetic acid
TFE: trifluoroethanol
THF: tetrahydrofuran
TIPS: *triisopropylsilyl*
TMS: trimethylsilyl
X: halogen, leaving group, generic group
Y: generic group
 Δ : heat, change

Abstract

The development of catalytic methods for critical bond-forming reactions has been vital in the progress of synthetic organic chemistry. Accessing straightforward, selective, and efficient methods for rapid assembly of biologically relevant motifs is important to the success of a variety of chemical industries. In particular, both divergent C–H functionalization, and glycosidic bond-formation, for glycoconjugate preparation, are underrepresented in the literature, despite being highly valued transformations. The work herein details progress made in the development of catalytic methods for the synthesis of unique molecular scaffolds.

Chapter 1 provides background on historic and current state-of-the-art approaches to transition metal-catalyzed C–H functionalization, which leverages various directing groups to achieve selective reactivity. Of central focus is the nitrile, which can engage in dual coordination modes, to direct C–H activation both at remote and proximal aromatic sites. This offers a versatile and divergent handle to guide synthetic strategy. Despite this, limitations exist in current methods. The components of these reactions that help determine selectivity are also explored. Following this introduction, Chapter 2 describes work towards accessing methods for traceless nitrile-directed C–H activation. Using a previously reported cyanoborylation, in combination with newly developed, highly regioselective C–H functionalization, and a mild reductive decyanation, transition metal catalysis enables rapid functionalization of aromatic systems. Optimization, scope, and mechanistic hypotheses regarding the four transformations (acetoxylation, pivalation,

methoxylation, and decyanation) are discussed in detail, along with a general demonstration of their orthogonality, when used in combination.

The second half of this dissertation focuses on glycosylation methods, specifically borane-catalyzed transformations to enable the synthesis of polysaccharides and glyco-dendrimers. Chapter 3 begins with a general overview of the innate challenges present in carbohydrate synthesis, and the applications of these biopolymers. Established strategies for the synthesis of polysaccharides are outlined, as well as the current solutions to the stereo-, regio- and chemo-selectivity challenges which inevitably arise in glycosidic bond formation. The utility of glycosyl fluoride donors in conjunction with silyl-ether protected acceptors, and their role in recently developed tris(pentafluorophenyl) borane ($\text{B}(\text{C}_6\text{F}_5)_3$ or BCF) catalysis are discussed in detail. Finally, the importance of dendrimers in molecular biology, and the drawbacks of current synthetic methods to access them are discussed. Following this brief introduction to carbohydrate chemistry, Chapter 4 demonstrates the progress made towards using BCF catalysis for one-pot polysaccharide synthesis. Strategy and experimental design are outlined, followed by initial insight into this challenging research area. The design and synthesis of a novel bifunctional silyl-ether protected glycosyl fluorides are discussed, and various systems to access mono-disperse oligosaccharides are explored. Approaches to mitigate unproductive deglycosylation pathways are also examined. Finally, the synthesis of fully glyco-based dendrimers, using BCF catalysis, is successfully demonstrated, and future work towards accessing complex glycoconjugates is outlined.

Chapter 1

Introduction to Nitrile-Directed C–H Activation and Reductive Decyanation

1.1 Introduction to C–H Functionalization

The areas of pharmaceutical, agrochemical, and materials development rely on efficient methods to construct highly functionalized molecules from basic synthetic building blocks.¹ One approach to address these needs, which has gained momentum in both academic and industrial

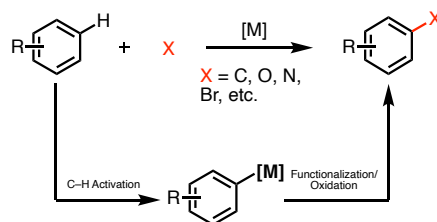


Figure 1-1 Transition metal-catalyzed C–H activation.

processes, is the functionalization of carbon–hydrogen bonds. C–H functionalization, the process of converting carbon–hydrogen bonds to other functional groups, serves as a viable approach to efficiently build up molecular complexity from inexpensive, simple, starting materials.^{1–3} This catalytic process circumvents the need to pre-install functional groups at the site of reactivity, thus reducing the number of synthetic steps, and improving overall atom-economy (Figure 1-1).² However, as molecular complexity increases, selectively functionalizing hydrocarbon portions of a molecule, without undesired reactivity at sensitive functional groups, becomes a challenge. Traditional approaches for chemoselectively functionalizing C–H bonds within a molecule utilize radical processes, acid–base chemistry, or electrophilic aromatic substitution (EAS) to cleave the desired C–H bond(s) in a substrate, but these methods have inherent limitations.^{1–3} In addition to lack of predictably

and over functionalization observed in classical transformations, harsh reaction conditions make for poor functional group tolerance. Finally, the tedious substrate and reagent preparation often required, make these systems unpopular for selective C–H activation.

Using the C–H bond as a synthetic handle to increase molecular complexity is fundamentally

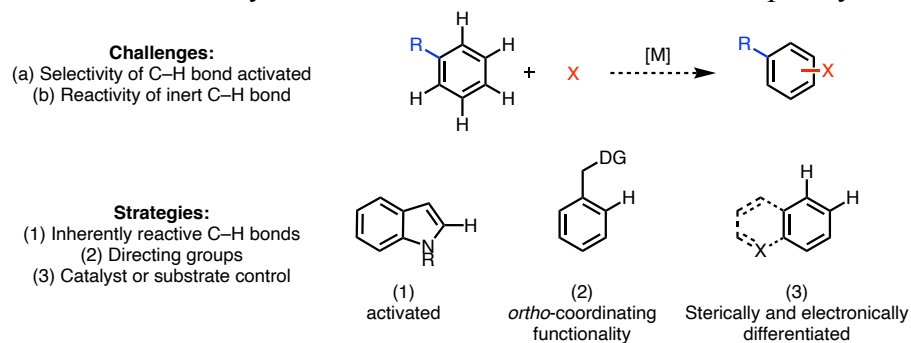


Figure 1-2 Classic challenges and strategies used in modern C–H activation.

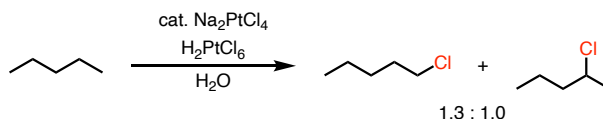
problematic. Specifically, (1) selectively functionalizing the desired C–H bond among others, and (2) overcoming the lack of reactivity at these sites, are among the largest challenges in this field (Figure 1-2). The first obstacle has frequently been addressed by employing coordinating functionality, such as an amide, hydroxyl, or amine, to direct metalation of proximal C–H bonds.¹ While these directing groups are robust, they are often remain incorporated in the molecule, which results in constraints regarding the structure of the final product. Other strategies for selective functionalization can be achieved through either catalyst control, substrate control, or a combination of the two. Work by Davies⁴, White⁵, and others² take this approach, wherein the ligand scaffold of the metal complex, and unique steric or electronic characteristics of one C–H bond, guide chemoselective oxidation in highly complex molecules.

The relatively inert nature of C–H bonds is owed to the low polarization of the C–H bond, high pKa (relative to other functional group-hydrogen bonds), and poor orbital overlap with metal *d*-orbitals. Many of the solutions discussed above aide in the activation of these inert bonds, but still make selection of the C–H bond for activation over other functionalities present in the molecule challenging. One solution, transition-metal promoted reactions, have evolved from stoichiometric

organometallic studies, to catalytic transformations. The resulting carbon-metal bond formation, results in a more reactive handle for oxidation. Regardless, insertion into hydrocarbons requires uniquely tailored electrophilic metal species and careful control of conditions.^{1,2}

Relevant literature exploring C–H functionalization has expanded rapidly since the initial

Shulpin and Shilov (1969)



Fujiwara (1969)

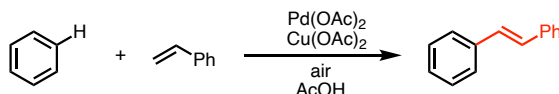


Figure 1-3 Early C–H functionalization work by Shulpin, Shilov, and Fujiwara.

reports by Shulpin and Shilov in the 1960s and 1970s, but motivations behind the study of C–H functionalization processes, have shifted. While the first research concentrated on activating C–H bonds in simple hydrocarbons, methods developed in recent years have focused on using C–H activation as a strategy for late-stage functionalization, and the tuning of reactions to selectively oxidize specific, otherwise unreactive, C–H bonds within a complex molecule.

Shilov, often considered the pioneer of modern C–H activation, studied primarily stoichiometric transformations, his influential insights igniting the field, and inspiring many to explore catalytic variants of his work.^{2,3,6} Stoichiometric findings opened the door for modern approaches to C–H functionalization. Selectivity patterns in Shilov’s platinum halogenation, and Hodges’ deuteration of hydrocarbons, differed from that typically observed by radical C–H functionalizations. This eluded to the presence of an alkylplatinum intermediate, and the potential to use metal species to further control selectivity. While Shilov focused on halogenations of alkanes, concurrently, Fujiwara observed C–H bond functionalization in the context of oxidative cross-coupling of arenes and olefins (Figure 1-3).⁷ Using stoichiometric $\text{Pd}(\text{OAc})_2$ and $\text{Cu}(\text{OAc})_2$ under air, the Fujiwara reaction laid ground for C–H activation studies involving transition metals bearing carboxylate ligands.^{2,7} These studies paved the

way for more extensive studies of C–H activation, and offered insight into the power of electrophilic palladium to functionalize these bonds, which were previously thought to be unreactive.

1.2 Directed C–H Functionalization via Palladium Catalysis

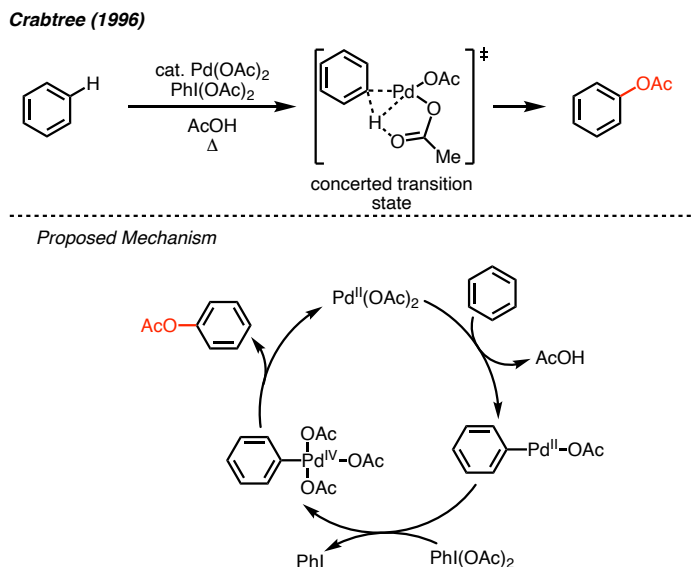


Figure 1-4 First Pd(OAc)₂ catalyzed aromatic acetoxylation with PhI(OAc)₂ as a terminal oxidant.

In 1996, Crabtree reported the first C–H acetoxylation of aromatic systems using catalytic Pd(OAc)₂ with (diacetoxyiodo)benzene (PhI(OAc)₂) as a terminal oxidant (Figure 1-4).⁸ Although excess benzene was required for the transformation, this discovery not only demonstrated that PhI(OAc)₂ could act as a productive terminal oxidant, and Pd(OAc)₂ as a viable C–H activation

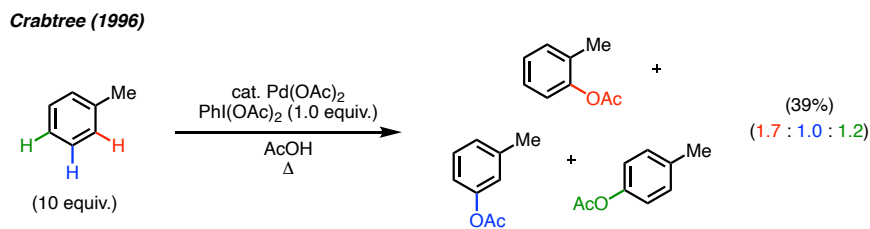


Figure 1-5 Non-selective Pd(OAc)₂ catalyzed aromatic acetoxylation by Crabtree and coworkers.

catalyst, but that a Pd^{II/IV} catalytic cycle was operative for the C–H acetoxylation reaction. Other simple arene substrates provided statistical mixtures of products dictated by solely electronic factors. (Figure 1-5). These seminal studies eventually led to the exploration of novel catalyst systems employing

various ligand scaffolds to overcome complex mixtures of products that arise from unselective C–H functionalization. In particular, the use of coordinating ligands or “directing groups,” became a solution, but still employed the reliable oxidative system of hypervalent iodine and catalytic palladium, to access the first regioselective products.¹ While answers to the selectivity and reactivity paradigm were addressed, mechanistic insight and reaction predictability was limited.

Early contributions to C–H activation field by the Fagnou group helped to de-convolute questions regarding mechanism and regioselectivity. This work probed the concerted-metalation-deprotonation (CMD) pathway, and disclosed support for the electronically-driven selectivity in these transformations. In this established mechanism, a C–H bond is deprotonated by a pendant acetate ligand while the palladium catalyst, on which the ligand is complexed, becomes metallated to the substrate. This seminal work, and studies that followed, laid the foundation for modern C–H

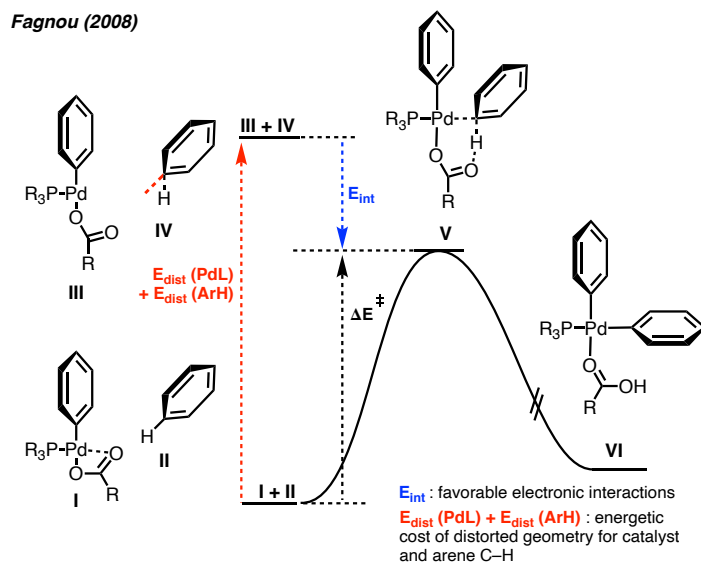


Figure 1-6 Distortion-interaction analysis for palladium-catalyzed arene CMD C–H activation.

functionalization. As important reaction parameters and physical organic techniques to study these systems were developed, the mechanisms of these transformations were elucidated, allowing for great advancements in understanding these processes.^{2,9–11} Of critical importance was distortion-interaction analysis, which provides the thermodynamic penalty of palladium-arene geometric strain as they move

away from ground state energy (distortion energy, ΔE_{dist}), versus the favorable interaction energy ΔE_{int}). Data was assessed to determine the specificity, and plausibility, of arene C–H functionalizations (Figure 1-6). This work suggested carboxylate deprotonation as key to understanding the regioselectivity in early, undirected C–H activation, as the hydrogen cleaved is often the most acidic, and minimizes transition state distortion. Recent literature^{2,12} continues to assess C–H activation through energetic strain and transition state analysis. It is used as a guiding feature for the development of transformations with more complex reaction parameters, and unique regioselectivity.

1.2.1 Nitrogen-Directed C–H Functionalization

Following Crabtree's results, pioneering work by Sanford, beginning in 2004, revealed the

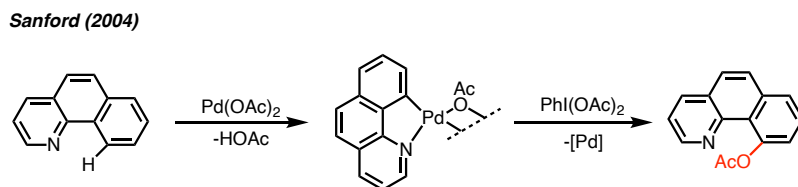


Figure 1-7 Sanford's seminal directed C–H acetoxylation.

powerful strategy of using functional groups within a molecule to control site selectivity of a reaction. This directing group strategy allowed for selective oxidation and accelerated C–H bond cleavage by bringing the metal in close proximity to the desired bond to be activated.^{13–15} The seminal work by Sanford utilized the coordinative capability of *N*-heterocycles, such as pyridine and phenanthrolines to direct proximal installation of acetoxy groups with catalytic $\text{Pd}(\text{OAc})_2$ via a 5-membered palladacyclic intermediate (Figure 1-7). Based on numerous stoichiometric and mechanistic investigations, these transformations were thought to occur via CMD thus making the acetate reagents present in the reaction not only crucial to determining the identity of the oxidation, but also play a role in the initial C–H activation step.

Within the last two decades, arene C–H functionalization has become a rapidly growing field, with key developments by Yu and Shi, though the use of oxazoline¹⁶ and amine¹⁷ groups, among other

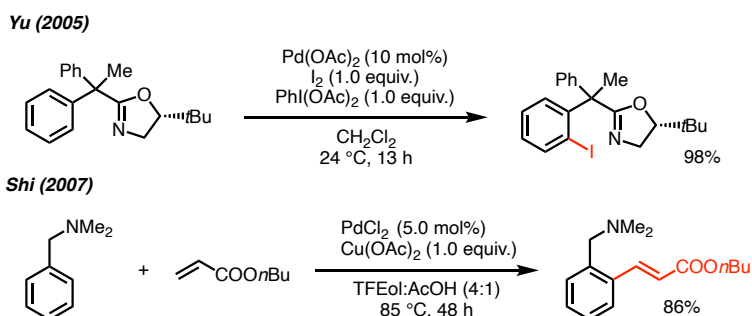


Figure 1-8 Representative examples of palladium-catalyzed directed C–H activation of arenes.

motifs,^{1,2} to direct C–H activation (Figure 1-8). Moreover, a variety of methodologies have been developed that utilize other transition metal catalysts, such as Ru, Rh, Pt, Pd and Ir, in directed C–H activation.^{2,3} Palladium has been an important focus in the literature though, due to Pd^{II} compatibility with a broad scope of oxidants and directing groups, as well as its stability in ambient moisture and air.¹⁸ Additionally, while a variety of directing groups are employed in C–H activation reactions, those containing nitrogen have accumulated particular interest due to their ease of installation and ability to strongly coordinate to transition metals. These chelating functionalities are well positioned to orient the palladium adjacent to the carbon *ortho* of the directing group. Thus, the bond activated by the metal catalyst in most directed C–H activations have been limited to functionalization at this position; sterics, ring strain, and thermodynamic instability of cyclopalladated intermediates are likely the reason. Further, once installed, directing groups are difficult (if even possible) to remove, and lack flexibility in site-selectivity. While the strategies mentioned above allowed for control in the installation of new functionality, selectively functionalizing C–H bonds distal to pre-installed directing groups remains a challenge for the synthetic community.

1.3 Nitrile-Directed C–H Functionalization

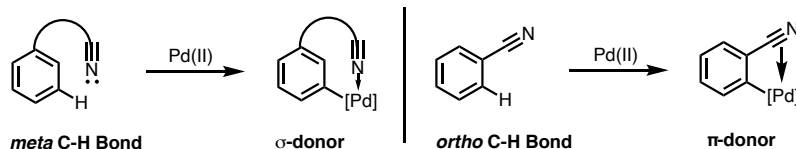


Figure 1-9 Dual directing capability of the nitrile functional group in C–H activation.

The nitrile is of great interest as a directing group in C–H functionalization due to its unique, dual modes of coordination. It has been used to access a variety of functionalized molecules, and has made previously inaccessible hydrogens available to directed metal catalysis.

Nitrile-based template methods that employ the weakly chelating property of the nitrile group have been shown to be effective strategies for remote C–H functionalization. These systems rely on the end-on coordination of the nitrogen lone pairs to an electron-deficient transition metal (through σ -donation) to allow for selective C–H activation (Figure 1-9).¹⁹ The efficiency and atom-economy of these transformations leave room for further development, though. These methods offer access to previously inert CH bonds, but chemistry accessing remote positions is still limited. Alternatively, nitriles have been shown to be effective π -acids, through coordination via the carbon-nitrogen triple bond. Although there has been some research into complementary methods for proximal C–H activation via π -coordination of nitriles, this paradigm also remains underexplored.²⁰

While multiple mechanisms have been proposed for each π - and σ -directed functionalization by the nitrile, no system which harnesses both chelation modes to differentially (and selectively) functionalize a single molecule has been developed. Mechanistic studies have been conducted to explain the nitriles' coordinative modes that allow for proximal or distal activation. Herein, a brief discussion of those factors, and important literature examples which demonstrate these patterns will be described.

1.3.1 Nitrile C–H Activation via σ -donation

The linear nature of nitriles, their propensity to reversibly coordinate to metal centers and stability to metal-catalyzed reactions make them an ideal directing group for distal functionalizations (via σ -donation). Unlike other directing groups, nitriles do not succumb to unfavorable conformations or steric strain as found in amide or carboxylic acid systems. For example, A-1,3 strain recognized in carbonyl-based directing groups is not present with nitriles. Moreover, while rotation of the bond linking the substrate and directing group can change which C–H bond the metal is interacting with for many directing groups, this pitfall is not observed with linearity of the nitrile. Further, the weak, reversible chelation by the nitrile's lone pairs is geometrically enabled by the linear nature of the C(sp)–N bond. This functionality is poised to bring the metal catalyst (typically palladium) in closer proximity to more remote positions in a molecule via an “end-on” coordination, and the weaker chelation allows for the transient directing capability. Because of this, nitriles are often used in auxiliary-based systems and have been used to access a wide array of C–C and C–heteroatom bond formations.^{12,21} These functionalities interact uniquely in macrocyclic transition states to allow for distal C–H oxidation. The success of many of these transformations relies on multiple reagents which work synergistically with the nitrile to achieve selectivity. These reaction components include (1) important reaction additives, (2) privileged ligands, and (3) unique solvent effects.

First, silver additives have been shown to play a vital role in acquiring the unique selectivity achieved in many of the template-based systems. This phenomenon was studied via computations in a

Yu and Houk (2014 and 2017)

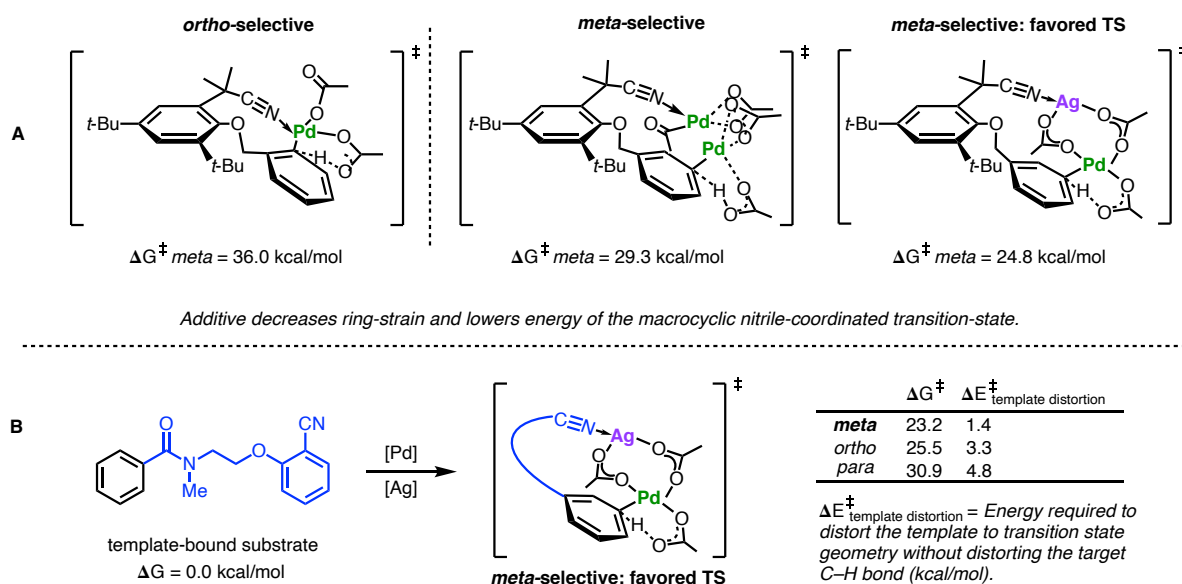


Figure 1-10 Computational analysis of palladium-catalyzed C–H activation with a nitrile-containing templates.

collaborative report by Yu and Houk, on the palladium-catalyzed C–H alkenylation of toluene derivatives with a nitrile-containing template.²² It was found that the inclusion of a silver species to these systems decreases the ring strain and lowers the energy barrier for the macrocyclic C–H activation transition state. While a dimeric palladium species also lowers energy to allow for the *meta*-selective transformation to favorably occur, ultimately a bimetallic silver-palladium coordination (Pd-Ag heterodimer) to the nitrile leads to the lowest energy transition state. This computational result correlates experimentally with the best yield and most selective olefination (Figure 1-10A). In a later study, looking at structurally similar systems, template distortion energy (related to ΔE_{dist} discussed in Chapter 1.2) was also found to be lowest for the *meta* isomer, as opposed to *ortho* and *para*, when silver was included, highlighting the interplay of additives and favorable template conformation on regioselectivity (Figure 1-10B).²³

Specific ligands also play a large role in the selectivity of C–H activation of remote arenes. Monoprotected amino acid (MPAA) ligands have been shown in work by the Yu and Houk groups, to aid in accelerating the palladium-catalyzed C–H activation step by stabilizing the Pd–Ag heterodimer

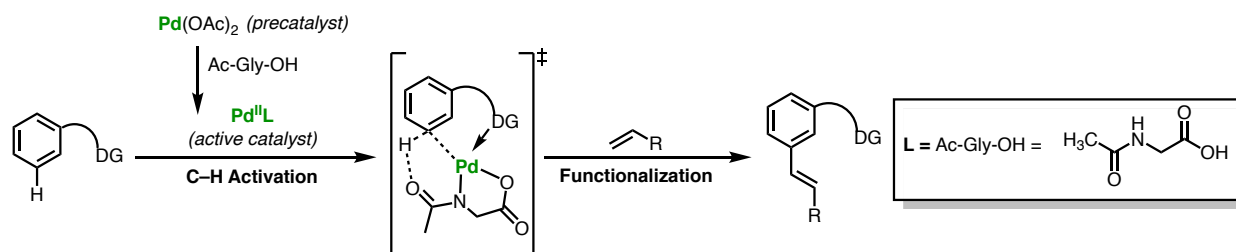


Figure 1-11 N-protected amino acid ligand has dual impact on reactivity and selectivity, when DG = CN.

(discussed above), and simultaneously act as the internal base in the CMD step, when used in conjunction with nitrile-template directing groups (Figure 1-11).²⁴ More recently, Stahl has shown evidence of rate-acceleration (via ligand-accelerated catalysis) enabled by these unique MPAA ligands,²⁵ while other groups have harnessed the modular properties of these ligands to apply them to other nitrile-based systems. Finally, these rigid ligands are known to prevent palladium from blacking out (a common challenge), lower the barrier for oxidative addition, and increase the rate of the reactions, which concurrently prevents off-cycle byproducts from forming.^{12,21} These results show that this highly privileged class of ligands are ideal reaction components for the development of selective, remote C–H activation directed by nitrile functional groups.

Finally, solvent choice is key when designing nitrile directed C–H activation enabled by the σ -donation mode. It has been found that fluorinated solvents, such as hexafluoroisopropanol (HFIP), and trifluoroethanol (TFE) have been crucial in the success of many directed C–H activation transformations, especially those using template auxiliaries for remote functionalization. The first nitrile-based system by Yu utilized HFIP as the chosen solvent as it was hypothesized to stabilize the large cyclophane-like transition state formed in the reaction.¹⁹ HFIP is known for its polar-protic character and hydrogen-bonding propensity, which has demonstrated beneficial effects in many recent

C–H functionalizations, as well.¹² While not fully explored, the coordinating solvent is thought to be vital to the structural rigidity of these systems, overcoming the entropic cost of the macrocycle to reach the distal *meta* and *para* C–H bonds. In many of the remote functionalization methods present in the current literature, non-fluorinated solvents show trace yields and low selectivity.^{26,27} Ultimately, expanding these remote, nitrile directed C–H activation methods must be guided by exploration of variety of factors including additive, ligand, and solvent choice, which current literature has shown to be important in the conversion and selectivity of this class of nitrile enabled transformations.

Harnessing the end-on coordination of the nitrile through σ -coordination to a transition metal has been shown to promote the installation of a variety of functional groups at distal positions within tethered arenes.^{12,21} The nitrile has become a crucial part in the design of auxiliary/template methods, but work to use the nitrile beyond these biased systems is desirable. Being able to utilize the innate function of the nitrile, rather than tediously designing a specific template, for one class of reaction would be key. Moreover, removing these molecular tethers without destroying the molecular integrity, is difficult; Hydrogenation reduces olefins; strong acid can racemize stereocenters, and slightly oxidizing conditions can completely degrade a late-stage intermediate. Thus, accessing methods which harness innate functional groups for regiodivergent functionalization would be an impactful addition to current directed C–H activation methods.

1.3.2 Distal-Directed C–H Functionalization

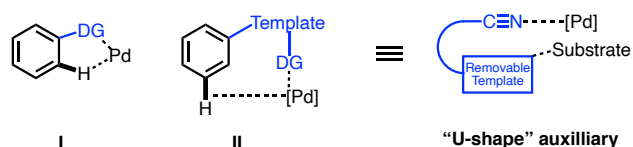


Figure 1-12 Yu's model for selective meta-C–H activation methodology by use of a removable template.

In 2012 the Yu group developed a nitrile-based, removable template to allow for direct C–H olefination at the *meta*-position of aromatic rings. , by inducing a large, conformationally strained pre-

transition state for activation of these bonds.¹⁹ While typical *ortho*-directed C–H activation proceeds via a rigid 5- or 6-membered palladacycle intermediates (**I**), Yu’s cyclophane-like pre-transition state forms via 12-membered rings or larger (**II**) (Figure 1-12). This large, organized, and conformationally strained pre-transition state is enabled by the use of a heterobimetallic palladium-silver species, which spatially positions selective functionalization of distal C–H bonds.¹⁹

While a large advancement for the field, the requirement to synthesize the nitrile-containing template through a 6-step procedure prior to attachment on the benzyl bromide substrate greatly limits the utility of this reaction. Following *meta*-directed C–H functionalization, this template must be

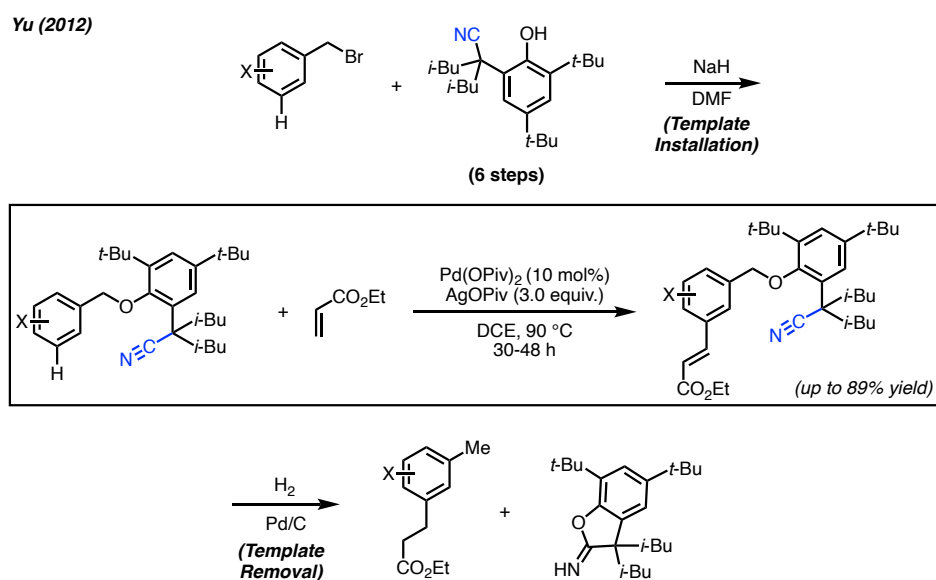


Figure 1-13 Yu’s seminal template-directed C–H activation.

removed via hydrogenolysis, which greatly limits the functional group compatibility of this reaction. Furthermore, template removal leaves a methyl substituent, which might not always be desirable, and generates a stoichiometric byproduct that must be removed during purification (Figure 1-13).

This strategy, which uses the end-on coordination of nitrile-groups, has been expanded to several substrates and bonds installed, but has consistently employed palladium catalysts.^{28–31} For example, later work by the Yu group has demonstrated a template (T₆), which is appended to the nitrogen functionality and subsequently removed (**II**) after the desired transformation (**I**), can be used

to achieve C–H acetoxylation at the *meta* position of tethered anilines in modest yields (Figure 1-14).³²

The authors emphasize the specific, highly rigid structural conformation achieved in the macrocyclic palladacycle as key to the regioselectivity of the transformation. This is achieved by the meticulously-designed template, with steric and electronic biases, including a linearly coordinating nitrile, as well as

Yu (2014)

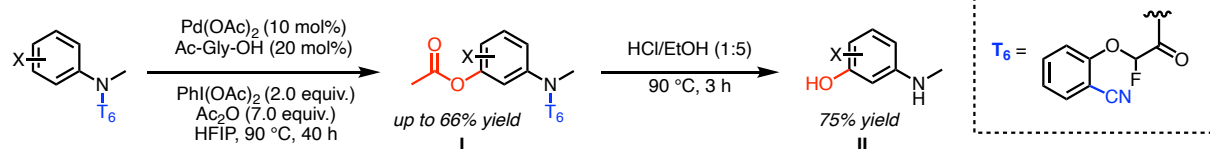


Figure 1-14 Yu’s template induced *meta*-C–H acetoxylation of anilines (I) and subsequent hydrolysis for template removal (II). a rotation-limiting carbonyl and fluorine substituent on the carbon chain. In addition to the highly geometrically-tailored directing template, it is notable that a silver additive and mono-protected amino acid (MPAA) ligand were important to reaction success, as omitting these additives led to significantly lower yield, and reaction rate. Finally, like their initial template-directed olefination, the newly installed acetoxy group is unfortunately incompatible with the cleavage of this auxiliary, though the valuable amine tether is left unscathed.

While this transformation, and extensions of the “U-shape” auxiliary methodology for *meta*-C–H activation by Maiti, Tan, and others are synthetically useful, the requirement for specific substrate classes, and need to synthesize, attach, and subsequently cleave each template is inefficient and cumbersome.^{33–40} Further, the functional groups which can be installed by these methods are relatively limited in scope, especially given the relatively harsh conditions necessary for template removal. Because of these limitations, a new, easy to install distal-directing groups that can enable the functionalization of C–H bonds are necessary. The common theme of all these systems is their employment of the nitrile to bring the metal in proximity to the bond which is to be functionalized. The systems differ though, in the identity of the linker, as well as the method by which the template is attached. Systems for these transformations range greatly; *N*-Methyliminodiacetic acid (MIDA) boronate derivatives have been used to install activated olefins at the *meta* C–H bonds⁴¹, silyl

tethers have been employed to access *para*-silylated arenes,⁴² among other species, and even distal deuteration has been demonstrated with ester-ligated templates.⁴³

Further, The Yu group has engaged reversible chelation of quinolones,²⁸ to functionalize arenes without covalently bonded-ligands, and more recently, and has merged template-directed chemistry with Catellani-like norbornene (NBE) reactivity⁴⁴ to achieve remote “differentiation” and C–H activation at more challenging positions (Figure 1-15). While a unique approach that solved issues regarding remote functionalization, the highly specialized, non-atom-economical template scaffolds, super-stoichiometric silver, and requirement for a heteroaromatic nitrogen in substrates are major pitfalls of this method.

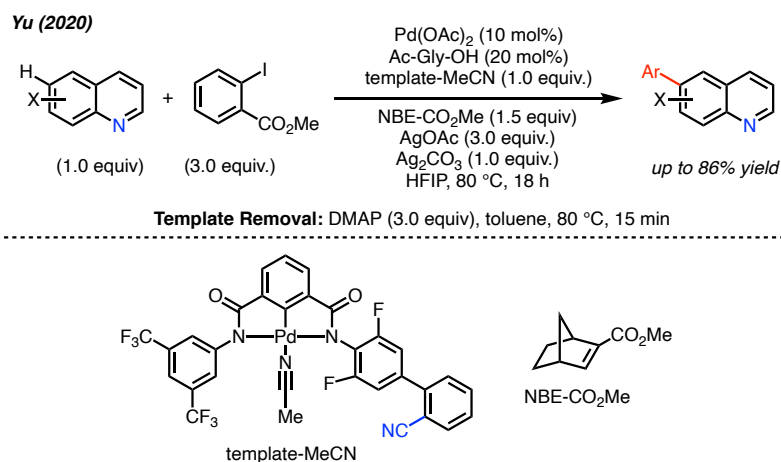


Figure 1-15 Yu’s remote site-selective arylation of benzoazines.

While all of these examples highlight the exquisite selectivity that can be achieved through the design of highly tuned template systems, the large synthetic effort necessary to carry-out these reactions, limits their wider utility. They cannot be broadly applied in general synthetic strategy, as each system is highly substrate dependent. Additionally, most of these directed functionalizations do not occur via innate functional groups, and installing and subsequently removing a template is not always possible to do without negatively perturbing the system. Finally, while these methods can be used to functionalize simple arenes, they have not been tested in more

complex systems in which multiple arenes with similar (unbiased) steric and electronic environments are present.

1.3.3 Nitrile C–H Activation via π -coordination

Orthogonal to the methods for σ -directed distal C–H functionalization, nitriles are capable of engaging transition metals through π -coordination, for proximal functionalization. The selectivity is due to proximity to the adjacent C–H bond, and geometric constraints of the resulting metallacycle, when coordinated via the π -system. This π -mode of coordination to nitriles is commonly proposed to

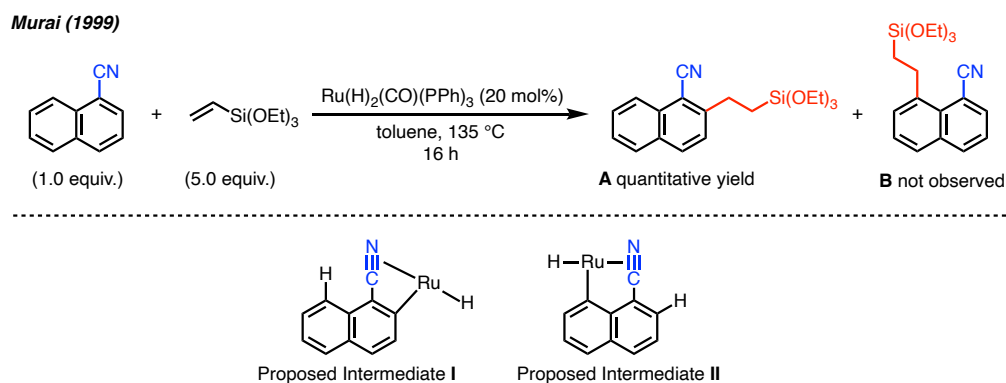


Figure 1-16 Selective ruthenium-catalyzed C–H activation of benzonitriles.

promote C–H cleavage in transition-metal catalyzed dimerization of acrylonitrile.⁴⁵ Despite the historical assumption of this mechanism, little evidence has established a clear understanding of the CN motif engaging in this binding mode. This type of labile coordination is not unlike that observed between π -acids and palladium (and other) metal catalysts and olefins,⁴⁶ or alkynes,^{1,47} to direct C–H functionalization. General π -metal-bonded systems are prevalent throughout the literature.

Early demonstrations of the nitrile's coordinative reactivity was reported by the Murai group in their ruthenium-catalyzed C–H olefination (Figure 1-16).⁴⁵ The authors exclusively observed product **A**, which they propose is the result of geometric constraints, as the nitrile is not capable of directing metallation to more distal sites. The implied cyclo-metallated intermediate **I** is necessary for

the selective *ortho*-nature of these π -coordinated systems, regardless of ring strain. Even a less distorted proposed intermediate **II**, does not lead to the specific naphthalene product observed in this transformation, emphasizing the unique, nitrile-driven, regioselectivity. Additionally, Murai proposes potential need for conjugation of the π -electrons of the nitrile group and those in the arene (at the *ortho* position), for activation, and that the C–H bond in **II** is simply too far from the nitrile-coordinated catalyst for functionalization. While this method demonstrated a new way to selectively functionalize benzonitriles, the scope is limited to activated olefins (triethoxysilane) as coupling partners, and difunctionalization was observed as the major product in substrates lacking an *ortho*-substituent.

Several palladium-based methods have been developed recently, and propose similar mechanistic pathways, emphasizing the importance of π -coordination in proximal nitrile-directed C–H bond functionalization. In particular, palladium-catalyzed methods for alkoxylation⁴⁸ and halogenation⁴⁹ have been demonstrated by the Sun group. While informative, both transformations suffer from limited substrate scope, with over functionalization and/or regioisomeric side products in almost all examples. The methoxylation protocol developed by Sun requires a blocking group to avoid undesirable di-functionalization, and the harsh reaction conditions limit the substrate scope to simple arenes, leaving much room for further improvement (Figure 1-17).

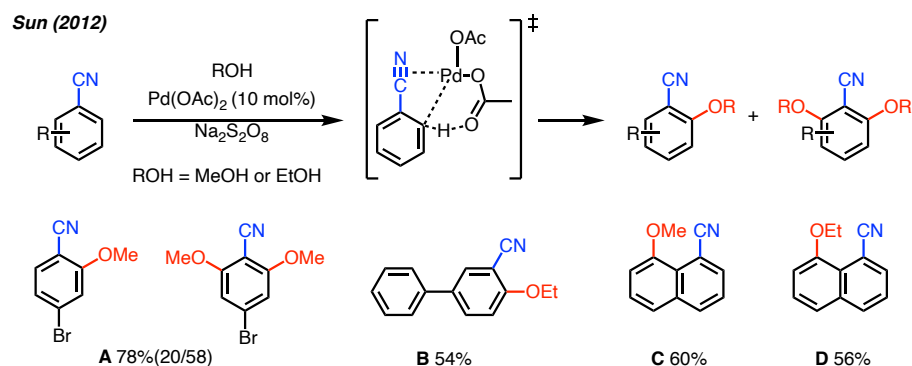


Figure 1-17 Sun's palladium-catalyzed C–H alkoxylation of benzonitriles.

Interestingly, when the alkoxylation was performed on 1-naphthonitrile (products **C** and **D**), exclusive functionalization at the 8-position was observed, rather than the 2-position, as in Murai's Ru-

catalyzed C–H activation. This suggests that different metal/ ligand combinations can be used to promote orthogonal reactivity in systems bearing C–H bonds in different steric and electronic environments. The selectivity change may result from a difference in mechanism due to the different metal/oxidant combination, or from the potential steric hindrance involved in the addition of a large silyloxy-substituted olefin, to the 2-position of naphthonitrile. Regardless, this result offers interesting selectivity for proximal functionalization enabled by a nitrile directing group, and insight into regioselectivity changes guided by catalyst control. Unfortunately, the forcing conditions for the methoxylation make it a less than desirable, and applicable transformation for molecules with sensitive functional groups.

Arylation⁵⁰ and fluorenone-synthesis⁵¹ have also been achieved with nitrile-directed palladium C–H functionalization, as well, but further study of the details behind the nitrile’s π -coordination to the catalyst is limited. Ruthenium-catalyzed C–H activation has also been used to install *ortho* aryl groups⁵² and olefins⁵³ to benzonitriles, but similar drawbacks persist, including over functionalization, low regioselectivity, and the necessity for particularly activated olefins or arenes. Improvements upon the selectivity and efficiency, as well as a broader application of these reactions is a gap in the literature. Regardless of methodology drawbacks though, Jeganmohan’s study of ruthenium catalyzed olefination⁵³, offers unique insights into potential selectivity-determining factors for *ortho*-activation

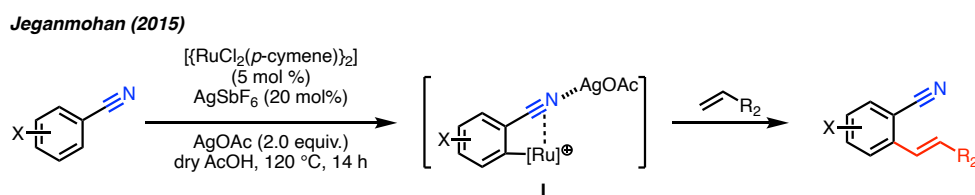


Figure 1-18 Jeganmohan’s ruthenium-catalyzed C–H olefination of benzonitriles.

by the nitrile. The transformation proposes intermediate **I** involving a ruthenium- π interaction, with silver acetate coordinated to the nitrogen’s lone pair (Figure 1-18).

Interestingly, the addition of a Lewis acid, such as a silver salt, is necessary for good yield and selectivity, as well as to reduce formation of a benzamide side-product. The additive is thought to coordinate to the lone pairs on the nitrile blocking Pd-coordination in an end-on fashion. Similarly, highly linear-nitrile-silver coordinated species have been shown in DFT calculations in the literature,⁵⁴ and are used to support Jeganmohan's proposal. This may apply to previously discussed CN *ortho*-directed functionalizations which necessitate an additive, or polar solvent, for good yield/and selectivity. The coordination of these reagents may play a role impeding the undesired, alternative (linear) chelation mode, and thus enhance π -direction. Although this finding may contradict the beneficial effect of silver additives in remote, σ -directed transformations, the difference in metal, oxidant and scope may suggest the silver additives play a different role in each reaction. Regardless, due to lack of mechanistic studies in this case, the specific role of this component is unclear. Overall, much work is needed on the selectivity, scope, and mechanistic details of these *ortho*-selective, nitrile-directed transformations.

Unlike previous methods employing nitriles as a directing group, which rely on either σ - or π -coordination, the Li group in 2015 reported a regiodivergent *ortho*- and *meta*-C–H olefination. Despite its ability to rapidly build up molecular complexity in simple benzamides, this reaction suffers from di-olefination, and ultimately requires extra synthetic steps to change inherent regioselectivity in a reaction.³⁹ Furthermore, the applicability of these transformations is limited due to the requirement of

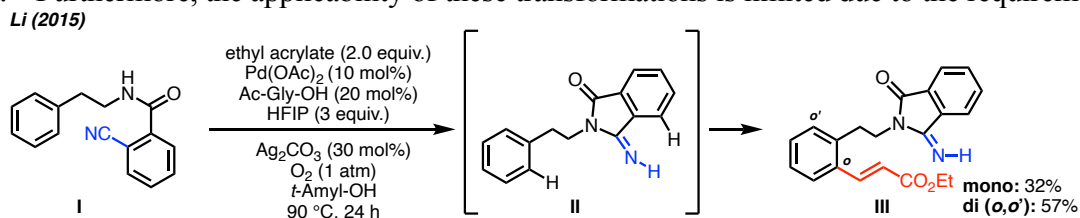


Figure 1-19 Distal *ortho*-olefination of biased substrate (**I**), requiring *in situ* generation of imidamide (**II**) to direct functionalization.

a privileged substrate, as selectivity achieved by a cyclic amide which forms due to reaction conditions (Figure 1-19). Ultimately, this method lacks functional group tolerance (e.g. *ortho* functional groups),

scope, and necessitates specific geometric parameters. While not ideal, this work alludes to the potential for regiodivergent functionalization, directed by a single group in a molecule.

In conclusion, the nitrile functional group offers complementary strategies for proximal and distal C–H functionalization, with the potential for selectivity via choice of metal, ligand, and Lewis acid additive. This bifunctional directing group is underutilized and underexplored, though, offering possibilities for scope- and mechanism-driven research. Further, harnessing both reversible chelation modes, to offer a broad approach to functionalization across complex scaffolds with multiple aromatic rings, has not yet been demonstrated.

1.4 Introduction to Catalytic Reductive Decyanation

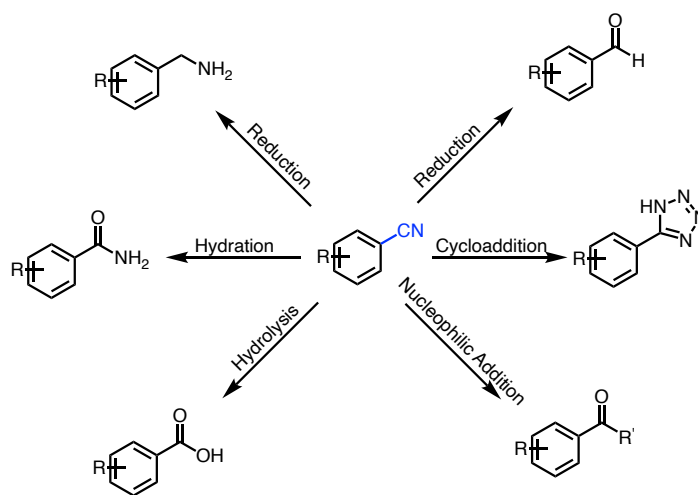


Figure 1-20 Conversion of the nitrile functional group via standard organic transformations.

While the dual directing capability of nitrile group is extremely valuable for catalytically diversifying aromatic motifs, like any directing group it will not always be desired in the final target. Although the nitrile is found in several drugs on the market, and can be potentially valuable in forming carboxylic acids, esters, amides, amines, and alcohols through oxidations, reductions, and other standard organic transformations, sometimes accessing the *ispro* C–H bond is most ideal (Figure 1-20).⁴⁸ The removal of directing groups is a common way to access functionalized molecules in a

traceless manner. Although many directing groups are challenging to remove, chemists have been able to cleave even high bond-dissociation energy (BDE) C–CN bonds by not only using harsh dissolving metal conditions, but also by employing more user-friendly stoichiometric, and substoichiometric, metal promoters. Removal of the nitrile group from the carbon scaffold offers a unique opportunity to leverage traceless directed C–H functionalizations. Proceeding selective C–H activation of the benzonitrile (which are widely available, and accessible^{3,55,56}) the functional handle could be removed to acquire the unbiased molecular scaffolds. In addition to methods developed for reductive decyanation,^{57,58} transition metal catalysis has enabled an array of chemical transformations including borylation,⁵⁹ silylation⁶⁰, and cross-coupling at the *ipso*-carbon. While this area of organometallic chemistry is less well understood, some work has been done to understand decyanation pathways, and develop methods to remove the group in a catalytic manner.

Existing methods primarily target activation of the C–CN group through direct metal-mediated insertion pathways, rather than *in-situ* modification of the functional group prior to the removal. Based on various mechanistic studies, there are generally two pathways which are widely accepted.^{57,60} First, the metal can insert directly into the C–C sigma bond via oxidative addition (Figure

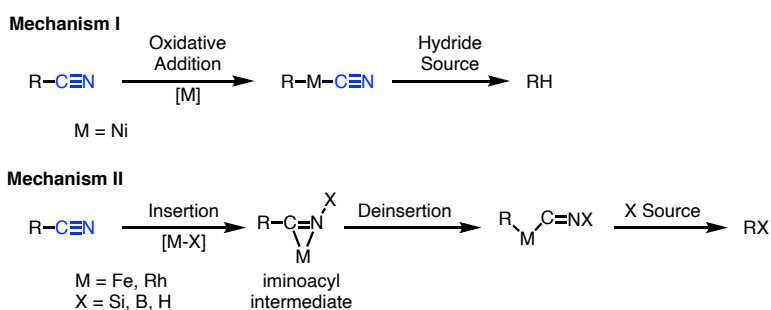


Figure 1-21 Standard pathways for transition-metal-catalyzed decyanative functionalizations.

1-21, Mechanism I). This type of mechanism proceeds with low-valent centers and is often proposed in nickel-based reductive decyanation cycles. For cross-coupling with stoichiometric reagents (e.g. boron, silanes), or nitrile-removal pathways employing other catalysts such as rhodium or iron,

mechanisms proposed often involve a 1,2-insertion, forming an iminoacyl intermediate (Figure 1-21, Mechanism II).

Although studies of transition-metal mediated mechanisms commenced with Yamamoto's work in 1982, on the cleavage of the C–CN bond in aryl and alkyl systems using stoichiometric cobalt,

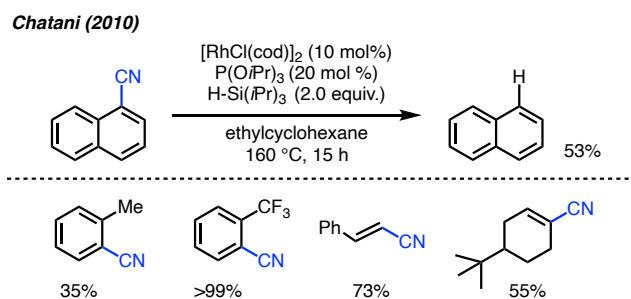


Figure 1-22 Chatani's rhodium-catalyzed reductive decyanation.

it was not until the early 2000s that catalytic methods gained traction.⁵⁷ One pertinent example developed by Chatani in 2010 was a rhodium-catalyzed reductive decyanation (Figure 1-22).⁶¹ This transformation uses an organosilane reducing agent, and was widely applied to numerous aryl-, heteroaryl- and vinyl-nitriles. High loadings of an expensive rhodium catalyst and extreme temperatures are necessary for good results, as well as being limited to simple systems and laboratory scales. Further, aromatic substrates with electron rich or neutral substituents, and non-extended pi-systems suffer from only moderate yields.

A more recent method, developed by Maiti in 2013, uses nickel, a more economical and environmentally benign metal in order to convert aryl nitriles to reduced arenes (Figure 1-23).⁶² Conversely though, this method requires the use of strong, stoichiometric quantities of pyrophoric Lewis acids like trimethylaluminum ($AlMe_3$), in stoichiometric quantities. These reagents are thought to coordinate to the nitrogen lone pairs, polarizing the C–CN bond, which aids in the oxidative addition step. These harsh additives are undesirable though, as they pose numerous safety concerns, and highly limit functional group tolerance. Maiti proposes that the silane serves as a hydride-source, using

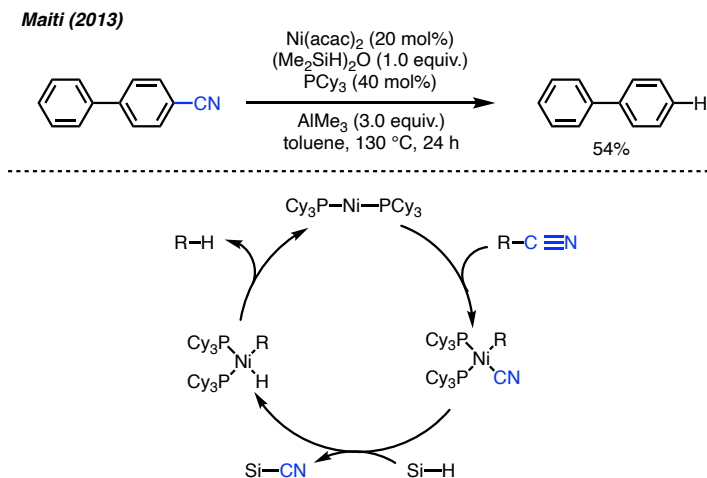


Figure 1-23 Maiti's catalytic nickel-catalyzed reductive-decyanation and proposed catalytic cycle.

deuterium labeling studies to support these claims, and proposes a catalytic cycle following the general pattern described as Mechanism I, discussed above.

Alternate methods in literature follow closely to these approaches, with most reductive decyanations employing a transition metal catalyst, ligand, Lewis acid (or other additive), and reducing agent. While the methods discussed here use silanes, other important hydride sources include hydrogen gas, borohydrides, tin-hydrides, among other reagents.⁵⁷ While these current literature examples offer access to various decyanated substrates, limitations exist. Most methods require forcing conditions, precious metals or undesirable additives, and are limited in scope.

1.5 Conclusion

The difficulties associated with remote C–H activation can be remedied by exploration of substrate conformation (via template auxiliary groups) and by use of linear directing groups like the nitrile functionality. Achieving selectivity at distal sites is attractive, and of current interest in the field. In addition, attaining regiodivergent outcomes of C–H activation, by simple changes in reaction conditions, is highly desirable. While extensive reports show end-on coordination of nitriles and their role in directing C–H functionalization, only a few have examined the π -coordination of the $\text{C}\equiv\text{N}$ bond

as a handle for directed reactivity. Further, using templates for the remote C–H functionalization by the nitrile groups requires the employment of highly specialized molecules which require cumbersome synthesis, and removal. If harnessed, the controllable, dual chelating property of organonitriles, through differentiable π - and σ -chelation, offers a powerful C–H activation strategy. Accessing the unique, multifaceted capabilities of the nitrile group, as well as potentially being able to activate the group for removal could be a promising solution to render highly functionalized motifs, devoid of unnecessary directing functionality in the final product.

1.6 References

- (1) Lyons, T. W.; Sanford, M. S. Palladium-Catalyzed Ligand-Directed C–H Functionalization Reactions. *Chem. Rev.* **2010**, *110* (2), 1147–1169. <https://doi.org/10.1021/cr900184e>.
- (2) Hartwig, J. F. Evolution of C–H Bond Functionalization from Methane to Methodology. *J. Am. Chem. Soc.* **2016**, *138* (1), 2–24. <https://doi.org/10.1021/jacs.5b08707>.
- (3) Davies, H. M. L.; Morton, D. Recent Advances in C–H Functionalization. *J. Org. Chem.* **2016**, *81* (2), 343–350. <https://doi.org/10.1021/acs.joc.5b02818>.
- (4) He, J.; Hamann, L. G.; Davies, H. M. L.; Beckwith, R. E. J. Late-Stage C–H Functionalization of Complex Alkaloids and Drug Molecules via Intermolecular Rhodium-Carbenoid Insertion. *Nat. Commun.* **2015**, *6* (1), 5943. <https://doi.org/10.1038/ncomms6943>.
- (5) White, M. C.; Zhao, J. Aliphatic C–H Oxidations for Late-Stage Functionalization. *J. Am. Chem. Soc.* **2018**. <https://doi.org/10.1021/jacs.8b05195>.
- (6) Roudesly, F.; Oble, J.; Poli, G. Metal-Catalyzed CH Activation/Functionalization: The Fundamentals. *J. Mol. Catal. Chem.* **2017**, *426*, 275–296. <https://doi.org/10.1016/j.molcata.2016.06.020>.
- (7) Jia, C.; Kitamura, T.; Fujiwara, Y. Catalytic Functionalization of Arenes and Alkanes via C–H Bond Activation. *Acc. Chem. Res.* **2001**, *34* (8), 633–639. <https://doi.org/10.1021/ar000209h>.
- (8) Yoneyama, T.; Crabtree, R. H. Pd(II) Catalyzed Acetoxylation of Arenes with Iodosyl Acetate. *J. Mol. Catal. Chem.* **1996**, *108* (1), 35–40. [https://doi.org/10.1016/1381-1169\(95\)00289-8](https://doi.org/10.1016/1381-1169(95)00289-8).
- (9) Stuart, D. R.; Fagnou, K. The Catalytic Cross-Coupling of Unactivated Arenes. *Science* **2007**, *316* (5828), 1172–1175. <https://doi.org/10.1126/science.1141956>.
- (10) Gorelsky, S. I.; Lapointe, D.; Fagnou, K. Analysis of the Concerted Metalation-Deprotonation Mechanism in Palladium-Catalyzed Direct Arylation Across a Broad Range of Aromatic Substrates. *J. Am. Chem. Soc.* **2008**, *130* (33), 10848–10849. <https://doi.org/10.1021/ja802533u>.
- (11) Gorelsky, S. I.; Lapointe, D.; Fagnou, K. Analysis of the Palladium-Catalyzed (Aromatic)C–H Bond Metalation–Deprotonation Mechanism Spanning the Entire Spectrum of Arenes. *J. Org. Chem.* **2012**, *77* (1), 658–668. <https://doi.org/10.1021/jo202342q>.
- (12) Shao, Q.; Wu, K.; Zhuang, Z.; Qian, S.; Yu, J.-Q. From Pd(OAc)₂ to Chiral Catalysts: The Discovery and Development of Bifunctional Mono-N-Protected Amino Acid Ligands for Diverse C–H Functionalization Reactions. *Acc. Chem. Res.* **2020**, *acs.accounts.9b00621*. <https://doi.org/10.1021/acs.accounts.9b00621>.
- (13) Dick, A. R.; Hull, K. L.; Sanford, M. S. A Highly Selective Catalytic Method for the Oxidative Functionalization of C–H Bonds. *J. Am. Chem. Soc.* **2004**, *126* (8), 2300–2301. <https://doi.org/10.1021/ja031543m>.
- (14) Kalyani, D.; Sanford, M. S. Regioselectivity in Palladium-Catalyzed C–H Activation/Oxygenation Reactions. *Org. Lett.* **2005**, *7* (19), 4149–4152. <https://doi.org/10.1021/ol051486x>.
- (15) Desai, L. V.; Stowers, K. J.; Sanford, M. S. Insights into Directing Group Ability in Palladium-Catalyzed C–H Bond Functionalization. *J. Am. Chem. Soc.* **2008**, *130* (40), 13285–13293. <https://doi.org/10.1021/ja8045519>.

- (16) Giri, R.; Liang, J.; Lei, J.-G.; Li, J.-J.; Wang, D.-H.; Chen, X.; Naggar, I. C.; Guo, C.; Foxman, B. M.; Yu, J.-Q. Pd-Catalyzed Stereoselective Oxidation of Methyl Groups by Inexpensive Oxidants under Mild Conditions: A Dual Role for Carboxylic Anhydrides in Catalytic C–H Bond Oxidation. *Angew. Chem. Int. Ed.* **2005**, *44* (45), 7420–7424. <https://doi.org/10.1002/anie.200502767>.
- (17) Cai, G.; Fu, Y.; Li, Y.; Wan, X.; Shi, Z. Indirect Ortho Functionalization of Substituted Toluenes through Ortho Olefination of N,N-Dimethylbenzylamines Tuned by the Acidity of Reaction Conditions. *J. Am. Chem. Soc.* **2007**, *129* (24), 7666–7673. <https://doi.org/10.1021/ja070588a>.
- (18) Chen, X.; Engle, K. M.; Wang, D.-H.; Yu, J.-Q. Palladium(II)-Catalyzed C–H Activation/C–C Cross-Coupling Reactions: Versatility and Practicality. *Angew. Chem. Int. Ed.* **2009**, *48* (28), 5094–5115. <https://doi.org/10.1002/anie.200806273>.
- (19) Leow, D.; Li, G.; Mei, T.-S.; Yu, J.-Q. Activation of Remote Meta -C–H Bonds Assisted by an End-on Template. *Nature* **2012**, *486* (7404), 518–522. <https://doi.org/10.1038/nature11158>.
- (20) Sambriago, C.; Schönbauer, D.; Blicke, R.; Dao-Huy, T.; Pototschnig, G.; Schaaf, P.; Wiesinger, T.; Zia, M. F.; Wencel-Delord, J.; Besset, T.; Maes, B. U. W.; Schnürch, M. A Comprehensive Overview of Directing Groups Applied in Metal-Catalysed C–H Functionalisation Chemistry. *Chem. Soc. Rev.* **2018**, *47* (17), 6603–6743. <https://doi.org/10.1039/C8CS00201K>.
- (21) Meng, G.; Lam, N. Y. S.; Lucas, E. L.; Saint-Denis, T. G.; Verma, P.; Chekshin, N.; Yu, J.-Q. Achieving Site-Selectivity for C–H Activation Processes Based on Distance and Geometry: A Carpenter’s Approach. *J. Am. Chem. Soc.* **2020**, *142* (24), 10571–10591. <https://doi.org/10.1021/jacs.0c04074>.
- (22) Yang, Y.-F.; Cheng, G.-J.; Liu, P.; Leow, D.; Sun, T.-Y.; Chen, P.; Zhang, X.; Yu, J.-Q.; Wu, Y.-D.; Houk, K. N. Palladium-Catalyzed *Meta* -Selective C–H Bond Activation with a Nitrile-Containing Template: Computational Study on Mechanism and Origins of Selectivity. *J. Am. Chem. Soc.* **2014**, *136* (1), 344–355. <https://doi.org/10.1021/ja410485g>.
- (23) Fang, L.; Saint-Denis, T. G.; Taylor, B. L. H.; Ahlquist, S.; Hong, K.; Liu, S.; Han, L.; Houk, K. N.; Yu, J.-Q. Experimental and Computational Development of a Conformationally Flexible Template for the Meta-C–H Functionalization of Benzoic Acids. *J. Am. Chem. Soc.* **2017**, *139* (31), 10702–10714. <https://doi.org/10.1021/jacs.7b03296>.
- (24) Cheng, G.-J.; Yang, Y.-F.; Liu, P.; Chen, P.; Sun, T.-Y.; Li, G.; Zhang, X.; Houk, K. N.; Yu, J.-Q.; Wu, Y.-D. Role of N-Acyl Amino Acid Ligands in Pd(II)-Catalyzed Remote C–H Activation of Tethered Arenes. *J. Am. Chem. Soc.* **2014**, *136* (3), 894–897. <https://doi.org/10.1021/ja411683n>.
- (25) Salazar, C. A.; Gair, J. J.; Flesch, K. N.; Guzei, I. A.; Lewis, J. C.; Stahl, S. S. Catalytic Behavior of Mono-N-Protected Amino-Acid Ligands in Ligand-Accelerated C–H Activation by Palladium(II). *Angew. Chem. Int. Ed.* *n/a* (n/a). <https://doi.org/10.1002/anie.202002484>.
- (26) Wencel-Delord, J.; Colobert, F. A Remarkable Solvent Effect of Fluorinated Alcohols on Transition Metal Catalysed C–H Functionalizations. *Org. Chem. Front.* **2016**, *3* (3), 394–400. <https://doi.org/10.1039/C5QO00398A>.
- (27) Colomer, I.; Chamberlain, A. E. R.; Haughey, M. B.; Donohoe, T. J. Hexafluoroisopropanol as a Highly Versatile Solvent. *Nat. Rev. Chem.* **2017**, *1* (11), 0088. <https://doi.org/10.1038/s41570-017-0088>.

- (28) Zhang, Z.; Tanaka, K.; Yu, J.-Q. Remote Site-Selective C–H Activation Directed by a Catalytic Bifunctional Template. *Nature* **2017**, *543* (7646), 538–542. <https://doi.org/10.1038/nature21418>.
- (29) Wan, L.; Dastbaravardeh, N.; Li, G.; Yu, J.-Q. Cross-Coupling of Remote Meta-C–H Bonds Directed by a U-Shaped Template. *J. Am. Chem. Soc.* **2013**, *135* (48), 18056–18059. <https://doi.org/10.1021/ja410760f>.
- (30) Deng, Y.; Yu, J.-Q. Remote Meta-C–H Olefination of Phenylacetic Acids Directed by a Versatile U-Shaped Template. *Angew. Chem. Int. Ed.* **2015**, *54* (3), 888–891. <https://doi.org/10.1002/anie.201409860>.
- (31) Yang, G.; Zhu, D.; Wang, P.; Tang, R.-Y.; Yu, J.-Q. Remote C–H Activation of Various N-Heterocycles Using a Single Template. *Chem. – Eur. J.* **2018**, *24* (14), 3434–3438. <https://doi.org/10.1002/chem.201800105>.
- (32) Tang, R.-Y.; Li, G.; Yu, J.-Q. Conformation-Induced Remote Meta -C–H Activation of Amines. *Nature* **2014**, *507* (7491), 215–220. <https://doi.org/10.1038/nature12963>.
- (33) Lee, S.; Lee, H.; Tan, K. L. Meta-Selective C–H Functionalization Using a Nitrile-Based Directing Group and Cleavable Si-Tether. *J. Am. Chem. Soc.* **2013**, *135* (50), 18778–18781. <https://doi.org/10.1021/ja4107034>.
- (34) Jayarajan, R.; Das, J.; Bag, S.; Chowdhury, R.; Maiti, D. Diverse Meta-C–H Functionalization of Arenes across Different Linker Lengths. *Angew. Chem.* **2018**, *130* (26), 7785–7789. <https://doi.org/10.1002/ange.201804043>.
- (35) Bera, M.; Modak, A.; Patra, T.; Maji, A.; Maiti, D. Meta-Selective Arene C–H Bond Olefination of Arylacetic Acid Using a Nitrile-Based Directing Group. *Org. Lett.* **2014**, *16* (21), 5760–5763. <https://doi.org/10.1021/ol502823c>.
- (36) Bera, M.; Maji, A.; Sahoo, S. K.; Maiti, D. Palladium(II)-Catalyzed Meta-C–H Olefination: Constructing Multisubstituted Arenes through Homo-Diolefination and Sequential Hetero-Diolefination. *Angew. Chem. Int. Ed.* **2015**, *54* (29), 8515–8519. <https://doi.org/10.1002/anie.201503112>.
- (37) Li, S.; Cai, L.; Ji, H.; Yang, L.; Li, G. Pd(II)-Catalysed Meta -C–H Functionalizations of Benzoic Acid Derivatives. *Nat. Commun.* **2016**, *7* (1), 1–8. <https://doi.org/10.1038/ncomms10443>.
- (38) Maity, S.; Hoque, E.; Dhawa, U.; Maiti, D. Palladium Catalyzed Selective Distal C–H Olefination of Biaryl Systems. *Chem. Commun.* **2016**, *52* (97), 14003–14006. <https://doi.org/10.1039/C6CC07861C>.
- (39) Li, S.; Ji, H.; Cai, L.; Li, G. Pd(II)-Catalyzed Remote Regiodivergent Ortho- and Meta-C–H Functionalizations of Phenylethylamines. *Chem. Sci.* **2015**, *6* (10), 5595–5600. <https://doi.org/10.1039/C5SC01737H>.
- (40) Modak, A.; Mondal, A.; Watile, R.; Mukherjee, S.; Maiti, D. Remote Meta C–H Bond Functionalization of 2-Phenethylsulphonic Acid and 3-Phenylpropanoic Acid Derivatives. *Chem. Commun.* **2016**, *52* (96), 13916–13919. <https://doi.org/10.1039/C6CC08302A>.
- (41) Williams, A. F.; White, A. J. P.; Spivey, A. C.; Cordier, C. J. Meta-Selective C–H Functionalisation of Aryl Boronic Acids Directed by a MIDA-Derived Boronate Ester. *Chem. Sci.* **2020**, *11* (12), 3301–3306. <https://doi.org/10.1039/D0SC00230E>.
- (42) Maji, A.; Guin, S.; Feng, S.; Dahiya, A.; Singh, V. K.; Liu, P.; Maiti, D. Experimental and Computational Exploration of Para-Selective Silylation with a Hydrogen-Bonded Template. *Angew. Chem. Int. Ed.* **2017**, *56* (47), 14903–14907. <https://doi.org/10.1002/anie.201708449>.

- (43) Xu, H.; Liu, M.; Li, L.-J.; Cao, Y.-F.; Yu, J.-Q.; Dai, H.-X. Palladium-Catalyzed Remote Meta-C–H Bond Deuteration of Arenes Using a Pyridine Template. *Org. Lett.* **2019**, *21* (12), 4887–4891. <https://doi.org/10.1021/acs.orglett.9b01784>.
- (44) Shi, H.; Lu, Y.; Weng, J.; Bay, K. L.; Chen, X.; Tanaka, K.; Verma, P.; Houk, K. N.; Yu, J.-Q. Differentiation and Functionalization of Remote C–H Bonds in Adjacent Positions. *Nat. Chem.* **2020**, *12* (4), 399–404. <https://doi.org/10.1038/s41557-020-0424-5>.
- (45) Kakiuchi, F.; Sonoda, M.; Tsujimoto, T.; Chatani, N.; Murai, S. The Ruthenium-Catalyzed Addition of C–H Bonds in Aromatic Nitriles to Olefins. *Chem. Lett.* **1999**, No. 10, 1083–1084. <https://doi.org/10.1246/cl.1999.1083>.
- (46) Gandeepan, P.; Cheng, C.-H. Allylic Carbon–Carbon Double Bond Directed Pd-Catalyzed Oxidative Ortho-Olefination of Arenes. *J. Am. Chem. Soc.* **2012**, *134* (13), 5738–5741. <https://doi.org/10.1021/ja300168m>.
- (47) Zheng, L.; Hua, R. C–H Activation and Alkyne Annulation via Automatic or Intrinsic Directing Groups: Towards High Step Economy. *Chem. Rec.* **2018**, *18* (6), 556–569. <https://doi.org/10.1002/tcr.201700024>.
- (48) Li, W.; Sun, P. Pd(OAc)₂-Catalyzed Alkoxylation of Arylnitriles via Sp² C–H Bond Activation Using Cyano as the Directing Group. *J. Org. Chem.* **2012**, *77* (18), 8362–8366. <https://doi.org/10.1021/jo301384r>.
- (49) Du, B.; Jiang, X.; Sun, P. Palladium-Catalyzed Highly Selective Ortho-Halogenation (I, Br, Cl) of Arylnitriles via Sp² C–H Bond Activation Using Cyano as Directing Group. *J. Org. Chem.* **2013**, *78* (6), 2786–2791. <https://doi.org/10.1021/jo302765g>.
- (50) Li, W.; Xu, Z.; Sun, P.; Jiang, X.; Fang, M. Synthesis of Biphenyl-2-Carbonitrile Derivatives via a Palladium-Catalyzed Sp² C–H Bond Activation Using Cyano as a Directing Group. *Org. Lett.* **2011**, *13* (6), 1286–1289. <https://doi.org/10.1021/ol103075n>.
- (51) Wan, J.-C.; Huang, J.-M.; Jhan, Y.-H.; Hsieh, J.-C. Novel Syntheses of Fluorenones via Nitrile-Directed Palladium-Catalyzed C–H and Dual C–H Bond Activation. *Org. Lett.* **2013**, *15* (11), 2742–2745. <https://doi.org/10.1021/ol401063w>.
- (52) Koseki, Y.; Kitazawa, K.; Miyake, M.; Kochi, T.; Kakiuchi, F. Ruthenium-Catalyzed Ortho C–H Arylation of Aromatic Nitriles with Arylboronates and Observation of Partial Para Arylation. *J. Org. Chem.* **2017**, *82* (13), 6503–6510. <https://doi.org/10.1021/acs.joc.6b02623>.
- (53) Chenna Reddy, M.; Jeganmohan, M. Ruthenium-Catalyzed Ortho Alkenylation of Aromatic Nitriles with Activated Alkenes via C–H Bond Activation. *Chem. Commun.* **2015**, *51* (53), 10738–10741. <https://doi.org/10.1039/C5CC03112E>.
- (54) Tamer Shoeib; Houssain El Aribi; K. W. Michael Siu, and; Hopkinson*, A. C. A Study of Silver (I) Ion–Organonitrile Complexes: Ion Structures, Binding Energies, and Substituent Effects <https://pubs.acs.org/doi/pdf/10.1021/jp002676m> (accessed Apr 22, 2020). <https://doi.org/10.1021/jp002676m>.
- (55) Zhao, W.; Montgomery, J. Functionalization of Styrenes by Copper-Catalyzed Borylation/Ortho-Cyanation and Silver-Catalyzed Annulation Processes. *Angew. Chem. Int. Ed.* **2015**, *54* (43), 12683–12686. <https://doi.org/10.1002/anie.201507303>.
- (56) Zhao, W.; Montgomery, J. Cascade Copper-Catalyzed 1,2,3-Trifunctionalization of Terminal Allenes. *J. Am. Chem. Soc.* **2016**, *138* (31), 9763–9766. <https://doi.org/10.1021/jacs.6b05216>.

- (57) Mattalia, J.-M. R. The Reductive Decyanation Reaction: An Overview and Recent Developments. *Beilstein J. Org. Chem.* **2017**, *13* (1), 267–284. <https://doi.org/10.3762/bjoc.13.30>.
- (58) Modak, A.; Maiti, D. Metal Catalyzed Defunctionalization Reactions. *Org. Biomol. Chem.* **2015**, *14* (1), 21–35. <https://doi.org/10.1039/C5OB01949D>.
- (59) Tobisu, M.; Kinuta, H.; Kita, Y.; Rémond, E.; Chatani, N. Rhodium(I)-Catalyzed Borylation of Nitriles through the Cleavage of Carbon–Cyano Bonds. *J. Am. Chem. Soc.* **2012**, *134* (1), 115–118. <https://doi.org/10.1021/ja2095975>.
- (60) Tobisu, M.; Kita, Y.; Chatani, N. Rh(I)-Catalyzed Silylation of Aryl and Alkenyl Cyanides Involving the Cleavage of C–C and Si–Si Bonds. *J. Am. Chem. Soc.* **2006**, *128* (25), 8152–8153. <https://doi.org/10.1021/ja062745w>.
- (61) Kita, Y.; Tobisu, M.; Chatani, N. Rhodium-Catalyzed Carbon-Cyano Bond Cleavage Reactions Using Organosilicon Reagents. *J. Synth. Org. Chem. Jpn.* **2010**, *68* (11), 1112–1122. <https://doi.org/10.5059/yukigoseikyokaishi.68.1112>.
- (62) Patra, T.; Agasti, S.; Akanksha; Maiti, D. Nickel-Catalyzed Decyanation of Inert Carbon–Cyano Bonds. *Chem. Commun.* **2012**, *49* (1), 69–71. <https://doi.org/10.1039/C2CC36883H>.

Chapter 2

Development of Methods for Nitrile-Directed C–H Functionalization and Reductive Decyanation

2.1 Motivation and Project Goals

The nitrile group is a highly versatile functional group. Its role in a variety of remote directed C–H oxidation transformations, through σ -chelation, as well as its ability to engage in π -coordination for proximal functionalization, makes this motif a potential tool for differentiated, regioselective C–H activation. Further, while both binding modes are known, examples of non-auxiliary based nitrile-directed distal transformations (via σ -coordination), as well as improved access to a proximal or π -directed reactions, are rare. Finally, divergent, selective C–H activation for functionalization of multiple sites within a complex molecule, is an appealing, yet understudied area in the literature.

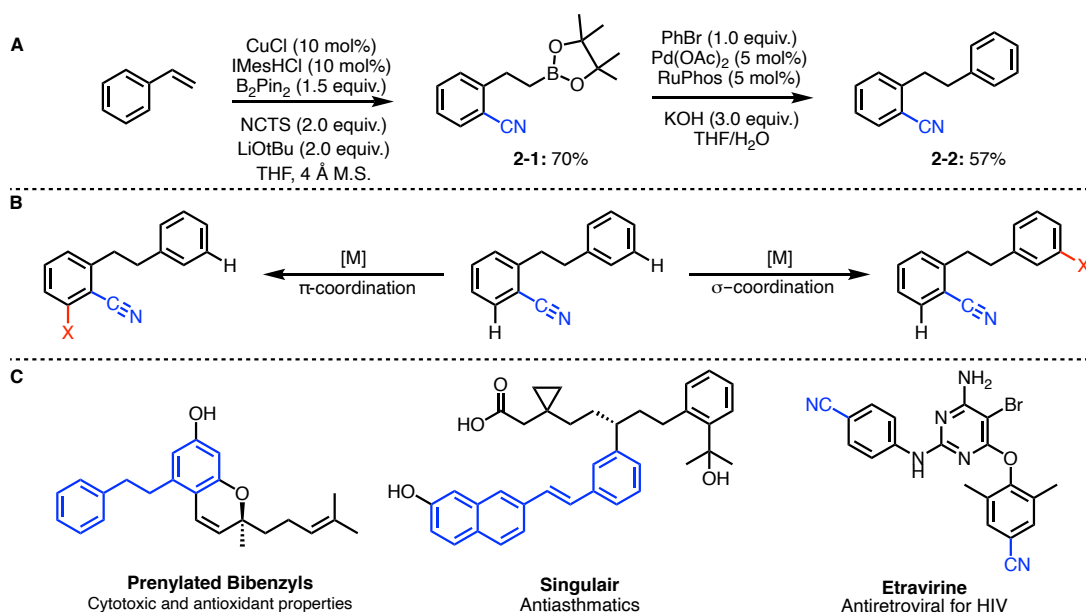


Figure 2-1 Model substrate synthesis, project goals, and biological relevance.

In 2015, the Montgomery group developed a one-pot multicomponent, copper-catalyzed protocol for borylation/*ortho*-cyanation of styrene derivatives.¹ Due to its ability to rapidly construct benzonitriles, we envisioned this strategy could be employed to develop a general method for nitrile-directed C–H activation (Figure 2-1A). We believed that this biaryl ethane substrate **2-2** would provide an excellent system to examine both the σ - and π -coordinating capability of the nitrile to functionalize distal and proximal C–H bonds, respectively (Figure 2-1B). This scaffold is not only reminiscent of natural products, and pharmaceuticals currently on the market, but the nitrile functionality is present in a number of biologically relevant motifs (Figure 2-1C).² Further, the nitrile can be converted into a number of other useful functional groups via standard organic transformations, or engaged in transition metal catalysis to provide more complex conversions.

We hypothesized that this would be an ideal system to examine the directing capabilities of the nitrile group in the late-stage functionalization of un-activated arenes, as there are multiple C–H bonds in similar steric and electronic environments. This model substrate **2-2** would also allow us to explore the factors that control nitrile-directed distal and proximal functionalization of arenes, and demonstrate remote functionalization with an *innate* directing group, as opposed to installing one prior. We envisioned that guiding σ - or π -chelation could be achieved through catalyst control, and careful examination of factors known to improve regioselectivity for each coordination mode. Ultimately, this project aims to develop a widely applicable, operationally simple methodology, to afford divergent reactivity in the late-stage functionalization of arene C–H bonds in the context of medicinally relevant biaryl ethane scaffolds. Following this strategy with a reductive decyanation would offer access to highly functionalized aromatic motifs in a traceless fashion

2.2 Development of a Distal Nitrile-Directed C–H Acetoxylation

2.2.1 Optimization Studies

While directed C–H functionalization transformations, specifically palladium-catalyzed processes, are efficient and expansive in scope, there is a void in the literature of remote C–H activation for late-stage functionalization.^{3–6} While the use of large templates and biased scaffolds is undesirable, this type of reactivity, notably that of within nitriles, found throughout the literature, reveals the viability of directing oxidation to isolated C–H bonds.^{6,7} Utilizing the nitrile functionality as a scaffold for directing remote C–H activation is not only feasible, but synthetically practical.

Based on previous work by Yu,⁶ we hypothesized that the σ -coordinating ability of the nitrile could be leveraged to facilitate regioselective distal acetoxylation. Employing conditions inspired by the template-directed methodology,⁷ model substrate **2-2** was assessed in the system. This proof-of-concept study provided product **2-3**, derived from selective *meta*-C–H acetoxylation of the pendant arene, isolated from a large mixture of additional unidentified products (Figure 2-2).

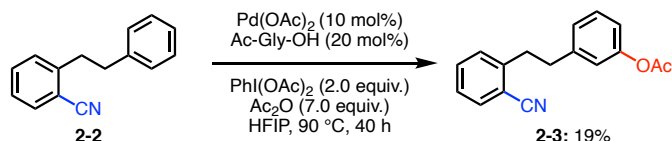


Figure 2-2 Lead result for distal *meta*-C–H acetoxylation.

Isolation of *meta*-acetoxyated compound **2-3** demonstrated that the nitrile is functioning as a directing group, allowing for selective oxidation of a single aromatic C–H bond among otherwise similar C(sp²)-H bonds, without a rigid, pre-synthesized template, but rather through use of an innate directing group. Extensive NMR characterization, as well as comparison with an authentic standard, confirmed the regioselectivity and allowed for streamlined reaction analysis.

To improve, and further study this unique transformation, we began to draw inspiration from mono-protected amino acid (MPAA) promoted selective C–H functionalization,^{6,7} and examine the role of additives in our system.^{8,9} Initial challenges associated with separation of regioisomers

prompted us to synthesize authentic standards for the distal *meta*-, *para*-, and *ortho*-acetoxyated products, and generate a calibration curve to determine the yield and regioisomeric ratio for a given reaction. This strategy allowed for ease of screening, and gave us insight into the highest yielding and

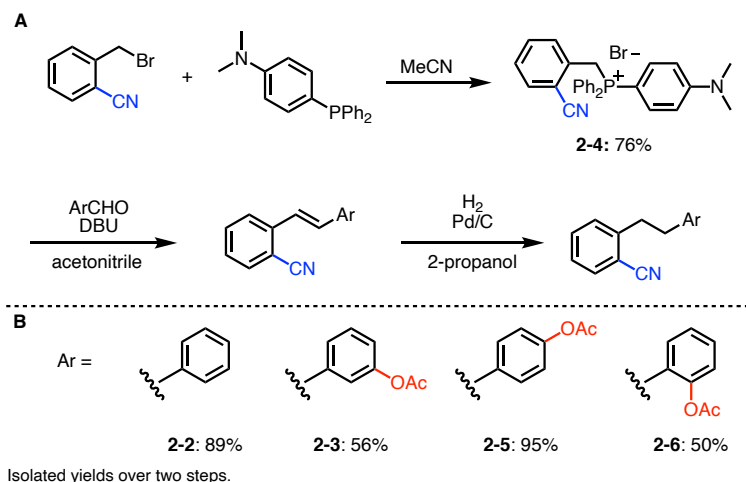


Figure 2-3 Regioisomer authentic standard synthesis.

most selective conditions for the newly developed method. The authentic standards were synthesized via Wittig-reaction¹⁰ between pre-synthesized **2-4** and benzaldehyde, followed by hydrogenation (Figure 2-3). This synthetic procedure was used for several biaryl motif substrates, as well (see Chapter 6).

With this lead result and analytical strategy in hand for determining product distributions, studies to improve the yield and selectivity of this transformation began. Preliminary work towards

Entry	Temperature (°C)	Yield (%)
1	70	40
2	80	22
3	90	19 ^{a,b}
4	90	23 ^{a,c}
5	90	51
6	100	21
7	110	38

GCFID yields based on internal standard tridecane. ^aIsolated yields. ^bReaction stirred for 40 hours. ^cReaction stirred for 48 hours.

Table 2-1 Temperature and time screen for distal *meta* C–H acetoxylation.

optimization of the transformation produced shorter reaction times with no loss in yield (Table 2-1, entries 3-4). This is likely due to over-oxidation with extended experiment duration. A temperature screen was also conducted to see if heating, or lowering the temperature of the reaction, could improve reaction conversion. After screening a small range, it was shown that 90 °C remained ideal (Table 2-1).

Surveying various oxidants for the palladium-catalyzed acetoxylation revealed that the hypervalent iodine reagents screened yielded more product **2-3** than did AgOAc, K₂S₂O₈ and Selectfluor (Table 2-2, entries 2-5). Consistent with Yu's work, the optimal choice appeared to be PhI(OAc)₂ (Table 2-2, entry 1). It was found that increasing PhI(OAc)₂ loading from 2.0 to 3.0 equivalents afforded higher yields, while further increasing oxidant to 4.0 equivalents, appeared to be detrimental to reaction yields (Table 2-2, entries 6-7).

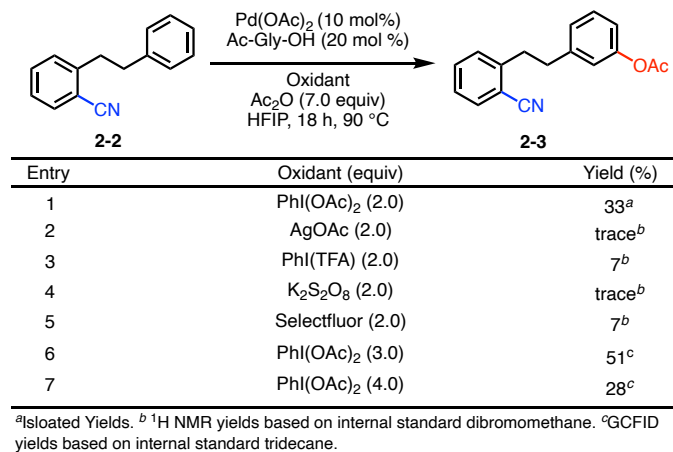


Table 2-2 Oxidant screen for distal *meta* C–H acetoxylation.

With moderate yields of the distal *meta* C–H acetoxylation, we hoped to study the important selectivity factors examined in other nitrile-directed remote C–H functionalizations, specifically the role of mono-protected amino acid (MPAA) ligands, and silver additives (for a more detailed discussion on these effects, see Chapter 1).¹¹ First, when the reaction was run in absence of the N-acyl amino acid ligand, yields were diminished to 48% *meta* product (Table 2-3, entry 1). This data may indicate the need for

higher levels of active catalyst in solution. Interesting, though, while increased loading of palladium acetate boosted yields significantly, an analogous increase in Ac-Gly-OH equivalents did not help product formation, but rather slightly decreased yields. Because of the need to access a specific ligated palladium-species to form the desired macrocyclic transition state, the system might be particularly

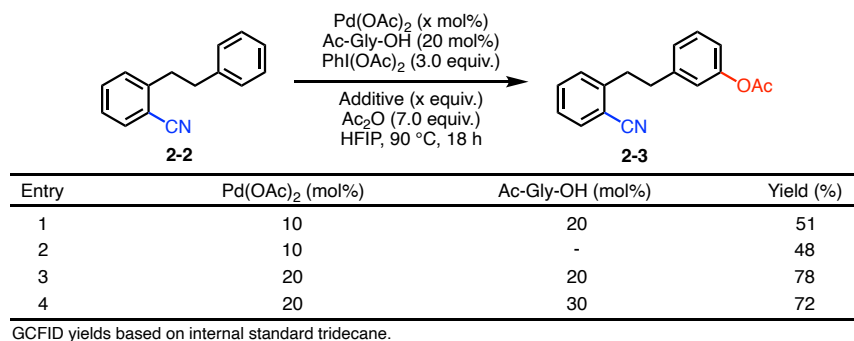


Table 2-3 Palladium and ligand screen for distal *meta* C–H acetoxylation.

sensitive to the ratio of palladium to ligand (1:1 in this case). As demonstrated by Yu and Houk, the conformational bias induced by these ligands, and their assistance in the C–H activation step, is necessary to ensure formation of the desired ligand-stabilized palladacycle, and thus product in good yield, and selectivity. Furthermore, too much ligand may lead to unproductive, over-ligated palladium; as Stahl showed, only minimal amounts of ligand is necessary impart the unique properties of this MPAA class of ligands to a catalytic system.¹²

While desired product is formed without additives, this may allude to results demonstrated by Yu and Houk that a dimeric palladium species may allow for the correct catalyst system to access remote *meta* C–H bonds.^{9,8} Thus the large, flexible palladacycle conformation likely formed when acetoxyating substrate **2-2** is sufficient to achieve selectivity without external ligands or metal salts, but to acquire the best yields and selectivity, a variety of additives were examined. As discussed in Chapter 1, it has been shown that Lewis acids may lower the ring strain and energy barrier for formation of the necessary nitrile σ -coordinated macrocyclic transition state.^{8,9} Silver salts were first

examined due to their ability to form hetero-bimetallic species that are poised for highly regioselective C–H functionalization.

Although the yield of this transformation was synthetically useful, we hoped to increase the selectivity to greater than 3 : 1 *meta* to *para* remote acetoxylation (Table 2-4, entry 1). As expected, selectivity benefited from the inclusion of silver acetate (AgOAc), but unfortunately, yield dropped (entry 2). We were able to lower loadings of the AgOAc to 1.0 equivalents, and regain good yield and selectivity, but substoichiometric loading eroded these results (entries 3-5). Ultimately, silver trifluoroacetate (AgTFA) proved beneficial to the reaction and could be used in substoichiometric amounts to give good yield (77%) and high selectivity of 15:2:1, *meta* : *para*: *ortho* (entry 6). As controls, various Lewis acids, and other additives with the acetate counterion were examined, but proved either unhelpful in yield or selectivity (entries 7-10). Molecular sieves were included in the

Entry	Additive (equiv.)	Yield (%) ^a	Ratio <i>m</i> : <i>p</i> : <i>o</i>
1	-	78	12: 4: 1
2	AgOAc (3.0)	29	20: 1: 4
3	AgOAc (2.0)	36	11: 1: 1
4	AgOAc (1.0)	70	10: 1: 1
5	AgOAc (0.2)	55	7: 1: 1
6	AgTFA (0.2)	77 (74^b)	15: 2: 1
7	KH ₂ PO ₄ (1.0)	74	15: 5: 1
8	NaH ₂ PO ₄ · H ₂ O (1.0)	34	20: 8: 1
9	KOAc (1.0)	15	8: 3: 1
10	NaOAc (1.0)	13	7: 1: 1
11	4 Å M.S.	55	18: 4: 1
12	-	70 ^c	10: 1: 1

GCFID yields based on internal standard tridecane. Reactions in 2.0 mL HFIP. ^aYield of *meta* product. ^b1.0 mmol scale reaction: Isolated yield as a mixture of acetoxylation products 2.0 :1.0 ratio *meta*: minor regioisomer. ^cReaction carried out with 10.0 equiv. Ac₂O.

Table 2-4 Additive screen for distal *meta* C–H acetoxylation.

reaction mixture to see if potentially moisture was prohibiting product formation, or deprotecting the desired acetate product, but yields and selectivity remained only modest (entry 11). Adding more acetic anhydride (Ac₂O), thus increasing the concentrations of acetate in solution, was essentially

inconsequential (entry 12). An extensive screen of modified norbornene was also carried out to potentially employ divergent, Catellani-type selectively changes,¹³ but no significant impact on

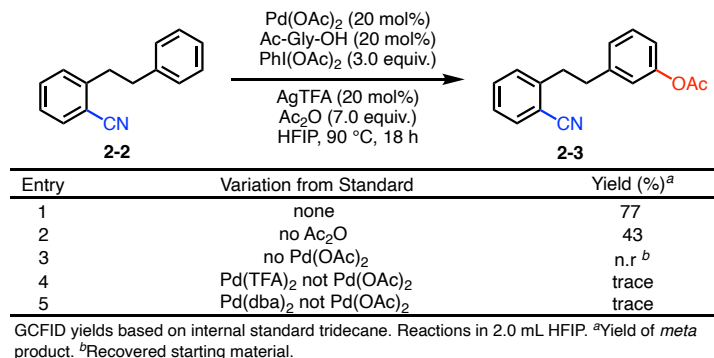


Table 2-5 Select control screens for distal *meta* C–H acetoxylation.

regiochemistry or yield was observed (see Chapter 6.2.2.1). Finally, control reactions with the finalized conditions solidified the need for a palladium catalyst (and the correct palladium precursor), and the acetic anhydride in the C–H acetoxylation (Table 2-5, entries 1-5).

In addition to testing the concentration of these transformations (Table 2-6, entries 1-2), the identity of the solvent was briefly studied as well (entries 3-5). The polar-protic solvent, hexafluoroisopropanol (HFIP), and other fluorinated solvents, are well established as essential for template-based C–H activation transformations.¹⁴ This is believed to be due to the ability of these bulky, highly electron-withdrawing alcohols to engage in robust hydrogen-bonding, and subsequently stabilize macrocyclic transition states, analogous to those which we propose. Employing HFIP was uniquely ideal for selectivity and yield (entry 1). Similar alcohols, such as isopropanol performed

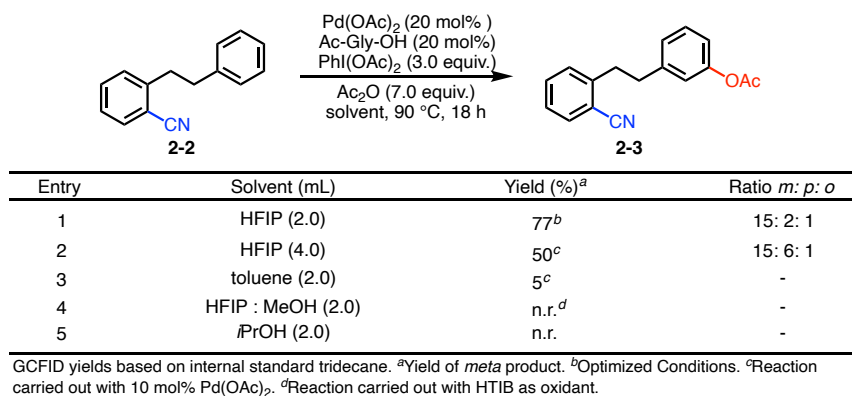
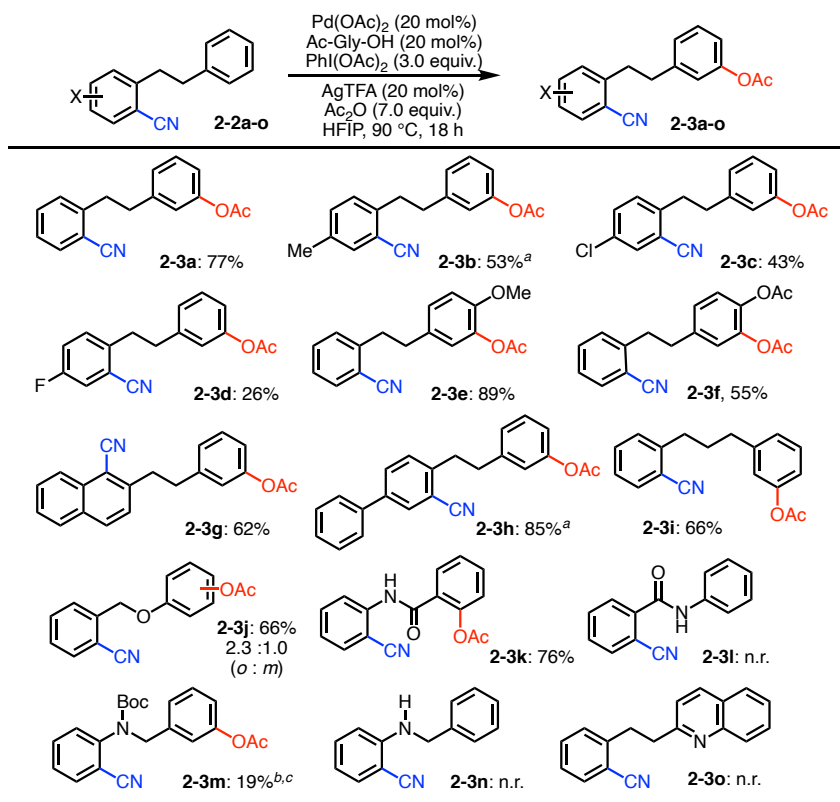


Table 2-6 Brief solvent screen for distal *meta* C–H acetoxylation.

poorly and switching to non-polar solvents, with no hydrogen bonding ability, appeared to also shut down the reaction (entry 5). Although its complete role is not fully understood. HFIP may favorably coordinate with the transition metal catalyst, and help stabilize the large, entropically disfavored, cyclophane-like intermediates in the template-based systems.

The optimization of this distal nitrile-directed, *meta*-selective C–H acetoxylation demonstrated not only the unique properties of a nitrile as a directing group, but its potential as an innate source of selectivity in aromatic motifs, without the need for an external template. Further, the exploration of various selectivity factors offered high yield and selectivity, reiterating the unique role of the nitrile's weak σ -chelation.

2.3 Substrate Scope for the Distal Nitrile-Directed C–H Acetoxylation



Isolated yields of *meta*-product. ^aProduct isolated as a mixture of 2.0 : 1.0 *meta* : minor regioisomer. ^bProduct Boc-deprotected during reaction. ^cIsolated as a mixture of 2.3 : 1.0 *meta* : minor regioisomer.

Table 2-7 Substrate scope of nitrile-directed *meta* C–H acetoxylation.

With optimized conditions in hand, this remote acetoxylation transformation was applied to a variety of different biaryl ethanes (Table 2-7). Selective distal *meta*-C–H acetoxylation was observed for neutral substrates with multiple functionalizable C(sp²)–H bonds (**2-3a**), as well as those bearing electron-withdrawing and electron-donating substituents on both the distal and proximal aromatic rings (**2-3b-f**). Changing the electronics on the proximal, nitrile-containing ring may have caused a change in the directing/metal coordination properties of the nitrile for substrates **2-3b-d**, and thus may have led to a lower yield. This trend was much more pronounced for a highly electron-withdrawing substituent like fluorine (**2-3d**). Further, while only moderate yields were observed for *para*-acetylated substrate **2-3f**, which could potentially be due to the sterics of the large ester, a higher yield was observed for the *para*-methoxy substrate **2-3e**, could be potentially due to this smaller group's blocking of the position that is next major isomer (*para*-acetoxylation) typically observed in this transformation. Other extended pi-systems such as naphthyl and biphenyl moieties performed well in this selective system (**2-3g** and **2-3h**). This observation showcased the method's high selectivity in large aromatic motifs. Furthermore, we were able to extend the length of the carbon chain between the arenes (**2-3i**) and maintain good yield and *meta*-selectivity. Several substrates with heteroatoms in the linker were also compatible in the reaction. Both the ether-type substrate (**2-3j**), and the amide-type substrate (**2-3k**) gave *ortho*-selectivity, with the complete switch in selectivity for **2-3k** likely resulting from the directing effects associated with carbonyl oxygen moieties. In order to elucidate these adverse directing effects, and potentially change selectivity, **2-3l** was synthesized, but no desired acetoxylation was observed, only starting material and decomposition products. Potentially, palladium coordination to the nitrile is favored, but the additional directing moiety, and increased rigidity of the amine-linker in **2-3k** changes the ultimate selectivity of the transformation (as no reactivity is observed with **2-3l**). Finally, a protected amine could be used in this reaction to give *meta*-acetoxylation, albeit in low yield

(**2-3m**). This reaffirmed our hypothesis in the directing affects attributed to the carbonyl in **2-3k**. An unprotected alkyl-amine (**2-3n**) was also examined, but gave only recovered starting material, and substrate decomposition. Finally, a quinolone substrate remained unreactive in our system (**2-3o**), likely due to the role of quinoline as a directing group in palladium catalysis. Overall, these substrates showcase the nitrile's unique capability in directing acetoxylation in a variety of systems. The ability to include heteroatoms in the linker, and to increase linker length expands this chemistry to a broad array of substrates.

2.3.1 Additional Studies and Discussion Regarding Substrate Scope

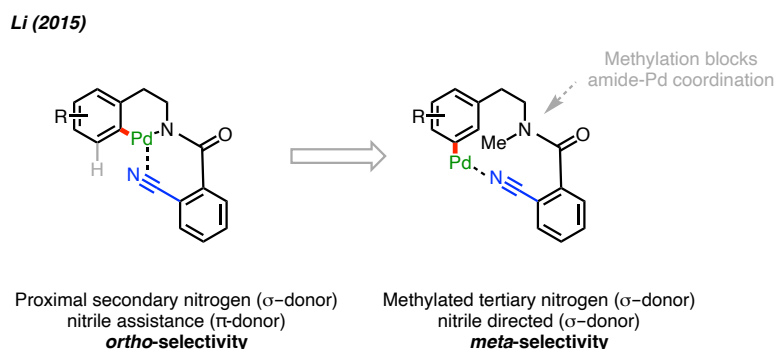


Figure 2-4 Regioselective olefination at *ortho* position due to secondary directing effect of proximal nitrogen.

Although the selectivity of the distal *meta*-C–H acetoxylation is consistent over a variety of substrates, certain outliers offered interesting insight into the interesting regiochemistry of nitrile directed reactions. First, the change in acetoxylation selectivity for **2-3k** is rationalized by looking at analogous reactivity in the template C–H activation literature (Figure 2-4).^{15,16} When coordinative functionality is proximal to the arene undergoing functionalization, a deviation from the typical selectivity can be expected. The Li group found that anilines within the template linker can intercept the catalyst, and act as a directing group for functionalization of the adjacent *ortho* C–H bond.¹⁵ It is thought that the nitrile engages in remote π -coordinative assistance to give this specific regiochemistry.

The change in regioselectivity for **2-3j** was more perplexing. The ratio of acetoxylation acquired in this case is 2.3:1.0 (*ortho*:*meta*), whereas the standard acetoxylation conditions give a ratio of 15: 2: 1 (*meta*:*para*:*ortho*) on the model biaryl. This regiochemistry is different from that observed in all other substrates. Not only is major (and minor) regioisomer not consistent, but the mixture also does not correspond to typical selectivity for electronically governed oxidations (i.e. *ortho* and *para* for an aryl-ether). To help tease out the factors accounting for this regioselectivity changes, a variety of control reactions were carried out (Figure 2-5). First, when the metal catalyst/additives are removed from reaction, the acetoxylation does not proceed, and the oxidation resulting from the background

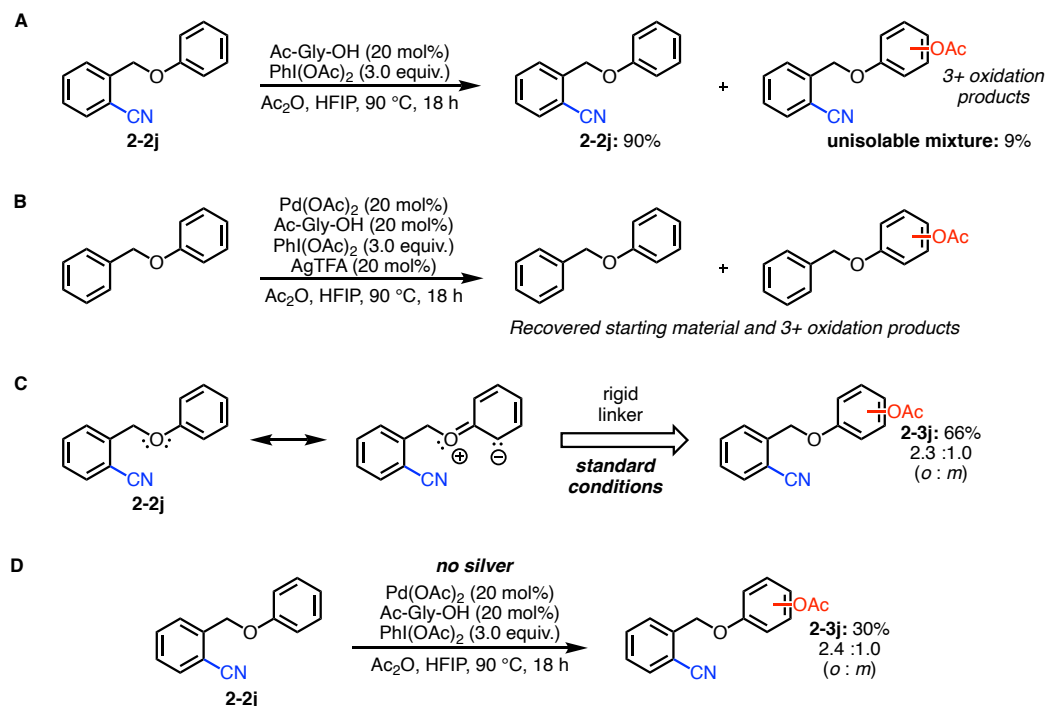


Figure 2-5 Control reactions for ether substrate **2-3j**.

reactivity gives no selectivity (Figure 2-5A). Next, when the nitrile is removed from the system, a large mixture of starting material and multiple oxidation products are observed by GCMS (Figure 2-5B). These two reactions imply that the reaction is nitrile-directed, and palladium-catalyzed. Likely, the change in selectivity for substrate **2-2j** results from the enhanced rigidity and diminished length of the

linker, as compared to the all carbon model system (**2-3a**)(Figure 2-5C). This diminished flexibility, and likely change in directionality of the coordinating functionality is reminiscent of the works by Yu, Houk, and others, which found that the flexibility of the template (or lack thereof), and resulting

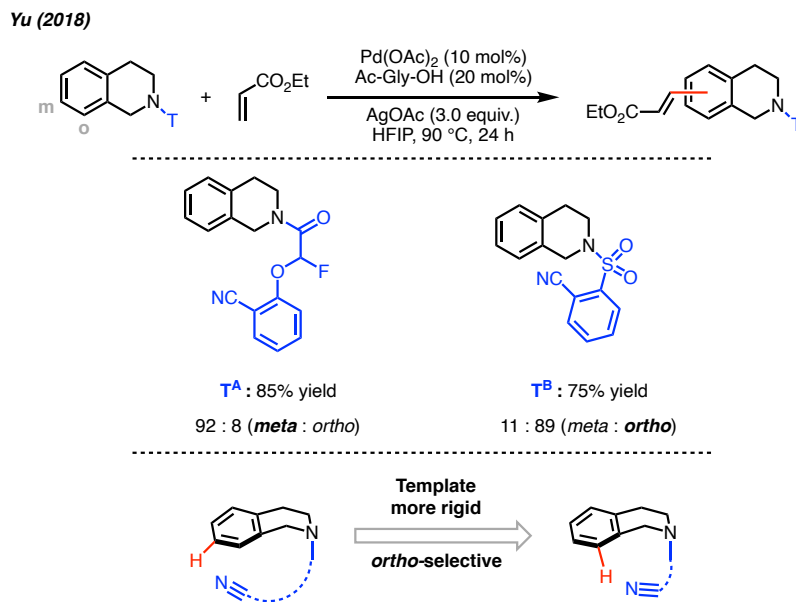


Figure 2-6 Effect of conformational rigidity of a template on C–H activation selectivity.

distortion energies, govern the stability of macrocyclic transition state, and thus selectivity of the reaction (Figure 2-6, also see Chapter 1.3.1).^{6,8,9,16,17} Finally, when the reaction is carried out without AgTFA, the same ratio of regioisomers, but much lower yield is obtained (Figure 2-5D). The silver additive is clearly required for high yields (and selectivity in more flexible systems), but confirmation

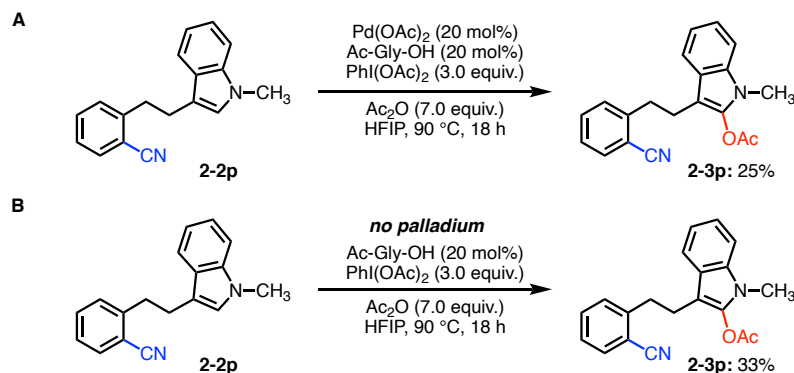


Figure 2-7 Indole substrate **2-2p** acetoxylation by palladium-catalyzed (**A**) and metal-free (**B**) methods.

strain induced with the **2-2j** linker still prevents acetoxylation of more distal (*meta* and *para*) bonds in the molecule.

Although the selectivity discussions are informative and scope of the acetoxylation transformation are quite wide, synthetic challenges regarding substrate preparation was a challenging aspect of this project.

Attempting to demonstrate our method on a heterocyclic substrate, methyl-protected indole **2-3p** was synthesized. While product was obtained under our acetoxylation conditions (Figure 2-7A), recent work detailing the hypervalent iodine-mediated, regioselective acetoxylation of indoles¹⁸ inspired us to examine the corresponding control reaction. As expected acetoxylation under these metal-free conditions could be achieved in slightly elevated yields, thus demonstrating our initial reactivity was likely not due to a palladium-catalyzed process (Figure 2-7B).

For several of our substrates, the previously developed cyanoborylation reaction was employed to rapidly assemble our biphenyl ethane substrates.¹ In addition to synthesis of the NCTS and IMesCuCl for the cyanoborylation procedure, the synthetic route for many substrates was challenging. The lengthy synthesis and challenging isolation of the desired cyanoborylation product (including the correct regioisomer) made expansion of the scope difficult. For example, many substrates required synthesis of the vinyl arene, as these materials are not commercially available, and the challenging Csp²–Csp³ Suzuki cross coupling¹⁹ is a non-trivial reaction, as seen not only by experience but across the literature. In some cases, the pinacol ester was converted to BF₃K salt. Once in hand, the very small isolated starting material meant the small scale of the acetoxylation reaction was challenging to purify, and characterize. As a representative example of the challenges associated with these heteroaromatic substrates, the multiple step sequence to access the carbazole substrate is shown (Figure 2-8). Because of the multiple steps with low yield, and multiple purifications necessary to obtain the correct regioisomers, little material was available to subject to the C–H activation conditions. While the major observed products appeared to be resulting from decomposition, a mass of unprotected carbazole with

acetate was observed by GCMS. Further, a mixture was isolated which indicated functionalization on the distal ring, but impurities and little material made further analysis futile. Ultimately, these obstacles lead us to the move toward synthesizing substrates **2-3j-o**, for scaffolds with extended and heteroatom-based linkers between the distal and proximal arenes. This served as alternative way to showcase the

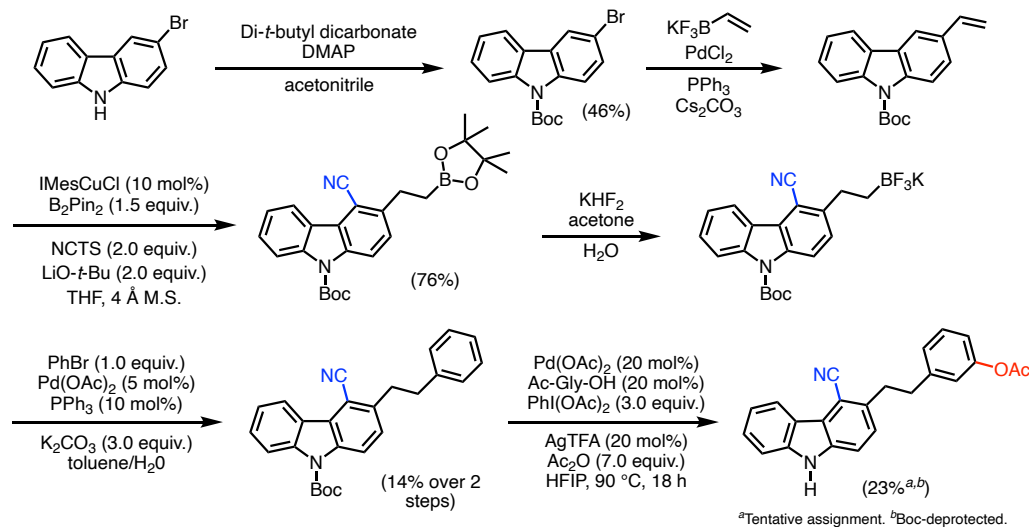


Figure 2-8 Representative heterocyclic substrate synthesis.

generality of our acetoxylation method. A variety of organic transformations which currently exist could be leveraged to provide substrates of interest for our investigation, including various oxidations, Wittig protocols, and other robust reactions (see Chapter 6.2.2).

Overall, we demonstrated our method to be viable across a range of biaryl motifs, tolerating a range of functionality, and offering interesting examples of selectivity paradigms important in the field of distal, nitrile-directed C–H functionalization.

2.4 Development of a Distal Nitrile-Directed C–H Pivalation

Intrigued by the unique *meta* selectivity of the distal nitrile-directed C–H acetoxylation, we hoped to expand this method to other remote C–H oxidative functionalization. In attempt to achieve a selective pivalation at this position, we applied conditions analogous to that of the acetoxylation, yet

switched the identity of the hypervalent iodine reagent to $\text{PhI}(\text{OPiv})_2$. No anhydride was included in the reaction mixture initially. Excitingly, in this first attempt towards installation of a pivalate ester to the distal ring we were able to achieve 28% isolated yield of the desired product (Table 2-8, entry 1).

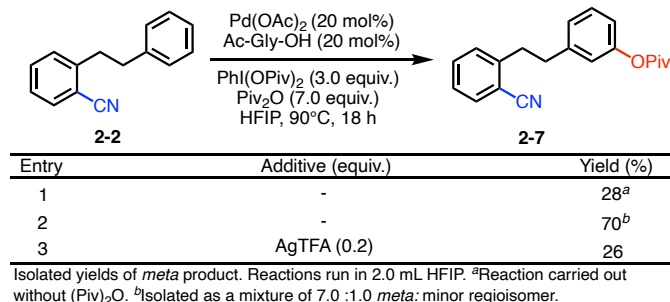


Table 2-8 Optimization of nitrile-directed distal *meta* C–H pivalation.

Further, simply switching the identity of the anhydride, we were able to achieve selective distal *meta*-C–H pivalation in 70% yield (entry 2). To our knowledge there is no other method for a remote *meta* nitrile-directed C–H pivalation. A very brief examination of additives in this transformation demonstrated a difference between this method and that of the acetoxylation, as substoichiometric silver did not afford higher yield or selectivity (entry 3). This may potentially be due to the steric bulk of the pivalate moiety being enough to increase size, and minimize ring strain of the macrocyclic transition state. The Pd/Ag heterodimeric metallacycle may thus be unnecessary in this case, but rather the mechanism might rely on a dimeric palladium macrocycle, which was also shown by Yu and Houk to give selective functionalization, even in the acetoxylation case (see Chapter 1). This high selectivity for the remote ring was also demonstrated when our method was applied to a naphthalene substrate (Figure 2-9).

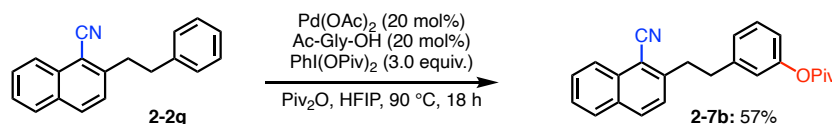


Figure 2-9 Nitrile-directed distal *meta* C–H pivalation of substrate **2-2g**.

Installation of a pivalate not only increases the scope of this reaction, but the utility of the pivalate is unique as it not only resists deprotection often observed with acetoxy groups,²⁰ and furthermore it can serve as functional handle for C–O activation strategies pioneered by the Montgomery group,^{21,22} and many others. Specifically, we hoped to engage our pivalic ester in Chatani’s C–O amination.²³ Using these known strategies, we were thus able to install a morpholine moiety at this meta position which was accessed through our new C–H activation protocol. We were

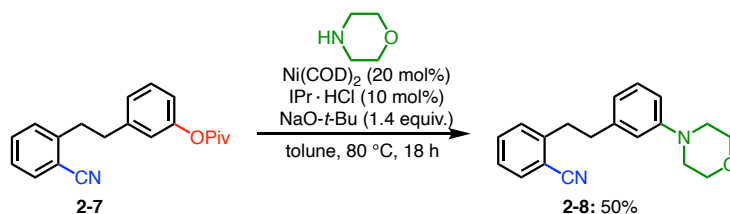


Figure 2-10 Optimized C–O amination of distal pivalation product.

pleased to see that minimal optimization was required to achieve good yield of the functionalized product **2-8** (Figure, 2-10 see Chapter 6.2.2.3 for optimization).

Overall, the distal *meta* C–H bond selectivity is a unique feature of the nitrile directed palladium catalysis. Furthermore, the installation of a robust pivalate group allows for further functionalization through C–O bond activation, with the C–CN bond left intact for subsequent catalysis, if desired.

2.5 Control Studies for the Distal Nitrile-Directed C–H Activation

Various control studies were carried out to assess the nitrile’s role in directing these remote C–H oxidations. Specifically, we wanted to evaluate whether the *meta* acetoxylation selectivity is due to nitrile coordination to palladium. First, a bibenzyl **2-9**, without the nitrile, was subjected to the standard acetoxylation conditions (Figure 2-11A). After analysis by GCMS and GC-FID, a statistical mixture of regioisomers was observed. Further, the specific macrocycle transition state size was probed. When a *para*- nitrile substrate **2-10** was engaged in the C–H acetoxylation conditions,

again, non-selective distribution of regioisomers was observed (Figure 2-11B). Experiment B demonstrated that it is not simply electronics of the benzonitrile substrate playing a role in the outcome of the acetoxylation, but as initially proposed, the specific metal coordination to the nitrile leading to reaction selectivity. These results reinforced the palladium directing-role of nitrile; not only is the position of nitrile (*ortho*-to the linker) important to the selectivity of the reaction, but also the nitrile's presence in the molecule at all, as a statistical mixture of oxidation is achieved otherwise.

Additional control experiments were carried out to better understand the importance of the

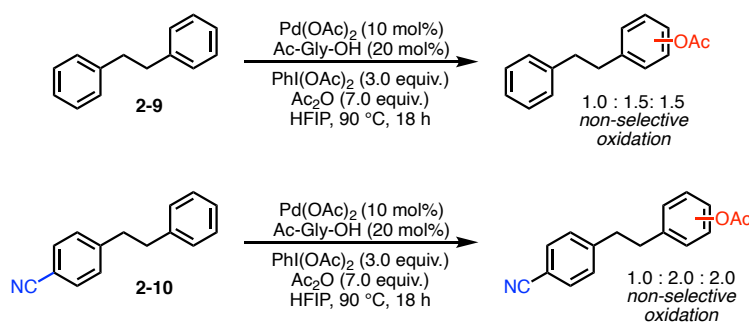


Figure 2-11 Control studies for distal nitrile-directed transformations.

anhydride in the acetoxylation and pivalation methods (Figure 2-12). Inclusion of acetic anhydride was vital to high yield in acetoxylation optimization, but we saw especially significant yield improvements (28% to 70%) with addition of pivalic anhydride in the pivalation transformation. We wondered what the necessity and specific role of these anhydride reagents was in the C–H activation mechanisms, and whether the particular anhydride structure (acetate or pivalate) was important for the functional group installed. In order to probe this, an experiment was set up to see if the specific anhydride employed affected yield and/or oxidation identity of the product. All conditions were kept constant, except the identity of the anhydride flipped: pivalic anhydride was used the acetoxylation and acetic anhydride in the pivalation.

When analyzed by GCMS and GC-FID, it was revealed that the identity of the major oxidation product depends on the anhydride added to the reaction, regardless of the oxidant used.

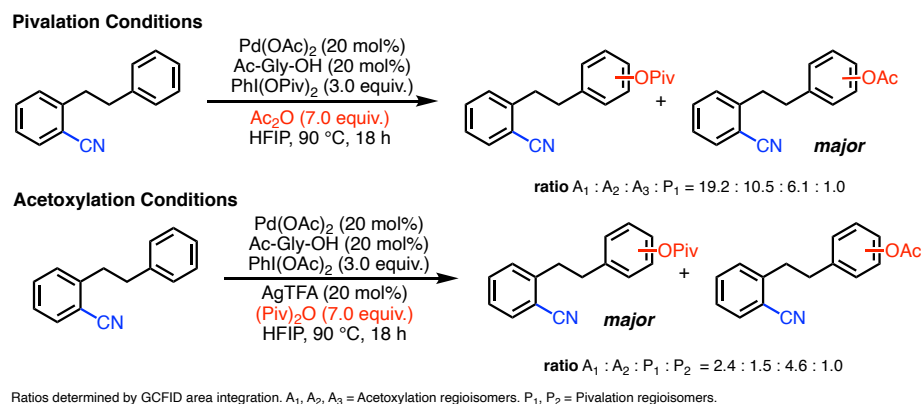


Figure 2-12 Experiments to probe the role of the anhydride in distal nitrile-directed C–H functionalization.

The competition experiment demonstrated that not only is the anhydride necessary for good yield for both pivalation and acetoxylation, but the specific anhydride is the ultimate source of the installed group. We believe it is likely that the anhydride engages in some sort of ligand exchange on the metal, or on the hypervalent iodine, which would result in the correctly oxidized palladium species to give the desired ester identity for the C–H functionalization.²⁴ Finally, with the importance of the anhydride shown to be key in the nitrile-directed C–H functionalization, a brief examination of other anhydrides was carried out, but no other anhydrides had a notable impact on reaction identity or conversion (see Chapter 6.2.2.2).

Overall, these control experiments confirm the necessity of the nitrile in the molecule and its position on the arene to direct selective distal *meta* C–H functionalization, and emphasize the importance of the anhydride to allow for desired oxidation product.

2.5.1 Mechanistic Hypothesis

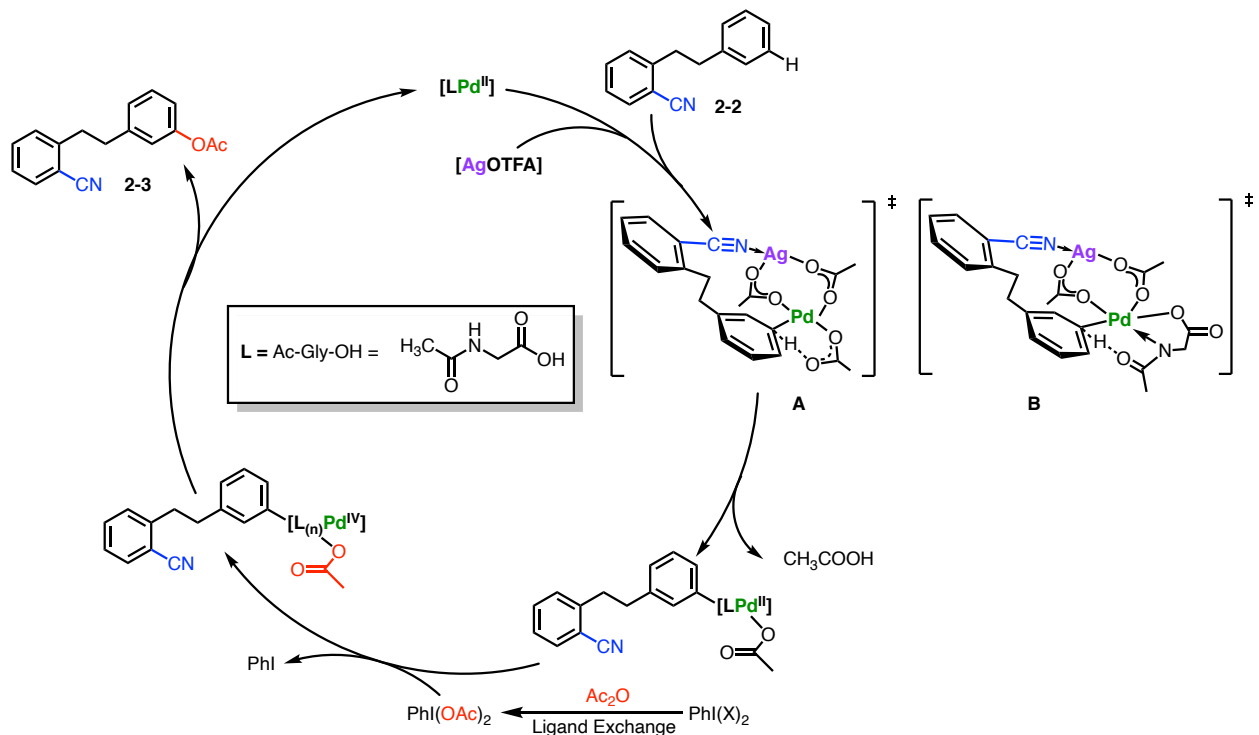


Figure 2-13 Mechanistic proposal for *meta* nitrile-directed C–H functionalization.

With the previously discussed control studies completed, we proposed the following mechanism. In discerning this pathway we paid specific attention to the experimental work regarding unexpected substrate selectivity cases, and key control studies looking at both the presence of the nitrile and anhydride. A thorough understanding of the important additives and ligands which control σ -nitrile-directed C–H transformations were also considered.

We hypothesized that our transformation occurs via a traditional Pd II/IV mechanism, analogous to the C–H acetoxylation studied in Sanford’s early work, as well as nitrile-directed, palladium catalyzed methods developed by the Yu lab.^{3,6} The catalytic cycle begins with a ligated Pd(II) species, which after concerted metalation-deprotonation to the substrate **2-2**, results in the formation of palladacycle **A** or **B** (Figure 2-13). Species **A** represents the palladium-silver, heterobimetallic dimer proposed by Yu and Houk, based on the enhanced selectivity and yield from

employment of silver additives. Alternatively, if the MPAA ligand is evoked in this step, a ligated palladium **B** species can be envisioned. After this nitrile-directed concerted-metalation-deprotonation step, the *meta*-palladated species is formed, which then can be oxidized to Pd(IV) by the hypervalent iodine oxidant, followed by reductive elimination to give the acetoxyated product **2-3**. We believe that due to the control studies which examined the role of the anhydride, that a ligand exchange occurs on the hypervalent iodine, resulting in the acetoxyated palladium IV (pictured in Figure 2-13). Alternatively, the oxidized palladium IV can undergo ligand exchange itself, to give the correct identity of the ester on the metal species (not pictured). Overall, this mechanistic proposal is guided by both literature and empirical observations of this palladium-catalyzed acetoxylation (and pivalation).

2.6 Development of a Proximal Nitrile-Directed C–H Methoxylation

2.6.1 Optimization Studies

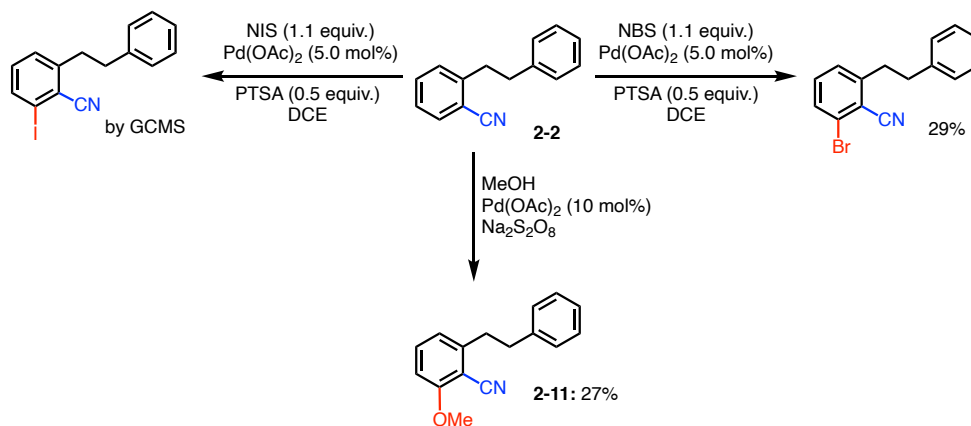


Figure 2-14 Lead results for *ortho*-nitrile-directed C–H functionalization.

With two distal-directed C–H functionalization methods established, we then focused our attention on developing an orthogonal method to direct proximal C–H oxidation through π -coordination of the nitrile triple bond. Using model biaryl ethane substrate **2-2**, preliminary results demonstrated C–H functionalization activation on the benzonitrile (proximal) aromatic ring.²⁵

Specifically, these lead results demonstrated *ortho*-methoxylation, -bromination, and -iodination achieved with moderate yields (Figure 2-14).

Proposed to proceed via π -coordination, this interesting reactivity demonstrates the capability to selectively functionalize the *ortho*-position with a typical *meta*-director in electrophilic-aromatic substitution (EAS).^{25–28} The C–H activation on the aryl nitrile not only reveals positional selectivity between sp^2 -hybridized carbon-hydrogen bonds, but demonstrates selective oxidation between distal and proximal arenes. This selectivity contrasts the nitrile lone-pair-directed methods discussed above, as acetoxylation/pivalation conditions yield selective *meta*-functionalization of the pendant arene. Initial iodination yields were low and bromination resulted in a mixture of two isomers (by GCMS), in addition to the isolated *ortho* product. While methoxylation GCMS data showed low yield, mainly lack of conversion was the issue, so in hopes of optimizing for a selective transformation, this method was further studied, rather than the others.

Entry	Reaction Conditions	Yield (%)
1	r.t. 7h, then 70 °C, 16 h	27
2	70 °C, 18 h	7
3	r.t., 18 h	18
4	r.t. 7h, then 70 °C, 16 h	trace ^a
5	r.t. 7h, then 100 °C, 16 h	trace

Isolated yields. ^aReaction carried out with 20 mol% Pd(OAc)₂.

Table 2-9 Initial temperature and time screen for nitrile-directed *ortho* C–H methoxylation

Initially, when assessing a range of conditions using methanol as a solvent, yields for the nitrile-directed *ortho*-methoxylation were low (Table 2-9). A very minor regioisomeric mass was also observed occasionally. Following literature procedures for nitrile-directed methoxylations, the best yield of **2-11** was 27% yield (Table 2-9, entry 1). Running the reaction overnight (18h) without the initial 7 hours at room temperature, as given for conditions in Sun’s work, led to palladium black

formation within minutes, as well as significantly lower yield and evaporated solvent at the end (entry 2). Performing the reaction at room temperature, increasing palladium loading and raising temperature also had no effect on yield at this point in our studies (entries 3-5).

A screen of oxidants revealed little productive change in the transformation (Table 2-10). Notably, potassium persulfate ($K_2S_2O_8$) show diminished yield, and interestingly, while $PhI(OAc)_2$ resulted in low reactivity employing hydroxy(tosyloxy)iodobenzene (HTIB) resulted in a slight increase in yield (entries 1-4). Further, yields were improved, and major evaporation

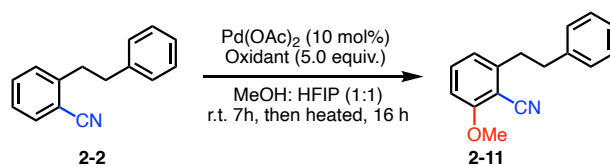
Entry	Oxidant	Yield (%)
1	$Na_2S_2O_8$	19
2	$K_2S_2O_8$	5
3	$PhI(OAc)_2$	trace
4	Hydroxy(tosyloxy)iodobenzene	25
5	$Na_2S_2O_8$	26 ^a

^aH NMR yields by internal standard dibromomethane. ^aReaction carried out with co-solvent HFIP.

Table 2-10 Oxidant screen for nitrile-directed *ortho* C–H methoxylation.

issues were resolved when a cosolvent was employed with the original $Na_2S_2O_8$ oxidant (entry 5). Hexafluoroisopropanol (HFIP) was used due to its success in the acetoxylation transformation and its high boiling point. HFIP could be helpful in stabilizing the strained palladacyclic intermediate or enhance binding to nitrile.^{14,29} Specifically, the high hydrogen bonding affinity could lend to blocking the nitrile lone-pairs for distal functionalization. This would be analogous to Lewis acid additives being beneficial in similar systems explored by Jegamohan.²⁸ For more discussion on Lewis acid additives

in this system, see below. Regardless, the HFIP co-solvent reduced solvent loss over the reaction period, improving reaction analysis.



Entry	Oxidant	Additive (equiv.)	Temperature (°C)	Yield (%)
1	Na ₂ S ₂ O ₈	-	70	26 ^a
2	Na ₂ S ₂ O ₈	-	70	trace ^{a,b}
3	Na ₂ S ₂ O ₈	-	90	10 ^a
4	Na ₂ S ₂ O ₈	Ac-Gly-OH (0.2)	70	18
5	Na ₂ S ₂ O ₈	Ac-Gly-OH (0.2)	70	6 ^c
6	Hydroxy(tosyloxy)iodobenzene	-	90	47
7	Hydroxy(tosyloxy)iodobenzene	Ac-Gly-OH (0.2)	90	8 ^c
8	Hydroxy(tosyloxy)iodobenzene	AgOAc (1.0)	90	22
9	Hydroxy(tosyloxy)iodobenzene	Ag ₂ O (1.0)	90	20
10	Hydroxy(tosyloxy)iodobenzene	AgSbF ₆ (1.0)	90	23
11	Hydroxy(tosyloxy)iodobenzene	4 Å M.S.	90	trace
12	Hydroxy(tosyloxy)iodobenzene	-	90	10 ^a
13	PhI(OAc) ₂	-	90	n.r.
14	PhI(OPiv) ₂	-	90	n.r.

¹H NMR yields by internal standard dibromomethane. ^aReaction carried out with 20 mol% Pd(OAc)₂.

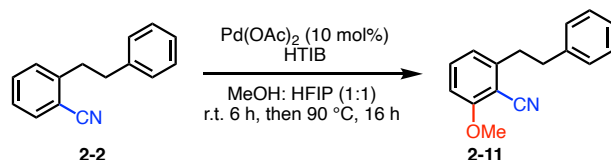
^bReaction carried out with 6.0 equiv. MeOH in HFIP as solvent. ^cNo HFIP cosolvent was used.

Table 2-11 Additive screens for nitrile-directed *ortho* C–H methoxylation.

Moving forward with moderate yields using the initial Na₂S₂O₈ oxidant (Table 2-11, entry 1), a more extensive conditions (time/temperature) and oxidant screen was carried out. Interestingly, while HFIP as a co-solvent (with methanol) resulted in moderate yields, simply adding MeOH as a reagent resulted in only trace product formation (entry 2). Increasing temperature and catalyst loading with these conditions seemed to have no effect or slightly decrease product formation as well (entries 1-3). Further, inclusion of the MPAA ligand (with and without HFIP) was detrimental (entries 4-5). As we seemed to be plateauing at only modest yield (26%) using Na₂S₂O₈, we switched to HTIB as an oxidant, which had provided similar results in early studies. Excitingly, simply increasing the temperature with the new oxidant almost doubled

yield to 47%, and thus further screening was conducted using HTIB (entry 6). The MPAA ligand, Ac-Gly-OH was still unneeded with HTIB, and silver additives were not helpful for this transformation either, even though these factors were important in the nitrile-directed C–H acetoxylation (entries 7-10). Because some hydroxylation products were observed by GCMS molecular sieves (4 Å M.S.) were added to help reduce byproduct formation, but this appeared to shut down the reaction (entry 11). Finally, because of the larger product formation now observed, we re-examined other hypervalent iodine reagents. Still, $\text{PhI}(\text{OAc})_2$ and $\text{PhI}(\text{OPiv})_2$ were not effective oxidants (entries 13-14).

With moderate yields of 47%, although conversion had improved, a minor C–H hydroxylation side product seemed to be forming as result of employing HTIB as an oxidant. We thus faced the challenge of improving the reaction selectively, hoping to arrive at higher conversions, with no unwanted side products. Further screens were carried out to address this problem. Dioxidation appeared to be one problem (as observed by GCMS), and thus oxidant loading was examined. Attempts seemed futile though, as these issues remained unsolved.



Entry	HTIB (equiv.)	Yield (%)
1	5.0	47
2	7.0	trace
3	5.0	5 ^a
4	5.0	22 ^{b,c}
5	5.0	11 ^c

¹H NMR yields by internal standard dibromomethane. HTIB = [Hydroxy(tosyloxy)iodo]benzene. ^aReaction was carried out with MeOH: HFIP (2:1) ^bReaction was carried out with MeOH: dioxanes (1:1). ^cReaction carried out with 20 mol% Pd(OAc)₂.

Table 2-12 Further screens for nitrile-directed *ortho* C–H methoxylation.

Increasing oxidant reduced yields significantly, likely due to over oxidation, both hydroxylation and methoxylation, as observed by GCMS (Table 2-12, entry 2). Including a higher

ratio of methanol, as well as switching to different co-solvents, and increasing palladium loading all resulted in lower yields for the current system (entries 3-5).

Ultimately, these issues were solved by running the reaction at room temperature for a longer period of time (Table 2-13, entry 2). Increasing the catalyst loading at the room temperature procedure was beneficial, and resulted in the highest isolated yield of *ortho* methoxylation (entry

Entry	Reaction Time (h)	Temperature (°C)	Yield (%)
1	24	90	9
2	24	r.t.	43
3	24	r.t.	73 ^{a,b}
4	24	r.t.	22 ^c
5	48	r.t.	35
6	48	r.t.	54 ^a

¹H NMR yields by internal standard dibromomethane. HTIB = [Hydroxy(tosyloxy)iodo]benzene. ^aReaction carried out with 20 mol% Pd(OAc)₂. ^bIsolated yield. ^cReaction carried out with 7.0 equiv. HTIB.

Table 2-13 Final time and temperature screens for nitrile-directed *ortho* C–H methoxylation.

3). Control studies revealed that stirring the reaction proceeded for 48 hours did not seem to increase conversion further, nor did increasing oxidant loading or catalyst with the longer time and lower temperature (entries 4-6)

Overall, examination of alternative oxidants improved yields and revealed Hydroxyl(tosyloxy)iodobenzene (HTIB) as superior in this system; while additives and ligands played

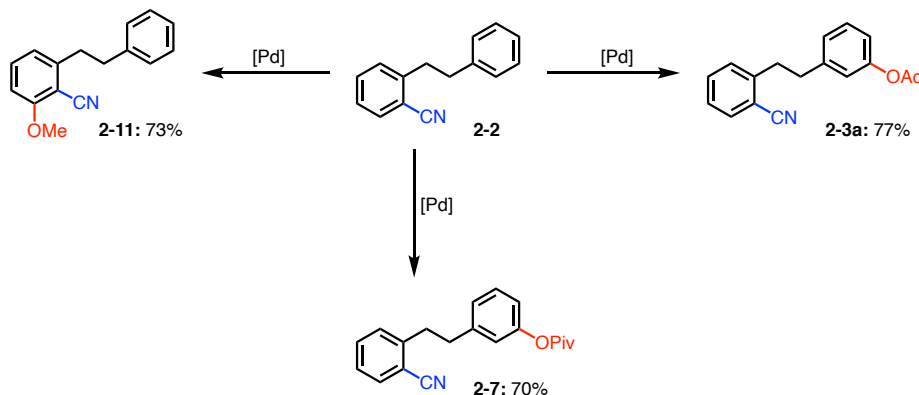


Figure 2-15 Regiodivergent nitrile-directed C–H functionalization.

a beneficial role in the distal acetoxylation chemistry, both of these components did not improve yields for this reaction. Further still, yields were improved by employing a co-solvent, hexafluoroisopropanol (HFIP), and running the reaction at room temperature, providing 73% *ortho*-methoxylation of our model substrate **2-2**. Using a simple nitrile containing starting material, we were now able to regioselectively oxygenate proximal or distal C–H bonds by varying the oxidant and nucleophile to access complex biaryl ethanes (Figure 2-15). With this we have now been able to demonstrate the selective oxidation of proximal and distal aryl C–H bonds, using the nitrile as the sole directing group.

2.6.2 Control Studies and Scope Investigation

As the optimization of the *ortho*-methoxylation was challenging, so was the application of this C–H functionalization method to additional substrates. Thus, only some work was done in this area, as other applications, and extensions of the nitrile-directed chemistry seemed more encouraging. A brief discussion of the substrates examined, and the problems encountered, are outlined below.

First, we wanted to demonstrate the divergent oxidation at both proximal and distal positions. Initial attempts were unfruitful, as we tried to apply our methoxylation conditions to the acetoxyated model compound **2-3a**, and only decomposition of starting material was observed (no identifiable products by GCMS) (Figure 2-16A). The palladium catalysis seemed to be the problematic factor, as hydrolysis of the acetate ester was not evident, and neither was methoxylation product formation, when

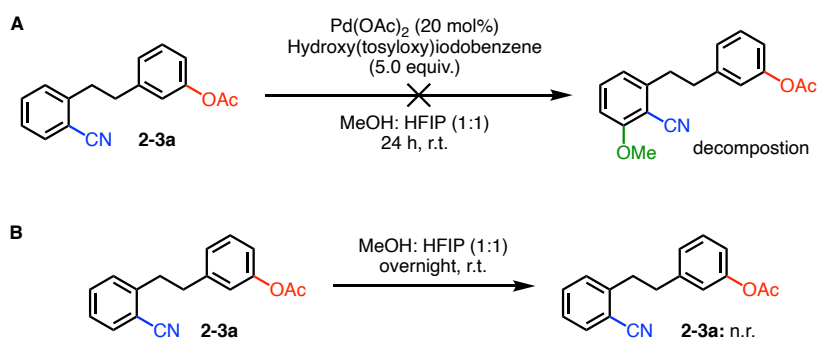


Figure 2-16 Methoxylation attempts on acetoxyated model substrate **2-3a**.

the starting material **2-3a** was stirred in methanol and hexfluoroisopropanol overnight (Figure 2-16B). Only unreacted starting material was observed. This suggested that the catalytic transformation with the methoxylation conditions did not tolerate the labile acetate, or the starting material underwent another decomposition pathway when the ester was already installed.

These findings were one of the motivations for developing the distal pivalation, as discussed in Chapter 2.4; A pivalic ester is a much more robust functional group than the acetate moiety, and can withstand forcing conditions in which the acetoxy is often deprotected to the hydroxyl. When the standard methoxylation conditions were employed with the pivalated model substrate **2-7**, oxidation was initially low yielding, and thus a bit of optimization was required

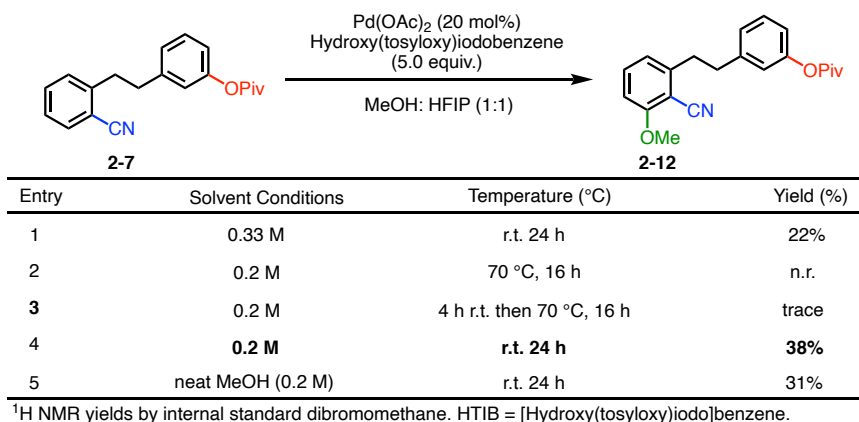


Table 2-14 Methoxylation optimization on pivalated substrate **2-7**.

(Table 2-14, entry 1). Increasing temperature, even with a slow ramp resulted in deleterious pathways leading to decomposition (entries 2-3). Ultimately a more dilute, co-solvent, reaction mixture gave the best yields, which topped-out around 40% (entry 4-5). The modest yields achieved for this reaction may be due to the deprotection, or even cleavage of the pivalate, as palladium has been known to insert into pivalic esters for C–O functionalization.²⁰

Moving forward with the methoxylation, we hoped to extend this transformation to additional substrates. One benzonitrile we were particularly interested in subjecting to the

methoxylation was the biaryl naphthalene substrate. This motif would be an ideal substrate to

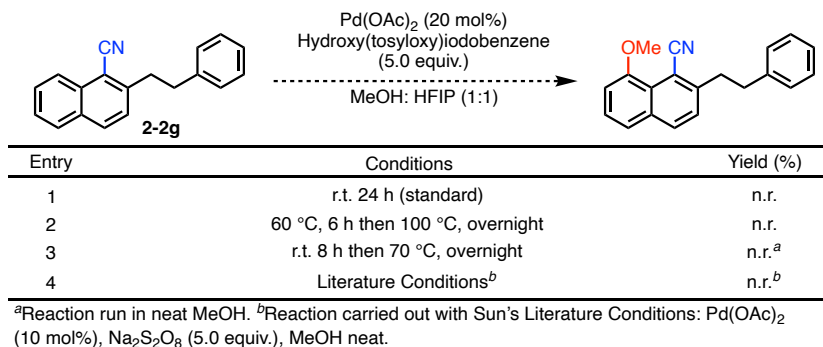


Table 2-15 Methoxylation attempts on naphthalene substrate **2-2g**.

showcase all of our nitrile-directed transformations, due to the multiple functionalizable aromatic C–H bonds. With successful distal acetoxylation and pivalation on this compound **2-2h** (see **2-3h** and **2-7b**), selective installation of methoxide was intriguing, and the next logical step in our method development. Unfortunately, after looking at various conditions (Table 2-15), no methoxylated product of any kind was detected on this substrate; only starting material was recovered. This could be due to the flexible methylene linker sterically blocking the catalyst coordination to the nitrile, and thus functionalization at the 8-position. Further, the more electron-rich, alkyl-substituted arene may make C–H abstraction more challenging. We reasoned this, as even exact literature conditions discussed in Chapter 1.3.2 by Sun (entry 4), which functionalized the 8-position selectively, proved futile.²⁵ Potentially our conditions may invoke metal catalyst coordination more apt to direct methoxylation to the 2-position of the naphthalene, as seen in the Jeganmohan's ruthenium catalyzed method (see Chapter 1.3.2),²⁸ which is blocked by the alkyl chain in our case with **2-2h**. No more work was done on this substrate, and few other substrates were investigated (see Chapter 6.2.2.4). Ultimately, these various methoxylation studies showcase the sensitive selectivity of our nitrile-directed *ortho*-methoxylation.

2.6.3 Mechanistic Hypothesis

We believe our catalytic cycle follows a pathway analogous to that proposed by Sun (Figure 2-17). The mechanism begins with palladium π -coordination to the nitrile C–N triple bond. This chelation brings the metal (Pd II) in proximity to the bond *ortho* to the nitrile, allowing for selective

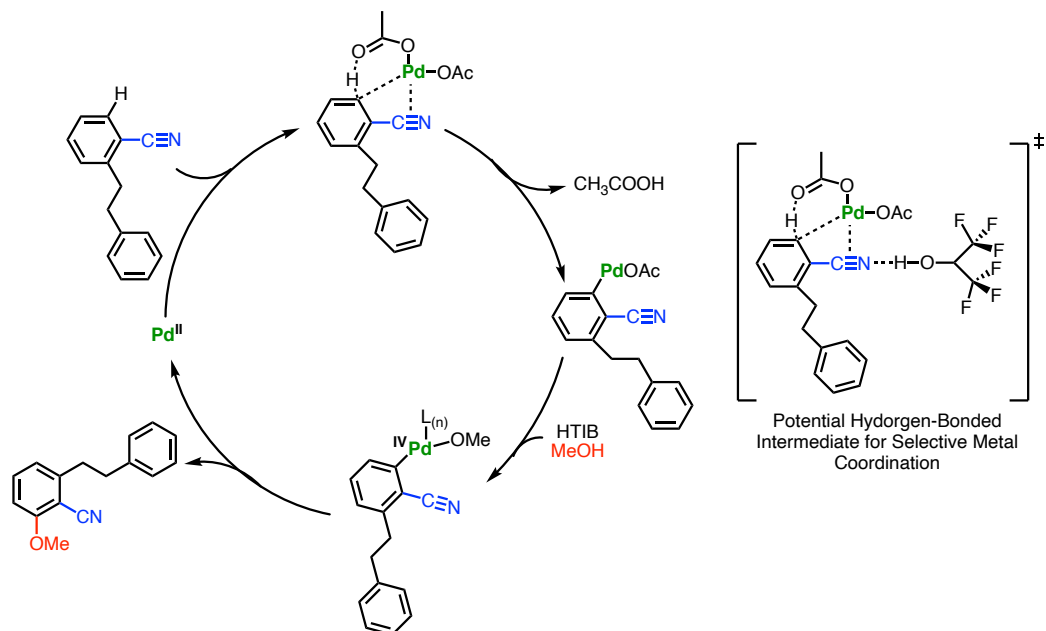


Figure 2-17 Mechanistic proposal for nitrile-directed *ortho* C–H methoxylation.

C–H insertion via CMD.³ The palladated-intermediate is then oxidized to palladium IV, reductive elimination gives the methoxylated product, and regenerates the active Pd II. As discussed above, the selectivity is imparted due to the geometrically constrained palladacycle, but may also be attributed to empirical findings, such as the need for co-solvent hexafluoroisopropanol, which may be coordinating to the lone pairs (via Hydrogen-Bonding) to block alternate coordination modes. This would be reminiscent of Jegamohan's mechanistic proposal²⁸ for nitrile-directed *ortho* C–H activation, which follows a similar cycle as depicted above, and by Sun,²⁵ but evokes a Lewis acid additive to block lone pair-metal binding (as opposed to Brønsted acid in our case). Regardless, this system appears consistent with other literature reports regarding palladium (and other metal) catalysis which evoke a π -chelated

metal to allow for selective functionalization. More work would need to be done to fully characterize the mechanism of this transformation.

2.7 Development of a Nickel-Catalyzed Reductive Decyanation

2.7.1 Motivation and Inspiration

Motivated by our lab's previous experience regarding reductive deoxygenation of silyloxyarenes, and other methods to functionalize inert electrophiles, we hypothesized that nickel-*N*-heterocyclic carbenes (Ni-NHCs) could be employed to conduct reductive decyanation.^{21,22} In 2017, the Montgomery group developed a set of conditions to chemoselectively install C–H or C–Si bonds at the *ispo*-position of these silyl-protected phenols (Figure 2-18). Notably, these transformations

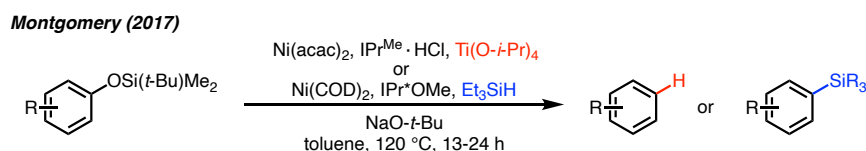


Figure 2-18 Montgomery nickel-NHC-catalyzed reduction of silyloxyarenes.

employ the mild reductants titanium-isopropoxide ($\text{Ti}(\text{o-}i\text{-Pr})_4$), or triethylsilane, to arrive at the reduced arenes. This work, like Chatani's and others, allows for nickel activation of aromatic C–O bonds, typically thought to be relatively inert.²³ These examples show that employing an NHC-ligated nickel species, along with high base loadings, results in an electron-rich metal center effective for oxidative addition. With our knowledge of nickel-catalysis,^{21,22} we wondered if our previous methodology would be amenable to accessing metal insertion at the analogously inert C–CN present in this work, to provide a traceless C–H functionalization strategy, and expand upon existing limitations in the de-functionalization literature.³⁰ Achieving a mild reductive decyanation would render the nitrile group a removable directing group for late-stage functionalization of un-activated arenes. Furthermore, while methods for decyanation do exist, many methods employ pyrophoric

reagents and precious metal catalysts, such as rhodium.³¹ Many systems also require conjugated cyanoarenes for good yields. Thus, safety, substrate compatibility, and cost concerns made development of a new reductive decyanation intriguing.

2.7.2 Optimization of the Nickel-Catalyzed Reductive Decyanation

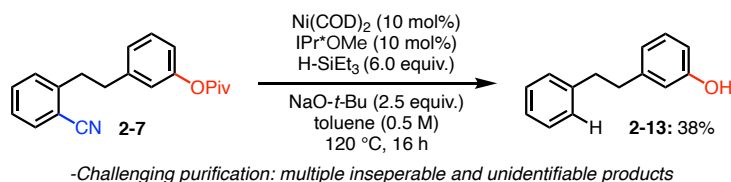
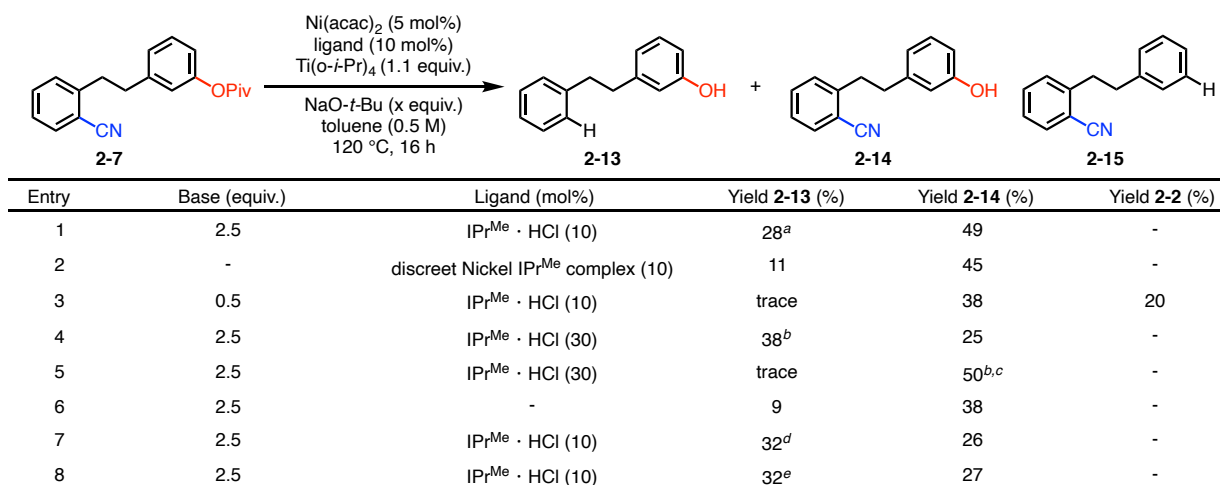


Figure 2-19 Reductive decyanation using Montgomery triethylsilane conditions.

We began our studies into the activation of the aromatic nitrile group by screening our previously reported C–O activation conditions on our pivalated biaryl **2-7**. First, the method which used triethylsilane provided desired product **2-13** in a reasonable yield of 38% (Figure 2-19), but provided a large mixture of products which were challenging to separate. Besides the decyanated product, the remaining mass balance was difficult to identify. Fortunately, when titanium-isopropoxide



Isolated yields. ^aExact conditions from Montgomery *ACS Catal.* **2017**, *7*, 5568. ^bReaction carried out with 15 mol% Ni(acac)₂. ^cReaction carried out at room temperature. ^dReaction stirred for 24h. ^eReaction carried out with 2.5 equiv. Ti(o-*i*-Pr)₄.

Table 2-16 Initial optimization of nickel-catalyzed reductive decyanation.

(Ti(O-*i*-Pr)₄) was used as a hydride source instead of the silane, a moderate yield of **2-13** could be

cleanly isolated along with deprotected starting material **2-14** (Table 2-16, entry 1). Although **2-14** was the major product, we believed the straightforward purification and product identification, along with almost full conversion of **2-7** offered more promise for developing a successful reductive decyanation.

Moving forward with initial optimization of this reductive transformation, we considered the role of the ligated nickel complex. Although we hypothesized that the excess base was detrimentally deprotecting our starting material, or that lack of active nickel-complex formation in solution was hampering product formation, when a discrete Nickel IPr^{Me} complex was used (and thus base excluded from the reaction), yield of desired **2-13** was minimal (entry 2). When substoichiometric base loading was used, only trace product was observed, but significant byproduct **2-14** was isolated, as well as a previously unobserved C–O activation product (**2-15**), in decent yields (entry 3). Conversely, increasing the amount of active catalyst in solution seemed to increase desired product formation slightly, but doing the same at room temperature for elongated reaction times was not helpful (entries 4-6). Control experiments confirmed the necessity of the ligand, and running the reaction longer (at elevated temperatures), or with increased reductant, showed no improvement (entries 7-8).

Entry	Ni(acac) ₂ (mol%)	Ligand (mol%)	Yield 2-13 (%)	Yield 2-14 (%)
1	15.0	IPr ^{Me} · HCl (30.0)	38	25
2	15.0	IPr ^{Me} · HCl (20.0)	31	31
3	15.0	IPr ^{Me} · HCl (15.0)	32	31
4	5.0	IPr ^{Me} · HCl (10.0)	31 ^a	42
5	5.0	PCy ₃ (10.0)	40	25
6	15.0	PCy ₃ (30.0)	68	32
7	15.0	PCy ₃ (30.0)	29 ^b	38

Isolated yields. Reactions carried out with 0.4 mL toluene. ^aReaction carried out with 0.8 mL toluene. ^bReaction stirred for 24h.

Table 2-17 Ligand screen for nickel-catalyzed reductive decyanation.

It has been shown that the ratio of ligand to metal in Nickel-NHC can have a large impact on active catalyst formation, and thus product yield. Unfortunately, manipulating these ratios seemed to show little impact though, and diluting the reaction mixture was futile, as well (Table 2-17, entries 1-4). Looking at previous work on defunctionalization reactions, the use of phosphine-ligands is common. Excitingly, a simple switch in ligand choice and ultimate increase in loading of it and Ni(acac)₂, gave good yield of 68% of the reductive decyanation the pivalated bibenzyl **2-13** (entries 5-7).

In order to speed-up optimization (due to synthesis of the model substrate) and see if the reductive decyanation could be expanded in scope, a 4-phenylbenzonitrile **2-16** was utilized (Table 2-18). Optimized conditions for the model substrate **2-7** gave good yields for the biphenyl (entry 1), and similar controls as discussed above showed no increase in yield with longer reaction times, lower temperatures, or when the Ti(O-*i*-Pr)₄ reductant is excluded (entries 2-4). Increasing the NaO-*t*-Bu base addition to 5.0 equivalents boosted yields in this system to 74% of **2-17** (entry 5). Switching the identity of the *tert*-butoxide base counter ion was detrimental in the case of LiO-*t*-Bu, and inconsequential for yields when KO-*t*-Bu was employed (entries 6-7).

c1ccc(cc1)-c2ccc(cc2)C#N $\xrightarrow[\text{Base (2.5 equiv.)}]{\text{Catalyst (x mol \%)} \text{ PCy}_3 \text{ (30 mol \%)} \text{ Ti(O-}i\text{-Pr)}_4 \text{ (1.1 equiv.)}}$ c1ccc(cc1)-c2ccc(cc2)H

2-16 **2-17**

toluene (0.5 M)
120 °C, 16 h

Entry	Catalyst (mol%)	Base	Yield (%)
1	Ni(acac) ₂ (15.0)	NaO- <i>t</i> -Bu	68
2	Ni(acac) ₂ (15.0)	NaO- <i>t</i> -Bu	65 ^a
3	Ni(acac) ₂ (15.0)	NaO- <i>t</i> -Bu	64 ^b
4	Ni(acac) ₂ (15.0)	NaO- <i>t</i> -Bu	n.r. ^c
5	Ni(acac) ₂ (15.0)	NaO- <i>t</i> -Bu	74 ^d
6	Ni(acac) ₂ (15.0)	LiO- <i>t</i> -Bu	38
7	Ni(acac) ₂ (15.0)	KO- <i>t</i> -Bu	73
8	Ni(acac) ₂ (20.0)	NaO- <i>t</i> -Bu	81
9	Ni(acac) ₂ (20.0)	KO- <i>t</i> -Bu	87
10	Ni(COD) ₂ (20.0)	KO- <i>t</i> -Bu	80

Isolated yields. Reactions carried out with 0.4 mL toluene. ^aReaction stirred for 24h. ^bReaction carried out at 100 °C. ^cReaction carried out without Ti(O-*i*-Pr)₄. ^dReaction carried out with 5.0 equiv. NaO-*t*-Bu.

Table 2-18 Optimization of nickel-catalyzed reductive decyanation on 4-phenylbenzonitrile.

Further screening revealed that increasing nickel loading was also helpful to product formation, and a subsequent switch of base ultimately provided the best yield of 87% for our decyanated biphenyl (entries 8-9). Finally, although not providing the best yields, Ni(COD)₂ was also demonstrated as competent nickel- source in this transformation (entry 10).

Taking inspiration from the success found in optimizing the reductive decyanation on the biphenyl **2-16**, we continued to optimize the transformation on **2-7** (Table 2-19). Beginning with our best results thus far (68% **2-13** and 30% **2-14**), we began by screening alternative nickel sources, but this change was unproductive, as was changing the *tert*-butoxide base identity (Table 2-19, entries 2-4). Contrary to the biphenyl substrate, increasing Ni(acac)₂ loading to 20% and keeping ligand loading

Entry	Catalyst (mol %)	Ligand (mol%)	Base	Yield 2-13 (%)	Yield 2-14 (%)
1	Ni(acac) ₂ (15.0)	PCy ₃ (30.0)	NaO- <i>t</i> -Bu	68	30
2	Ni(COD) ₂ (15.0)	PCy ₃ (30.0)	NaO- <i>t</i> -Bu	40	38
3	Ni(acac) ₂ (20.0)	PCy ₃ (30.0)	KO- <i>t</i> -Bu	45	23
4	Ni(acac) ₂ (15.0)	PCy ₃ (30.0)	LiO- <i>t</i> -Bu	40	54
5	Ni(acac) ₂ (20.0)	PCy ₃ (30.0)	NaO- <i>t</i> -Bu	19	49
6	Ni(COD) ₂ (20.0)	PCy ₃ (30.0)	NaO- <i>t</i> -Bu	58	32
7	Ni(COD) ₂ (15.0)	PCy ₃ (30.0)	LiO- <i>t</i> -Bu	30	35
8	Ni(COD) ₂ (20.0)	PCy ₃ (30.0)	NaO- <i>t</i> -Bu	32 ^a	24
9	Ni(COD) ₂ (20.0)	PCy ₃ (40.0)	NaO- <i>t</i> -Bu	32 ^a	24
10	Ni(COD) ₂ (20.0)	PCy ₃ (30.0)	NaO- <i>t</i> -Bu	63 ^b	13

Isolated yields. Reactions run with 0.4 mL toluene. ^aReaction run with 2.5 equiv. Ti(*o*-*i*-Pr)₄. ^bReaction carried out with 5.0 equiv. NaO-*t*-Bu.

Table 2-19 Final optimization of nickel-catalyzed reductive decyanation.

at 30%, caused yields dropped (entry 5). When the 2 : 3 metal to ligand ratio was employed with Ni(COD)₂, though, the higher yields were promising (entry 6). Changing base identity and increasing reductant proved unhelpful, but increasing base loading not only regained yields to 63%, but reduced formation of the undesired product (entries 7-10). Increased base was also seen in previous Montgomery and Chatani transformations to boost generation of desired products. The alkoxide bases

are thought to coordinate to the nickel catalyst, making an electron rich-metal species, improving the efficiency of challenging oxidative additions, such as C–O or C–C activations.^{21,22,32}

In conclusion, we found that an electron-rich nickel catalyst, in conjunction with Ti(O-*i*-Pr)₄ as a both the Lewis acid, and mild hydride source, provided moderate yields of desired product. Further optimization revealed that by switching the ligand from an NHC to tricyclohexylphosphine, and increasing the amount of base, good yields of the decyanated product could be achieved. Although some deprotection of the pivalate group is observed, no de-oxygenation was detected with our final conditions. Bibenzyl phenols (**2-13**), are not only desired precursors to many medicinally relevant products, but are both challenging to synthesize independently, and expensive to purchase wholesale. Regardless, these products showcase the selective C–H oxidation by a removable directing group, and offer access to *meta*-substitution of arenes with alkyl substituents, substrates which would typically result in *ortho*- or *para*- substitution with electrophilic aromatic substitution.

2.7.3 Substrate Scope for the Nickel-Catalyzed Reductive Decyanation

With two variants of a reductive decyanation transformation in hand we wanted to examine the scope of this reaction, and better understand the divergence in yield for the 4-phenylbenzotrile (**2-16**) and the model bibenzyl (**2-7**) systems. In particular, we wondered if the deprotection of pivalate **2-7**, or the resulting phenol was impeding catalysis, but when **2-18** was synthesized, and subjected to optimized conditions, high yields were still achieved (Figure 2- 20A). Additionally, a bibenzyl lacking a pivalated group **2-2** decyanated in moderate yield (Figure 2-20B). These results informed us that it is likely the lack of conjugation in bibenzyl **2-7**, and potentially the addition of the electron-rich linker, which results in only moderate yields, as compared to biphenyl **2-16**. Finally, 2-

(3-morpholinophenethyl)benzonitrile **2-8**, proceeded in good yield with slight modifications, but additional isolated aromatic substrates examined showed no productive decyanation (Figure 2- 20C).

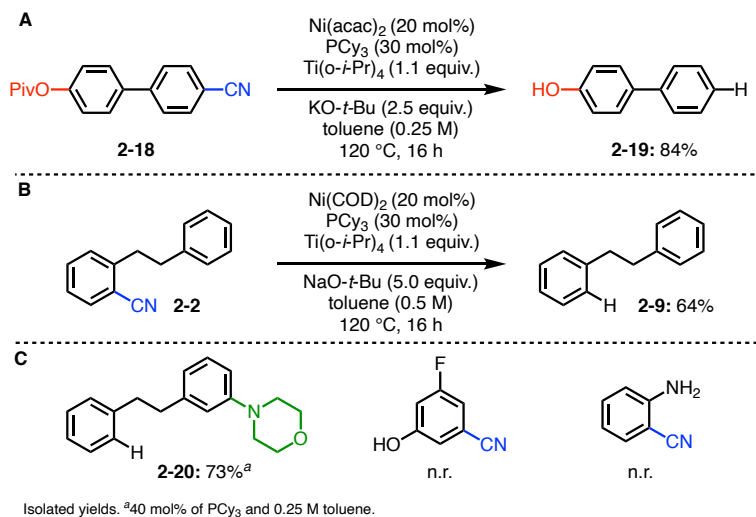


Figure 2-20 Substrate scope examined for the nickel-catalyzed reductive decyanation.

2.8 Synthetic Demonstrations and Conclusions

Moving forward we hoped to demonstrate the orthogonality of our recently developed transformations (Figure 2-21). When **2-7** is subjected to our optimized C–H methoxylation conditions, it can be further functionalized to incorporate a second C–O-bond, while keeping the pivalate intact (**2-12**). Second, we can further functionalize the distal portion of the molecule at the open *meta*-position, using our C–H acetoxylation procedure (**2-21**) (with *para*-functionalization also occurring). This showcases how the dual activation modes of the nitrile can be used to conduct sequential, highly regioselective oxidations of complex arene systems at both proximal and distal sites. We are then able to further diversify our C–H activation product using Chatani’s C–O amination conditions (**2-8**), and finally, employ our reductive decyanation conditions to arrive at the traceless-functionalized product (**2-20**).⁸ Thus, starting with simple vinyl arenes, using borylation/*ortho*-cyanation chemistry, followed

by our newly developed nitrile-directed C–H activation strategies, one can rapidly acquire highly decorated aromatic motifs in a sequential and selective fashion.

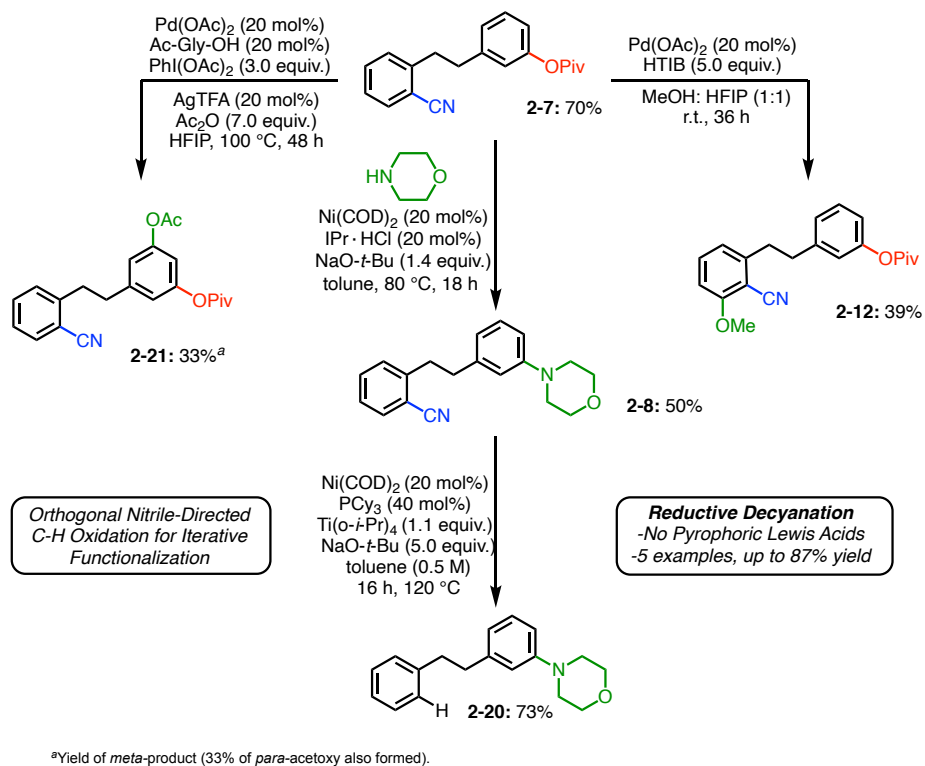


Figure 2-21 Rapid molecular diversification via traceless nitrile-directed C–H functionalization.

In conclusion, Montgomery group cascade borylation chemistry, in unison with the dual directing capability of the nitrile, and if desired, reductive decyanation, offer a simple and rapid entrance into highly decorated aromatic motifs, starting from commercially available starting materials via a traceless directing group strategy. Through use of the σ -binding mode for distal C–H functionalization, or through donation from the π -system for proximal C–H functionalization, one can envision the use of this versatile directing group for late-stage, regiodivergent functionalization of medicinal targets, and ultimately, removal of the directing group, if desired. In this work, three different nitrile-directed C–H activation methods were developed, including remote *meta*-acetoxylation and pivalation, as well as, proximal *ortho*-methoxylation. Further, a reductive decyanation was developed to access these products in a traceless manner. All of these reactions were demonstrated on a variety

of motifs and various studies into the importance of different additives and reactivity parameters were examined. In general, this work highlights the power of combinational, divergent C–H functionalization in accessing uniquely oxidized aromatic systems. If future work on this project was to be carried out, one would work to expand the scope of the acetoxylation, methoxylation, pivalation, and decyanation to more complex substrates. Additionally, gaining more insight into the mechanism of each transformation would be helpful to advancing general research in C–H functionalization and reductive denationalization method development. Finally, computationally exploring the exact nature of nitrile-palladium coordination, in each case, as well as more specific parameters to better understand factors which control divergent selectivity, is needed.

2.9 References

- (1) Zhao, W.; Montgomery, J. Functionalization of Styrenes by Copper-Catalyzed Borylation/Ortho-Cyanation and Silver-Catalyzed Annulation Processes. *Angew. Chem. Int. Ed.* **2015**, *54* (43), 12683–12686. <https://doi.org/10.1002/anie.201507303>.
- (2) Ping, Y.; Ding, Q.; Peng, Y. Advances in C–CN Bond Formation via C–H Bond Activation. *ACS Catal.* **2016**, *6* (9), 5989–6005. <https://doi.org/10.1021/acscatal.6b01632>.
- (3) Lyons, T. W.; Sanford, M. S. Palladium-Catalyzed Ligand-Directed C–H Functionalization Reactions. *Chem. Rev.* **2010**, *110* (2), 1147–1169. <https://doi.org/10.1021/cr900184e>.
- (4) Hartwig, J. F. Evolution of C–H Bond Functionalization from Methane to Methodology. *J. Am. Chem. Soc.* **2016**, *138* (1), 2–24. <https://doi.org/10.1021/jacs.5b08707>.
- (5) Davies, H. M. L.; Morton, D. Recent Advances in C–H Functionalization. *J. Org. Chem.* **2016**, *81* (2), 343–350. <https://doi.org/10.1021/acs.joc.5b02818>.
- (6) Shao, Q.; Wu, K.; Zhuang, Z.; Qian, S.; Yu, J.-Q. From Pd(OAc)₂ to Chiral Catalysts: The Discovery and Development of Bifunctional Mono-N-Protected Amino Acid Ligands for Diverse C–H Functionalization Reactions. *Acc. Chem. Res.* **2020**, *acs.accounts.9b00621*. <https://doi.org/10.1021/acs.accounts.9b00621>.
- (7) Leow, D.; Li, G.; Mei, T.-S.; Yu, J.-Q. Activation of Remote Meta -C–H Bonds Assisted by an End-on Template. *Nature* **2012**, *486* (7404), 518–522. <https://doi.org/10.1038/nature11158>.
- (8) Fang, L.; Saint-Denis, T. G.; Taylor, B. L. H.; Ahlquist, S.; Hong, K.; Liu, S.; Han, L.; Houk, K. N.; Yu, J.-Q. Experimental and Computational Development of a Conformationally Flexible Template for the Meta-C–H Functionalization of Benzoic Acids. *J. Am. Chem. Soc.* **2017**, *139* (31), 10702–10714. <https://doi.org/10.1021/jacs.7b03296>.
- (9) Yang, Y.-F.; Cheng, G.-J.; Liu, P.; Leow, D.; Sun, T.-Y.; Chen, P.; Zhang, X.; Yu, J.-Q.; Wu, Y.-D.; Houk, K. N. Palladium-Catalyzed *Meta* -Selective C–H Bond Activation with a

- Nitrile-Containing Template: Computational Study on Mechanism and Origins of Selectivity. *J. Am. Chem. Soc.* **2014**, *136* (1), 344–355. <https://doi.org/10.1021/ja410485g>.
- (10) Husemoen, G.; Olsson, R.; Andersson, C.-M.; Harvey, S. C.; Hansen, H. C. Solution-Phase Parallel Wittig Olefination: Synthesis of Substituted 1,2-Diarylethanes. *J. Comb. Chem.* **2003**, *5* (5), 606–609. <https://doi.org/10.1021/cc0300210>.
- (11) Cheng, G.-J.; Yang, Y.-F.; Liu, P.; Chen, P.; Sun, T.-Y.; Li, G.; Zhang, X.; Houk, K. N.; Yu, J.-Q.; Wu, Y.-D. Role of N-Acyl Amino Acid Ligands in Pd(II)-Catalyzed Remote C–H Activation of Tethered Arenes. *J. Am. Chem. Soc.* **2014**, *136* (3), 894–897. <https://doi.org/10.1021/ja411683n>.
- (12) Salazar, C. A.; Gair, J. J.; Flesch, K. N.; Guzei, I. A.; Lewis, J. C.; Stahl, S. S. Catalytic Behavior of Mono-N-Protected Amino-Acid Ligands in Ligand-Accelerated C–H Activation by Palladium(II). *Angew. Chem. Int. Ed.* *n/a* (n/a). <https://doi.org/10.1002/anie.202002484>.
- (13) Shen, P.-X.; Wang, X.-C.; Wang, P.; Zhu, R.-Y.; Yu, J.-Q. Ligand-Enabled Meta-C–H Alkylation and Arylation Using a Modified Norbornene. *J. Am. Chem. Soc.* **2015**, *137* (36), 11574–11577. <https://doi.org/10.1021/jacs.5b08914>.
- (14) Wencel-Delord, J.; Colobert, F. A Remarkable Solvent Effect of Fluorinated Alcohols on Transition Metal Catalysed C–H Functionalizations. *Org. Chem. Front.* **2016**, *3* (3), 394–400. <https://doi.org/10.1039/C5QO00398A>.
- (15) Li, S.; Ji, H.; Cai, L.; Li, G. Pd(II)-Catalyzed Remote Regiodivergent Ortho- and Meta-C–H Functionalizations of Phenylethylamines. *Chem. Sci.* **2015**, *6* (10), 5595–5600. <https://doi.org/10.1039/C5SC01737H>.
- (16) Meng, G.; Lam, N. Y. S.; Lucas, E. L.; Saint-Denis, T. G.; Verma, P.; Chekshin, N.; Yu, J.-Q. Achieving Site-Selectivity for C–H Activation Processes Based on Distance and Geometry: A Carpenter’s Approach. *J. Am. Chem. Soc.* **2020**, *142* (24), 10571–10591. <https://doi.org/10.1021/jacs.0c04074>.
- (17) Tang, R.-Y.; Li, G.; Yu, J.-Q. Conformation-Induced Remote Meta -C–H Activation of Amines. *Nature* **2014**, *507* (7491), 215–220. <https://doi.org/10.1038/nature12963>.
- (18) Xu, D.; Sun, W.-W.; Xie, Y.; Liu, J.-K.; Liu, B.; Zhou, Y.; Wu, B. Metal-Free Regioselective Hypervalent Iodine-Mediated C-2 and C-3 Difunctionalization of N-Substituted Indoles. *J. Org. Chem.* **2016**, *81* (22), 11081–11094. <https://doi.org/10.1021/acs.joc.6b02078>.
- (19) Mlynarski, S. N.; Schuster, C. H.; Morken, J. P. Asymmetric Synthesis from Terminal Alkenes by Cascades of Diboration and Cross-Coupling. *Nature* **2014**, *505* (7483), 386–390. <https://doi.org/10.1038/nature12781>.
- (20) Becica, J.; Gaube, G.; Sabbers, W. A.; Leitch, D. C. Oxidative Addition of Activated Aryl-Carboxylates to Pd(0): Divergent Reactivity Dependant on Temperature and Structure. *Dalton Trans.* **2020**. <https://doi.org/10.1039/D0DT01119C>.
- (21) Wiensch, E. M.; Todd, D. P.; Montgomery, J. Silyloxyarenes as Versatile Coupling Substrates Enabled by Nickel-Catalyzed C–O Bond Cleavage. *ACS Catal.* **2017**, *7* (9), 5568–5571. <https://doi.org/10.1021/acscatal.7b02025>.
- (22) Wiensch, E. M.; Montgomery, J. Nickel-Catalyzed Amination of Silyloxyarenes through C–O Bond Activation. *Angew. Chem. Int. Ed.* **2018**, *57* (34), 11045–11049. <https://doi.org/10.1002/anie.201806790>.

- (23) Shimasaki, T.; Tobisu, M.; Chatani, N. Nickel-Catalyzed Amination of Aryl Pivalates by the Cleavage of Aryl C–O Bonds. *Angew. Chem. Int. Ed.* **2010**, *49* (16), 2929–2932. <https://doi.org/10.1002/anie.200907287>.
- (24) Yoshimura, A.; Zhdankin, V. V. Advances in Synthetic Applications of Hypervalent Iodine Compounds. *Chem. Rev.* **2016**, *116* (5), 3328–3435. <https://doi.org/10.1021/acs.chemrev.5b00547>.
- (25) Li, W.; Sun, P. Pd(OAc)₂-Catalyzed Alkoxylation of Arylnitriles via Sp² C–H Bond Activation Using Cyano as the Directing Group. *J. Org. Chem.* **2012**, *77* (18), 8362–8366. <https://doi.org/10.1021/jo301384r>.
- (26) Du, B.; Jiang, X.; Sun, P. Palladium-Catalyzed Highly Selective Ortho-Halogenation (I, Br, Cl) of Arylnitriles via Sp² C–H Bond Activation Using Cyano as Directing Group. *J. Org. Chem.* **2013**, *78* (6), 2786–2791. <https://doi.org/10.1021/jo302765g>.
- (27) Li, W.; Xu, Z.; Sun, P.; Jiang, X.; Fang, M. Synthesis of Biphenyl-2-Carbonitrile Derivatives via a Palladium-Catalyzed Sp² C–H Bond Activation Using Cyano as a Directing Group. *Org. Lett.* **2011**, *13* (6), 1286–1289. <https://doi.org/10.1021/ol103075n>.
- (28) Chenna Reddy, M.; Jeganmohan, M. Ruthenium-Catalyzed Ortho Alkenylation of Aromatic Nitriles with Activated Alkenes via C–H Bond Activation. *Chem. Commun.* **2015**, *51* (53), 10738–10741. <https://doi.org/10.1039/C5CC03112E>.
- (29) Colomer, I.; Chamberlain, A. E. R.; Haughey, M. B.; Donohoe, T. J. Hexafluoroisopropanol as a Highly Versatile Solvent. *Nat. Rev. Chem.* **2017**, *1* (11), 0088. <https://doi.org/10.1038/s41570-017-0088>.
- (30) Mattalia, J.-M. R. The Reductive Decyanation Reaction: An Overview and Recent Developments. *Beilstein J. Org. Chem.* **2017**, *13* (1), 267–284. <https://doi.org/10.3762/bjoc.13.30>.
- (31) Modak, A.; Maiti, D. Metal Catalyzed Defunctionalization Reactions. *Org. Biomol. Chem.* **2015**, *14* (1), 21–35. <https://doi.org/10.1039/C5OB01949D>.
- (32) Xu, L.; Chung, L. W.; Wu, Y.-D. Mechanism of Ni-NHC Catalyzed Hydrogenolysis of Aryl Ethers: Roles of the Excess Base. *ACS Catal.* **2016**, *6* (1), 483–493. <https://doi.org/10.1021/acscatal.5b02089>.

Chapter 3

Introduction to Glycosylation and Polysaccharide Synthesis

3.1 Introduction to Carbohydrates and Glycosylation

Carbohydrates are stereochemically rich, polar building blocks that offer an immense amount of molecular complexity. Each carbohydrate building block, known as a monosaccharide, can be linked to another via one of the multiple hydroxyl groups, and each anomeric linkage that is formed, introduces a new stereocenter. The vast number of permutations available to even short carbohydrate chains makes these essential biomolecules, which govern intercellular molecular recognition events, amongst many other functions. The ability to serve in a myriad of functions is owed to their highly complex, diverse, and modular structure.¹ Studying the cellular interactions precisely and then disrupting them, through structural modifications, is a proven strategy to develop novel therapeutics.^{1,2} However, this effort is hindered by the limitations of existing carbohydrate chemistry to efficiently synthesize complex oligo- and polysaccharides. Non-trivial purifications following each iterative glycosylation step between the donor and acceptor monosaccharide units, and necessary protecting-group manipulations, makes obtaining monodisperse biopolymers synthetically challenging, tedious, and time-consuming.

Although biomolecules exist with *O*-, *S*-, *N*- and *C*- glycosides, *O*-glycosidic linkages are the most common found in nature, and will be the focus of discussion herein. Two of the most common sugar moieties in *O*-glycosides are glucose and mannose, which are C-2 epimers. Each of these sugars can exist as two stereoisomers (anomers), known as α - or β -glycosides, based on

the orientation of the anomeric oxygen (Figure 3-1A).³ This stereochemical diversity that results

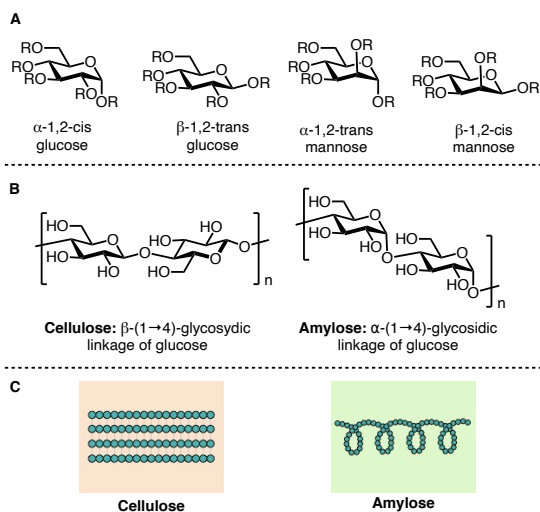


Figure 3-1 Common mono- and polysaccharides found in nature.

from a simple change in the orientation of the anomeric linkage leads to drastic changes in macroscopic properties. For example, while amylose, or starch, consists of 1,2-*cis* glucose units linked together, the polysaccharide which gives cellulose, and thus wood, its rigid structure is a 1,2-*trans* glucoside (Figure 3-1B). The α -(1,4) glycosidic linkage of amylose does not result in straight chain of monosaccharide units, but rather the bound monomeric sugars twist into a coil-like shape to relieve steric strain between units. Conversely, cellulose, consisting of β -(1,4) glycosidic bonds, allows for highly linear polysaccharide chains, and thus results in densely packed cell fiber (Figure 3-1C).⁴ Clearly, the resulting application and functional differences which result from the specific stereo- and regio-configurations of polymeric glycosides make synthesizing the desired isomers of great importance. The field of glycoscience is rich in methods to make and manipulate carbohydrates in a selective fashion for an array of applications. Work in this area is far from finished, though, as simple transformations to rapidly access to pure, large, and chemically diverse glycoconjugates are scarce.

3.1.1 Introduction to Glycosylation

To fully understand the challenges which come with the preparation of oligo- or polysaccharides, the obstacles which result from constructing simple disaccharides must first be understood. Several components make up a successful glycosylation reaction, and the selection of promoter, glycosyl donor, and method to attain stereoselectivity are key.

Generally, a glycosylation reaction is the formation of a bond between the anomeric carbon of the glycosyl donor and the nucleophilic component of a glycosyl accepter (Figure 3-2). Specifically, the mechanism proceeds via activation by an electrophilic promoter to induce loss of a leaving group of the of the glycosyl donor, to form an oxocarbenium ion, which can then be attacked, at either the axial or equatorial face, to form the α - or β - anomer, respectively.^{3,5-7} Notably, if the C-2 hydroxyl protecting group is an ester (most often an acetate), then this group can participate, forming a dioxalenium ion intermediate, which can then react with the glycosyl acceptor to form predominantly the 1-2- *trans* product, due to steric blocking of the *cis* face. Conversely, if the C-2 protecting group is a non-participating functional group (such as a benzyl ether), then no steric preference results in a thermodynamic mixture of α - and β - anomers. For

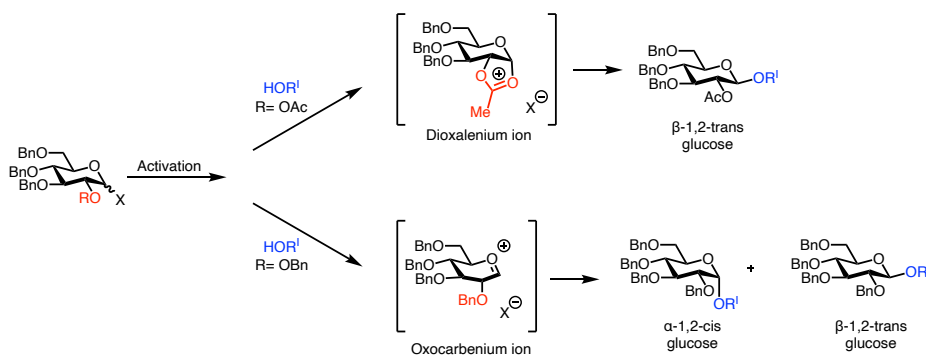


Figure 3-2 Standard glycosylation mechanism with neighboring group participation for stereoselectivity.

mannosides, the α -isomer is the major product due to the stability of the axial anomer (i.e. the anomeric effect), while in glucose, a thermodynamic mixture favors the β - anomer approximately

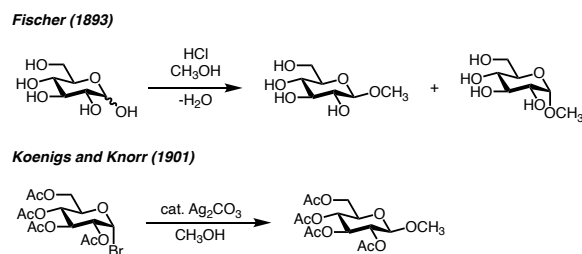


Figure 3-3 Seminal glycosylation methods by Fischer, Koenigs, and Knorr.

2:1. These stability- and equilibrium-driven processes were first observed in early Fischer glycosylations. Demonstration of the neighboring group effect by Koenigs and Knorr in 1901, though, allowed *trans*-glycosides to be reliably accessed (Figure 3-3).⁸ This pioneering method employed glycosyl bromides as the glycosyl donor, with alcoholic acceptors and silver salts to promote the formation of α - or β - anomers selectively, via substrate control.⁹ While the participating group-strategy has been successfully employed in many stereoselective oligosaccharide syntheses, other efficient methods include solvent participation, remote group participation, steric blocking strategies, intramolecular aglycone delivery, and catalyst control over selectivity, have also been developed to enable stereo-control.

While Koenigs and Knorr showed the first examples of bromide donors, and these types of monosaccharides are still commonly used, many other glycosyl donors are employed in modern

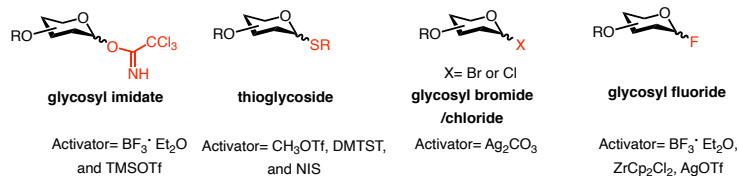


Figure 3-4 Commonly employed glycosyl donor leaving groups for chemical glycosylation.

carbohydrate chemistry including, but not limited to, trichloroacetimidates thioglycosides, glycosyl chlorides, and glycosyl fluorides (Figure 3-4). Finding cooperative promotors which selectively activate the leaving group (and do not erode other functionality on the carbohydrate molecule) is also important. These promotors range from precious transition metals to Brønsted acids, and may require super-stoichiometric loadings in some cases, while catalytic in others, and

are often highly specific to each type of glycosyl donor used. Protecting groups, which impact the electronic and steric profile of glycosides, can also have a large effect on the success of a glycosylation. Specifically, reactive glycosyl acceptors (often containing electron-donating protecting groups) are known as armed, while those with electron-poor/withdrawing protecting groups, and thus unreactive as glycosyl acceptors, are often referred to as disarmed.³ Finally, and most importantly, the choice of anomeric leaving group on the glycosyl donor faces delicate reactivity/stability balance. While the donors must be stable enough for storage and carrying through intermediate synthetic manipulations, they must also be reactive enough to allow for efficient glycosylation, when functionalization is desired. For instance, trichloroacetimidates (*O*-derivatives) and glycosyl bromides and iodides are attractive due to their activation by mild promoters, but are labile in purification or subsequent reactions on the glycan. Other leaving groups, such as thioglycosides, and disarmed chloride and bromide donors are both stable through various protecting group manipulations and reactive to a variety of promoters. Thus, while somewhat less reactive in catalytic activation methods, are used widely in the synthetic field. Finally, while rarely degrading, the stable *n*-pentenyl glycosides are minimally reactive and thus require much more forcing promoters, making them less desirable, on the opposite end of the spectrum as the more labile esters or imidates.⁹ This delicate reactivity/stability balance makes glycosyl donor choice imperative.

Ultimately, it is these challenges which result from constructing simple disaccharides that dictate the successful synthesis of oligo- or polysaccharides. In addition to stereoselectively synthesizing the correct anomer, and choosing an ideal glycosyl donor within the reactivity/stability continuum, a specific protecting group strategy is often necessary to allow for the reaction to occur between adequately reactive acceptor and donor partners. While there is a

breadth of glycosylation methodology in the literature, making improvements in synthetic efficiency of donors and acceptors, protecting group compatible and mild catalytic promoter systems is of need.

3.1.2 Glycosyl Fluorides as Glycosyl Donors

Glycosyl fluorides are attractive and commonly utilized glycosyl donor choice due to their intermediate stability and reactivity. Fluorous sugars are typically unreactive to the standard Koenigs and Knorr conditions employed with other halide donors.^{3,10} Thus, the enhanced stability of this leaving group has led to the increased employment in standard oligosaccharide synthesis and natural product glycosylation.^{3,11} These glycosyl donors are typically synthesized by nucleophilic substitution of anomeric hydroxyl or thioethers by HF-pyridine, (diethylamino)sulfur trifluoride (DAST), or a combination of DAST and NBS. They can also be used as glycosyl acceptors (armed or disarmed) to perform glycosylation with other glycosyl donors, such as thioglycosides. In comparison, glycosyl bromides and chlorides are usually too reactive to serve as glycosyl acceptors. Glycosyl fluorides not only have enhanced stability, but also can be activated under mild conditions. This provides an ideal balance between reactivity and stability.

The balanced attributes of the glycosyl fluorides were uncovered by Mukaiyama in 1981 (Figure 3-5).¹² The protocol employed stoichiometric stannous chloride (SnCl_2) and silver perchlorate (AgClO_4) to arrive at good yield of the disaccharide in a mixture of anomers. Further

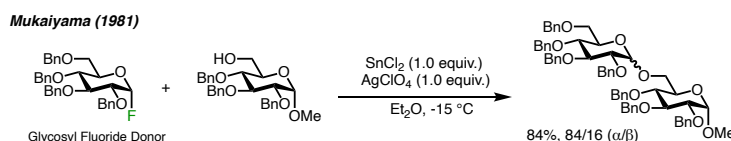


Figure 3-5 Seminal glycosylation method using glycosyl fluoride donors.

work has extended this method to employ other silver sources such as silver triflate (AgOTf), or Lewis acids like trityl perchlorate (TrClO_4), in conjunction with Tin.^{3,5,6} Other valuable reagents

for this transformation, SiF₄ and TMSOTf, were initially reported by Noyori in 1984.¹³ Boron-based Lewis acid promoters have been employed as well, due to their highly fluorophilicity. Notably, BF₃•Et₂O was the first to be reported as successful in these fluoride abstraction mechanisms; Nicolau¹⁰, Kunz¹⁴, and Vozny³ independently disclosed this approach for glycosylation, which paired these fluoride donor glycosides with silyl-ether acceptors (Figure 3-6). The strength of the silicon-fluoride bond is commonly denoted as the driving force for many of these reactions, and is another characteristic which makes the use of glycosyl fluorides attractive for synthesis. The widely available silyl-based protecting groups are not only easy to install, but through this glycosylation process, they can be ultimately removed *in-situ*.^{3,5,6} Modern glycosylations employ stoichiometric BF₃•Et₂O, but scope is limited, and generation of HF

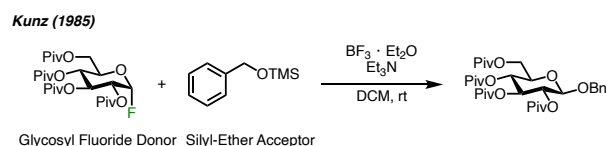


Figure 3-6 Glycosylation of silyl ethers using glycosyl fluorides and boron trifluoride etherate.

requires inclusion of triethyl amine, which precludes large scale reactions. In attempts to move away from stoichiometric promoters for these transformation, various groups have employed ZrCp₂Cl₂ and AgOTf in catalytic amounts. Mukaiyama has also gone on to disclose boron Lewis acids and certain Brønsted acids as competent promoters in sub-stoichiometric quantities.^{11,15} In

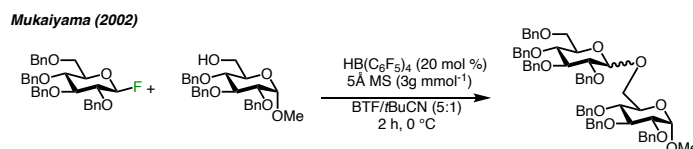


Figure 3-7 Stereoselective glycosylation of using glycosyl fluoride donors and catalytic boron trifluoride etherate.

one particular example, β- selectivity can even be achieved using counterion and solvent effects (Figure 3-7).¹⁶ Armed donors and careful temperature and moisture control are commonly required to access catalytic methods. These generalized setbacks unfortunately continue to limit glycosyl fluoride usage in the synthesis of complex oligosaccharides.

While it is clear that glycosyl fluoride donors offer a variety of appealing attributes in terms of stability and reactivity, many current methods that promote the loss of the fluoride anion are not catalytic.² Thus, accessing a mild, efficient catalytic protocol for activating glycosyl fluorides would be highly valuable for the synthetic carbohydrate community.

3.2 Montgomery Group Contributions to the Glycosylation Literature

The Montgomery group has developed a variety of glycosylation methods over the last decade. While initial reports outlined the expansion of Intramolecular Aglycone Delivery (IAD) to access 1,2-*cis* glycosides using sugar silanes,¹⁷⁻¹⁹ more recent carbohydrate chemistry has focused on using catalytic amounts of boron Lewis acids to promote glycosylations of glycosyl fluorides.²⁰

3.2.1 Fluoride Migration Catalysis for Iterative Glycosylation

Glycosyl fluorides are desirable donor species in glycosylation reactions due to their intermediate stability, reactivity, and relatively straightforward synthesis. Although these attributes make their use in oligomer synthesis appealing, the lack of catalytic methods for activating the anomeric fluoride has precluded their extensive use.

Inspired by gold-catalyzed fluoride rebound trifluoromethylations by the Toste group,²¹ and Stephan's fluoride migration work,²² our group developed a Lewis acid-catalyzed glycosylation method using glycosyl fluoride donors, and silyl ether acceptors.²⁰ Specifically, this work highlighted the unique properties of boron and its affinity for fluoride to enable catalytic loading of promoters.

By using substrate control for selectivity (neighboring group participation or IAD), the transformation offers access to all four stereochemical glycoside configurations. This operationally simple method is moisture and air tolerant, and can be carried out at room temperature with extremely low loadings of catalyst (0.5 mol %) (Figure 3-8A). Further, because

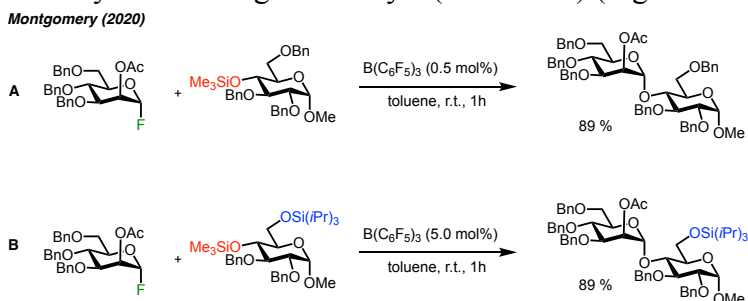


Figure 3-8 Montgomery fluoride migration catalysis for iterative glycosylation.

the acceptors are silyl ethers, a range of common protecting groups can be used, and are deprotected *in situ*. The tris(pentafluorophenyl)borane catalyst ($B(C_6F_5)_3$ or BCF) allows for chemoselective glycosylation, as the catalyst will select for the smaller silyl ethers over the larger ones, thus overriding inherent selectivity for 1° alcohols (Figure 3-8B). With DFT calculations and experimental studies, the following mechanism was proposed (Figure 3-9). Beginning with the free BCF catalyst, the anomeric fluoride is abstracted from the glycosyl donor **I**. The abstraction

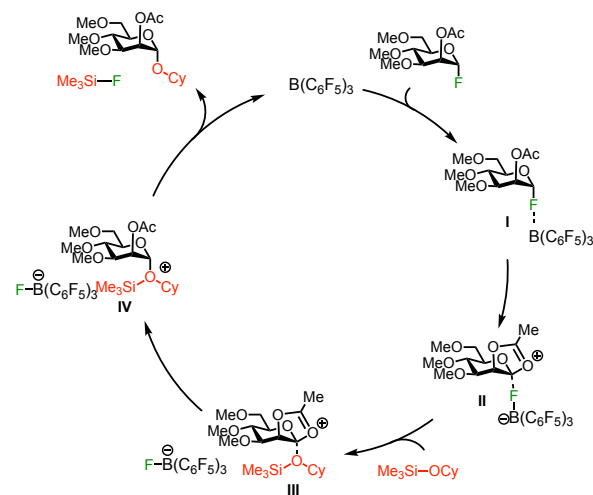


Figure 3-9 Mechanism for BFC-catalyzed glycosylation.

results in a charged oxocarbenium or dioxalenium ion intermediate **II** due to the neighboring group effect from the acetate group. The oxygen of the silylated acceptor then attacks the anomeric

position of the donor (**III**), forming a positively charged intermediate **IV**, which exists as a frustrated Lewis acid-base with the fluoro-boronate. The BCF—F anion then redelivers the fluorine to the silyl protecting group, which results in releasing the desired glycosylation product. Thus, the driving force of the reaction is the silicon-fluorine bond formed in the final step, and the boron delivery of the abstracted fluorine to the recently deprotected silyl group ultimately turns over the catalytic system.

This work achieved the iterative synthesis of oligosaccharides via a mild, user-friendly BCF-catalyzed glycosylation method. The glycosyl fluoride donors are shelf-stable and modifiable intermediates, whereas the silicon-protected acceptors make dictating regioselectivity straightforward. The fluoride migration strategy enables a glycosylation transformation that is wide in scope and potential, as it offers insights into overcoming other challenges in carbohydrate chemistry.

3.3 Introduction to Polysaccharides and Glycoconjugates

Carbohydrates play many vital roles, from signaling units in microbiological processes, to forming massive structural frameworks for tree bark. These macroscopic structural and functional properties result from small stereo- and regio-chemical changes and branching complexity, in the basic structures of these polysaccharides (see Figure 3-1).^{3,23,24} Closely related glycoconjugates, carbohydrates covalently linked to proteins or lipids, have similar purposes in the cell are also highly dependent on small structural features.² The study of these biomolecules is critical to a variety of fields from medicine to materials, and thus synthesizing them in a fast and efficient manner, is key.

3.3.1 Introduction to Polysaccharides and Glycobiology

Polysaccharides, the most abundant organic materials on earth, are diverse in structure and function. Although they are the keys to biological signaling, serve as structural support and energy sources, and offer indispensable applications in materials and food industries, the study of these unique biopolymers has lagged in comparison to proteins and polynucleotides.^{9,23} This challenge is rooted in the enhanced three-dimensional complexity of carbohydrate monomers. In comparison to their amino acid and nucleotide counterparts, sugars can have five stereo-defined branching units at each hydroxyl on a monosaccharide. Furthermore, each glycosidic linkage results in the formation of a new stereocenter at the anomeric carbon. The stereochemical variations are evident in the number of unique combinations possible from the combination of three biopolymeric units. While up to 1,056 unique trisaccharide permutations can be generated from three hexoses, only six different trimers can be derived from three nucleic or amino acids.³ This potential for wide structural variations leads to the diverse role carbohydrates, and their mimetics.

As discussed in the introduction, glucose polymers, such as cellulose and glycogen (amylose) serve in vital structure and energy storage roles. These natural polysaccharides, and others, have also found use in an array of industries.^{9,25} For example, the three-dimensional helical configuration of glycogen (amylose) offers application in the iodine test for starch, while chitin's acetyl group offers structural rigidity through inter-chain hydrogen bonding (Figure 3-10).

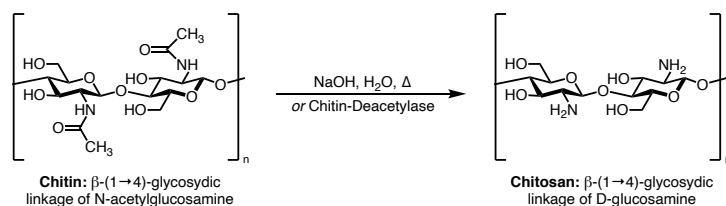


Figure 3-10 Synthesis of chitosan from chitin.

Modification of chitin, through base-catalyzed de-acetylation, results in formation of chitosan, a biomaterial with applications in medical devices and bioplastics. Other unnatural polysaccharides

have found use in the food and cosmetic industries, due to their enhanced water solubility, and biocompatibility. The inter- and intramolecular hydrogen-bonding and molecular rigidity of the polysaccharides modify aqueous solutions to extend shelf life, emulsify liquids and enhance other desired properties.²⁴ Synthetic and natural polysaccharides function in advanced materials, separation and biotechnology platforms. Synthetic carbohydrates have been inspired by natural structure-function properties, and thus studying of these biopolymers is critical.

In addition to harnessing the macroscopic properties of carbohydrates, scientists have come to understand the critical mechanism in which polysaccharides dictate biology. Glycobiology is the research area which encompasses the complex area of carbohydrate chemistry in conjunction with the study of the biological processes in which these complex structures function independently and in conjunction with other biomolecules.^{26,27} While carbohydrate materials, like glycogen are important to cellular function, many biologically-relevant oligosaccharides are associated with proteins, lipids and natural products. These aglycone-linked

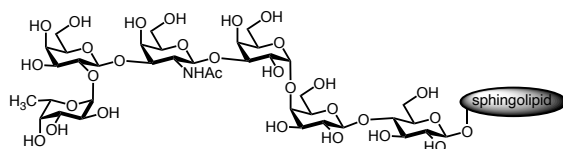


Figure 3-11 Glycoconjugate example: tumor-associated *globo H antigen*.

carbohydrates are known as glycoconjugates. Most cell surfaces are coated with sugars, as they allow for signaling between cells. There are also several types of glycoconjugates which exist as independent biomacromolecules. Some of these typically *O*- or *N*- linked glycoprotein categories include mucins and proteoglycans, whereas the most common glycolipids are often considered to be gangliosides.²⁶ For example, tumor-associated *globo H antigen* is a sphingolipid-linked hexasaccharide with potent anti-cancer properties (Figure 3-11).²⁸ The natural properties and (bio)synthesis of this important biomolecule, and others is a current research focus in the field.

Improving synthetic access to oligosaccharides is not only necessary to progress biomedical applications of these polymers, but also critical to study biological systems effectively.

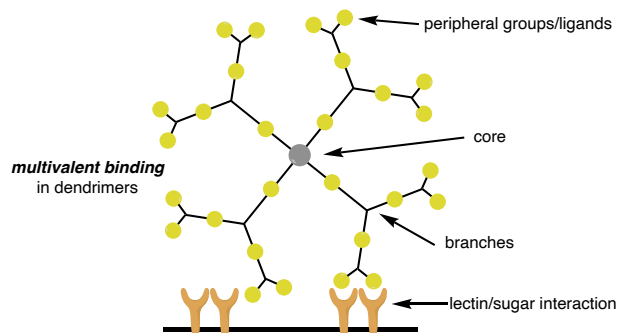


Figure 3-12 Dendrimer structure and propensity to engage in multivalent intercellular interactions.

One specific class of glycoconjugates which have gained considerable traction in recent years is glyco-dendrimers. In general, dendrimers are structural motifs which contain a central core unit from which extend ligand units of typically uniform length and branching pattern.²⁹ Biological macromolecules such as saccharide-appended peptides, and other carbohydrate decorated cores, offer unique applications. These glyco-dendrimers promote highly favorable, highly specific, protein-carbohydrate associations for cell-cell (or cell-pathogen) communication. These strong binding coefficients result from the “multivalent interactions,” or sum of the interactions between the target protein and the multiple branching units on the dendrimer (Figure 3-12). This concept, explored extensively by Kiessling and others, explains the immense effect that a synergistic, cumulative affinity can have on activation of a binding target, even though the single binding of a monosaccharide to an individual active site tends to be quite weak.^{2,30,31} This multivalent interaction phenomenon has been shown to be more effective than proximity or statistical effects resulting from a simple increase concentration of a binding agent.³¹ Further, the specific atomic architecture, and small disruptions within it (e.g. hydrogen-bond manipulations) can have large changes in the bulk, three-dimensional properties, and binding-efficacy of glycoconjugates.²⁴ Because of this unique structure-function relationship, dendrimers have been applied to various

industrial and medicinal uses, ranging from vehicles for targeted drug-delivery to serving roles in bioimaging.^{29,32,33}

3.3.2 Strategies for the Synthesis of Polysaccharides

Just as work on structural elucidation and microbiological role of polysaccharides has lagged in comparison to proteins and polynucleotides, due the complexity of polysaccharide architecture, so has the development of efficient syntheses toward these elaborate biopolymers. Due to the stereochemical and structural diversity of polysaccharides, synthesizing the desired molecule, and especially those of large length is a continued challenge.^{26,27,34}

In the most common strategy, stepwise synthesis of a polysaccharide from monosaccharides requires the construction of each glycosidic linkage from an independent reaction setup, workup, and purification.^{3,27,35} In most cases, the growing carbohydrate serves as the glycosyl acceptor, while the new glycoside is typically the glycosyl donor, as the leaving group

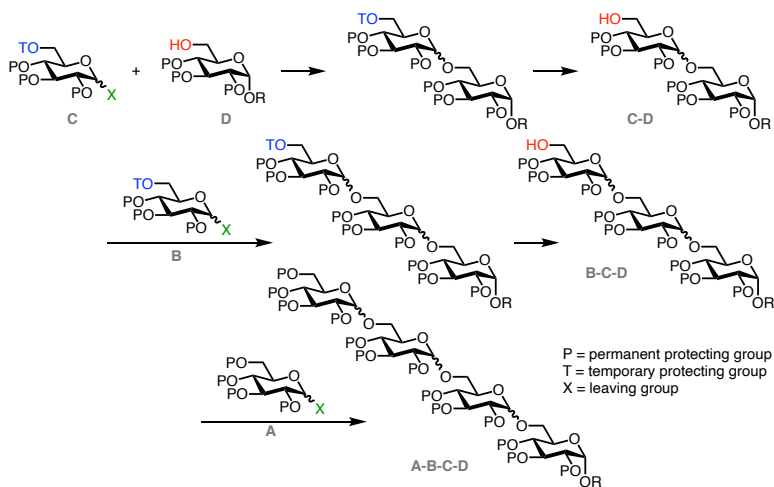


Figure 3-13 Stepwise synthesis of oligosaccharides.

on the donor may be too reactive/unstable to be carried through workup and purification (before the next glycosylation). Further, before each the resulting glycan can be carried forward, a “temporary protecting group,” which was previously, selectively installed, must be removed in an

additional step, before the subsequent glycosylation can occur (Figure 3-13). These protecting group manipulations add another challenge to the already tedious synthesis of stereo- and regio-specific polysaccharides. Although as early as 1926, Helferich demonstrated the viability of this iterative approach, scope and oligomer length was limited.³⁶ It was not until decades later, in the 1950s, that systematic demonstrations of polysaccharide synthesis were published. Further, with

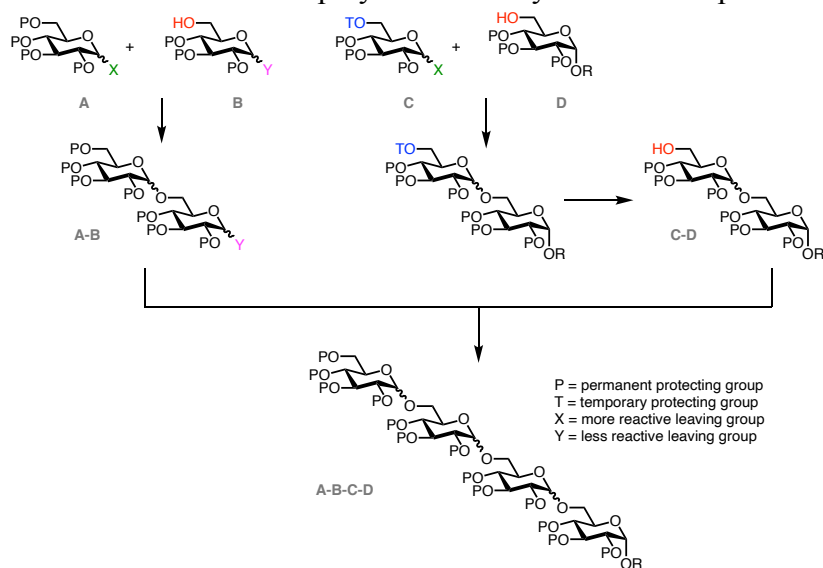


Figure 3-14 Block synthesis of oligosaccharides.

the emergence of more efficient glycosylation and protection/deprotection strategies, stepwise access oligosaccharides have been achieved selectively, and high yielding, by many. One notable example was Nicolau's elegant synthesis of the sialyl-Le^x tetrasaccharide, an oligosaccharide involved in leucocyte recruitment.³⁷ While most steps are high yielding, selective and leading to the desired product, this strategy is still time-consuming and laborious. To address some of the synthetic challenges of accessing large chains, a derivative of the stepwise strategy, is block synthesis. In this case, two separately synthesized units are engaged in a final glycosylation, one serving as a donor, and the other as an acceptor (Figure 3-14).³ In order to synthesize efficient blocks, the donor components must be both suitably stable to be carried through initial synthetic steps, and reactive enough for the last, convergent glycosylation. If the initial anomeric leaving

group is not sufficient, reactivation can be achieved by exchange of the anomeric substituent. However more synthetic steps will be involved. Common anomeric temporary protecting groups include silyl ether, allyl, *p*-methoxyphenyl, and 2-(trimethylsilyl)ethyl. Additionally, block synthesis of polysaccharides can be carried out with different types of glycosyl donors on each unit, in which the last donor is the most stable. This strategy circumvents unnecessary synthetic maneuvers.

To avoid time and material- inefficient protecting group manipulations, other strategies for chemoselective block syntheses of oligosaccharides have been explored. Some examples include the armed-disarmed glycosylations, and active-latent glycosylations. Initially developed by Fraser-Reid³⁸ on *n*-pentenyl glycosides, which couples electron-rich (armed) saccharides with electron-poor (disarmed) saccharides, allow for use of the same donor group on both components, as reactivity is determined by the greater electronic stability of the armed

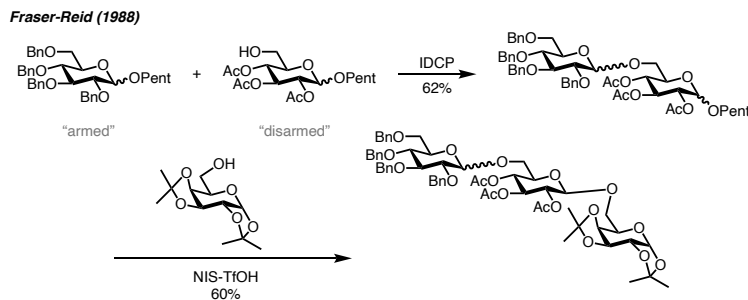


Figure 3-15 Armed-disarmed glycosylation for the synthesis of oligosaccharides.

oxocarbenium ion enables the use of the same anomeric leaving group on both the glycosyl acceptor and donor. The differences in electronic profiles prevent self-glycosylation, and streamlines the synthesis (Figure 3-15).

Latent- active strategies, on the other hand, allow for the donor capability (of a sugar previously used as the acceptor) to be activated by small chemical modification before the subsequent glycosylation. Examples range from deprotection of *p*-Nitrophenyl thioglycosides into their active donor form,³⁹ to isomerization of alkenes by Wilkinson's catalyst,⁴⁰ such as described

by Boons (Figure 3-16). While this allows for the synthesis of homoglycans or homopolymers, as different protecting group schemes are not required for each glycoside, the method still involves the cumbersome stepwise synthesis of growing oligosaccharide.

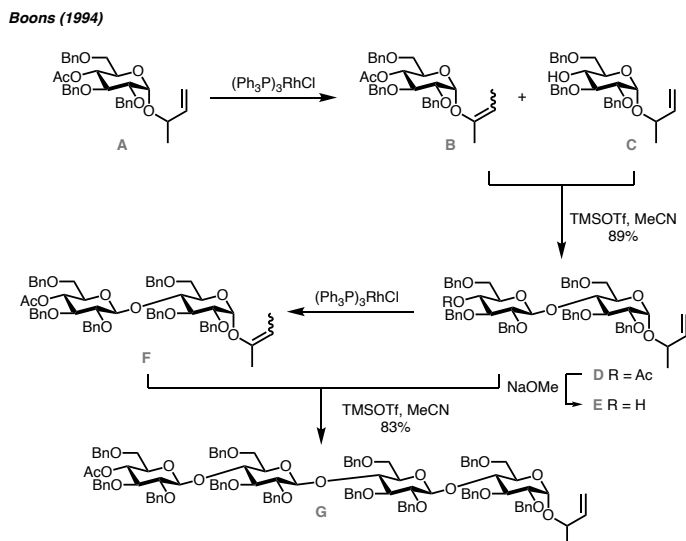


Figure 3-16 Active-latent glycosylation (with alkenyl glycosides) for the synthesis of oligosaccharides.

The methods above have offered pure glycans in good yield and selectivity, but are costly in time and material consumption. To overcome these inefficiencies, one-pot multistep oligosaccharide synthesis was first reported by Raghavan in 1993. Conversely to the traditional, iterative methods, these oligosaccharide syntheses preclude the need for workup and purification at each glycosylation step, but rather the product of the first reaction can react in the subsequent glycosylation selectively due to inherent reactivity on the donor units. Pioneering work by

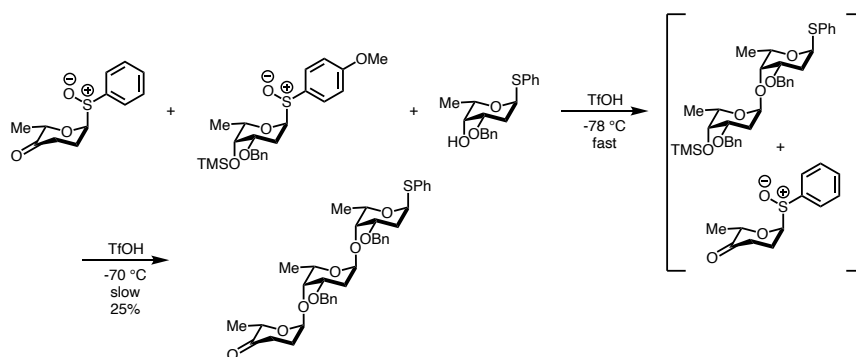


Figure 3-17 One-pot synthesis of ciclamycin trisaccharide.

Takahashi showed that not only is it possible to use various donor identities, but that the isolated, final yield of these one-pot glycosylations are higher than when carried out stepwise (Figure 3-17).⁴¹ Other seminal one-pot transformations have been reported by Kahne, Fraser-Reid, and Ley. Although decades of work have gone toward accessing long-chain, selective polysaccharides, chemical means to synthesize these biopolymers average at about only twelve units. One answer to this void in synthetic carbohydrate chemistry is automation. Wong developed one-pot programmable, automated methods which utilize virtual libraries to pair ideal combinations, but obstacles still persist, as reactivity is reliant on the donor design and known chemical methodology.^{27,42} Regardless of the intriguing selectivity and efficiency of these reactions, they still require the painstaking synthesis of each unique donor with particular, electronically-tailored protecting group schemes, and very specific overall reaction conditions.

Solid supported glycosylation transformations to access polysaccharides without the need for workup and purification, although were not initially, have recently become automated, as well. Seeberger's Automated Glycan Assembly (AGA), has been able to generate up to 50-unit polysaccharides, but requires the use of pre-programmed donor/acceptor combinations, thus limiting the extension to novel, potentially more efficient methods being developed. Though currently limited in scope and availability of equipment for use in organic labs, the work in the automation of glycosylation is slowly catching up to systems for the synthesis of other biopolymers.^{23,43}

Most of the glycosylations discussed above, while varying in strategic use of glycosylation methods, all tend to use well established glycosylation procedures, most of which employ

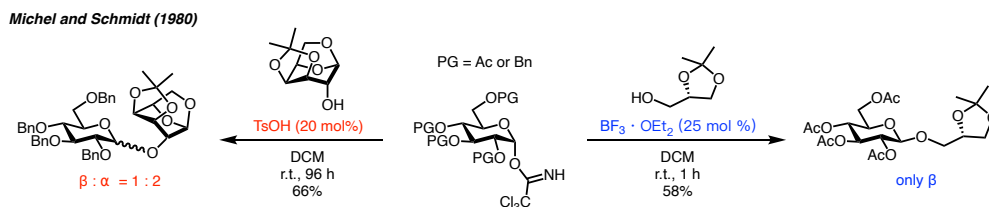


Figure 3-18 Early catalytic glycosylations in oligosaccharide synthesis.

stoichiometric, or superstoichiometric promoters to activate the anomeric leaving group. Inspired by early work by Sinaÿ, Michel and Schmidt demonstrated some of the first catalytic glycosylations (Figure 3-18).⁴⁴ This work has made trichloroacetimidates become the most heavily employed donor in catalytic glycosylations.¹¹ N-(phenyl)trifluoroacetimidate donors have also

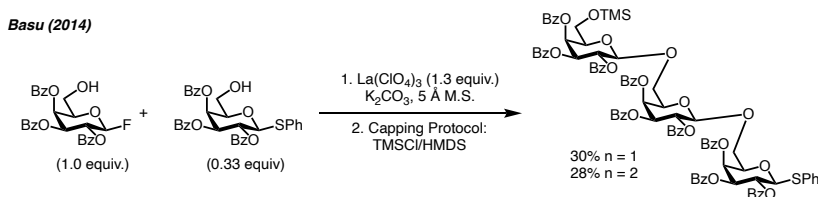


Figure 3-19 Lanthanum perchlorate promoted oligomerization of glycosyl fluorides.

found success in catalytic glycosylations developed by Yu.⁴⁵ Glycosyl fluorides were popularized by Mukaiyama (see Chapter 3.1.2), to offer boron-catalyzed procedures in a stepwise-type oligomer synthesis. The catalytic promoters range from Brønsted acids and organocatalysts, to standard transition metal complexes. While catalytic variants have been developed for various anomeric donors, these methods are still plagued with chemo- and stereoselectivity issues, necessary acceptor protecting group manipulations (after each iterative glycosylation), and often require workup and purification with each monosaccharide added (i.e. stepwise synthesis), thus limiting access to large oligosaccharides. Although few groups have shown success in using monosaccharides that act as both a donor and acceptor to allow for one-pot methods, scopes are narrow and oligomeric lengths remain low. Additionally, post-reaction protecting group manipulations are often required, moisture sensitivity is problematic, and stoichiometric metal catalysts are necessary for good conversion (Figure 3-19).⁴⁶ Current research in the field, including in the Montgomery lab,²⁰ aims to solve some of these challenges in the development of catalytic chemical glycosylations.

Enzymatic methods have been demonstrated on both on automated solid support, and in solution, with high stereo- and chemoselectivity for specific glycoside linkages.⁴⁷ Even so,

substrate specificity and narrow scope of enzymes, as well as the specialized equipment and knowledge-base required, limit access to effective biocatalytic polysaccharide synthesis.

Overall, the synthesis of polysaccharides is not a straightforward endeavor. Achieving a single chemo- and stereoselective glycosidic linkage, is challenging, but doing so in multiple successive iterations, can be insurmountable. Overcoming the inherent obstacles in preparing long-chain and/or branched glycan is of continued pursuit in the literature. While traditional chemical methods have been used for decades, the evolution of automated and enzymatic procedures have more recently allowed synthesis of longer polysaccharides. Yet, the limits of the solid support and enzymatic methods lie in access to specialized equipment and knowledge, which often precludes the average organic chemist from acquiring oligosaccharides in an efficient manner.

3.3.3 Strategies for the Synthesis of Dendrimers

Saccharide-dendrimers are not only are plagued by similar synthetic challenges faced in the construction of oligo- and polysaccharides, but also face new ones. The synthetic barriers and solutions, discussed regarding the synthesis of independent linear and branched oligosaccharides are the same for the glycans which decorate dendrimers, but due to the steric crowding around the central core, these challenges are attenuated.^{29,31,33} Further, the need for monodisperse oligomer length is critical for the three-dimensional shape and function of these nanomaterials. As previously discussed, the coveted multivalent interactions in which these dendric-materials engage, require well defined structural manipulations.^{2,24} In addition to these though, dendrimer synthesis faces challenges involving sugar appendage to the core, as well as choosing a glycosidic linkage which is not labile to final deprotection strategies, as the unprotected free hydroxyls are the state in which glycans function biologically. Most glyco-dendrimers are attached (via the N-

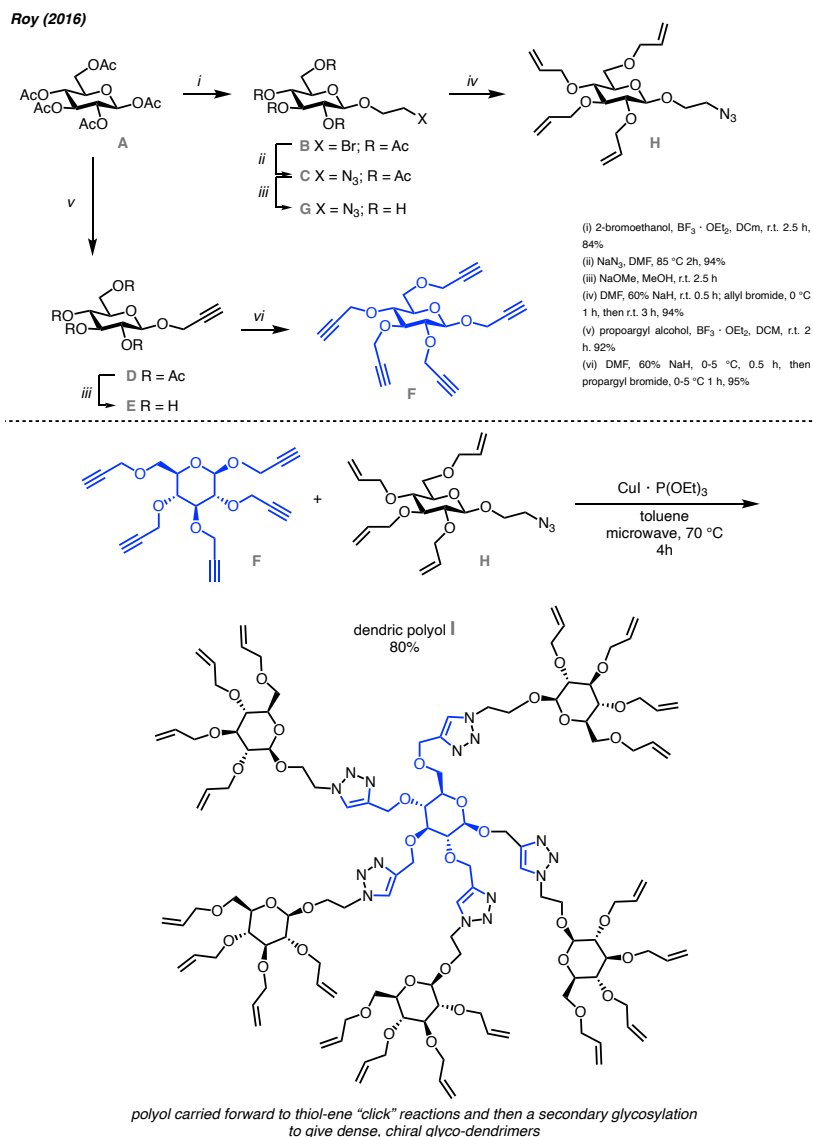


Figure 3-20 Representative glycol-dendrimer synthesis.

terminus) to commercially available alkylamines, like (propylene)imine (PPI), or polypeptides, such as polyamidoamine (PAMAM). Other cores, such as glycerol, cyclic polyols, and even simple glycosides have been explored as core structures, too, as they offer differing polarity, and potential for chirality at the center structure (Figure 3-20).^{33,48} The procedures necessary to construct the carbohydrate dendrimers that have been reported require numerous complex steps, protections, and purifications, though. Efficient transformations to synthesize dense, dendric-polyol sugars are limited. In general, full carbohydrate-based dendrimers are sparse in the literature. Typically, only

peripheral groups, rather than the branches, consist of glycosides (see Figure 3-20). This is likely due to the synthetic challenges in oligosaccharide synthesis. Accessing these types of these specific glyco-dendric architectures, and developing better methods to obtain them, could better allow study into their structure-function relationship, and potential biological applications.

3.4 Conclusion

Carbohydrates are the most common, and arguably, the most important biomolecules. Their value though, derives from the variations which exist in their polymeric forms, which unfortunately make them the most difficult biopolymers to synthesize. Because of this, the study of glycobiology has also lagged. Therefore, developing ways to efficiently construct basic glycosidic linkages is a very fruitful area of research. Furthermore, applying and optimizing these methods to make them amenable to the synthesis of large glycans and glycoconjugates (e.g. dendrimers), in a straightforward, user-friendly manner, is of need.

3.5 References

- (1) Bertozzi, C. R.; Kiessling, and L. L. Chemical Glycobiology. *Science* **2001**, *291* (5512), 2357–2364. <https://doi.org/10.1126/science.1059820>.
- (2) Kiessling, L. L. Chemistry-Driven Glycoscience. *Bioorg. Med. Chem.* **2018**, *26* (19), 5229–5238. <https://doi.org/10.1016/j.bmc.2018.09.024>.
- (3) *The Organic Chemistry of Sugars*; Levy, D. E., Fügedi, P., Eds.; Taylor & Francis: Boca Raton, 2006.
- (4) Sugar Polymers | BioNinja <https://ib.bioninja.com.au/standard-level/topic-2-molecular-biology/23-carbohydrates-and-lipids/sugar-polymers.html> (accessed Jun 15, 2020).
- (5) Das, R.; Mukhopadhyay, B. Chemical O-Glycosylations: An Overview. *ChemistryOpen* **2016**, *5* (5), 401–433. <https://doi.org/10.1002/open.201600043>.
- (6) *Handbook of Chemical Glycosylation*, 1st ed.; John Wiley & Sons, Ltd, 2008. <https://doi.org/10.1002/9783527621644>.
- (7) Adero, P. O.; Amarasekara, H.; Wen, P.; Bohé, L.; Crich, D. The Experimental Evidence in Support of Glycosylation Mechanisms at the SN1–SN2 Interface. *Chem. Rev.* **2018**, *118* (17), 8242–8284. <https://doi.org/10.1021/acs.chemrev.8b00083>.

- (8) Koenigs, W.; Knorr, E. Ueber Einige Derivate Des Traubenzuckers Und Der Galactose. *Berichte Dtsch. Chem. Ges.* **1901**, *34* (1), 957–981. <https://doi.org/10.1002/cber.190103401162>.
- (9) *Carbohydrates: The Essential Molecules of Life*; Elsevier, 2009. <https://doi.org/10.1016/B978-0-240-52118-3.X0001-4>.
- (10) Nicolaou, K. C.; Chucholowski, A.; Dolle, R. E.; Randall, J. L. Reactions of Glycosyl Fluorides. Synthesis of O-, S-, and A/-Glycosides. 2.
- (11) Nielsen, M. M.; Pedersen, C. M. Catalytic Glycosylations in Oligosaccharide Synthesis. *Chem. Rev.* **2018**, *118* (17), 8285–8358. <https://doi.org/10.1021/acs.chemrev.8b00144>.
- (12) Mukaiyama, T.; Murai, Y.; Shoda, S. An Efficient Method for Glucosylation of Hydroxy Compounds Using Glucopyranosyl Fluoride. *Chem. Lett.* **1981**, *10* (3), 431–432. <https://doi.org/10.1246/cl.1981.431>.
- (13) Hashimoto, S.; Hayashi, M.; Noyori, R. Glycosylation Using Glucopyranosyl Fluorides and Silicon-Based Catalysts. Solvent Dependency of the Stereoselection. *Tetrahedron Lett.* **1984**, *25* (13), 1379–1382. [https://doi.org/10.1016/S0040-4039\(01\)80163-5](https://doi.org/10.1016/S0040-4039(01)80163-5).
- (14) Kunz, H.; Sager, W. Stereoselective Glycosylation of Alcohols and Silyl Ethers Using Glycosyl Fluorides and Boron Trifluoride Etherate. *Helv. Chim. Acta* **1985**, *68* (1), 283–287. <https://doi.org/10.1002/hlca.19850680134>.
- (15) Mukaiyama, T. Explorations into New Reaction Chemistry. *Angew. Chem. Int. Ed.* **2004**, *43* (42), 5590–5614. <https://doi.org/10.1002/anie.200300641>.
- (16) Jona, H.; Mandai, H.; Chavasiri, W.; Takeuchi, K.; Mukaiyama, T. Protic Acid Catalyzed Stereoselective Glycosylation Using Glycosyl Fluorides. *Bull. Chem. Soc. Jpn.* **2002**, *75* (2), 291–309. <https://doi.org/10.1246/bcsj.75.291>.
- (17) Buchan, Z. A.; Bader, S. J.; Montgomery, J. Ketone Hydrosilylation with Sugar Silanes Followed by Intramolecular Aglycone Delivery: An Orthogonal Glycosylation Strategy. *Angew. Chem. Int. Ed.* **2009**, *48* (26), 4840–4844. <https://doi.org/10.1002/anie.200901666>.
- (18) Partridge, K. M.; Bader, S. J.; Buchan, Z. A.; Taylor, C. E.; Montgomery, J. A Streamlined Strategy for Aglycone Assembly and Glycosylation. *Angew. Chem. Int. Ed.* **2013**, *52* (51), 13647–13650. <https://doi.org/10.1002/anie.201307680>.
- (19) Walk, J. T.; Buchan, Z. A.; Montgomery, J. Sugar Silanes: Versatile Reagents for Stereocontrolled Glycosylation via Intramolecular Aglycone Delivery. *Chem. Sci.* **2015**, *6* (6), 3448–3453. <https://doi.org/10.1039/C5SC00810G>.
- (20) Sati, G. C.; Martin, J. L.; Xu, Y.; Malakar, T.; Zimmerman, P. M.; Montgomery, J. Fluoride Migration Catalysis Enables Simple, Stereoselective, and Iterative Glycosylation. *J. Am. Chem. Soc.* **2020**, jacs.0c03165. <https://doi.org/10.1021/jacs.0c03165>.
- (21) Levin, M. D.; Chen, T. Q.; Neubig, M. E.; Hong, C. M.; Theulier, C. A.; Kobylanskii, I. J.; Janabi, M.; O’Neil, J. P.; Toste, F. D. A Catalytic Fluoride-Rebound Mechanism for C(Sp³)-CF₃ Bond Formation. *Science* **2017**, *356* (6344), 1272–1276. <https://doi.org/10.1126/science.aan1411>.
- (22) Chitnis, S. S.; LaFortune, J. H. W.; Cummings, H.; Liu, L. L.; Andrews, R.; Stephan, D. W. Phosphorus Coordination Chemistry in Catalysis: Air Stable P(III)-Dications as Lewis Acid Catalysts for the Allylation of C–F Bonds. *Organometallics* **2018**, *37* (24), 4540–4544. <https://doi.org/10.1021/acs.organomet.8b00686>.
- (23) Delbianco, M.; Kononov, A.; Poveda, A.; Yu, Y.; Diercks, T.; Jiménez-Barbero, J.; Seeberger, P. H. Well-Defined Oligo- and Polysaccharides as Ideal Probes for Structural

- Studies. *J. Am. Chem. Soc.* **2018**, *140* (16), 5421–5426. <https://doi.org/10.1021/jacs.8b00254>.
- (24) Yu, Y.; Tyrikos-Ergas, T.; Zhu, Y.; Fittolani, G.; Bordoni, V.; Singhal, A.; Fair, R. J.; Grafmüller, A.; Seeberger, P. H.; Delbianco, M. Systematic Hydrogen-Bond Manipulations To Establish Polysaccharide Structure–Property Correlations. *Angew. Chem. Int. Ed.* **2019**, *58* (37), 13127–13132. <https://doi.org/10.1002/anie.201906577>.
- (25) Lapasin, R.; Pricl, S. *Rheology of Industrial Polysaccharides: Theory and Applications*; Springer US: Boston, MA, 1995. <https://doi.org/10.1007/978-1-4615-2185-3>.
- (26) *Essentials of Glycobiology*, 2nd ed.; Varki, A., Cummings, R. D., Esko, J. D., Freeze, H. H., Stanley, P., Bertozzi, C. R., Hart, G. W., Etzler, M. E., Eds.; Cold Spring Harbor Laboratory Press: Cold Spring Harbor (NY), 2009.
- (27) Krasnova, L.; Wong, C.-H. Oligosaccharide Synthesis and Translational Innovation. *J. Am. Chem. Soc.* **2019**, *141* (9), 3735–3754. <https://doi.org/10.1021/jacs.8b11005>.
- (28) Mandal, S. S.; Liao, G.; Guo, Z. Chemical Synthesis of the Tumor-Associated Globo H Antigen. *RSC Adv.* **2015**, *5* (30), 23311–23319. <https://doi.org/10.1039/C5RA00759C>.
- (29) Abbasi, E.; Aval, S. F.; Akbarzadeh, A.; Milani, M.; Nasrabadi, H. T.; Joo, S. W.; Hanifehpour, Y.; Nejati-Koshki, K.; Pashaei-Asl, R. Dendrimers: Synthesis, Applications, and Properties. *Nanoscale Res. Lett.* **2014**, *9* (1), 247. <https://doi.org/10.1186/1556-276X-9-247>.
- (30) Wolfenden, M. L.; Cloninger, M. J. Mannose/Glucose-Functionalized Dendrimers To Investigate the Predictable Tunability of Multivalent Interactions. *J. Am. Chem. Soc.* **2005**, *127* (35), 12168–12169. <https://doi.org/10.1021/ja053008n>.
- (31) Wolfenden, M. L.; Cloninger, M. J. Carbohydrate-Functionalized Dendrimers To Investigate the Predictable Tunability of Multivalent Interactions. *Bioconjug. Chem.* **2006**, *17* (4), 958–966. <https://doi.org/10.1021/bc060107x>.
- (32) Madaan, K.; Kumar, S.; Poonia, N.; Lather, V.; Pandita, D. Dendrimers in Drug Delivery and Targeting: Drug-Dendrimer Interactions and Toxicity Issues. *J. Pharm. Bioallied Sci.* **2014**, *6* (3), 139–150. <https://doi.org/10.4103/0975-7406.130965>.
- (33) Liu, J.; Gray, W. D.; Davis, M. E.; Luo, Y. Peptide- and Saccharide-Conjugated Dendrimers for Targeted Drug Delivery: A Concise Review. *Interface Focus* **2012**, *2* (3), 307–324. <https://doi.org/10.1098/rsfs.2012.0009>.
- (34) Xiao, R.; Grinstaff, M. W. Chemical Synthesis of Polysaccharides and Polysaccharide Mimetics. *Prog. Polym. Sci.* **2017**, *74*, 78–116. <https://doi.org/10.1016/j.progpolymsci.2017.07.009>.
- (35) Panza, M.; Pistorio, S. G.; Stine, K. J.; Demchenko, A. V. Automated Chemical Oligosaccharide Synthesis: Novel Approach to Traditional Challenges. *Chem. Rev.* **2018**, *118* (17), 8105–8150. <https://doi.org/10.1021/acs.chemrev.8b00051>.
- (36) Ueber einige bei den versuchen zur Synthese des Tyrosins gewonnene Derivate der Zimmtsäure. *Justus Liebigs Ann. Chem.* **1883**, *219* (2), 179–233. <https://doi.org/10.1002/jlac.18832190204>.
- (37) Nicolaou, K. C. Stereocontrolled Synthesis of Sialyl Lex, the Oligosaccharide Binding Ligand to ELAM-I (Sialyl = A/-Acetylneuramin). 3.
- (38) Mootoo, D. R.; Konradsson, Peter.; Udodong, Uko.; Fraser-Reid, Bert. Armed and Disarmed N-Pentenyl Glycosides in Saccharide Couplings Leading to Oligosaccharides. *J. Am. Chem. Soc.* **1988**, *110* (16), 5583–5584. <https://doi.org/10.1021/ja00224a060>.

- (39) Cao, S.; Gan, Z.; Roy, R. Active-Latent Glycosylation Strategy toward Lewis X Pentasaccharide in a Form Suitable for Neoglycoconjugate Syntheses. *Carbohydr. Res.* **1999**, *318* (1–4), 75–81. [https://doi.org/10.1016/s0008-6215\(99\)00080-4](https://doi.org/10.1016/s0008-6215(99)00080-4).
- (40) Boons, G.-J.; Isles, S. Vinyl Glycosides in Oligosaccharide Synthesis (Part 1): A New Latent-Active Glycosylation Strategy. *Tetrahedron Lett.* **1994**, *35* (21), 3593–3596. [https://doi.org/10.1016/S0040-4039\(00\)73249-7](https://doi.org/10.1016/S0040-4039(00)73249-7).
- (41) Yamada, H.; Harada, T.; Miyazaki, H.; Takahashi, T. One-Pot Sequential Glycosylation: A New Method for the Synthesis of Oligosaccharides. *Tetrahedron Lett.* **1994**, *35* (23), 3979–3982. [https://doi.org/10.1016/S0040-4039\(00\)76718-9](https://doi.org/10.1016/S0040-4039(00)76718-9).
- (42) Cheng, C.-W.; Zhou, Y.; Pan, W.-H.; Dey, S.; Wu, C.-Y.; Hsu, W.-L.; Wong, C.-H. Hierarchical and Programmable One-Pot Synthesis of Oligosaccharides. *Nat. Commun.* **2018**, *9* (1), 5202. <https://doi.org/10.1038/s41467-018-07618-8>.
- (43) Guberman, M.; Seeberger, P. H. Automated Glycan Assembly: A Perspective. *J. Am. Chem. Soc.* **2019**, *141* (14), 5581–5592. <https://doi.org/10.1021/jacs.9b00638>.
- (44) Schmidt, R. R.; Michel, J. Facile Synthesis of α - and β -O-Glycosyl Imidates; Preparation of Glycosides and Disaccharides. *Angew. Chem. Int. Ed. Engl.* **1980**, *19* (9), 731–732. <https://doi.org/10.1002/anie.198007311>.
- (45) Yu, B.; Tao, H. Glycosyl Trifluoroacetimidates. Part 1: Preparation and Application as New Glycosyl Donors. *Tetrahedron Lett.* **2001**, *42* (12), 2405–2407. [https://doi.org/10.1016/S0040-4039\(01\)00157-5](https://doi.org/10.1016/S0040-4039(01)00157-5).
- (46) Dräger, M.; Basu, A. Galactan Synthesis in a Single Step via Oligomerization of Monosaccharides. *Beilstein J. Org. Chem.* **2014**, *10* (1), 2658–2663. <https://doi.org/10.3762/bjoc.10.279>.
- (47) Wen, L.; Edmunds, G.; Gibbons, C.; Zhang, J.; Gadi, M. R.; Zhu, H.; Fang, J.; Liu, X.; Kong, Y.; Wang, P. G. Toward Automated Enzymatic Synthesis of Oligosaccharides. *Chem. Rev.* **2018**, *118* (17), 8151–8187. <https://doi.org/10.1021/acs.chemrev.8b00066>.
- (48) Shiao, T. C.; Rej, R.; Rose, M.; Pavan, G. M.; Roy, R. Synthesis of Dense and Chiral Dendritic Polyols Using Glyconanosynthon Scaffolds. *Molecules* **2016**, *21* (4). <https://doi.org/10.3390/molecules21040448>.

Chapter 4

Progress Towards the Synthesis of Complex Polysaccharides via Triarylborane

Catalysis

4.1 Motivation and Project Goals

The Montgomery group recently developed a catalytic method for the rapid and selective glycosylation of glycosyl fluoride donors and silyl protected acceptor monosaccharides, employing tris(pentafluorophenyl)borane (BCF).¹ With insights gained from these studies, we hypothesized that if we could synthesize bifunctional glycosyl fluoride donors with silyl-protected hydroxyl acceptor groups within the same unit, polysaccharides of various length and branching characteristic could be accessed via a one-pot, rapid and systematic chain-growth polymerization

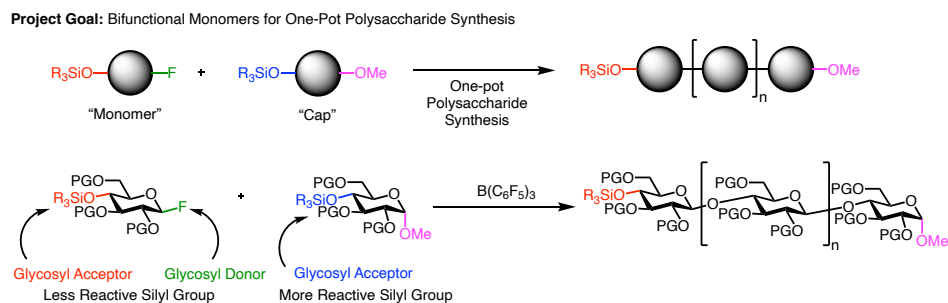


Figure 4-1 Project goals for a triarylborane-catalyzed polysaccharide synthesis.

(Figure 4-1). Although the report details iterative access to oligosaccharides, straightforward methods to synthesize long-chain, uniform polydispersity polysaccharides is still a gap in the carbohydrate literature.^{2,3}

One key feature of this report by Montgomery was the use of different sized the silyl ethers, which can act as orthogonal protecting groups. Smaller, less sterically hindered silicon protecting

groups led to faster reactions with BCF, allowing for chemoselective glycosylations. Therefore, we believed that inclusion of a “cap,” with a more reactive, sterically accessible (smaller) silane under our catalytic conditions could serve as the initiator for the growing polysaccharide chain, and result in a controlled oligomerization. Further, the unreactive (under BCF conditions) anomeric methoxide group would ensure the glycoside would act only as an acceptor in the reaction mixture. Ideally, optimizing the stoichiometry between cap and bifunctional monomer could offer access to programmable polysaccharide lengths and identity.

Sparse examples of one-step polymerizations with glycosyl fluorides do exist, but in addition to only short oligosaccharides formed, the glycan synthesis requires precious metal catalysts, and do not employ versatile silyloxy-acceptors.^{4,5} In summary, this project aims to synthesize a variety of glycosyl fluoride monomers and access complex glycans via a systematic, one-pot polymerization method.

4.2 Initial Strategy for Polysaccharide Synthesis

Our initial experimental design for the polymerization, is outlined below (Figure 4-2). We hypothesized that our bifunctional monomer **4-4**, with the given protecting group scheme, would

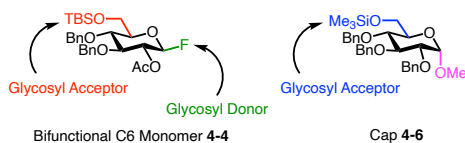


Figure 4-2 Initial hypothesis and bifunctional C6 monomer.

be most successful in the glycosylation reaction. We installed the silyl group at C6, as the primary hydroxyl situated above the plane of the hexose would make it the most accessible acceptor for the fluoride migration catalysis. We chose to protect with *tert*-butyldimethylsilyl chloride (TBSCl), as this group is relatively large, which would allow for a slower, and thus, more

controlled glycosylation. Benzylating the remaining free hydroxyls would ensure the sugar units were armed for glycosylation. These armed (electron-rich, reactive) glycosyl donors, would ensure rapid formation of the oxocarbenium ion after fluoride abstraction by the BCF catalyst, and thus efficient addition to the growing polymer. Finally, as discussed above, inclusion of a monosaccharide (4-6) protected with a less sterically encumbered silyloxy protecting group, trimethylsilyl, might provide a predictable chain initiation event.

4.2.1 Synthesis of the C6 Monomer

My work in this area began with the development of various syntheses to access silyloxy-protected glycosyl fluorides. These glycosyl fluorides are challenging to synthesize, requiring meticulous route scouting and judicious selection of orthogonal protecting groups.

While the C6 position is typically straightforward to protect selectively, due to acidity (and nucleophilicity) differences between the hydroxyls on glucose,⁶ stereo- and chemo-selectively installing a fluorine atom into the monomer was expected to be more of a challenge. The highly nucleophilic fluoride, and the strong fluoro-philicity of silicon, makes installing these reactive units within the same molecule, challenging. Further, most nucleophilic fluoride sources, such as HF and HF-pyridine, pose safety concerns. In surveying the literature, we found that the more mild fluorine source, diethylaminosulfurtrifluoride (DAST), which is typically used for the nucleophilic displacement of free hydroxyls, had been shown to selectively attack the anomeric position of fully-protected glycoside ortho-esters.⁷ Although sparse in examples, promising results with much

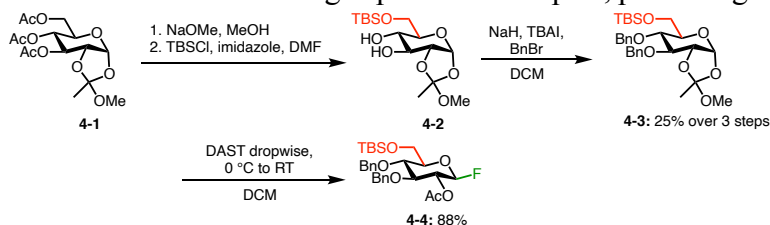


Figure 4-3 Synthesis of bifunctional C6 monomer.

stronger HF-pyridine reassured us that fluoride could be installed in the presence of bulky silyl groups with mild success.⁸

With this insight, we carried out the synthesis of a bifunctional glucose fluoride (Figure 4-3). Beginning with an ortho-ester derived from glucose penta-acetate (**4-1**), the glycoside was deprotected to give the triol, leaving the ortho-ester intact. The C6 hydroxyl was then selectively silylated, based on the higher nucleophilicity of the primary hydroxyl. Benzyl-ether protection of the C3 and C4 give intermediate **4-3**. Finally, we were pleased to observe that, under temperature-controlled conditions, DAST added dropwise, gave stereospecific fluorination of the anomeric carbon, and thus our desired bifunctional fluoride **4-4** in high yield. A mannose variant (**4-5**) was also synthesized using the same synthetic approach.

4.2.2 Initial Polymerization Results

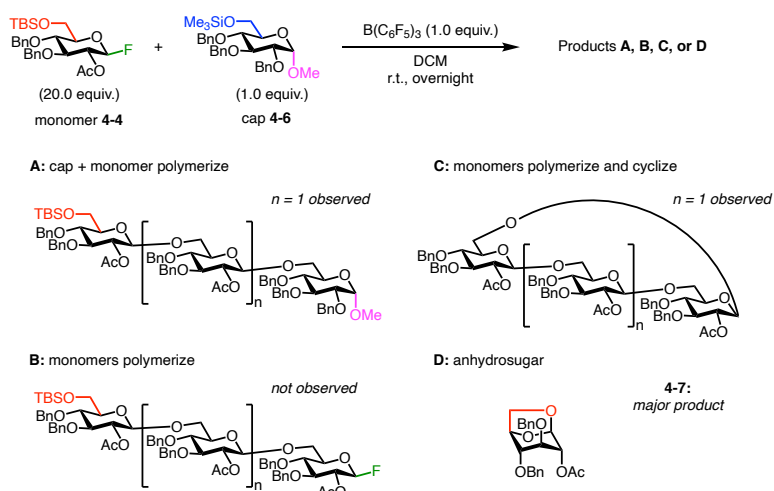


Figure 4-4 Initial C6 monomer polymerization results.

With our bifunctional monomer in hand, we began initial screens for the tris(pentafluorophenyl)borane-catalyzed polymerization. Under air-free conditions, BCF was added to a round-bottom flask, followed by a solution of our cap **4-6**. Our glucose bifunctional monomer (**4-4**) was added as a solution to the rapidly stirring mixture. This setup was chosen,

under the assumption that with this specific addition sequence, 1.0 equivalent of BCF would activate 1.0 equivalent of glycosyl fluoride, which would then react with all capped-acceptors (**4-6**). The remaining bifunctional monomer would then be activated by the regenerated BCF catalyst and enable glycosylation on the growing chain. Reactions were stirred overnight and analyzed (Figure 4-4).

Unfortunately, only trace amount of desired product **A** ($n = 1$, trimer) was observed, with the major product isolated as product **D** (**4-7**), the 1,6-anhydrosugar. This undesired product is formed due to a ring-flip followed by the intramolecular reaction between the donor and acceptor unit on the same monosaccharide. Another potential product outcome, which was not observed, is the homopolymerization of the silyl-protected glycosyl fluorides (product **B**). Product **C** ($n = 1$, cyclic trimer) though, resulting from the intramolecular reaction between the reactive ends of a homopolymer was observed by HRMS and crude ^1H NMR.

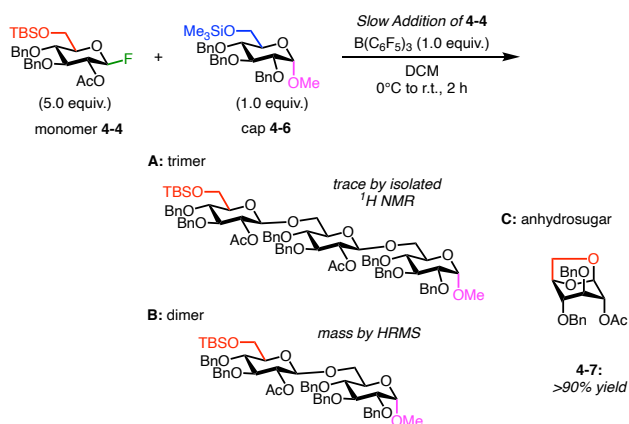


Figure 4-5 Initial C6 monomer polymerization with slow addition.

Moving forward we wondered if employing a slow addition protocol could aid in the formation of longer oligomers and preclude anhydrosugar formation. Theoretically, under this setup, with each dropwise addition of glycosyl fluoride, once the more reactive silyl acceptor was consumed (cap), glycosylation would continue in a controlled fashion on the growing chain. We were excited to see no formation of homopolymers, as the trimers (Product **A**) and dimers (Product

B) observed by HRMS and ^1H NMR appeared to have incorporated the capping monosaccharide (Figure 4-5). Unfortunately, though, slow-addition procedures did not prove to be helpful in terms of the intramolecular reaction (4-7). The anhydrosugar was the major product, isolated in 90% yield. It became apparent to us that the reaction between the intramolecular donor and acceptor was much faster than the desired, intermolecular glycosylation.

4.3 Progress Towards Strategic Polysaccharide Synthesis

Current work in borane-catalyzed polysaccharide synthesis focuses on optimizing conditions and exploring potential roadblocks, such as deglycosylation, in accessing large polysaccharides. In doing so, various bifunctional monomers were synthesized to address issues, as they arose.

4.3.1 Modified Strategy and C4 Monomer Synthesis

We postulated that if we installed the silyl acceptor at the C4 of bifunctional monosaccharide, we could geometrically prevent the intramolecular product (Figure 4-6). To do this, a very particular synthetic strategy was envisioned, as selective protection of the C3 and C4 hydroxyls of hexose is not typically straightforward, due to their minimal reactivity differences.^{6,9}

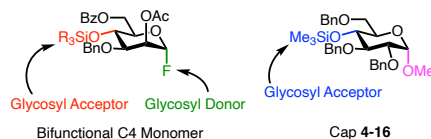


Figure 4-6 Modified hypothesis and bifunctional C4 monomer.

In addition to the previous discussed installation of a fluoride and silyl group together, other synthetic hurdles were likely due to the tedious protecting group manipulations required for the appropriate regio- and stereoselective design. We were pleased to see that after a significant

amount of tuning of reaction and purification conditions, we were able to selectively and cleanly synthesize mannose fluoride **4-15** on large scale, and in moderate yield (Figure 4-7).

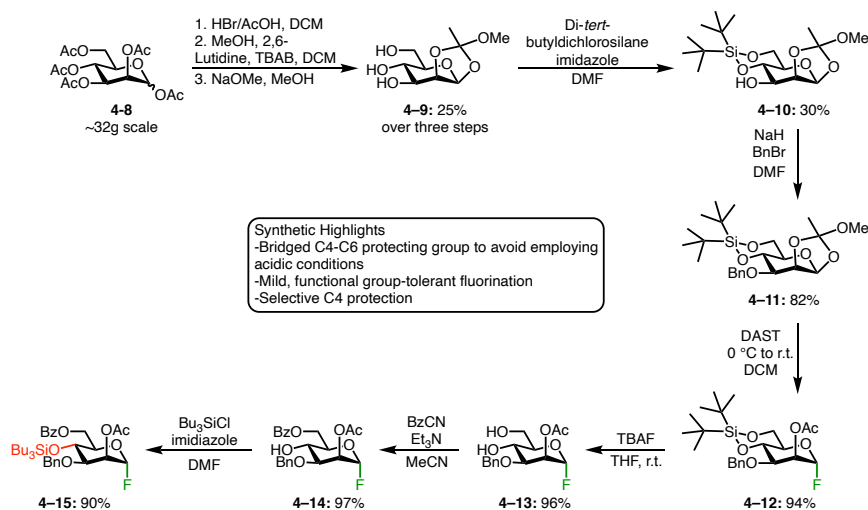


Figure 4-7 Synthesis of bifunctional C4 monomer.

The synthesis was carried out in nine linear steps, starting with mannose- pentaacetate **4-8**. After carrying out bromination at the anomeric carbon, orthoester formation, and methanolysis, the triol (**4-9**) could be isolated in moderate yield. To achieve selective silylation of the C4 hydroxyl, we first needed to protect the C6 and C3 positions. While typically employing a benzylidene protecting group might achieve this, because of the ortho-ester acid sensitivity, this strategy would not work. Fortunately though, after assessing various synthetic routes in the literature,¹⁰ we found employing a bridged silyl C4-C6 protecting group, **4-10** could be isolated cleanly, which allowed for the subsequent C3 selective benzylation (**4-11**). Although initial concerns were raised again regarding the installation of the alpha fluoride in the presence of this more labile silyl group, we were pleased to see clean, stereoselective mono-fluorination at only the anomeric position. At this point, **4-12** could be deprotected to give high yields of **4-13**. Next, employing a technique known as the cyanide effect,¹¹ the primary C6 hydroxyl could be regioselectively benzoylated (**4-14**), which left a free alcohol to be silylated with the silyl chloride of choice. In addition to the tributylsilyl-protected bifunctional monomer depicted in this synthesis

(4-15), other monomers with varying sized-silyloxy groups were also synthesized using the same route (Figure 4-8), as well as the corresponding 4-trimethylsilyl protected cap (4-16). Finally, other C4 silyl-protected glycosyl fluorides (4-19 and 4-20) were synthesized from maltose after initial screening begun. Although it is used as a mixture of anomers, its more expedient synthetic route (discussed in Chapter 4.3.5) allowed for faster access to material and more rapid optimization.

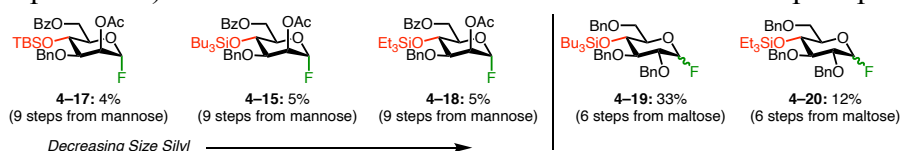


Figure 4-8 Initial C4 monomers examined.

4.3.2 Polymerization Results with a C4 Monomer

With our ideal bifunctional monosaccharides and capping units in hand, screening for ideal polymerization conditions began. Initially, a similar setup was used as when analyzing the viability of the C2 monomer; Under nitrogen, a mixture of catalyst and cap were stirred, and the highly-diluted monosaccharide of choice was slowly added by syringe pump (Figure 4-9), and then stirred until complete by TLC, often overnight. Because of positive results observed in both the C6 and now C4 oligosaccharide synthesis, this procedure was continued.

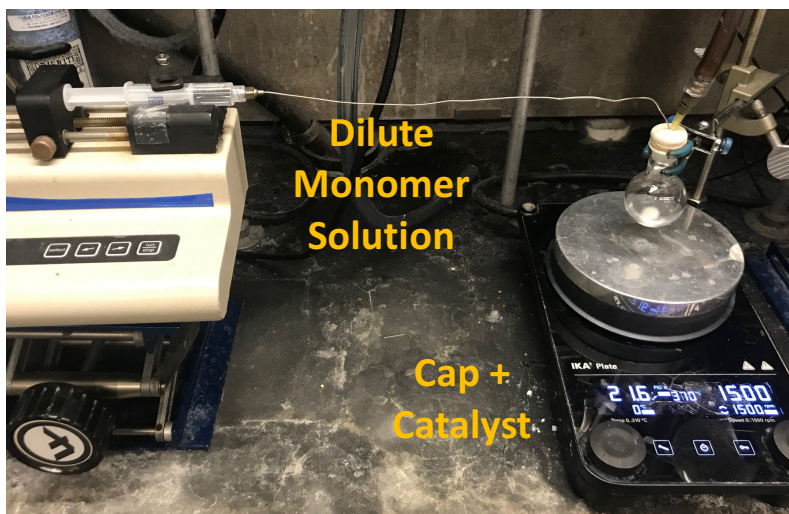


Figure 4-9 Syringe-pump polymerization setup.

It is important to note that higher loading of catalyst was initially used for ease handling, under the assumption that in the early fluoride migration work, extremely low to relatively high loadings of BCF resulted in generally equal, high yielding product formations. Regardless, changes in catalyst loading appeared to have little to no effect on polymerization results. Additionally, the monomer solution added dropwise was kept at very dilute concentration, and although held consistent in the experiments discussed in his chapter, variation in this parameter also showed no effect on polymerization results.

Early results were promising. Immediate analysis of the reaction revealed that, as we had predicted, the new monosaccharide design had precluded the formation of the anhydrosugar.

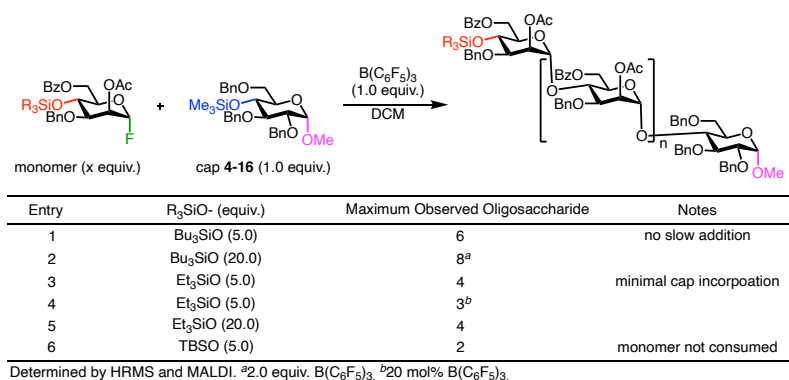


Table 4-1 Initial screen of C4 monomers in triarylborane catalyzed polysaccharide synthesis.

Moderately sized oligosaccharides were formed instead. Reaction optimization analyzed by MALDI and HRMS, revealed a clear relationship between size of silyl acceptor, and length of oligomer (Table 4-1). Specifically, the tributyl silyl protecting group was found to be ideal (entries 1-2). Likely, the intermediate size of this silyloxy protected acceptor gives the best reactivity for the BCF catalyst; slow enough to react with the cap, and small enough to participate in the fluoride migration, and thus consumed in the transformation. Smaller triethylsilyl-protected acceptors were consumed more rapidly (as monitored by TLC), and primarily resulted in masses corresponding to homo-polymerization of **4-18**, with significant lack of cap **4-16** incorporation. The formation of

these undesired “hydrolysis products,” with a hydroxyl at either end of the polymer was surprising to us, and was attributed to the fast reactivity of triethylsilyl acceptors, but the mechanism by which these oligosaccharides were formed, was unclear. Interestingly, changing the loading of catalyst and altering the ratio of monomer to cap seemed to have little effect on the reaction results (entries 3-5). On the contrary, the much bulkier *tert*-butyldimethylsilyl (TBS) acceptor was not consumed in the reaction, even when left to stir overnight after syringe-pump addition of the monomer (entry 6). The major problems which plagued our system included both experimental setup complications, and the “undesired” oligomer formation. Namely, evaporation of solvent during the slow addition, due to rapid stirring and high nitrogen pressure, would alter the final concentration of the reaction, but results remained unchanged after experiments were properly repeated. More detrimental though, was the lack of cap incorporation, as well as oligosaccharides without silyl protecting groups consistently observed by MALDI, and those (initially) analyzed by ¹H NMR. No change in conditions seemed to favor formation of the desired product over the large

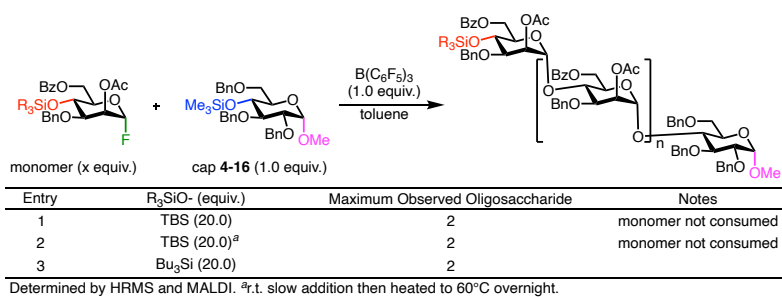


Table 4-2 Preliminary solvent and temperature screen of C4 monomers in triarylborane catalyzed polysaccharide synthesis.

unpredictable mixture of deprotected, homopolymerized, and hydrolyzed oligosaccharides.

Moving forward, we examined the effect of solvent on the polymerization, as the original fluoride migration can be performed in both polar (DCM) and non-polar solvents, and result in equally effective glycosylations (Table 4-2). We believed the higher boiling point of toluene might also solve evaporation problems. Additionally, we wondered if potentially the lack of reactivity

with TBS-saccharides could be resolved with elevated temperatures, but unfortunately, low monomer conversion and oligomer length prevailed (entries 1-2). Even the tributylsilyl acceptors gave only up to disaccharides in toluene (entry 3). Furthermore, the desilylation, and lack of cap incorporation persisted.

We also examined the maltose-derived bifunctional monomers (**4-19**), as they offered a different protecting group scheme, specifically one was slightly more electron-rich, and thus

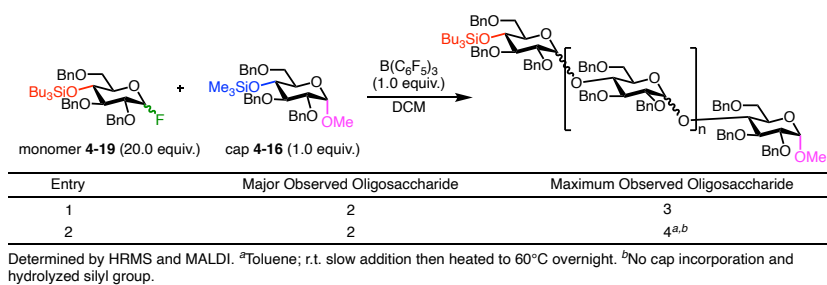


Table 4-3 Preliminary screen of monomer 4-19 in triarylborane catalyzed polysaccharide synthesis.

“armed” for glycosylation (Table 4-3). Additionally, this other monomer was a glucoside (as opposed to mannoside typically used), existed as a mixture of anomers, and offered a potentially different steric profile. These characteristics seemed to be inconsequential, or potentially unhelpful in the one-pot glycosylation. The same **4-15** trimethylsilyl cap was used as the initiator, as well as the most efficient, intermediate-sized silyl protecting group (Bu_3Si) on the acceptor unit. Slightly larger product masses were observed with increased temperatures, but the larger oligomers lacked both cap incorporation and a silyl protecting group. This monomer is potentially more reactive than **4-15**, and thus only results in smaller oligosaccharides than those observed in early studies. With fast fluoride abstraction, homodimerization seemed to be a major problem, as well as deprotection of the necessary acceptor unit.

Changing directions, we wondered if sequentially, or iteratively adding a range of different-sized silyl protected monomers to the single-pot reaction would give a slow oligomerization. Because the major oligosaccharides were limited to about two or three units, we

thought that potentially this approach could serve to control the growth of these glycans, and moreover serve as a proof of concept for the synthesis of polysaccharides with alternating blocks

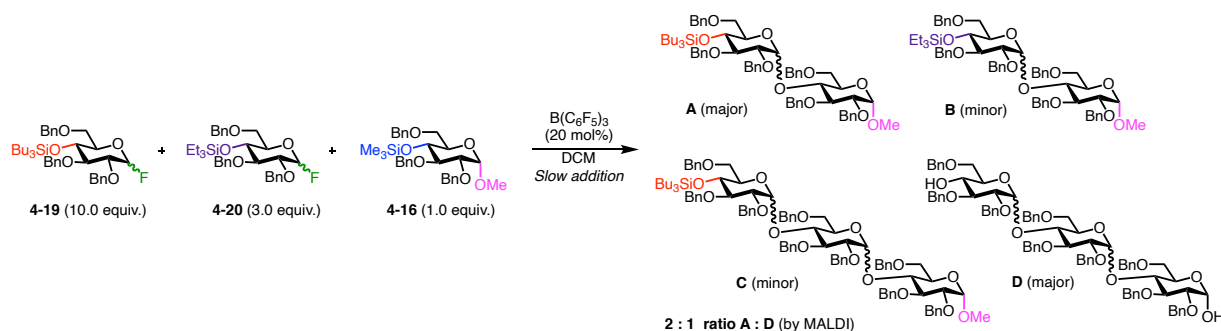


Figure 4-10 Iterative addition polymerization experiment.

of sugars. The glycosides would be added in order of reactivity of the silyl acceptor, as previously described correlation with size, which would allow for full consumption of each monomer before injection of the next.

In the first experiment, with the cap (**4-16**) stirring in a flask with the BCF catalyst, **4-20** was added via syringe, and after about 30 minutes, when **4-20** was consumed by TLC, **4-19** was incorporated to the reaction mixture (Figure 4-10). We were surprised to find that while the desired tributylsilyl-protected trimer **C** (with cap incorporation) was formed in the reaction, this was not the major product, but rather observed in only trace amounts. Rather, MALDI analysis revealed the major glycan to be a disaccharide **A** which corresponded to a tributylsilyl donor/acceptor linked to a trimethylsilyl-cap. This result suggested that either there was unreacted TMS cap before addition of the last monomer **4-19**, or some deglycosylation, or silyl-migration event occurring within the reaction mixture, to form the mis-matched disaccharide. Due to the rapid rates of the fluoride migration catalysis and reaction monitoring, the possibility of having unreacted cap in solution is highly unlikely. The other major oligosaccharide observed was a trisaccharide with no anomeric methoxide or protected terminus (**D**). Even attempting to bias the system, following a

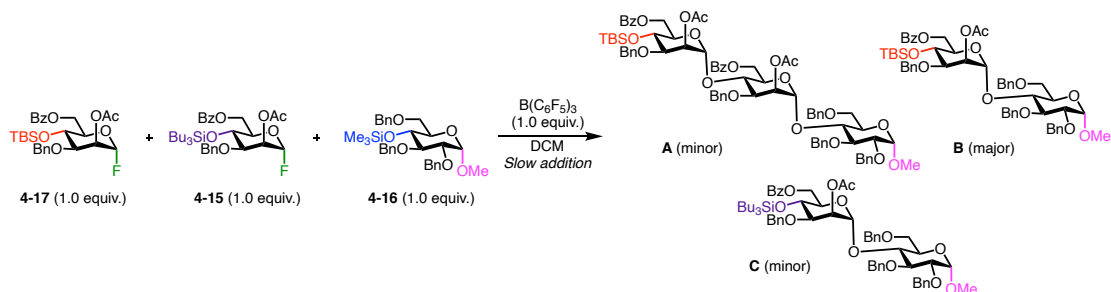


Figure 4-11 Follow up iterative addition polymerization experiment.

similar experimental setup, but with less reactive (larger) silyloxy sugar monomers (**4-17**), and one equivalent of each unit, resulted in major products (**B**) of deglycosylation and dimer (**C**) were still the major glycosides (Figure 4-11).

With these extensive screens completed, we still faced issues regarding not only minimal oligosaccharide lengths, but more perplexing, the lack of cap incorporation, and apparent desilylation. Mass of these hydrolyzed products, as well as no presence of fluoride in the crude NMRs led us to believe some detrimental pathway was occurring, rather than simply lack of substrate conversion. We postulated that this mass observed for the oligosaccharides with hydroxyl groups either end was due to the cleavage (in some yet to be determined mechanism) of a longer polysaccharide, which once contained the correct terminus (silyl) and/or the initiator (cap). The potential for deglycosylation was explored in more detail for this polysaccharide project, as well as in follow-up work in the fluoride migration work which is discussed further in Chapter 4.3.4.

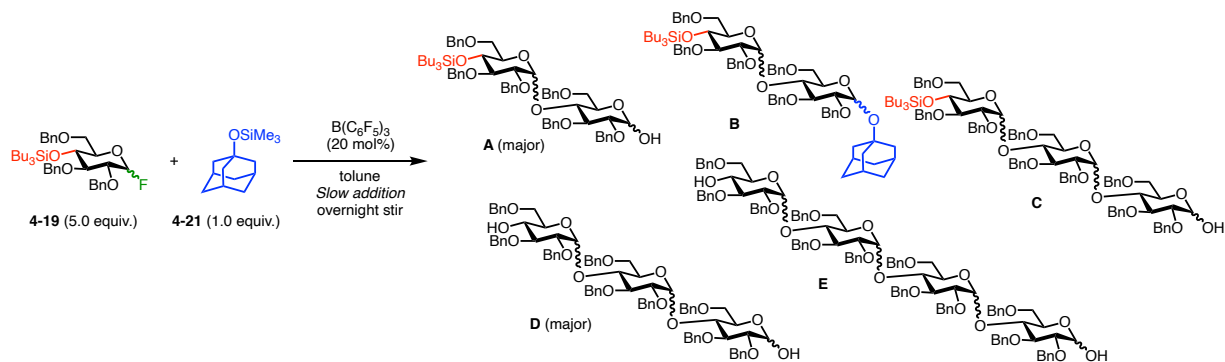


Figure 4-12 Polymerization experiment with adamantol acceptor: slow addition, extended stir.

Hoping to better understand and potentially amend some of these issues, we chose to test our poly-glycosylation using a more reactive aglycone acceptor, which could also allow for clear

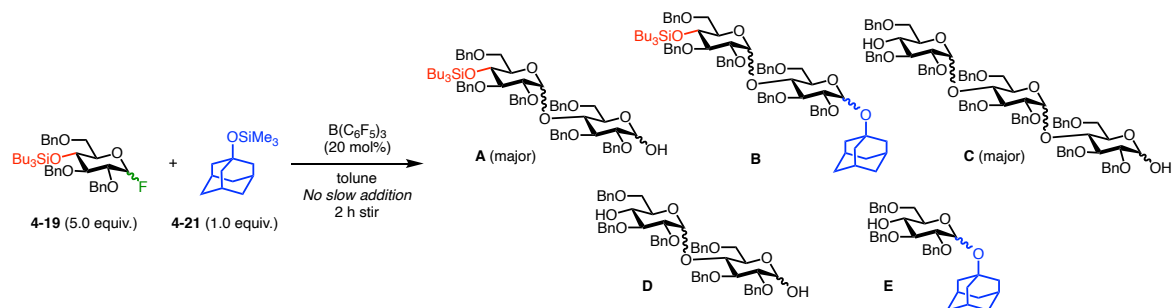


Figure 4-13 Polymerization experiment with adamantol acceptor: no slow addition, two hour stir.

mass analysis of capping unit incorporation (Figure 4-12). With 2-(trimethylsilyloxy)adamantane (**4-21**) and a catalytic amount of BCF, our bifunctional monosaccharide was introduced by syringe drive, and then stirred overnight. Although three-unit oligomers with adamantol incorporated (**B**), the major products were corresponding to not only those that did not have glycosylated adamantol, but more importantly those which had no silyl group, either. This confirmed our previous results. Interestingly, when this experiment was repeated without slow addition (2 hours), while oligomer masses were the same and smaller (thus apparently supporting our initial realization that slow, controlled growth was ideal), cap-incorporated glycoconjugates were not major (Figure 4-13). Surprisingly though, in a final experiment using the TMS-protected adamantol acceptor (**4-21**), when the reaction was added in whole after the slow addition had begun, and then let stir for only

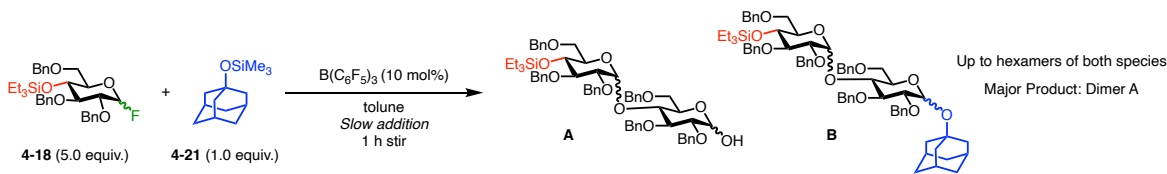


Figure 4-14 Polymerization experiment with adamantol acceptor: slow addition, one hour stir.

an hour, much larger oligomers were observed by MALDI, (Figure 4-14). This result contradicted our previous hypothesis that the longer slow addition (and subsequent stir times) were needed to allow for growth of the polymer. Looking back at previous results in this new light revealed that,

while slow addition might be beneficial for this C4 monomer, longer reaction times following the syringe pump addition was detrimental. Potentially the deglycosylation event is happening concurrently with the glycosylation, but once the polysaccharide has reached its given polydispersion, due to the monomer/cap loading, decomposition pathways degrade the previously formed oligomers. This is currently a working hypothesis and must be explored more fully.

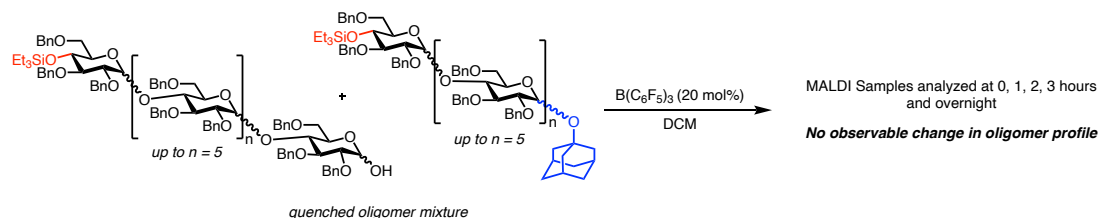


Figure 4-15 Adamantol oligosaccharides: deglycosylation experiment.

Various control experiments were carried out to further investigate this. First, the mixture of oligomers obtained in the adamantol experiment outlined in Figure 4-14 was subjected to catalytic BCF. MALDI samples were taken at various time points, but no observable changes in oligomer profile was noted (Figure 4-15). This result was complicated, as it implied that deglycosylation or decomposition of oligomers was not occurring by catalyst insertion alone. We believed that it was likely necessary to have a fluoride source, or some other basic moiety in solution, but no further work was done to this end.

Overall, despite prevention of the undesired anhydride sugar formation, as well as desired formation of oligomers of moderate length (up to ~8 units), complication plagued the reaction. Although larger oligosaccharide lengths could be achieved, the major products were typically disaccharides. Most unfortunately though, the mixtures of products were dominated by hydrolyzed homopolymer units, lacking both the chain initiator (cap) and silyl-protected terminus, which ultimately informed us of an irremediable glycan-degradation pathway.

4.3.3 Polymerization Results with a C2 Monomer

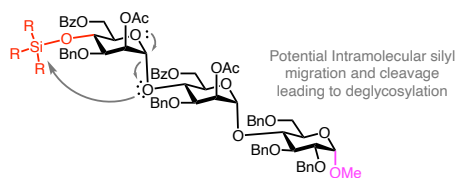


Figure 4-16 Potential silyl migration occurring with C4 bifunctional monosaccharide.

Despite the moderate oligosaccharides accomplished, the challenges regarding deglycosylation and accessing more monodisperse glycans was desired. Going back to our original approach to the polysaccharide synthesis, we re-examined the design of our C4 bifunctional monomers, discussed above (**4-15,17, 18, 19** and **20**). While its protecting group scheme prevented the unwanted intramolecular reaction, we wondered if we could tailor our monomer to avoid degradation of the resulting polysaccharide. Although it is not clear the cause of this deglycosylation (see Chapter 4.3.4), one rationale was silyl-group migration. This transfer of silicon across hydroxyls is a well known, problematic phenomenon in carbohydrate chemistry.⁹ Conceivably, the protecting group migration could transfer to an internal (anomeric) oxygen resulting in cleavage of the glycosidic linkage and leave a free hydroxyl at the terminal monosaccharide C6 (Figure 4-16). We thought that place the silyl group at the axial C2 oxygen of mannose may geometrically limit this migration (if occurring intramolecularly) and lead to longer oligomers. Further, we considered that this silyloxy group, due to its axial chirality, and position above the plane of the chair conformation, is a much more accessible to fluoride delivery in the proposed mechanism. Lastly, because the original glycosylation method^{1,12} is relatively unreactive

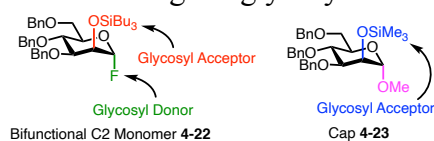
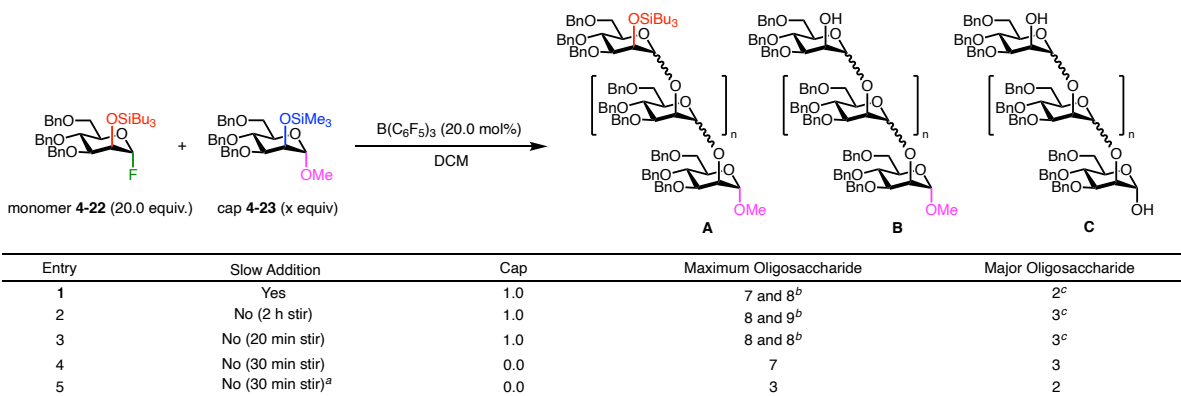


Figure 4-17 C2 monomer and cap examined.

with disarmed α -fluorides, potentially moving to the more electron rich (armed) glycoside **4-22** could aid in the catalytic polymerization. Although this monomer would offer no stereocontrol

(as previously provided by the neighboring group effect), this simple switch from a more sterically hindered C4 may make for more facile glycosylations. If promising, other methods could be employed to promote stereoselectivity at a later point in the project.

After synthesizing this monomer (**4-22**, synthesis Chapter 4.3.5), as well as an analogous cap (**4-23**), we began screening conditions (Figure 4-17). We were pleased to see that the initial polymerization resulted in high order oligosaccharides, as well as incorporation of the major disaccharide (Table 4-4, entry 1). Surprisingly, we found that with the control reaction, where no syringe pump addition was employed, the reaction produced longer oligomers, both with and without cap, and a longer major product (entry 2). Further reducing the stir time had minimal impact on maximum oligomer length, as did exclusion of the cap (entries 3-4). In addition to



^aReaction carried out with 10 mol% catalyst and 10 mol% 2,6-di-*tert*-butyl-4-methyl pyridine. ^bFirst number refers to mass with cap, second number mass without cap. ^cMajor oligomer with cap incorporated.

Table 4-4 Screen of C2 monomer 4-22 in triarylborane catalyzed polysaccharide synthesis.

slightly diminishing length, the trisaccharide remained as the predominant species in the mixture. Lastly, as hydrolysis (of the silyl protecting group) products were still detected, a hindered base, 2,6-di-*tert*-butyl-4-methyl pyridine, was added to the reaction mixture to probe whether proteolysis as the source of decomposition, but this just shut down the reaction (entry 5).

From this data, we had a few general takeaways. First, some of these results were reminiscent of general observations made during the C4 and adamantol studies, as longer post-monomer injection was detrimental to oligosaccharide formation. Further, although slow addition

appears to be inconsequential here, potentially the more sterically accessible C2 silyl acceptor allows for more efficient glycosylation. There are examples in the literature of one-pot glycosyl fluoride polymerizations, in which slow addition is unnecessary, but not necessarily harmful.⁵ Finally, while results were encouraging, hydrolyzed products were still observed in all cases, and major oligosaccharide lengths remained low. Excluding a cap inherently eliminated the mixture of capped-and non-capped products, but also eliminated this theoretical source of initiation for the polymer. Ultimately, while redesigning the bifunctional monomer alleviated some detrimental reactivity (e.g. silyl migration or sterically hindered glycosylations), and tedious setup, clearly a mixture of problems were present. We hoped to address this further with some catalyst-design insights discovered recently in the group.

4.3.4 Assessment of Modified Boranes in Polysaccharide Synthesis

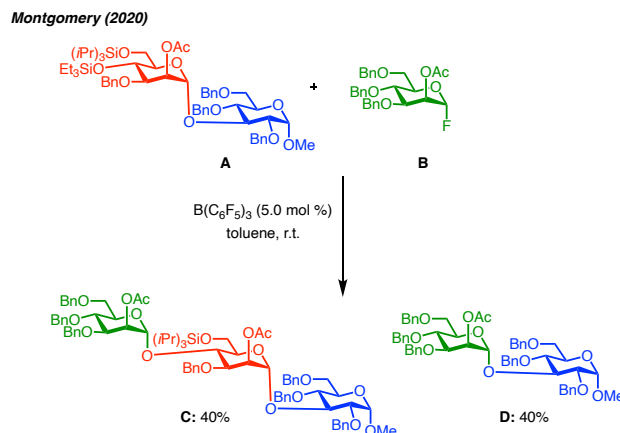


Figure 4-18 Isolation of deglycosylation/hydrolyzed products in Montgomery fluoride migration catalysis.

In a more recent attempt to minimize deglycosylation, and therefore synthesize larger oligosaccharides, I began examining some the recent results from my colleagues' work on modified triaryl boranes to address similar challenges in their work. Namely, Joshua Martin and Girish Sati showed that even in their iterative glycosylation, the undesired hydrolyzed and mixed saccharides could be isolated in good yield.^{1,12} For example, when disaccharide acceptor **A** is

subjected to $B(C_6F_5)_3$ catalysis with glycosyl fluoride donor **B**, not only is moderate yield of product saccharide **C** isolated, but so is an equal amount of product **D**, which results from

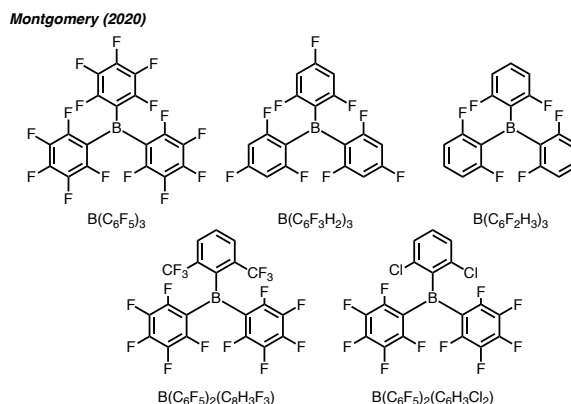
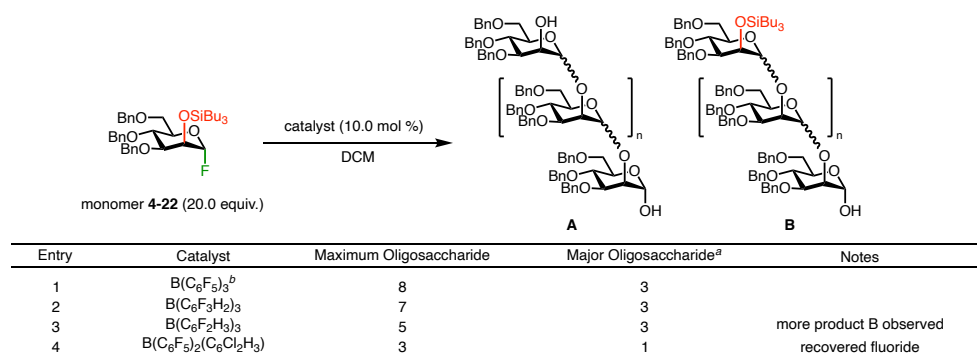


Figure 4-19 Modified boranes synthesized for Montgomery fluoride migration catalysis.

deglycosylation (Figure 4-18).

In the hope of solving the problems associated with the deglycosylation I examined various modified borane catalysts (Figure 4-19). We wondered if changing the electronic or steric properties of borane catalysts employed in the polysaccharide synthesis would minimize unproductive fluoride abstraction, redelivery, or other unproductive catalyst-driven pathways. Excitingly, most of the catalysts had a beneficial effect on the deglycosylation problem. For the iterative fluoride migration work, this was demonstrated through increased yields of the desired trisaccharide (**C**), and diminished production of the side product (**D**).¹² In particular, the more sterically hindered, and less Lewis acidic boranes gave the best results. Carrying out reactions



^aMajor product always **A**. ^bStandard C2 cap (**4-23**, 1.0 equiv.) included in reaction.

Table 4-5 Preliminary screen of modified boranes in triarylborane-catalyzed polysaccharide synthesis.

using the new catalysts showed a minimized effect for the oligomerization protocol, but results were potentially promising.

The less electron deficient boranes served as less active catalysts, overall. Specifically, while the major oligomer observed seemed to unchanged with the new catalysts, the less Lewis acidic nature of the catalysts did appear to make them less active in this system, as the maximum length of oligosaccharide was reduced substantially (Table 4-5, entries 1-3). Further, more of product **B**, relative to **A**, was observed, which implies a few potential outcomes. First, the boranes may result in fewer oxocarbenium intermediates for reaction with the silyl ether acceptors, second, detrimental fluoride delivery to neutral silyl ethers might be minimized with these boranes, or finally, intramolecular silyl migration may be shut-down under this manifold. Regardless, these results indicate that the less active catalysts do not rapidly degrade the silyl moiety, but rather, it remains intact it for subsequent glycosylation and oligomer growth, or isolation. These findings show while long-chain glycoconjugates might not be accessible, our method may be more suitable to controlled synthesis of smaller, monodispersed oligosaccharides (or application of these glycans). Interestingly though, when a the dichloro-modified borane was employed (entry 4), the reaction was shut-down completely, giving mostly recovered fluoride. This catalyst, $B(C_6F_5)_2(C_6Cl_2H_3)$, is known to be more Lewis acidic than the other modified boranes studied (in comparison to $B(C_6F_5)_3$, as the most Lewis acidic of those in Table 4-5).¹³ This result suggests that not only is the Lewis acidity important to fluoride abstraction and re- delivery, but so is the steric environment dictated by the *ortho*-fluoro substituents in the other catalysts. Similar loss in yield was observed for the chlorine-substituted boranes in the iterative glycosylation work.¹² Further work on utilizing these catalysts to access an ideal oligosaccharide profile, and studies regarding the mechanism behind the deglycosylation is underway in the Montgomery lab.

4.3.5 Synthesis of Additional Monosaccharide Monomers

The synthesis of various bifunctional monomers was a large portion of my work on this project, due to the specific protecting group manipulations necessary for installation of a fluoride and silyl ether within the same unit. As previously discussed, the first of those included the C6 protected monosaccharide (**4-4**), as well as the initial C4 monomer (**4-15**), which circumvented anhydrosugar formation observed in our first explorations of the polymerization. Both were synthesized successfully from glucose and mannose, albeit various synthetic challenges

The other C4 protected bifunctional monosaccharide **4-19** was derived from maltose, a

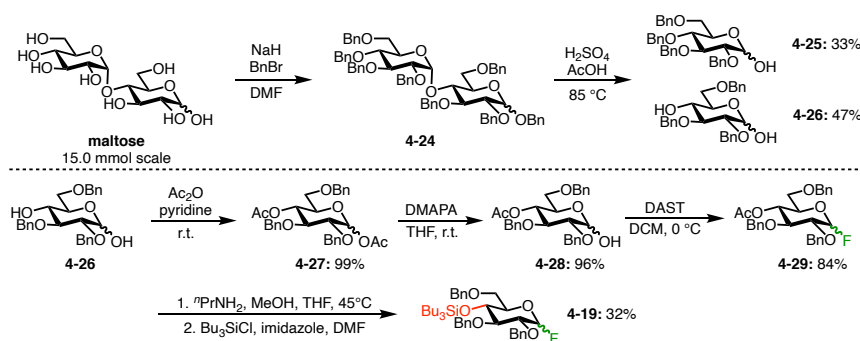


Figure 4-20 Synthesis of maltose-derived bifunctional C4 monomer.

naturally occurring disaccharide consisting of two glucosides (Figure 4-20). Inspired by literature precedent,^{14–16} we found that if we could cleave the glycosidic linkage of this glycan, we could selectively access free hydroxyl at both the C4 and anomeric (C1) positions, the only two carbons within the molecule that we needed to divergently functionalize. Our large-scale synthesis of **4-15** began with global protection of the disaccharide to give benzylated maltose **4-24**, which was directly carried on to acidic cleavage of the glycoside to give two unique monosaccharides, **4-25** and **4-26**. Tri-benzylated glucose **4-26** was carried forward, while tetra-benzylated glucose **4-25** was separated from the mixture for other purposes in the lab. Following acylation of the free hydroxyls (**4-27**), we selectively deacetylated the anomeric position using 3-(dimethylamino)-1-propylamine (DMAPA), which allowed for a mild reaction, with high yield, and no

chromatographic purification (**4-28**).¹⁷ DAST was then employed to selectively fluorinate at anomeric position(**4-29**), followed by another selective procedure for acyl group removal using amines too give a C4 free hydroxyl, and finally, after silyl protection, our bifunctional monomer **4-19**. Monomer **4-20** was synthesized in a similar fashion, but protected with triethylsilylchloride in the final step.

More recently, the efficacy of a C2 monomer (**4-22**) was explored. Below is the synthetic scheme for the C2 monomer, as well as the corresponding cap (**4-23**) (Figure 4-21). Starting from

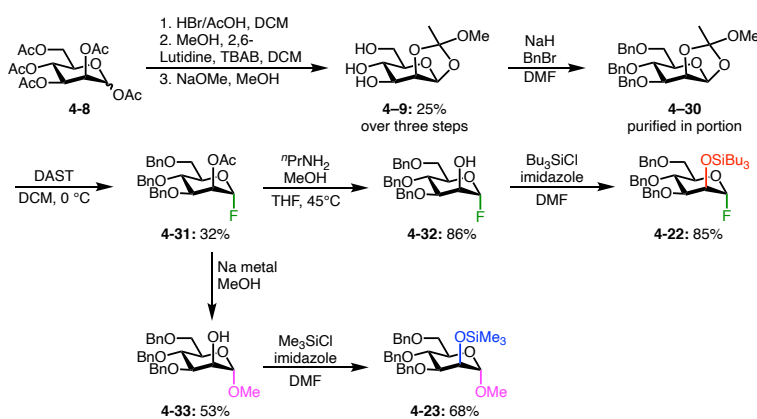


Figure 4-21 Synthesis of bifunctional C2 monomer and cap.

pentaacetate mannose (**4-8**), carried through the standard anomeric bromination, orthoester formation, and de-acetylation (**4-9**), global benzylation of the triol was carried out to give **4-30**, which was purified in portion. Opening of the orthoester gave α -mannosyl fluoride (**4-31**) in high yield. At this point the material was divergently synthesized to give our two C2 saccharides. Following fluorination with deacetylation (**4-32**) and protection with tributylchlorosilane (Bu₃SiCl), provided the bifunctional **4-22**. When glycosyl fluoride **4-31** was instead subjected to sodium metal methanolysis conditions, **4-33** was isolated, and carried on to be deprotected (**4-34**), and silylate at C2 with trimethylchlorosilane (Me₃SiCl) (**4-23**).

Through careful use of literature precedent, evaluation of reaction setup, and purification efficiency, these synthetic routes have offered relatively high yielding and scalable access to monosaccharide starting materials.

4.4 Progress towards the Synthesis of Glyco-Dendrimers

4.4.1 Motivation for Dendrimer Synthesis

Recent results for the synthesis of oligomers via our group's Lewis acid catalyzed glycosylation elucidated our method's potential to access medium length oligosaccharides. Additionally, experimental data regarding modified boranes demonstrates the potential for more controlled synthesis of these homoglycans. An underexplored class of glycoconjugates to that

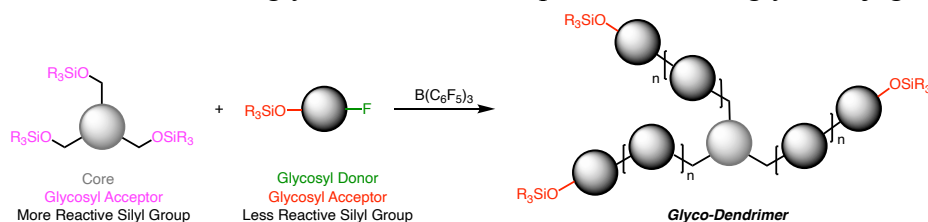


Figure 4-22 Project goals for triarylborane catalyzed dendrimer synthesis.

would be feasible to synthesize, with our synthetic limits, is carbohydrate dendrimers.¹⁸ Dendrimers have important functions in biological systems, and potential in the materials industry, due to multivalent interactions, and unique structure-driven functionality.^{19,20} The small oligosaccharides which branch off the central core, giving the dendric-architecture, may be a unique application of the triarylborane catalyzed glycosylation and bifunctional monomers (Figure 4-22). Furthermore, dendrimers with carbohydrate moieties typically consist of non-glyco (other organic functional group-based) branches, with the glycosides simply decorating the terminus. An uncommon glycan-based dendrimer architecture would be a unique addition to the literature, and the borane catalyzed glycosylation would offer an efficient method to synthesize these motifs, which might otherwise be challenging. Further, the potential of these densely-functionalized

molecules to offer multivalent, and other modifiable structure-function interactions, in a biological setting, is intriguing.²⁰ Ultimately, while the one-pot method discussed in the chapters above would be a rapid way to access glycol-dendrimers, building these oligosaccharide ligands via stepwise BCF glycosylation would also offer advantages to current methods in scope and synthetic effort.

4.4.2 Attempts Towards Dendrimer Synthesis via Polymerization

Initial work on dendrimer synthesis began with polymerization efforts. Rapid access to these biological motifs could be highly beneficial and cut down on routine glycoside manipulation

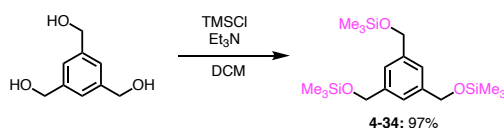


Figure 4-23 Silyl-protection of benzyl alcohol dendrimer core.

and purification with stepwise synthesis. Because the bioactivity is primarily dictated by the peripheral groups ligated to the central unit, and not the core synthon itself, we started with a TMS-

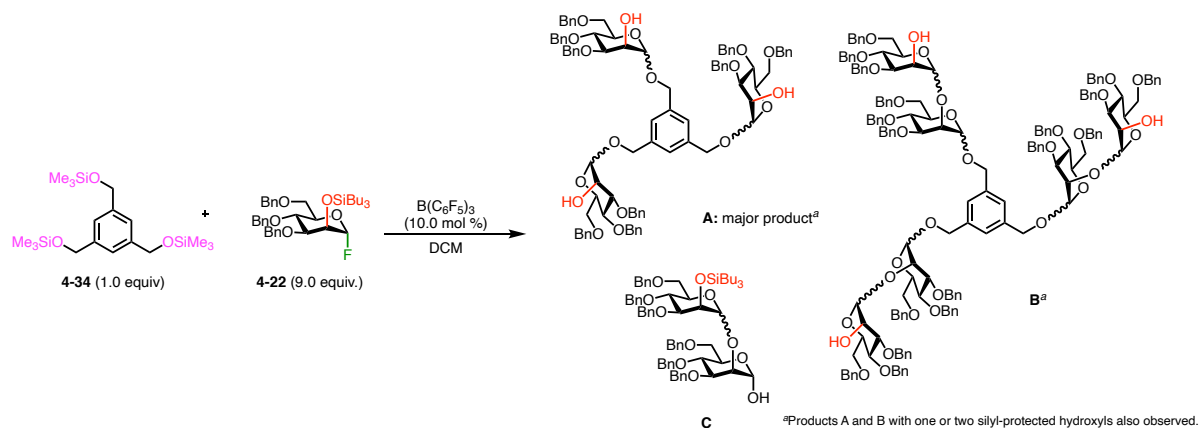


Figure 4-24 Poly-glycosylation of silyl-protected dendrimer core with a bifunctional monosaccharide.

protected tribenzyl alcohol core **4-34**. This simple unit would serve as a proof of concept for investigating the construction of the oligosaccharide ligands. The trisilyloxy core was easily synthesized in high yield form standard conditions (Figure 4-23). Bearing a relatively unhindered trimethylsilyl group, the core would serve as the acceptor in the glycosylation, while the

bifunctional fluoride monomer would serve as the first donor unit. Specifically, due to the relatively rapid synthesis, and promising results in the oligosaccharide work, the C2 monomer **4-22** was examined first.

With our core and silyl-protected glycosyl fluoride in hand, the glycosylation partners were subjected to BCF catalysis (Figure 4-24). The acceptor to donor ratio of 1.0 : 9.0 was set to test the feasibility of trisaccharide growth. Trisaccharides were regularly observed as the major products in our polysaccharides syntheses, but other challenges persist in dendrimer

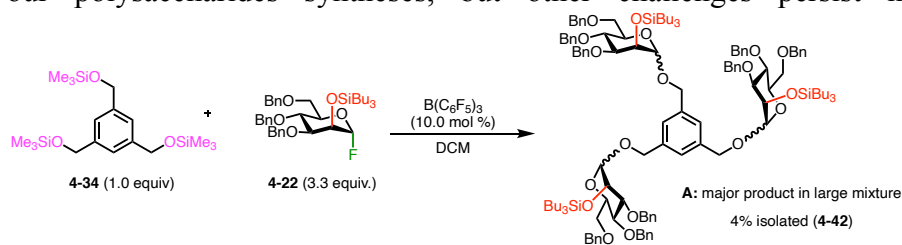


Figure 4-25 Mono-glycosylation of silyl-protected dendrimer core with a bifunctional monosaccharide.

polymerization, often due to steric hindrance of the reactions on a central functionality, and side reactions. Not only do the correct amount of monomer units need to add to each connection point on the core, but also, undesirable homopolymerization external to the benzyl alcohol, is possible as well. MALDI data displayed a wide array of products. Excitingly, fully glycosylated masses were present, as well as small peaks suggesting full di-glycosylation of each acceptor (products **A** and **B**; varying degrees of silyl protection retained). Also, in the mixture was disaccharide formation (product **C**), as well as unreacted bifunctional monosaccharides and masses which appear to be dendrimers with incomplete glycosylation (four or five units added).

To parse out the problems, and simplify the system before extending to longer ligands, we wanted to see if a full glycosylation could be cleanly observed. Accessing a mono-glycosylation using a bifunctional building block would reduce protecting group manipulations in the dendrimer synthesis. Now using a one to three ratio of core to glycoside, we carried out the catalytic glycosylation (Figure 4-25). Although the major product was the fully, mono glycosylated

dendrimer core, purification was onerous, and yielded minimal isolated product. More work on this polymeric dendrimer synthesis as BCF oligosaccharide synthesis is further optimized.

4.4.3 Progress Towards the Iterative Synthesis of Dendrimers

Even though the oligosaccharides which branch off the central core of dendrimers are sometimes shorter in length, their synthesis in an iterative fashion (as opposed to polymerization) is still not straightforward. As with synthesizing any glycosidic linkage, selectivity, protecting group manipulations, purification and stability concerns pose issues for chemists. Moreover, when dendrimer synthesis is desired, new steric environments, unexpected reactivity at the core, and biological considerations, such as a final deprotection, make this feat more difficult. BCF fluoride migration catalysis may offer solutions to these problems. Moreover, due to the wide range of silyl protecting groups, it offers branching and orthogonal reactivity opportunities, otherwise limited in standard glycosylation strategies, even when not grown one-pot. Finally, while many of these

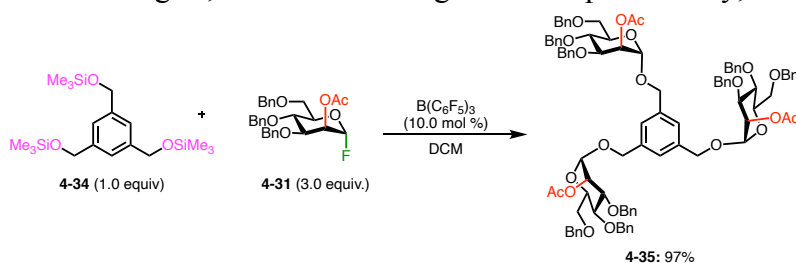


Figure 4-26 Mono-glycosylation of silyl-protected dendrimer core.

systems simply glycosylate existing dendrimers at the periphery,²¹ we believed that the efficiency of our glycosylation method could offer a stand-alone strategy for synthesis of interesting multivalent, dendric-carbohydrates.

Exploration of the iterative synthesis of an ideal carbohydrate dendrimer required multiple synthetic approaches. Herein is a discussion of the various routes and substrate combinations examined, and those of future interest.

First, TMS-protected tribenzyl alcohol core **4-34** was glycosylated rapidly using BCF catalysis with fluoride **4-31**, to provide functionalized dendrimer **4-35** in high yield. (Figure 4-26). Carrying on this glycosylated dendrimer to the C2-acetate deprotection caused several issues. First, although fully deacetylated dendrimer (**4-36**) was isolated in moderate yield, remaining product co-eluted with the mono- and di-acetylated species upon several chromatographic purifications (Figure 4-27A). Even re-subjecting mixed material to harsher reaction conditions resulted in decomposition (Figure 4-27B). Ultimately, in further screens of this reaction optimization, full conversion of starting material and formation of pure white solid was achieved when the

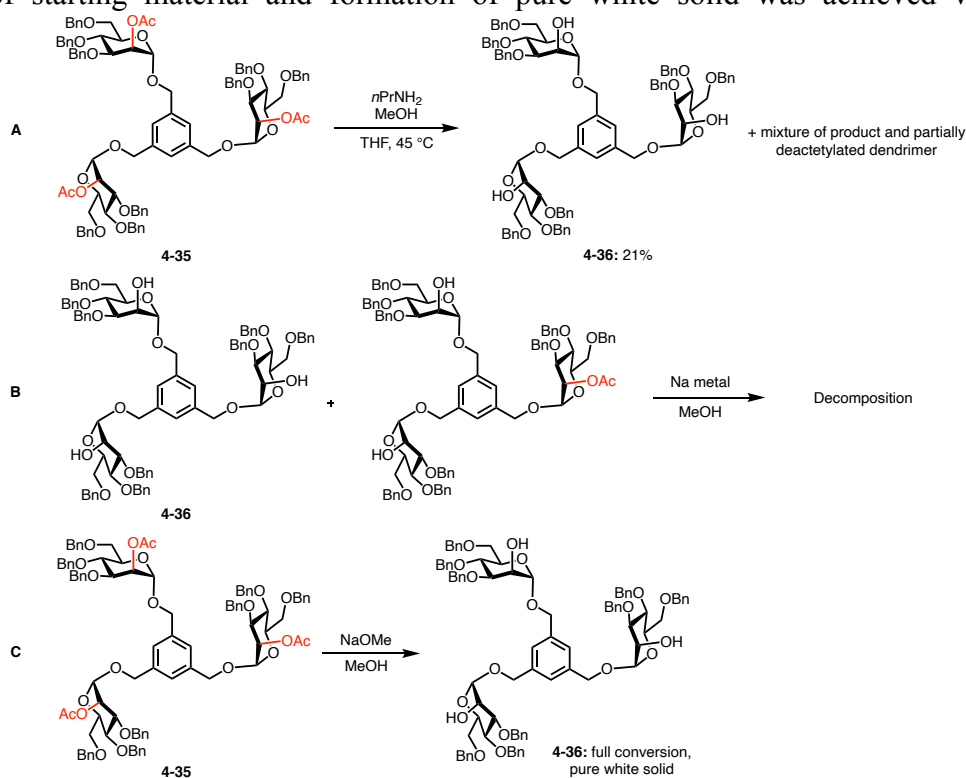


Figure 4-27 Deacetylation optimization for dendrimer synthesis.

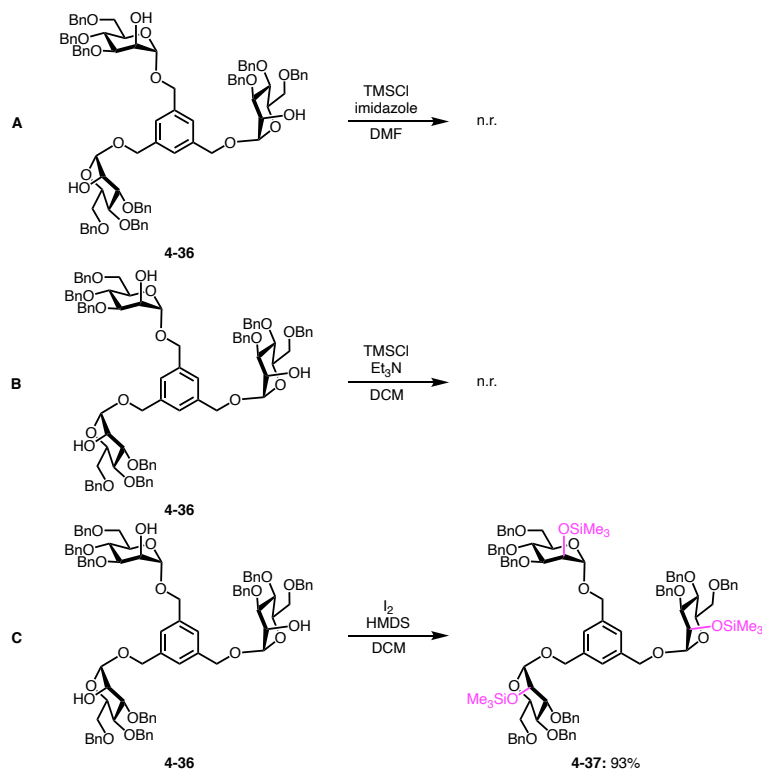


Figure 4-28 TMS-protection optimization for dendrimer synthesis.

methanolysis procedure was used at the outset (Figure 4-27C). This material could be directly carried forward without further purification. The tri-hydroxy dendrimer **4-36** was then carried on to trimethylsilyl protection to poise it for the subsequent fluoride migration catalysis. Likely due to the highly steric environment of the dendrimer, and potentially electron-rich nature of the armed sugars, the protection was more challenging than expected. After various standard strategies were tried, a more unusual TMS installation, using HMDS,²² was successfully implemented to give the

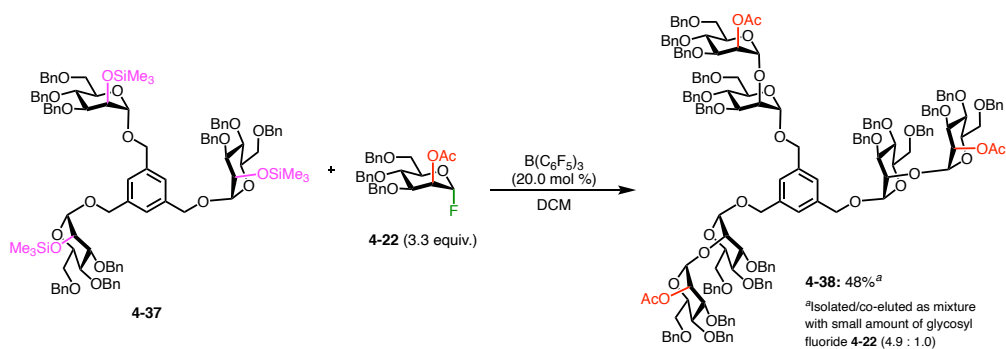


Figure 4-29 Secondary glycosylation for dendrimer synthesis.

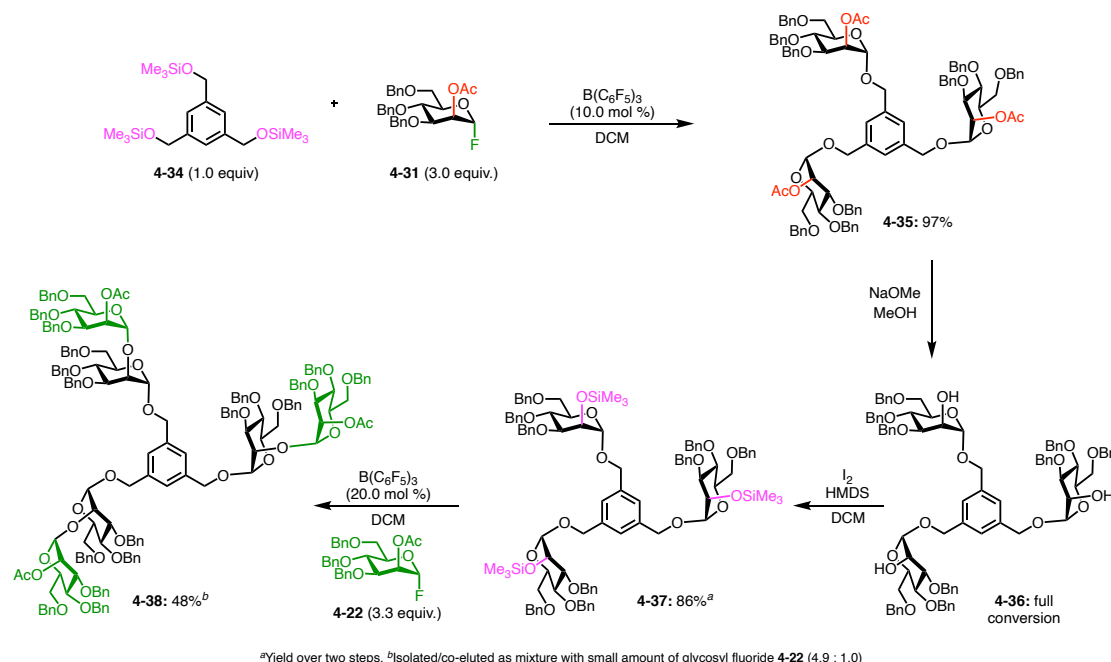


Figure 4-30 Iterative glyco-dendrimer synthesis.

silyloxy dendrimer acceptor **4-37** (Figure 4-28). Finally, a secondary glycosylation of the resulting glycan gave good yield of the desired product (**4-38**), but further condition and purification optimizations are underway (Figure 4-29). Figure 4-30 depicts the optimized synthesis thus far.

In addition to linear carbohydrate ligands, branching density on carbohydrate dendrimers is also a desirable feature in certain cases. In hopes of synthesizing branched systems, a glycoside that would allow for selective deprotection and thus divergent glycosylation, was required. Therefore, a monomer with different acyl protecting groups was designed (Figure 4-31). Ultimately, due to synthetic challenges, monomer **4-39** was synthesized instead. Glycosylation of the donor **4-39** with standard benzyl alcohol core **4-34** gave dendrimer in modest yield, with the

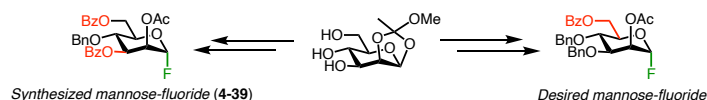


Figure 4-31 Alternative glycosyl fluoride for branched dendrimer synthesis.

only recovered starting material as the remaining mass balance (Figure 4-32A). Unfortunately, although previous publications²³ have demonstrated selective *O*-acetyl deprotection (over *O*-

benzoyl groups), the reaction with **4-40** was a messy, inseparable mixture of varying degrees of protection (Figure 4-32B).

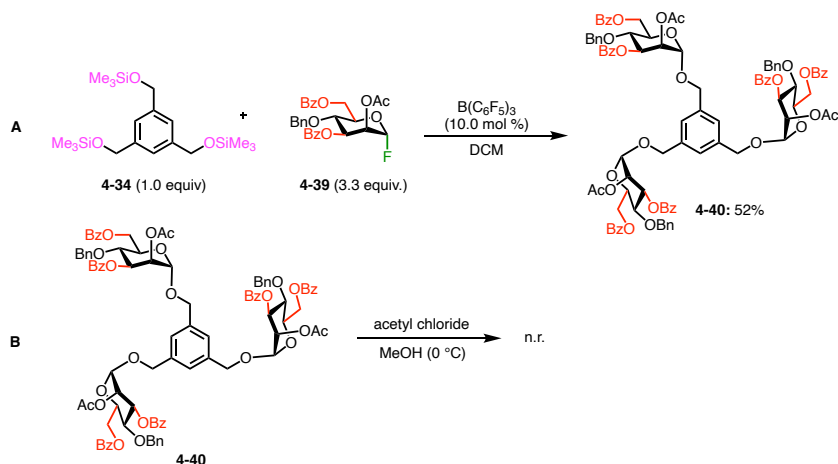


Figure 4-32 Alternative glycosyl fluoride glycosylation and attempted deprotection for branched dendrimer synthesis.

More recent work has explored alternative dendrimer cores. In addition to structural diversity, we wanted to examine the potential to grow dendrimer branches from the fluoride end, which would highlight the diversity of our method within the dendrimer application. This strategy also precludes the need to deprotect and re-protect, which would help illustrate the numerous advantages of the fluoride migration catalysis for glycoconjugates, and highlight the unique bifunctional monomer synthesis. Finally, because there are benzyl-protecting groups on the sugar, avoiding the use of the benzyl ether core would allow us to potentially fully deprotected at the end, and thus highlight the biological relevance of these systems. First attempts seemed promising as

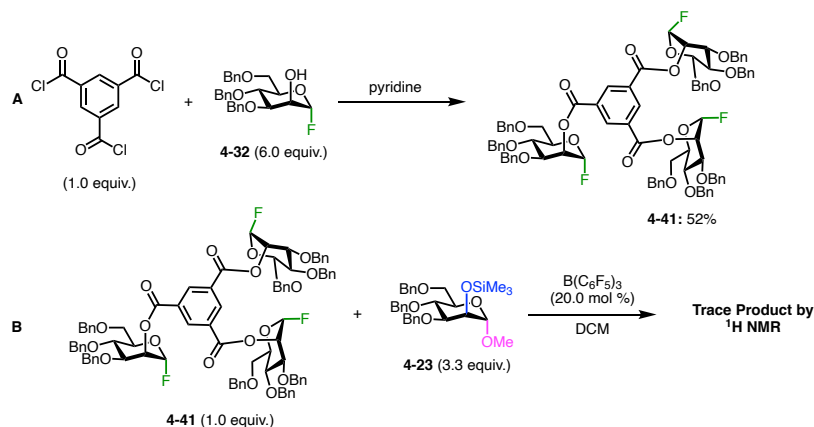


Figure 4-33 Dendrimer synthesis with alternate core.

glycosyl fluoride **4-32** was acylated²⁴ in modest yield, giving dendrimer **4-41**. A secondary glycosylation only gave trace desired dendrimer, with mostly recovered starting material, and hydrolyzed **4-23** as the major products isolated (Figure 4-33). This lack of reactivity is likely due to the deactivated glycosyl fluoride, as well as the extremely sterically hindered environment of the anomeric carbon. Further work on new dendrimers, including this acyl scaffold, is underway.

4.5 Conclusion and Future Directions

The initial goals of the borane-catalyzed oligosaccharide synthesis involved using a bifunctional monomer (which contained both a silyl ether acceptor and glycosyl fluoride donor), a capping molecule (from which the growing chain would initiate), and triarylborane catalyst to access polymeric glyco-conjugates in a one-pot fashion. Although initial results were promising, with up to 9-unit oligosaccharides formed, the major oligosaccharide observed hovered around 2 or 3 units. Further, as similarly observed in the standard glycosylation method in our lab, a deglycosylation pathway seemed to be occurring. We hypothesized that this impacted not only the short length of major oligosaccharide observed, but also was the reason as to why oligomers with no cap-monosaccharides were frequently observed. Our initial goal was to synthesize large polysaccharides in a one-pot method. After surveying the polysaccharide literature, and exploring the potential of BCF glycosylations in this context, we came to the conclusion that our work is

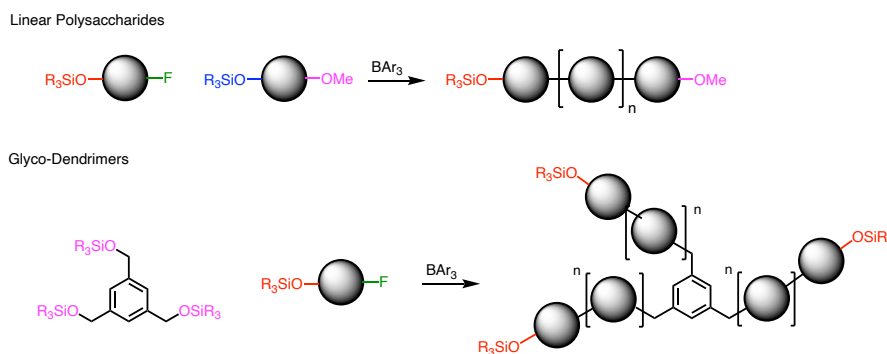


Figure 4-34 Glycoconjugate project summary and outlook.

more ideally positioned in the literature for the efficient synthesis smaller homoglycans. Current automated and enzymatic methods can efficiently synthesize large (10-100 unit) glycosides, but accessing intermediate glycoconjugates in a straightforward manner is still an unmet need.²

The polysaccharide work has ultimately evolved into two sub-projects which center upon applications of the borane-catalyzed glycosylation (Figure 4-34). In addition to examining potential for oligomerization of bifunctional monosaccharides, more recently, the synthesis of dendrimeric materials using our method has become an interesting opportunity. Both directions have required the careful synthesis of various complex monosaccharides, both bifunctional, and otherwise.

Currently, optimization of the oligomerization of these monomers is underway. Initial challenges, including homodimerization have been overcome by dilution and slow addition of the monomer, and tailoring or monomer structure to avoid degradation pathways. Amending these

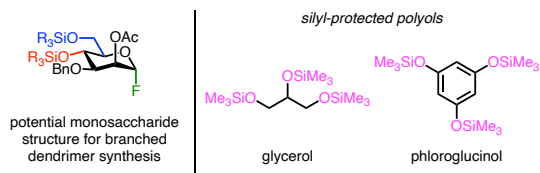


Figure 4-35 Potential monosaccharide and core structures for dendrimer synthesis.

issues will be the focus of the short-term, while long-term work might aim to access block copolymers and branched-chain polymers. For the glycoconjugate applications of this work, efforts will be aimed at using di-silyl-protected monomers to allow for multiple glycosylations on a single sugar, for branched dendrimer construction. Finally, additional cores such as silyl ether-protected glycerol, or Phloroglucinol (1,3,5-Trihydroxybenzene), will be important structures to consider for highlighting biological applications of this project (Figure 4-35).

4.6 References

- (1) Sati, G. C.; Martin, J. L.; Xu, Y.; Malakar, T.; Zimmerman, P. M.; Montgomery, J. Fluoride Migration Catalysis Enables Simple, Stereoselective, and Iterative Glycosylation. *J. Am. Chem. Soc.* **2020**, jacs.0c03165. <https://doi.org/10.1021/jacs.0c03165>.
- (2) Guberman, M.; Seeberger, P. H. Automated Glycan Assembly: A Perspective. *J. Am. Chem. Soc.* **2019**, *141* (14), 5581–5592. <https://doi.org/10.1021/jacs.9b00638>.
- (3) Delbianco, M.; Kononov, A.; Poveda, A.; Yu, Y.; Diercks, T.; Jiménez-Barbero, J.; Seeberger, P. H. Well-Defined Oligo- and Polysaccharides as Ideal Probes for Structural Studies. *J. Am. Chem. Soc.* **2018**, *140* (16), 5421–5426. <https://doi.org/10.1021/jacs.8b00254>.
- (4) Nielsen, M. M.; Pedersen, C. M. Catalytic Glycosylations in Oligosaccharide Synthesis. *Chem. Rev.* **2018**, *118* (17), 8285–8358. <https://doi.org/10.1021/acs.chemrev.8b00144>.
- (5) Dräger, M.; Basu, A. Galactan Synthesis in a Single Step via Oligomerization of Monosaccharides. *Beilstein J. Org. Chem.* **2014**, *10* (1), 2658–2663. <https://doi.org/10.3762/bjoc.10.279>.
- (6) *The Organic Chemistry of Sugars*; Levy, D. E., Fügedi, P., Eds.; Taylor & Francis: Boca Raton, 2006.
- (7) Cumpstey, I.; Fairbanks, A. J.; Redgrave, A. J. Stereospecific Synthesis of 1,2- *Cis* Glycosides by Allyl-Mediated Intramolecular Aglycon Delivery. 2. The Use of Glycosyl Fluorides. *Org. Lett.* **2001**, *3* (15), 2371–2374. <https://doi.org/10.1021/ol016175a>.
- (8) López, J. C.; Ventura, J.; Uriel, C.; Gómez, A. M.; Fraser-Reid, B. Reaction of 1,2-Orthoesters with HF–Pyridine: A Method for the Preparation of Partly Unprotected Glycosyl Fluorides and Their Use in Saccharide Synthesis. *Org. Lett.* **2009**, *11* (18), 4128–4131. <https://doi.org/10.1021/ol901630d>.
- (9) Dimakos, V.; Taylor, M. S. Site-Selective Functionalization of Hydroxyl Groups in Carbohydrate Derivatives. *Chem. Rev.* **2018**, *118* (23), 11457–11517. <https://doi.org/10.1021/acs.chemrev.8b00442>.
- (10) Hanashima, S.; Yamaguchi, Y.; Ito, Y.; Sato, K. Synthesis of the Starfish Ganglioside AG2 Pentasaccharide. *Tetrahedron Lett.* **2009**, *50* (45), 6150–6153. <https://doi.org/10.1016/j.tetlet.2009.08.071>.
- (11) Peng, P.; Linseis, M.; Winter, R. F.; Schmidt, R. R. Regioselective Acylation of Diols and Triols: The Cyanide Effect. *J. Am. Chem. Soc.* **2016**, *138* (18), 6002–6009. <https://doi.org/10.1021/jacs.6b02454>.
- (12) Sati, G.; Martin, J.; Xu, Y.; Montgomery, J. Unpublished.
- (13) Lewis Acidity of Boron Compounds. *Coord. Chem. Rev.* **2014**, *270–271*, 75–88. <https://doi.org/10.1016/j.ccr.2013.10.017>.
- (14) Cribiù, R.; Eszter Borbas, K.; Cumpstey, I. On the Synthesis of Vinyl and Phenyl C-Furanosides by Stereospecific Debenzylative Cycloetherification. *Tetrahedron* **2009**, *65* (10), 2022–2031. <https://doi.org/10.1016/j.tet.2009.01.014>.
- (15) Sato, T.; Nakamura, H.; Ohno, Y.; Endo, T. Synthesis of 1,4-Anhydro-2,3,6-Tri-O-Benzyl- α -D-Glucopyranose by *Cis*-Ring-Closure of a Glycosyl Chloride. *Carbohydr. Res.* **1990**, *199* (1), 31–35. [https://doi.org/10.1016/0008-6215\(90\)84090-H](https://doi.org/10.1016/0008-6215(90)84090-H).
- (16) Micheel, F.; Kreutzer, U. Synthese des kristallinen D-Glucose-anhydrids- α . β . *Justus Liebigs Ann. Chem.* **1969**, *722* (1), 228–231. <https://doi.org/10.1002/jlac.19697220124>.

- (17) Andersen, S. M.; Heuckendorff, M.; Jensen, H. H. 3-(Dimethylamino)-1-Propylamine: A Cheap and Versatile Reagent for Removal of Byproducts in Carbohydrate Chemistry. *Org. Lett.* **2015**, *17* (4), 944–947. <https://doi.org/10.1021/acs.orglett.5b00041>.
- (18) Liu, J.; Gray, W. D.; Davis, M. E.; Luo, Y. Peptide- and Saccharide-Conjugated Dendrimers for Targeted Drug Delivery: A Concise Review. *Interface Focus* **2012**, *2* (3), 307–324. <https://doi.org/10.1098/rsfs.2012.0009>.
- (19) Kiessling, L. L. Chemistry-Driven Glycoscience. *Bioorg. Med. Chem.* **2018**, *26* (19), 5229–5238. <https://doi.org/10.1016/j.bmc.2018.09.024>.
- (20) Yu, Y.; Tyrikos-Ergas, T.; Zhu, Y.; Fittolani, G.; Bordoni, V.; Singhal, A.; Fair, R. J.; Grafmüller, A.; Seeberger, P. H.; Delbianco, M. Systematic Hydrogen-Bond Manipulations To Establish Polysaccharide Structure–Property Correlations. *Angew. Chem. Int. Ed.* **2019**, *58* (37), 13127–13132. <https://doi.org/10.1002/anie.201906577>.
- (21) Wolfenden, M. L.; Cloninger, M. J. Carbohydrate-Functionalized Dendrimers To Investigate the Predictable Tunability of Multivalent Interactions. *Bioconjug. Chem.* **2006**, *17* (4), 958–966. <https://doi.org/10.1021/bc060107x>.
- (22) Karimi, B.; Golshani, B. Mild and Highly Efficient Method for the Silylation of Alcohols Using Hexamethyldisilazane Catalyzed by Iodine under Nearly Neutral Reaction Conditions. *J. Org. Chem.* **2000**, *65* (21), 7228–7230. <https://doi.org/10.1021/jo005519s>.
- (23) Byramova, N. É.; Ovchinnikov, M. V.; Backinowsky, L. V.; Kochetkov, N. K. Selective Removal of O-Acetyl Groups in the Presence of O-Benzoyl Groups by Acid-Catalysed Methanolysis. *Carbohydr. Res.* **1983**, *124* (1), C8–C11. [https://doi.org/10.1016/0008-6215\(83\)88370-0](https://doi.org/10.1016/0008-6215(83)88370-0).
- (24) Ma, T.; Li, C.; Zhang, Z.; Wang, Z.; Yu, L.; Xue, W. Indium(III) Iodide-Catalyzed Stereoselective Synthesis of β -Glucopyranosides by Using a Glucosyl Fluoride Donor with 2-O-Benzoyl-3,4,6-Tri-O-Benzyl Protection. *Synlett* **2017**, *28* (19), 2633–2636. <https://doi.org/10.1055/s-0036-1589121>.

Chapter 5

Conclusion

5.1 Conclusion

The development of methods for nitrile-directed C–H functionalization and Lewis acid-catalyzed oligosaccharide synthesis, outlined in this dissertation, offer improved access to molecular complexity in the context of two distinct fields. First, inspired by the multicomponent, copper-catalyzed borylation/*ortho*-cyanation of styrene derivatives, and the versatility of the nitrile as a valuable directing group for dual C–H activation, a remote, *meta*-selective C–H acetoxylation

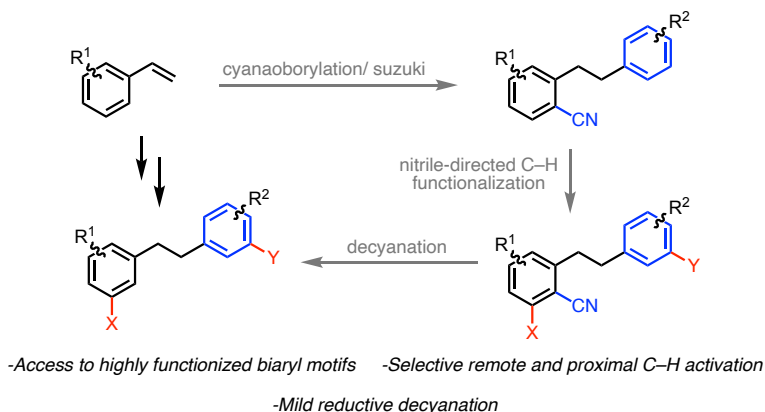


Figure 5-1 Development of divergent methods for traceless nitrile-directed C–H functionalization.

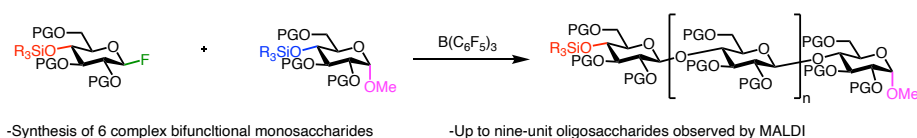
(directed by σ -coordination) was developed (Figure 5-1). The methodology was expanded to a variety of biaryl motifs and allowed for the demonstration of an analogous nitrile-directed C–H pivalation to the distal *meta* position, as well. This work also showcased the bimodal reactivity of the nitrile, which enabled selective, *ortho*-C–H functionalization at the proximal ring (via π -coordination). Following several studies examining selectivity outliers, and specific additives paramount to reaction selectivity, work was focused on development of a nickel-catalyzed transformation for the reductive decyanation

across various benzonitriles. This method is significantly more mild than those currently employed in the literature, especially for isolated aromatic systems. We then proceeded to demonstrate the orthogonality of our new transformations, selectively functionalizing multiple C–H bonds across a biaryl system in an iterative, reagent-controlled fashion. Ultimately a newly installed functional handle was used for C–O activation, and the nitrile was reductively cleaved. Overall, this work yielded a widely applicable, operationally simple methodology, to afford divergent reactivity in the late-stage functionalization of arene C–H bonds, in the context of medically relevant biaryl ethane scaffolds, starting from simple styrene derivatives.

The second research focus centered upon development of a one-pot triaryl borane-catalyzed polysaccharide synthesis. The Montgomery lab has developed a catalytic method for the rapid and selective glycosylation of glycosyl fluoride donors and silyl protected acceptor monosaccharides, employing a tris(pentafluorophenyl)borane catalyst. We demonstrated that by using a novel bifunctional glycosyl fluoride donor bearing silyl-protected hydroxyl acceptor groups within the same unit, polysaccharides of various length and branching characteristic could be accessed (Figure 5-2A). Work in this area began with the development of various syntheses to access silyl-protected glycosyl fluorides. These glycosides were challenging to synthesize and required meticulous route scouting and judicious selection of orthogonal protecting groups. Polymerization optimization revealed challenges, such as anhydrosugar formation and homodimerization, but have been overcome by dilution, slow addition of the monomer, and structurally tailoring the bifunctional monosaccharide. Polysaccharides of up to nine monomer units were observed by MALDI analysis, and convergence to more mono-dispersed oligomeric mixtures (and minimized deglycosylation) was obtained when less Lewis acidic boranes were employed.

Our fluoride migration catalysis also provides promising solutions to problems associated with dendrimer synthesis, due to the wide range of silyl protecting groups, which offer branching and orthogonal reactivity opportunities. Accessing these type of architectures, and developing better methods to access them, could allow study into their unique structure-function relationships, and potential biological applications. Thus far, diverse, and fully glycosylated dendrimers have been isolated in good yield (Figure 5-2B). Ultimately these ongoing projects aim (1) to access

A: One-Pot Oligosaccharide Synthesis



B: Iterative and One-Pot Synthesis of Glyco-Dendrimers

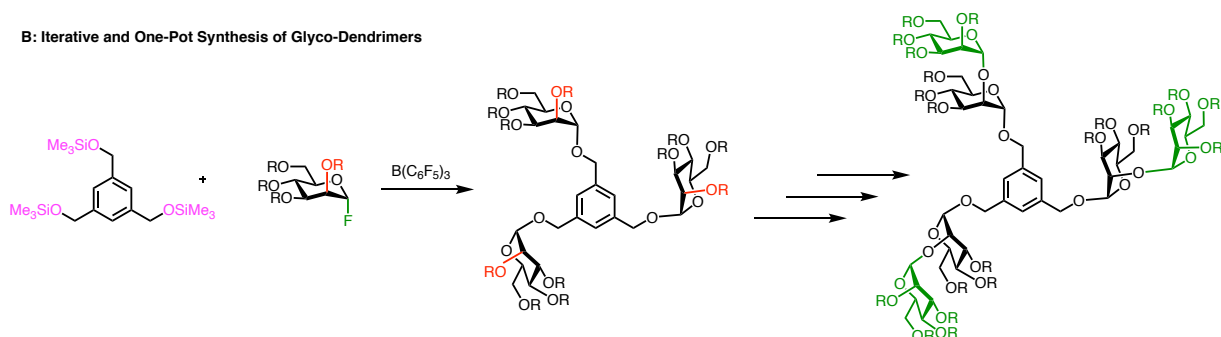


Figure 5-2 Progress towards triarylborane-catalyzed polysaccharide and glycoconjugate synthesis.

complex glycans via a systematic, one-pot polymerization and (2) explore applications of triarylborane catalysis in iterative dendrimer synthesis.

Overall while the research areas of described above are dissimilar in many ways, each addresses an important gap in organic synthesis. Taken as whole, they provide novel strategies for forging important bonds in industrial and biologically relevant molecular structures.

Chapter 6

Experimental Details

6.1 General Considerations

All reactions were conducted in a flame-dried or oven dried (120 °C) glassware with magnetic stirring under an atmosphere of dry nitrogen. Solvents were purified under nitrogen using a solvent purification system (Innovative Technology, Inc. Model # Sps-400-3 and PS-400-3). Unless otherwise noted all reagents were used as received. For Chapter 2, Styrene, titanium-isopropoxide and methanol (from CaH₂) were distilled. Silver salts (Sigma Aldrich, Strem Chemicals, Inc), palladium pre-catalysts (Sigma Aldrich), copper salts (Sigma Aldrich), nickel pre-catalysts (Sigma Aldrich, Strem), *N*-heterocyclic carbene salts (Sigma Aldrich, Strem), KO-*t*-Bu (Strem), NaO-*t*-Bu (Strem) B₂pin₂ (Combi Blocks, recrystallized from pentane), 4Å molecular sieves, and NCTS were stored and weighed in an inert atmosphere. For Chapter 4, tris(pentafluorophenyl) borane (Strem Chemicals, Inc.), D-mannose (Sigma Aldrich), 2,3,4,6-tetra-*O*-acetyl- α -D-glucose, and D-galactose (Sigma Aldrich) were used as received.

Analytical thin layer chromatography (TLC) was performed on Kieselgel 60 F254 (250 μ m silica gel) glass plates and compounds were visualized with UV light and *p*- anisaldehyde, potassium permanganate or ceric ammonium molybdate stains. ¹³C were obtained at r.t. (unless otherwise noted) in a Varian Mercury 400 MHz instrument, a Varian Unity 500 MHz, or a Varian Unity 700 MHz instrument. Chemical shifts of ¹H NMR spectra were recorded in parts per million (ppm) on the δ scale from an internal standard of deuterated solvent (δ 7.26 for CHCl₃). Chemical shifts of ¹³C NMR spectra were recorded in ppm from the standard of

deuterated solvent (δ 77.00 for Chloroform-d) on the δ scale. ^{19}F NMR were collected in a Varian Mercury 400 MHz instrument. High-resolution mass spectra (HRMS, ESI-TOF) were obtained at the University of Michigan Mass Spectrometry Laboratory in a VG-70-250-s spectrometer manufactured by Micromass Corp. (Manchester UK) or and Agilent Technologies 6230 TOF LC/MS. Regioisomeric ratios were determined on crude reaction mixtures using GC. GCMS analysis was carried out on a HP 6980 Series GC System with HP-5MS column (30 m x 0.250 mm x 0.25 μm). GC-FID was used for crude yield analysis (see Chapter 6.2.8), and was carried out on a HP 6980N Series GC system with a HP-5 column (30 m x 0.32 mm x 0.25 μm).

Matrix- assisted laser desorption/ionization mass spectrometry was performed on a Bruker AutoFlex Speed MALDI-TOF in positive-ion reflection mode. Samples were prepared by mixing matrix (2',4', 6'- trihydroxyacetophenone) in a solution of acetonitrile (10 mg/mL) with water (1:1 matrix solution: water). This matrix/water solution was then combined with the quenched polysaccharides dissolved in acetonitrile (1:1 mixture). The final sample was spotted on a 96-well MALDI plate and air-dried. The MALDI-TOF results were analyzed using flexAnalysis.

Flash column chromatography was performed using Kieselgel 60 (230-400 mesh) silica gel. When noted, Biotage purification was performed on an Isolera One purification system with SNAP silica columns.

6.2 Chapter 2 Experimental

6.2.1 Additional Experiments and Optimization Tables

6.2.1.1 Norbornene Experiments

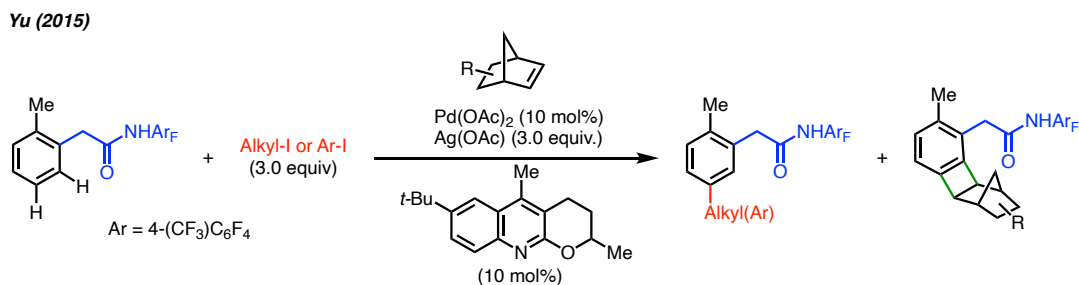
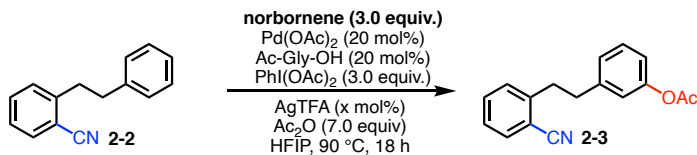


Figure 6-1 Yu's ligand-enabled C–H functionalization using modified norbornenes.

Additional experiments were carried out to examine the possibility of extending the selectivity of our system to divergent functionalization. This was inspired by work by the Yu group, that used modified norbornenes to alter the selectivity of amide-amide-directed C–H activation from *ortho*- to *meta*-functionalization (Figure 6-1).¹ Although acetoxylation has not been explored in these Catellani-type reactions, we thought it would be interesting to see if we could switch the regioselectivity of the distal acetoxylation from *meta* to *para*, as *para* is the next major regioisomer in the observed product mixture.



Entry	AgTFA (mol%)	Base (equiv.)	Yield <i>meta</i> (%)	ratio <i>m</i> : <i>p</i> : <i>o</i>
1	20	-	77 ^a	15.0: 2.0: 1.0
2	20	K ₂ CO ₃ (3.0)	n.r.	-
3	-	-	10	2.2: 1.0: 1.0
4	20	-	4	2.3: 1.0: 1.0
5	-	K ₂ CO ₃ (3.0)	n.r.	-
6	-	AgOAc (3.0)	n.r.	-
7	-	-	n.r. ^b	-

^aOptimized acetoxylation conditions: no norbornene. ^bModified norbornene (2-phenyl-2-norbornene used instead of standard norbornene).

Table 6-1 Acetoxylation selectivity with norbornene additives.

Screens were carried out to examine, this, and while the ratio of *meta* : *para* show some inclination toward more *para*-acetoxylation, as compared to our original conditions, a major

byproduct was continually observed by GCMS, as well as unreacted starting material (Table 6-1). Additionally, yields of the were quite low. Thus, no other work was done to this end.

6.2.1.2 Anhydride and Hypervalent Iodine Experiments

The anhydride was shown to be key in the remote nitrile-directed C–H functionalization. Thus, a brief examination of other anhydrides was carried out. The use of trifluoacetic (TFA)

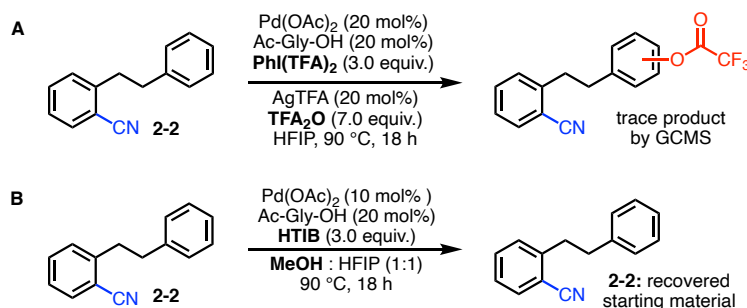
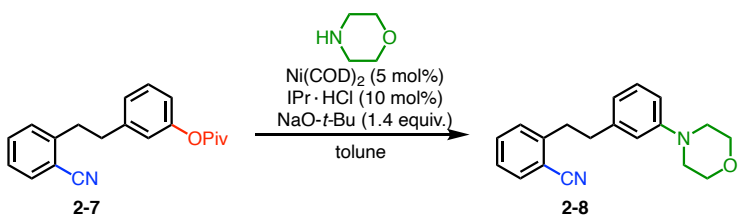


Figure 6-2 Additional anhydride/hypervalent iodine studies.

anhydride, and the analogous hypervalent iodine to install the TFA group on the distal arene, was inspired by these findings. Product was observed by GCMS, but no additional experiments were carried out (Figure 6-2A). Further, because the identity of the oxidation was influenced by the predominant species in solution, we wondered if C–H methoxylation (or hydroxylation) could be directed to the remote arene using conditions similar to those employed the selective acetoxylation. Hydroxy(tosyloxy)iodobenzene (HTIB) in methanol were used (as analogous to the proximal C–H functionalization), but only recovered starting material was observed (Figure 6-2B).

6.2.1.3 C–O Amination Optimization

Minimal optimization of Chatani's C–O amination² was required in order to achieve good yield of the functionalized product **2-8**. We found that both elevated temperatures, and longer reaction times were beneficial to this system (Table 6-2, entries 1-3), as well as increased nickel and ligand loading (entry 4). These findings are likely due to the non-conjugated bibenzyl. Most of Chatani's substrates consisted of conjugated aromatic systems, and many yields were also only moderate in the original



Entry	Conditions	Yield (%)
1	80 °C, 3 h	18
2	60 °C, 18 h	14
3	80 °C, 18 h ^a	38
4	80 °C, 18 h ^{a,b}	50
5	80 °C, 3 h ^c	trace

Isolated Yields. ^aCatalyst, ligand, and base pre-stirred for 10 minutes. ^bReaction carried out with 20 mol% Ni(COD)₂ and 20 mol% IPr·HCl. ^cReaction carried out with pyrrolidine as amine in place of morpholine.

Table 6-2 Brief optimization for C–O activation of distal pivalate.

method, due to the common phenol byproduct, which resulted from deprotection of the ester (at the C–O bond to be functionalized). Finally, a pyrrolidine variant was attempted in this case, but only gave trace product by GCMS (entry 5).

6.2.1.4 Additional Methoxylation Experiments

In a final attempt to expand the scope before moving on to the decyanation, and other

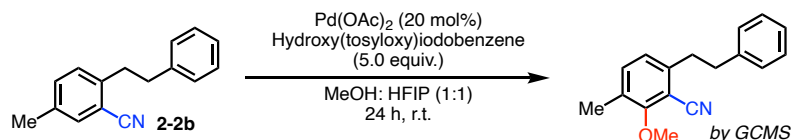


Figure 6-3 Attempted scope expansion for nitrile-directed ortho C–H methoxylation.

applications of our newly developed methods, the methyl-substituted substrate **2-2b** was also examined, and minimal product was observed by GCMS (Figure 6-3).

6.2.2 General Procedures for Chapter 2 (A-G)

6.2.2.1 General Procedure (A) for the Synthesis of Biaryl Substrates (via cyanoborylation/Suzuki)

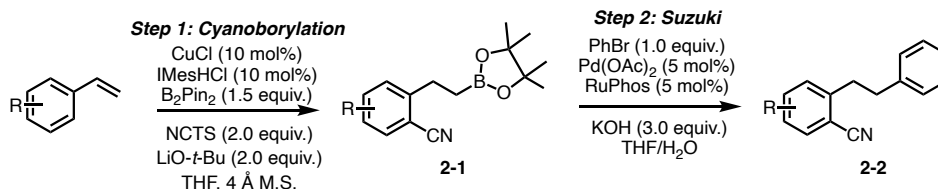


Figure 6-4 General procedure (A) for the synthesis of biaryl substrates (via cyanoborylation/Suzuki).

Step 1: The following cyanoborylated arenes were synthesized following literature procedure.³ 2-(2-(4,4,5,5-Tetramethyl-1,3,2-dioxaborolan-2-yl)ethyl)benzotrile (**2-1a**), 5-Methyl-2-(2-(4,4,5,5-tetramethyl-1,3,2-dioxaborolan-2-yl)ethyl)benzotrile (**2-1b**), 5-Chloro-2-(2-(4,4,5,5-tetramethyl-1,3,2-dioxaborolan-2-yl)ethyl)benzotrile (**2-1c**), 2-(2-(4,4,5,5-Tetramethyl-1,3,2-dioxaborolan-2-yl)ethyl)-1-naphthonitrile (**2-1g**), 4-(2-(4,4,5,5-Tetramethyl-1,3,2-dioxaborolan-2-yl)ethyl)-[1,1'-biphenyl]-3-carbonitrile (**2-1h**). All spectra characterization data are in accordance with the literature.³

Step 2: Following literature procedure,⁴ to an oven-dried round-bottom flask, with stir bar, was added palladium acetate (5.0 mol%) and RuPhos (5.0 mol%) under nitrogen atmosphere. Potassium hydroxide (3.0 equiv.) was then added and the flask was evacuated and filled with nitrogen (3x). Cyanoborylated arene (1.0 equiv.), bromobenzene (1.5 equiv.), THF (0.1 M), and H₂O (1.0 M) were then added. The resulting suspension was stirred overnight, under nitrogen, at 80 °C. After cooled to room temperature, the reaction was quenched with H₂O, extracted with ethyl acetate, dried with Na₂SO₄, filtered, concentrated, and chromatographed on silica gel.

6.2.2.2 General Procedure (B) for the Synthesis of Biaryl Substrates (via Wittig/hydrogenation)

Substrates **2-2d**, **f**, **i**, **o**, and **p** were synthesized by a streamlined three step synthesis utilizing a Wittig reaction and subsequent reduction of the olefin. All aldehydes and 2-bromomethyl benzonitriles were purchased and used as received.

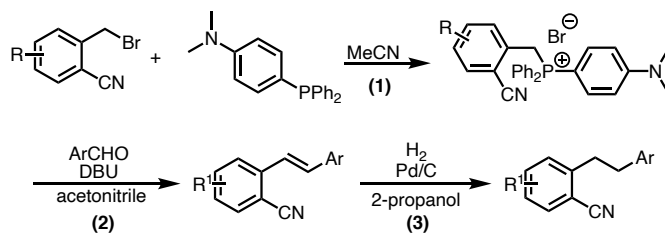


Figure 6-5 General procedure (B) for the synthesis of biaryl substrates (via Wittig/hydrogenation).

Step 1: Following literature procedure,⁵ to an oven-dried round-bottom flask, with stir bar, was added 2-bromomethyl benzonitrile derivative (1.0 equiv.) and 4-(Dimethylamino)phenyldiphenylphosphine (1.0 equiv.). The reagents were dissolved in acetonitrile (0.125 M), and stirred at reflux overnight. After cooling to room temperature, the phosphonium salt was collected by filtration and rinsed with cold acetonitrile. The crude material was dried and moved on to the next step without further purification. All spectra for the benzonitrile phosphonium salt match published data.

Step 2: Following literature procedure,⁵ to an oven-dried round-bottom flask, with stir bar, was added phosphonium salt (1.0 equiv.), benzaldehyde (0.66 equiv.), and DBU (1.0 equiv.), and acetonitrile (0.22 M). The mixture was stirred at 100 °C, overnight. After cooling to room temperature, the reaction mixture was quenched with ammonium chloride, extracted with ether, washed with brine, dried over magnesium sulfate, and concentrated. The reaction mixture was

filtered through a fritted funnel with celite and silica, and the crude material was concentrated, dried, and moved on to the next step without further purification.

Step 3: Following literature procedure,⁵ The olefin was dissolved in 2-propanol and a catalytic amount of 10.0 wt.% palladium on carbon (10.0 mol%) was added to the reaction vessel. The flask was purged with nitrogen and hydrogen gas, and then stirred under hydrogen gas for 18 hours. The mixture was filtered over silica gel, concentrated, and chromatographed by biotage, to afford the pure biaryl substrate.

6.2.2.3 General Procedure (C) for the Distal *meta*-Acetoxylation of Biaryl Substrates

To an oven-dried 8 mL culture tube with stir bar was added palladium acetate (20.0 mol%), silver trifluoroacetic acid (20.0 mol%), *N*-Acetylglycine (200 mol%), and (diacetoxyiodo)benzene (3.0 equiv.) and 1 mL hexafluorosopropanol (HFIP). The mixture was stirred at room temperature for 10 minutes. Acetic anhydride (7.0 equiv.) the biaryl substrate (1.0 equiv), and another 1 mL hexafluorisopropanol were then added. The tube was capped and the reaction was stirred at 90 °C for 18h. After cooled to room temperature, the reaction mixture was filtered through a pad of silica, concentrated, and chromatographed on silica gel.

6.2.2.4 General Procedure (D) for the Distal *meta*-Pivalation of Biaryl Substrates

To an oven-dried 8 mL culture tube with stir bar was added palladium acetate (20.0 mol%), *N*-Acetylglycine (20.0 mol%), and di-(pivaloyloxy)iodobenzene (3.0 equiv.) and 1 mL hexafluorosopropanol (HFIP). The mixture was stirred at room temperature for 10 minutes. Pivalic anhydride (7.0 equiv.) the biaryl substrate (1.0 equiv.), and another 1 mL hexafluorisopropanol were then added. The tube was capped and the reaction was stirred at 90 °C for 18h. After cooled

to room temperature, the reaction mixture was filtered through a pad of silica, concentrated, and chromatographed on silica gel (9:1 hexanes: ethyl acetate), to afford the pivalated product.

6.2.2.5 General Procedure (E) for the Proximal *ortho*-Methoxylation of Biaryl Substrates

To an oven-dried 8 mL culture tube with stir bar was added hydroxyl(tosyloxy)iodobenzene (5.0 equiv.) and palladium acetate (20.0 mol%). The tube was evacuated and purged three times, and the tube as capped. The biaryl substrate (1.0 equiv.), methanol (0.3 mL) and hexafluoroisopropanol (0.3 mL) were then added via syringe. The reaction was stirred for 24 hours at room temperature. The mixture was extracted with dichloromethane, washed with brine, dried over sodium sulfate, concentrated, and chromatographed on silica gel (100:0 to 9:1 hexanes: ethyl acetate), to afford the methoxylated product.

6.2.2.6 General Procedure (F) for the Decyanation of Bibenzyl Benzonitriles

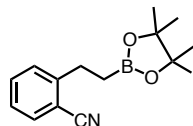
To an oven-dried 8 mL culture tube with stir bar was added, under Nitrogen atmosphere, Ni(COD)₂ (20.0 mol%), tricyclohexylphosphine (30.0 mol%), and sodium *tert*-butoxide (1.1 equiv) and toluene (0.5M). The mixture was stirred at room temperature for 5 minutes. The bibenzyl benzonitrile (1.0 equiv.) was added, and the mixture was stirred for another 5 minutes. Ti(*o-i*-pr)₄ (1.1 equiv) was added, the tube was capped and the reaction was stirred at 120 °C for 16h. After cooled to room temperature, the reaction mixture was filtered through a pad of silica, concentrated, and chromatographed by biotage (ethyl acetate/hexanes) to afford the decyanated product and the deprotected product.

6.2.2.7 General Procedure (G) for the Decyanation of Biphenyl Benzonitriles

To an oven-dried 8 mL culture tube with stir bar was added, under Nitrogen atmosphere, Ni(acac)₂ (20.0 mol%), tricyclohexylphosphine (30.0 mol%), and potassium *tert*-butoxide (2.5 equiv) and toluene (0.5 M). The mixture was stirred at room temperature for 5 minutes. The biphenyl benzonitrile (1.0 equiv.) was added, and the mixture was stirred for another 5 minutes. Ti(*o-i*-pr)₄ (1.1 equiv) was added, the tube was capped and the reaction was stirred at 120 °C for 16h. After cooled to room temperature, the reaction mixture was filtered through a pad of silica, concentrated, and chromatographed by biotage (ethyl acetate/hexanes) to afford the decyanated product.

6.2.3 Starting Material Synthesis for Chapter 2

2-(2-(4,4,5,5-Tetramethyl-1,3,2-dioxaborolan-2-yl)ethyl)benzonitrile (2-1a)

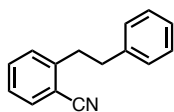


(Sample Scaled-up Procedure)

To an oven-dried round-bottom flask with stir bar, in an inert atmosphere, was added IMesHCl (170.4 mg, 0.5 mmol), copper chloride (49.5 mg, 0.5 mmol), LiO-*t*-Bu (800.5 mg, 10.0 mmol) and 4Å molecular sieves. Anhydrous THF (5 mL) was added, and the mixture was stirred at room temperature for 30 minutes. To the flask was added B₂Pin₂ (1.9046 g, 7.5 mmol), dropwise, as a solution in anhydrous THF (4 ml), and the reaction was stirred for another 30 minutes. A solution of styrene (0.5748 mL, 5.0 mmol) and N-Cyano-N-phenyl-*p*-toluenesulfonamide (2.7232 g, 10.0 mmol) in anhydrous THF (4 mL) was added dropwise, over a period of 30 minutes, while the reaction was stirring. The resulting solution was stirred under nitrogen, at room temperature, overnight. The final reaction mixture was filtered through a fritted funnel with sand and silica gel,

and the silica was rinsed with hexanes and ethyl acetate. The organic solution was concentrated and purified by gradient chromatography on silica gel (1% to 10 % ethyl acetate/hexanes), to afford 895.9 mg (70%) of the cyanoborylated substrate as a pale yellow, viscous oil. All spectra characterization data are in accordance with the literature.³

2-phenylbenzonitrile (2-2a)



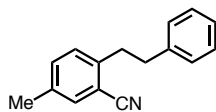
Following general procedure A for the synthesis of biaryl substrates (via cyanoborylation/Suzuki), 2-(2-(4,4,5,5-Tetramethyl-1,3,2-dioxaborolan-2-yl)ethyl)benzonitrile (180 mg, 0.7 mmol), palladium acetate (8.0 mg, 0.035 mmol), RuPhos (16.3 mg, 0.035 mmol), Potassium hydroxide (117.8 mg, 2.1 mmol), bromobenzene (0.11 mL, 1.05 mmol), THF (7.0 mL), and H₂O (0.7 mL) were used to produce after purification on silica gel (100:0 to 95:5 hexanes: ethyl acetate), 81.9 mg (57%) of the biaryl model substrate as a yellow solid.

¹H NMR (500 MHz cdCl₃) δ 7.63 (dd, *J* = 7.7, 1.5 Hz, 1H), 7.48 (td, *J* = 7.6, 1.4 Hz, 1H), 7.33 – 7.27 (m, 3H), 7.24 (d, *J* = 5.7 Hz, 1H), 7.21 (dd, *J* = 7.1, 5.4 Hz, 3H), 3.15 (dd, *J* = 9.6, 6.5 Hz, 2H), 2.98 (dd, *J* = 9.5, 6.6 Hz, 2H).

¹³C NMR (126 MHz, cdCl₃) δ 145.89, 140.88, 133.23, 133.08, 130.10, 128.93, 128.86, 127.03, 126.67, 118.40, 112.80, 37.54, 37.15.

MS(ESI+) calc'd for C₁₅H₁₃N: 207.1048, found: 207.1048 [M⁺]

5-methyl-2-phenethylbenzonitrile (2-2b)



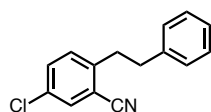
Following general procedure A for the synthesis of biaryl substrates (via cyanoborylation/Suzuki), 5-Methyl-2-(2-(4,4,5,5-tetramethyl-1,3,2-dioxaborolan-2-yl)ethyl)benzonitrile (590 mg, 2.2 mmol), palladium acetate (24.7 mg, 0.11 mmol), RuPhos (51.3 mg, 0.11 mmol), Potassium hydroxide (370.3 mg, 6.6 mmol), bromobenzene (0.35 mL, 3.3 mmol), THF (22.0 mL), and H₂O (2.20 mL) were used to produce, after purification on silica gel (100:0 to 95:5 hexanes: ethyl acetate), 308.3 mg (63%) of the biaryl substrate as a viscous, colorless oil.

¹H NMR (700 MHz, cdcl₃) δ 7.43 – 7.41 (m, 1H), 7.30 – 7.26 (m, 3H), 7.23 – 7.18 (m, 3H), 7.12 (d, *J* = 7.9 Hz, 1H), 3.09 (dd, *J* = 9.5, 6.7 Hz, 2H), 2.94 (dd, *J* = 9.4, 6.7 Hz, 2H), 2.35 (s, 3H).

¹³C NMR (176 MHz, cdcl₃) δ 142.47, 140.61, 136.50, 133.57, 133.02, 129.54, 128.52, 128.41, 126.18, 118.16, 112.15, 37.21, 36.24, 20.64.

MS(ESI+) calc'd for C₁₆H₁₅N: 222.1238, found: 222.1277 [M+H]⁺

5-chloro-2-phenethylbenzonitrile (2-2c)



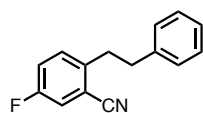
Following general procedure A for the synthesis of biaryl substrates (via cyanoborylation/Suzuki), 5-Chloro-2-(2-(4,4,5,5-tetramethyl-1,3,2-dioxaborolan-2-yl)ethyl)benzonitrile (7765 mg, 1.3 mmol), palladium acetate (14.5 mg, 0.065 mmol), RuPhos (30.3 mg, 0.065 mmol), Potassium hydroxide (218.8 mg, 3.9 mmol), bromobenzene (0.21 mL, 1.95 mmol), THF (13.0 mL), and H₂O (1.3 mL) were used to produce, after purification on silica gel (100:0 to 80:20 hexanes: ethyl acetate), 37.4 mg (12%) of the biaryl substrate as a viscous, colorless oil.

¹H NMR (700 MHz, cdcl₃) δ 7.44 (dd, *J* = 8.3, 2.3 Hz, 1H), 7.29 (t, *J* = 7.6 Hz, 2H), 7.24 – 7.21 (m, 1H), 7.17 – 7.15 (m, 3H).

¹³C NMR (176 MHz, cdcl₃) δ 143.90, 139.95, 132.94, 132.40, 132.22, 131.07, 128.50, 128.49, 126.38, 116.68, 113.84, 36.91, 36.10.

MS(ESI+) calc'd for C₁₆H₁₂ClN: 264.0550, found: 264.0557 [M+Na]⁺

5-fluoro-2-phenethylbenzonitrile(2-2d)



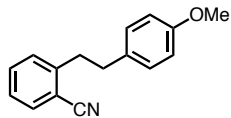
Following general procedure B for the synthesis of biaryl substrates (via Wittig/hydrogenation), the phosphonium salt (320.0 mg, 0.6 mmol), benzylaldehyde (0.4 mL, 0.396 mmol), DBU (0.09 mL, 2.72 mmol), and acetonitrile (7 mL) were used to produce the crude material which was moved on to the next step without further purification. After reduction of the resulting olefin and purification on silica gel by biotage, 109.3 mg (84% yield over 2 steps) of the biaryl substrate as a viscous, colorless oil, was obtained.

¹H NMR (700 MHz, cdcl₃) δ 7.33 – 7.27 (m, 3H), 7.24 – 7.20 (m, 1H), 7.17 (ddd, *J* = 17.0, 7.5, 1.6 Hz, 4H), 3.12 (dd, *J* = 9.2, 6.7 Hz, 2H), 2.95 (dd, *J* = 9.2, 6.8 Hz, 2H).

¹³C NMR (176 MHz, cdcl₃) δ 160.43 (d, *J* = 248.1 Hz), 141.47 (d, *J* = 3.6 Hz), 140.07, 131.52 (d, *J* = 8.0 Hz), 128.50, 128.48, 126.34, 120.26 (d, *J* = 21.0 Hz), 119.26 (d, *J* = 24.4 Hz), 116.80 (d, *J* = 2.9 Hz), 113.46 (d, *J* = 9.2 Hz), 37.11, 35.93.

MS(ESI+) calc'd for C₁₅H₁₂FN: 226.0987, found: 226.1027 [M+H]⁺

2-(4-methoxyphenethyl)benzonitrile (2-2e)



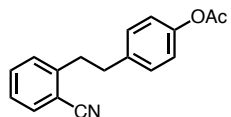
Following general procedure A for the synthesis of biaryl substrates (via cyanoborylation/Suzuki), 2-(2-(4,4,5,5-Tetramethyl-1,3,2-dioxaborolan-2-yl)ethyl)benzonitrile (257 mg, 1.0 mmol), palladium acetate (11.2 mg, 0.01 mmol), RuPhos (23.3 mg, 0.01 mmol), Potassium hydroxide (168.3 mg, 3.0 mmol), 4-bromoanisole (0.187 mL, 1.5 mmol), THF (10.0 mL), and H₂O (1.0 mL) were used to produce, after purification on silica gel (100:0 to 80:20 hexanes: ethyl acetate), 512.0 mg (22%) of the biaryl substrate as a viscous, colorless oil.

¹H NMR (700 MHz, cdcl₃) δ 7.62 (dd, *J* = 7.7, 1.4 Hz, 1H), 7.48 – 7.46 (m, 1H), 7.29 (td, *J* = 7.6, 1.2 Hz, 1H), 7.23 (dd, *J* = 7.7, 1.1 Hz, 1H), 7.10 (d, *J* = 8.6 Hz, 2H), 6.83 (d, *J* = 8.6 Hz, 2H), 3.79 (s, 3H), 3.12 – 3.09 (m, 2H), 2.93 – 2.90 (m, 2H).

¹³C NMR (176 MHz, cdcl₃) δ 158.04, 145.55, 132.77, 132.61, 132.54, 129.70, 129.44, 126.54, 118.01, 113.82, 112.35, 55.22, 36.97, 36.24.

MS(ESI+) calc'd for C₁₆H₁₅NO: 237.1154, found 237.1146 [M+H]⁺

4-(2-cyanophenethyl)phenyl acetate (2-2f)



Following general procedure B for the synthesis of biaryl substrates (via Wittig/hydrogenation), the phosphonium salt (1.37 mg, 2.72 mmol), 4-formylphenyl acetate (295.5 mg, 1.8 mmol), DBU (0.28 mL, 2.72 mmol), and acetonitrile (33 mL) were used to produce the crude material which was moved on to the next step without further purification. After reduction of the resulting olefin

and purification on silica gel by biotage, 453.0 mg (95% yield over 2 steps) of the biaryl substrate as a viscous, colorless oil, was obtained.

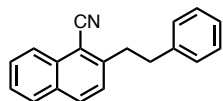
This compound also served as the para acetoxylation standard (2-5).

¹H NMR (700 MHz, cdcl₃) δ 7.63 (dd, *J* = 7.8, 1.8 Hz, 1H), 7.49 (tt, *J* = 7.6, 1.5 Hz, 1H), 7.32 – 7.29 (m, 1H), 7.25 (d, *J* = 7.9 Hz, 1H), 7.20 (dd, *J* = 8.3, 1.6 Hz, 2H), 7.00 (dd, *J* = 8.4, 1.7 Hz, 2H), 3.13 (dd, *J* = 9.1, 7.3 Hz, 2H), 2.96 (dd, *J* = 9.3, 7.1 Hz, 2H), 2.29 (s, 3H).

¹³C NMR (176 MHz, cdcl₃) δ 169.55, 149.09, 145.25, 138.04, 132.85, 132.72, 129.45, 126.70, 121.50, 117.95, 112.37, 36.71, 36.51, 21.11.

MS(ESI+) calc'd for C₁₇H₁₅NO₂: 266.1176, found: 266.1176 [M+H]⁺

2-phenethyl-1-naphthonitrile (2-2g)



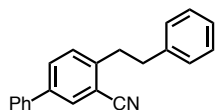
Following general procedure A for the synthesis of biaryl substrates (via cyanoborylation/Suzuki), 2-(2-(4,4,5,5-Tetramethyl-1,3,2-dioxaborolan-2-yl)ethyl)-1-naphthonitrile (1.0 g, 3.2 mmol), palladium acetate (35.9 mg, 0.16 mmol), RuPhos (74.6 mg, 0.16 mmol), Potassium hydroxide (539 mg, 9.6 mmol), bromobenzene (0.5 mL, 4.8 mmol), THF (32.0 mL), and H₂O (3.20 mL) were used to produce after purification on silica gel (100:0 to 95:5 hexanes: ethyl acetate), 508.1 mg (62%) of the biaryl substrate, as a pale yellow solid.

¹H NMR (500 MHz, cdcl₃) δ 8.23 (d, *J* = 8.4 Hz, 1H), 7.96 (d, *J* = 8.5 Hz, 1H), 7.88 (d, *J* = 8.1 Hz, 1H), 7.68 (ddd, *J* = 8.3, 6.9, 1.3 Hz, 1H), 7.57 (ddd, *J* = 8.2, 7.0, 1.2 Hz, 1H), 7.35 (d, *J* = 8.5 Hz, 1H), 7.29 (dd, *J* = 8.3, 7.1 Hz, 2H), 7.23 (d, *J* = 7.4 Hz, 3H), 3.38 – 3.32 (m, 2H), 3.06 (dd, *J* = 9.3, 6.8 Hz, 2H).

^{13}C NMR (126 MHz, cdCl_3) δ 146.35, 140.32, 132.74, 132.62, 132.57, 131.34, 128.46, 128.41, 128.28, 126.86, 126.70, 126.22, 124.99, 116.76, 108.97, 37.45, 37.22.

MS(ESI+) calc'd for $\text{C}_{19}\text{H}_{15}\text{N}$: 258.1238, found: 258.1277 [M+H]⁺

4-phenethyl-[1,1'-biphenyl]-3-carbonitrile (2-2h)



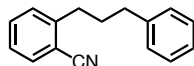
Following general procedure A for the synthesis of biaryl substrates (via cyanoborylation/Suzuki), 4-(2-(4,4,5,5-Tetramethyl-1,3,2-dioxaborolan-2-yl)ethyl)-[1,1'-biphenyl]-3-carbonitrile (373 mg, 1.1 mmol), palladium acetate (12.6 mg, 0.056 mmol), RuPhos (26.0 mg, 0.056 mmol), Potassium hydroxide (186.8 mg, 3.3 mmol), bromobenzene (0.18 mL, 1.67 mmol), THF (11.0 mL), and H_2O (1.11 mL) were used to produce after purification on silica gel (100:0 to 95:5 hexanes: ethyl acetate), 99.3 mg (32%) of the biaryl substrate as a viscous, colorless oil.

^1H NMR (700 MHz, cdCl_3) δ 7.84 (d, $J = 2.0$ Hz, 1H), 7.70 (dd, $J = 8.1, 2.0$ Hz, 1H), 7.57 – 7.54 (m, 2H), 7.47 (t, $J = 7.7$ Hz, 2H), 7.42 – 7.38 (m, 1H), 7.32 – 7.29 (m, 3H), 7.24 – 7.22 (m, 3H), 3.20 – 3.17 (m, 2H), 3.01 (dd, $J = 9.4, 6.8$ Hz, 2H).

^{13}C NMR (126 MHz, cdCl_3) δ 144.09, 140.37, 139.81, 138.64, 131.23, 131.10, 130.09, 128.97, 128.46, 128.40, 128.04, 126.80, 126.20, 117.93, 112.80, 37.05, 36.29.

MS(ESI+) calc'd for $\text{C}_{17}\text{H}_{17}\text{N}$: 283.1361, found: 283.1361 [M⁺]

2-(3-phenylpropyl)benzonitrile (2-2i)



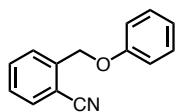
Following general procedure B for the synthesis of biaryl substrates (via Wittig/hydrogenation), the phosphonium salt (1.1 g, 2.2 mmol), phenylacetaldehyde (0.37 mL, 3.33 mmol), DBU (0.5 mL, 3.33 mmol), and acetonitrile (40 mL) were used to produce the crude material which was moved on to the next step without further purification. After reduction of the resulting olefin and purification on silica gel by biotage, 451.0 mg (62% yield over 2 steps) of the biaryl substrate as a viscous, colorless oil, was obtained.

¹H NMR (700 MHz, *cdcl*₃) δ 7.62 (dd, *J* = 7.7, 1.4 Hz, 1H), 7.50 (td, *J* = 7.7, 1.4 Hz, 1H), 7.32 – 7.27 (m, 4H), 7.22 – 7.19 (m, 3H), 2.92 – 2.88 (m, 2H), 2.73 – 2.70 (m, 2H), 2.05 – 1.99 (m, 2H).

¹³C NMR (176 MHz, *cdcl*₃) δ 146.58, 141.89, 133.16, 133.04, 129.78, 128.72, 128.70, 126.78, 126.28, 118.42, 112.70, 35.76, 34.53, 32.73.

MS(ESI+) calc'd for C₁₆H₁₅N: 222.1277, found: 222.1273 [M+H]⁺

2-(phenoxyethyl)benzonitrile (2-2j)



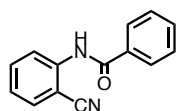
To an oven-dried 100 mL round-bottom flask with stir bar was added phenol (188.2 mg, 2.0 mmol), 2-bromomethyl-benzonitrile (431.3 mg, 2.2 mmol), cesium carbonate (776.2 mg, 2.2 mmol) and 40 mL acetonitrile. The mixture was stirred at room temperature for 5 hours under nitrogen. The reaction mixture was poured into dichloromethane. The organic solution was washed with water and brine, dried over Na₂SO₄, filtered, concentrated, and chromatographed by biotage, to afford 373 mg (89%) biaryl ether substrate as a white solid.

¹H NMR (700 MHz, cdcl₃) δ 7.73 – 7.69 (m, 2H), 7.63 (td, *J* = 7.7, 1.3 Hz, 1H), 7.43 (td, *J* = 7.6, 1.2 Hz, 1H), 7.32 (dd, *J* = 8.8, 7.2 Hz, 2H), 7.03 – 6.99 (m, 3H), 5.28 (s, 2H).

¹³C NMR (176 MHz, cdcl₃) δ 158.11, 140.73, 133.04, 132.83, 129.61, 128.34, 128.30, 121.58, 117.02, 114.89, 111.02, 67.42.

MS(ESI+) calc'd for C₁₄H₁₁NO: 210.0913, found: 210.0909 [M+H]⁺

N-(2-cyanophenyl)benzamide (2-2k)



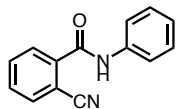
In an oven-dried round-bottom flask with stir bar, 2-aminobenzonitrile and trimethylamine were dissolved in dichloromethane and the solution was cooled to 0 °C. Benzylchloride was added dropwise, and the mixture was stirred at room temperature for 24 hours. The pH of the reaction mixture was then adjusted to 7-8 with saturated sodium bicarbonate solution. The reaction mixture was extracted, washed with water and brine, dried over magnesium sulfate, filtered, and concentrated. The concentrate was recrystallized with ethanol to afford 95.0 mg (21%) amide substrate as a white solid.

¹H NMR (700 MHz, Benzene-*d*₆) δ 8.77 (d, *J* = 8.5 Hz, 1H), 8.11 (s, 1H), 7.78 (dd, *J* = 8.3, 1.3 Hz, 2H), 7.06 – 7.01 (m, 1H), 6.98 – 6.93 (m, 3H), 6.86 (dd, *J* = 7.7, 1.6 Hz, 1H), 6.42 (td, *J* = 7.6, 1.1 Hz, 1H).

¹³C NMR (176 MHz, cdcl₃) δ 165.41, 140.64, 134.37, 133.66, 132.67, 132.15, 129.09, 127.16, 124.21, 120.98, 116.43, 101.96.

MS(ESI+) calc'd for C₁₄H₁₀N₂O: 223.0866, found: 223.0867 [M+H]⁺

2-cyano-N-phenylbenzamide (2-2l)



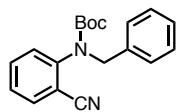
In an oven-dried round-bottom flask with stir bar, 2-cyanobenzoic acid (588.5, 4.0 mmol) was dissolved in dichloromethane (15 mL). Dimethylformamide (0.5 mL) and oxalyl chloride (0.69 mL, 8.0 mmol) were added dropwise. The reaction was refluxed overnight. After cooled to room temperature, the solvent was pumped off the crude mixture. To the crude 2-cyanobenzoylchloride was added dropwise aniline (1.09 mL, 12.0 mmol) dissolved in dichloromethane (15 mL). Triethylamine (0.56 mL, 4.0 mmol) was then added dropwise, and the mixture was refluxed overnight. The reaction mixture was extracted with ethyl acetate, washed with 1.0 M hydrochloric acid, washed with water and brine, dried over sodium sulfate, filtered, and concentrated. The concentrate was chromatographed by biotage, to afford 84 mg (10% over two steps) amide substrate as a white solid.

¹H NMR (700 MHz, cdcl₃) δ 7.95 (d, *J* = 7.8 Hz, 1H), 7.89 (s, 1H), 7.82 (d, *J* = 7.7 Hz, 1H), 7.74 (t, *J* = 7.7 Hz, 1H), 7.68 – 7.62 (m, 3H), 7.40 (t, *J* = 7.8 Hz, 2H), 7.22 – 7.19 (m, 1H).

¹³C NMR (176 MHz, cdcl₃) δ 163.03, 138.63, 137.15, 134.22, 133.12, 131.43, 129.21, 128.96, 125.33, 120.40, 117.41, 110.48.

MS(ESI+) calc'd for C₁₄H₁₀N₂O: 223.0866, found: 223.0865 [M+H]⁺

tert-butyl benzyl(2-cyanophenyl)carbamate (2-2m)



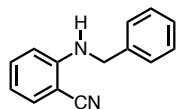
In an oven-dried round-bottom flask with stir bar, amine substrate (**2-2n**, see below)(218 mg, 1.3 mmol) was dissolved in acetonitrile(6 mL). Di-*tert*-butyl dicarbonate (539.1 mg, 2.47 mmol) was then added and the reaction mixture was added as a solid. 4-dimethylaminopyridine (DMAP)(158.8 mg, 1.3 mmol) was added in portion and the reaction was stirred overnight at room temperature. The mixture was quenched with water, extracted with ethyl acetate, washed with brine, dried over magnesium sulfate, filtered, and concentrated. The concentrate was chromatographed by biotage, to afford 389 mg (97%) boc-amine substrate as a white solid. Substrate was analyzed as a mixture of rotamers (mixture 1.0:1.9), with the spectra taken at -30 °C.

¹H NMR (700 MHz, CDCl₃, -30 °C) δ 7.67 (d, *J* = 7.7 Hz, 0.32H), 7.58 (d, *J* = 7.7 Hz, 0.61H), 7.55 – 7.49 (m, 1H), 7.33 (t, *J* = 7.5 Hz, 1H), 7.31 – 7.27 (m, 2H), 7.24 (d, *J* = 7.6 Hz, 3H), 7.20 (d, *J* = 8.2 Hz, 0.33H), 7.14 (d, *J* = 8.1 Hz, 0.61fH), 4.93 (d, *J* = 15.0 Hz, 1H), 4.83 (d, *J* = 15.2 Hz, 1H), 1.52 (s, 3H), 1.41 (s, 6H).

¹³C NMR (176 MHz, cdcl₃, -30 °C) (rotamers) δ 154.12, 153.52, 144.78, 144.05, 137.18, 136.57, 133.56, 133.38, 133.33, 133.04, 128.55, 128.43, 128.38, 128.30, 127.87, 127.52, 127.49, 127.47, 127.16, 126.99, 116.97, 116.83, 112.88, 112.55, 82.06, 81.66, 54.04, 53.04, 28.10, 27.79.

MS(ESI+) calc'd for C₁₉H₂₀N₂O₂: 331.1417, found: 331.1422 [M+Na]⁺

2-(benzylamino)benzonitrile (**2-2n**)



In an oven-dried round-bottom flask with stir bar, 2-aminobenzonitrile (1.1814g, 10.0 mmol) was dissolved in N,N-dimethylformamide (50 mL) with benzylbromide (0.59 mL, 5.0 mmol). Potassium carbonate (0.8292, 6.0 mmol) was added, and the reaction was stilled under nitrogen at

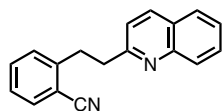
60 °C, overnight. The reaction mixture was cooled to room temperature, quenched with water, diluted with ethyl acetate, and extracted with ethyl acetate. The organic layer was washed with water (x3) and washed with brine (x2). The mixture was dried over Na₂SO₄, filtered, concentrated, and chromatographed by biotage, to afford 213 mg (21%) amine substrate as a white solid.

¹H NMR (500 MHz, cdcl₃) δ 7.42 (dd, *J* = 7.7, 1.6 Hz, 1H), 7.39 – 7.28 (m, 6H), 6.69 (t, *J* = 7.5 Hz, 1H), 6.64 (d, *J* = 8.5 Hz, 1H), 5.01 (s, 1H), 4.44 (d, *J* = 5.5 Hz, 2H).

¹³C NMR (126 MHz, cdcl₃) δ 149.95, 137.59, 134.17, 132.65, 128.77, 127.56, 127.07, 117.76, 116.77, 110.92, 95.85, 47.39.

MS(ESI+) calc'd for C₁₄H₁₂N₂: 209.1073, found: 209.1074 [M+H]⁺

2-(2-(quinolin-2-yl)ethyl)benzonitrile (2-2o)



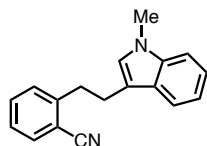
Following general procedure B for the synthesis of biaryl substrates (via Wittig/hydrogenation), the phosphonium salt (501.4 mg, 1.0 mmol), 2-quinoline-carboxaldehyde (103.7 mg, 0.66 mmol), DBU (0.15 mL, 1.0 mmol), and acetonitrile (10 mL) were used to produce the crude material which was moved on to the next step without further purification. After reduction of the resulting olefin and purification on silica gel by biotage, 121.8 mg (47% yield over 2 steps) of the biaryl substrate as a viscous, colorless oil, was obtained.

¹H NMR (500 MHz, cdcl₃) δ 8.07 (dd, *J* = 8.2, 5.7 Hz, 2H), 7.79 (dd, *J* = 8.3, 1.4 Hz, 1H), 7.71 (ddd, *J* = 8.4, 6.8, 1.5 Hz, 1H), 7.64 (dd, *J* = 7.7, 1.4 Hz, 1H), 7.53 – 7.45 (m, 2H), 7.36 (dd, *J* = 7.9, 1.2 Hz, 1H), 7.31 (d, *J* = 8.4 Hz, 1H), 7.29 (dd, *J* = 7.7, 1.2 Hz, 1H), 3.43 – 3.39 (m, 2H), 3.35 (ddd, *J* = 9.5, 6.1, 2.0 Hz, 2H).

^{13}C NMR (176 MHz, cdcl_3) δ 160.51, 147.92, 145.43, 136.46, 132.83, 132.77, 129.78, 129.45, 128.89, 127.54, 126.86, 126.67, 125.93, 121.45, 118.08, 112.41, 39.82, 34.31.

MS(ESI+) calc'd for $\text{C}_{18}\text{H}_{14}\text{N}_2$: 259.1235, found: 259.1237 [M+H] $^+$

2-(2-(1-methyl-1H-indol-3-yl)ethyl)benzonitrile (2-2p)



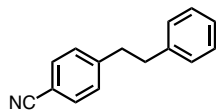
Following general procedure B for the synthesis of biaryl substrates (via Wittig/hydrogenation), phosphonium salt (1.1g, 2.2 mmol), 1-methyl-indole-3-carboxaldehyde (530.1 mg, 3.33 mmol), DBU (0.5 mL, 3.33 mmol), and acetonitrile (40 mL) were used to produce the crude material which was moved on to the next step without further purification. After reduction of the resulting olefin and purification on silica gel by biotage (ethyl acetate/hexanes), 317.2 mg (60% yield over 2 steps) of indole starting material, as a yellow solid, was obtained.

^1H NMR (700 MHz, Benzene- d_6) δ 7.71 – 7.69 (m, 1H), 7.26 (ddd, $J = 8.1, 6.9, 1.3$ Hz, 1H), 7.24 – 7.22 (m, 1H), 7.10 (dd, $J = 7.7, 1.3$ Hz, 1H), 7.04 (d, $J = 8.3$ Hz, 1H), 6.82 (td, $J = 7.6, 1.4$ Hz, 1H), 6.74 (dd, $J = 7.7, 1.2$ Hz, 1H), 6.61 (td, $J = 7.6, 1.2$ Hz, 1H), 6.33 (s, 1H), 3.13 – 3.09 (m, 2H), 3.04 (dd, $J = 9.3, 6.4$ Hz, 2H), 2.93 (s, 3H).

^{13}C NMR (176 MHz, cdcl_3) δ 146.20, 136.99, 132.77, 132.62, 129.67, 127.63, 126.47, 126.46, 121.53, 118.84, 118.78, 118.17, 113.50, 112.32, 109.15, 35.87, 32.56, 26.61.

MS(ESI+) calc'd for $\text{C}_{18}\text{H}_{16}\text{N}_2$: 261.1386, found: 261.1384 [M+H] $^+$

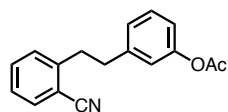
4-phenethylbenzonitrile (2-10)



This compound was prepared according to literature procedure (Sonogashira cross-coupling and hydrogenation), and all spectra match published data.^{6,7}

6.2.4 Spectral Characterization of Acetoxylation Products

3-(2-cyanophenethyl)phenyl acetate (2-3a)



(Scaled- up procedure (1.0 mmol))

Following general procedure C for the distal *meta*-acetoxylation of biaryl substrates, 2-phenylbenzonitrile (20.73 mg, 1.0 mmol), palladium acetate (44.9 mg, 0.2 mmol), silver trifluoroacetic acid (44.18 mg, 0.2 mmol), *N*-Acetylglycine (23.4 mg, 0.2 mmol), (diacetoxyiodo)benzene (96.63 mg, 3.0 mmol), acetic anhydride (0.66 mL, 7.0 mmol), and 5 mL (x2) hexafluoroisopropanol (HFIP) were used to produce, after purification on silica gel (9:1 hexanes: ethyl acetate), 19.6 mg (74%) of the acetoxyated product, as a viscous, colorless oil. Product was isolated as a mixture of major *meta*-product with a minor regioisomer (2.0 : 1.0 *meta* : minor isomer). Ratio based on major to minor aromatic peaks as determined by COSY analysis.

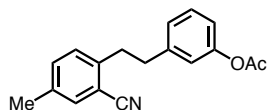
¹H NMR peak. The *meta*-acetoxyated product is characterized below.

¹H NMR (401 MHz, cdCl₃) δ 7.63 (dd, *J* = 7.7, 1.4 Hz, 1H), 7.48 (td, *J* = 7.6, 1.4 Hz, 1H), 7.33 – 7.27 (m, 2H), 7.25 – 7.22 (m, 1H), 7.06 (d, *J* = 8.0 Hz, 1H), 6.94 (dd, *J* = 7.8, 1.2 Hz, 2H), 3.14 (dd, *J* = 9.7, 6.3 Hz, 2H), 2.99 – 2.93 (m, 2H), 2.29 (s, 3H).

¹³C NMR (126 MHz, cdcl₃) δ 171.02, 150.65, 144.98, 142.04, 132.75, 132.65, 129.61, 129.29, 126.62, 125.94, 121.51, 119.39, 117.82, 112.22, 36.71, 36.34, 20.90.

MS(ESI+) calc'd for C₁₇H₁₅NO₂: 266.1136, found: 266.1176 [M+H]⁺

3-(2-cyano-4-methylphenethyl)phenyl acetate (2-3b)



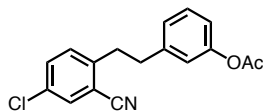
Following general procedure C for the distal *meta*-acetoxylation of biaryl substrates, 5-methyl-2-phenethylbenzonitrile (44.2 mg, 0.2 mmol), palladium acetate (8.9 mg, 0.04 mmol), silver trifluoroacetic acid (8.8 mg, 0.04 mmol), *N*-Acetylglycine (5.0 mg, 0.04 mmol), (diacetoxyiodo)benzene (193.3 mg, 0.6 mmol), acetic anhydride (0.13 mL, 1.4 mmol), and 1 mL (x2) hexafluoroisopropanol (HFIP) were used to produce, after purification on silica gel (9:1 hexanes: ethyl acetate), 29.5 mg (53%) of the acetoxyated product as a viscous, colorless oil. Product was isolated as a mixture of major *meta*-product with a minor regioisomer (2.0 : 1.0 *meta* : minor isomer). Ratio based on major to minor aromatic peaks as determined by COSY analysis. ¹H NMR peak. The *meta*-acetoxyated product is characterized below.

¹H NMR (700 MHz, cdcl₃) δ 7.42 (s, 1H), 7.30 – 7.27 (m, 2H), 7.12 (d, *J* = 7.8 Hz, 1H), 7.06 (d, *J* = 7.7 Hz, 1H), 6.94 (d, *J* = 6.2 Hz, 2H), 3.09 (dd, *J* = 9.7, 6.5 Hz, 2H), 2.94 (dd, *J* = 9.5, 6.8 Hz, 2H), 2.34 (s, 3H), 2.29 (s, 3H).

¹³C NMR (176 MHz, cdcl₃) δ 169.55, 169.46, 150.74, 149.04, 142.31, 142.23, 142.10, 138.18, 136.64, 136.61, 133.66, 133.63, 133.06, 130.84, 129.56, 129.45, 129.36, 126.05, 121.59, 121.45, 119.43, 118.12, 112.08, 36.92, 36.59, 36.21, 35.95, 21.12, 20.64.

MS(ESI+) calc'd for C₁₈H₁₇NO₂: 280.1338, found: 280.1198 [M+H]⁺

3-(4-chloro-2-cyanophenethyl)phenyl acetate (2-3c)



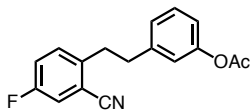
Following general procedure C for the distal *meta*-acetoxylation of biaryl substrates, 5-chloro-2-phenethylbenzonitrile (18.8 mg, 0.088 mmol), palladium acetate (4.0 mg, 0.018 mmol), silver trifluoroacetic acid (4.0 mg, 0.018 mmol), *N*-Acetylglycine (2.1 mg, 0.018 mmol), (diacetoxyiodo)benzene (85.0 mg, 0.264 mmol), acetic anhydride (0.06 mL, 0.616 mmol), and 0.44 mL (x2) hexafluoroisopropanol (HFIP) were used to produce, after purification on silica gel (9:1 hexanes: ethyl acetate), 11.4 mg (43%) of the acetoxyated product as a viscous, pale yellow oil.

¹H NMR (700 MHz, cdcl₃) δ 7.60 (d, *J* = 2.3 Hz, 1H), 7.44 (dd, *J* = 8.3, 2.3 Hz, 1H), 7.29 (t, *J* = 7.8 Hz, 1H), 7.15 (d, *J* = 8.4 Hz, 1H), 7.03 (d, *J* = 7.7 Hz, 1H), 6.95 (ddd, *J* = 8.1, 2.5, 0.9 Hz, 1H), 6.90 (s, 1H), 3.12 – 3.10 (m, 2H), 2.96 – 2.94 (m, 2H), 2.30 (s, 3H).

¹³C NMR (176 MHz, cdcl₃) δ 169.47, 150.76, 143.53, 141.65, 133.05, 132.55, 132.29, 131.12, 129.50, 126.04, 121.63, 119.65, 116.65, 113.80, 36.62, 35.83, 21.12.

MS(ESI+) calc'd for C₁₇H₁₄ClNO₂: 300.0786, found: 300.0786 [M+H]⁺

3-(2-cyano-4-fluorophenethyl)phenyl acetate (2-3d)



Following general procedure C for the distal *meta*-acetoxylation of biaryl substrates, 5-fluoro-2-phenethylbenzonitrile (45.1 mg, 0.2 mmol), palladium acetate (8.9 mg, 0.04 mmol), silver

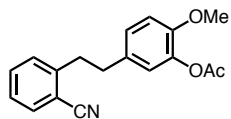
trifluoroacetic acid (8.8 mg, 0.04 mmol), *N*-Acetylglycine (5.0 mg, 0.04 mmol), (diacetoxyiodo)benzene (193.3 mg, 0.6 mmol), acetic anhydride (0.13 mL, 1.4 mmol), and 1 mL (x2) hexafluoroisopropanol (HFIP) were used to produce, after purification on silica gel (9:1 hexanes: ethyl acetate), 14.6 mg (26%) of the acetoxyated product as a viscous, pale yellow oil.

¹H NMR (700 MHz, cdcl₃) δ 7.32 (dd, *J* = 8.0, 2.6 Hz, 1H), 7.29 (t, *J* = 7.9 Hz, 1H), 7.21 – 7.16 (m, 2H), 7.03 (d, *J* = 7.6 Hz, 1H), 6.94 (dd, *J* = 8.0, 2.3 Hz, 1H), 6.90 (d, *J* = 2.0 Hz, 1H), 3.11 (dd, *J* = 9.2, 6.7 Hz, 2H), 2.95 (dd, *J* = 9.2, 6.8 Hz, 3H), 2.30 (d, *J* = 0.8 Hz, 3H).

¹³C NMR (176 MHz, CDCl₃) δ 169.51, 160.52 (d, *J* = 248.2 Hz), 150.77, 141.79, 141.13 (d, *J* = 2.4 Hz), 131.62 (d, *J* = 8.2 Hz), 129.50, 126.09, 121.68, 120.41 (d, *J* = 21.0 Hz), 119.63, 119.38 (d, *J* = 24.5 Hz), 116.82, 113.45 (d, *J* = 9.1 Hz), 36.85, 35.71, 21.16.

MS(ESI+) calc'd for C₁₇H₁₄FNO₂: 284.1042, found: 284.1081 [M+H]⁺

5-(2-cyanophenethyl)-2-methoxyphenyl acetate (2-3e)



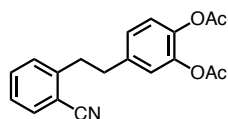
Following general procedure C for the distal *meta*-acetoxylation of biaryl substrates, 2-(4-methoxyphenethyl)benzonitrile (29.0 mg, 0.12 mmol), palladium acetate (5.4 mg, 0.024 mmol), silver trifluoroacetic acid (5.0 mg, 0.024 mmol), *N*-Acetylglycine (2.8 mg, 0.024 mmol), (diacetoxyiodo)benzene (116.0 mg, 0.36 mmol), acetic anhydride (0.08 mL, 0.84 mmol), and 0.6 mL (x2) hexafluoroisopropanol (HFIP) were used to produce, after purification on silica gel (8:2 hexanes: ethyl acetate), 31.7 mg (89%) of the acetoxyated product as a viscous, yellow oil.

¹H NMR (700 MHz, Chloroform-*d*) δ 7.62 (d, *J* = 7.7 Hz, 1H), 7.48 (td, *J* = 7.6, 1.3 Hz, 1H), 7.29 (t, *J* = 7.6 Hz, 1H), 7.22 (d, *J* = 7.8 Hz, 1H), 7.02 (dd, *J* = 8.4, 2.2 Hz, 1H), 6.90 – 6.86 (m, 2H), 3.81 (s, 3H), 3.10 (dd, *J* = 9.4, 6.7 Hz, 2H), 2.90 (dd, *J* = 9.4, 6.7 Hz, 2H), 2.31 (d, *J* = 0.8 Hz, 3H).

¹³C NMR (176 MHz, cdcl₃) δ 169.02, 149.52, 145.26, 139.55, 133.09, 132.83, 132.71, 129.74, 126.69, 126.65, 122.87, 121.77, 117.97, 112.38, 55.93, 36.71, 36.13, 20.65.

MS(ESI+) calc'd for C₁₈H₁₇NO₃: 296.1287, found: 296.1281 [M+H]⁺

4-(2-cyanophenethyl)-1,2-phenylene diacetate (2-3f)



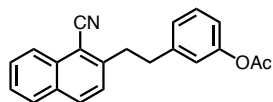
Following general procedure C for the distal *meta*-acetoxylation of biaryl substrates, 4-(2-cyanophenethyl)phenyl acetate (53.1 mg, 0.2 mmol), palladium acetate (8.9 mg, 0.04 mmol), silver trifluoroacetic acid (8.8 mg, 0.04 mmol), *N*-Acetylglycine (5.0 mg, 0.04 mmol), (diacetoxyiodo)benzene (193.3 mg, 0.6 mmol), acetic anhydride (0.13 mL, 1.4 mmol), and 1 mL (x2) hexafluoroisopropanol (HFIP) were used to produce, after purification on silica gel (9:1 hexanes: ethyl acetate), 35.3 mg (55%) of the acetoxyated product as a viscous, colorless oil.

¹H NMR (700 MHz, Chloroform-*d*) δ 7.63 (dd, *J* = 7.8, 1.4 Hz, 1H), 7.49 (td, *J* = 7.6, 1.4 Hz, 1H), 7.31 (td, *J* = 7.6, 1.2 Hz, 1H), 7.24 (d, *J* = 7.7 Hz, 1H), 7.12 – 7.07 (m, 2H), 7.03 (d, *J* = 1.9 Hz, 1H), 3.15 – 3.11 (m, 2H), 2.96 (dd, *J* = 9.5, 6.8 Hz, 2H), 2.28 (d, *J* = 2.1 Hz, 6H).

¹³C NMR (176 MHz, cdcl₃) δ 168.39, 168.29, 144.92, 141.89, 140.43, 139.34, 132.88, 132.82, 129.72, 126.79, 126.66, 123.36, 123.29, 117.91, 112.27, 36.47, 20.62.

MS(ESI+) calc'd for C₁₉H₁₇NO₄: 346.1055, found: 346.1048 [M+Na]⁺

3-(2-(1-cyanonaphthalen-2-yl)ethyl)phenyl acetate (2-3g)



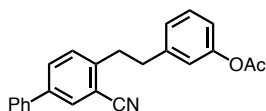
Following general procedure C for the distal *meta*-acetoxylation of biaryl substrates, 2-phenethyl-1-naphthonitrile (51.5 mg, 0.2 mmol), palladium acetate (8.9 mg, 0.04 mmol), silver trifluoroacetic acid (8.8 mg, 0.04 mmol), *N*-Acetylglycine (5.0 mg, 0.04 mmol), (diacetoxyiodo)benzene (193.3 mg, 0.6 mmol), acetic anhydride (0.13 mL, 1.4 mmol), and 1 mL (x2) hexafluoroisopropanol (HFIP) were used to produce, after purification on silica gel (9:1 hexanes: ethyl acetate), 39.2 mg (62%) of the acetoxyated product as a viscous, yellow oil.

¹H NMR (¹H NMR (700 MHz, cdcl₃) δ 8.23 (d, *J* = 8.4 Hz, 1H), 7.96 (d, *J* = 8.5 Hz, 1H), 7.88 (d, *J* = 8.1 Hz, 1H), 7.68 (ddd, *J* = 8.3, 6.9, 1.2 Hz, 1H), 7.59 – 7.56 (m, 1H), 7.34 (dd, *J* = 8.5, 4.4 Hz, 1H), 7.29 (t, *J* = 7.8 Hz, 1H), 7.10 – 7.08 (m, 1H), 6.98 (d, *J* = 1.9 Hz, 1H), 6.95 (dd, *J* = 8.1, 2.3 Hz, 1H), 3.36 – 3.32 (m, 2H), 3.07 – 3.03 (m, 2H), 2.29 (s, 2H).

¹³C NMR (176 MHz, cdcl₃) δ 169.48, 150.81, 146.09, 142.13, 132.83, 131.49, 129.47, 128.60, 128.40, 126.92, 126.85, 126.09, 125.09, 121.65, 121.56, 119.58, 116.82, 109.07, 37.26, 37.03, 21.14.

MS(ESI+) calc'd for C₂₁H₁₇NO₂: 316.1332, found: 316.1327 [M+H]⁺

3-(2-(3-cyano-[1,1'-biphenyl]-4-yl)ethyl)phenyl acetate (2-3h)



Following general procedure C for the distal *meta*-acetoxylation of biaryl substrates, 4-phenethyl-[1,1'-biphenyl]-3-carbonitrile (56.7 mg, 0.2 mmol), palladium acetate (8.9 mg, 0.04 mmol), *N*-

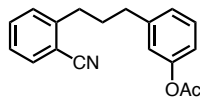
Acetylglycine (5.0 mg, 0.04 mmol), (diacetoxyiodo)benzene (193.3 mg, 0.6 mmol), acetic anhydride (0.13 mL, 1.4 mmol), and 1 mL (x2) hexafluoroisopropanol (HFIP) were used to produce, after purification on silica gel (9:1 hexanes: ethyl acetate), 57.7 mg (85%) of the acetoxyated product as a viscous, yellow oil. Product was isolated as a mixture of major *meta*-product with a minor regioisomer (2.0 : 1.0 *meta* : minor isomer). Ratio based on major to minor aromatic peaks as determined by COSY analysis. ¹H NMR peak. The *meta*-acetoxyated product is characterized below.

¹H NMR (700 MHz, cdcl₃) δ 7.84 (d, *J* = 2.0 Hz, 1H), 7.70 (dd, *J* = 8.0, 2.0 Hz, 1H), 7.56 – 7.54 (m, 2H), 7.47 (t, *J* = 7.7 Hz, 2H), 7.41 – 7.39 (m, 1H), 7.30 (d, *J* = 8.1 Hz, 1H), 7.23 (d, *J* = 8.4 Hz, 1H), 7.09 (d, *J* = 7.9 Hz, 1H), 6.96 (dd, *J* = 4.6, 2.4 Hz, 2H), 3.19 – 3.15 (m, 2H), 3.00 (qd, *J* = 7.8, 6.8, 3.8 Hz, 2H), 2.30 (s, 3H).

¹³C NMR (126 MHz, cdcl₃) δ 169.89, 151.20, 149.54, 144.20, 142.56, 140.44, 139.13, 131.65, 130.63, 129.87, 129.47, 128.56, 127.31, 126.50, 122.07, 119.96, 118.37, 113.27, 37.24, 36.50, 21.54.

MS(ESI+) calc'd for C₂₃H₁₉NO₂: 364.1313, found: 364.1248 [M+Na]⁺

3-(3-(2-cyanophenyl)propyl)phenyl acetate (2-3i)



Following general procedure C for the distal *meta*-acetoxylation of biaryl substrates, 2-(3-phenylpropyl)benzotrile (44.3 mg, 0.2 mmol), palladium acetate (8.9 mg, 0.04 mmol), silver trifluoroacetic acid (8.8 mg, 0.04 mmol), *N*-Acetylglycine (5.0 mg, 0.04 mmol), (diacetoxyiodo)benzene (193.3 mg, 0.6 mmol), acetic anhydride (0.13 mL, 1.4 mmol), and 1 mL (x2) hexafluoroisopropanol (HFIP) were used to produce, after purification on silica gel (9:1

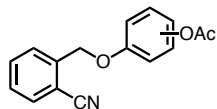
hexanes: ethyl acetate), 37.0 mg (66%) of the acetoxyated product as a colorless, viscous oil. Product was isolated as a mixture of major *meta*-product, with a small amount of starting material and a minor regioisomer. The *meta*-acetoxyated product is characterized below.

¹H NMR (500 MHz, , cdcl₃) δ 7.63 – 7.60 (m, 1H), 7.50 (td, *J* = 7.7, 1.4 Hz, 1H), 7.31 – 7.27 (m, 3H), 7.08 – 7.05 (m, 1H), 6.94 – 6.90 (m, 2H), 2.89 (dd, *J* = 8.8, 6.9 Hz, 2H), 2.73 – 2.69 (m, 2H), 2.29 (s, 2H), 2.05 – 1.98 (m, 3H).

¹³C NMR (126 MHz, cdcl₃) δ 169.45, 150.64, 145.93, 143.17, 132.74, 132.65, 129.39, 129.22, 126.42, 125.80, 121.34, 119.02, 117.98, 112.25, 35.03, 34.04, 31.98, 21.05.

MS(ESI+) calc'd for C₁₈H₁₇NO₂: 280.1332, found: 280.1335 [M+H]⁺

3-((2-cyanobenzyl)oxy)phenyl acetate and 2-((2-cyanobenzyl)oxy)phenyl acetate (2-3j)



Following general procedure C for the distal *meta*-acetoxylation of biaryl substrates, 2-(phenoxyethyl)benzotrile (41.8 mg, 0.2 mmol), palladium acetate (8.9 mg, 0.04 mmol), silver trifluoroacetic acid (8.8 mg, 0.04 mmol), *N*-Acetylglycine (5.0 mg, 0.04 mmol), (diacetoxyiodo)benzene (193.3 mg, 0.6 mmol), acetic anhydride (0.13 mL, 1.4 mmol), and 1 mL (x2) hexafluoroisopropanol (HFIP) were used to produce, after purification on silica gel (gradient 8:2 hexanes: ethyl acetate), a mixture of *meta*- and *ortho*-acetoxyated products in a 2.3:1.0 *ortho* : *meta* ratio 36.5 mg (66%) as a viscous, pale yellow oil.

¹H NMR (401 MHz, cdcl₃) δ 7.71 – 7.65 (m, 2H), 7.64 – 7.59 (m, 2H), 7.45 – 7.38 (m, 2H), 7.29 (t, *J* = 8.1 Hz, 1H), 7.18 (ddd, *J* = 8.2, 7.3, 1.8 Hz, 1H), 7.09 – 7.04 (m, 1H), 6.99 (td, *J* = 7.9, 7.5,

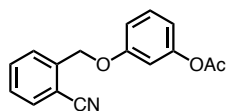
1.2 Hz, 2H), 6.86 (ddd, $J = 8.4, 2.4, 1.0$ Hz, 1H), 6.77 – 6.71 (m, 1H), 5.30 (s, 2H), 5.24 (s, 1H), 2.29 (s, 3H), 2.28 (s, 1H).

^{13}C NMR (126 MHz, cdCl_3) δ 169.20, 168.91, 158.84, 151.58, 149.42, 140.24, 140.18, 140.13, 133.04, 133.02, 132.78, 132.68, 129.95, 128.35, 128.29, 128.26, 128.02, 126.87, 123.02, 121.85, 116.88, 116.81, 114.72, 114.07, 112.27, 110.94, 110.66, 108.68, 67.93, 67.53, 21.04, 20.58.

MS(ESI+) calc'd for $\text{C}_{16}\text{H}_{13}\text{NO}_3$: 268.0968, found: 268.0969 [M+H]⁺

The authentic standards were synthesized by literature protocol, and are characterized below.

3-((2-cyanobenzyl)oxy)phenyl acetate (2-3j-std-meta) (authentic standard)

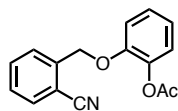


To an oven-dried round-bottom flask with stir bar was added resorcinol monoacetate (304.3 mg, 2.0 mmol), 2-bromomethyl-benzonitrile (431.3 mg, 2.2 mmol), cesium carbonate (776.2 mg, 2.2 mmol) and 40 mL acetonitrile. The mixture was stirred at room temperature for overnight, under nitrogen. The reaction mixture was poured into dichloromethane. The organic solution was washed with water and brine, dried over Na_2SO_4 , filtered, concentrated, and chromatographed using Biotage isolera, to afford 351.4 mg (66%) of the ether standard as a white solid.

^1H NMR (700 MHz, cdCl_3) δ 7.71 (dd, $J = 7.7, 1.3$ Hz, 1H), 7.69 – 7.67 (m, 1H), 7.64 (td, $J = 7.7, 1.3$ Hz, 1H), 7.46 – 7.43 (m, 1H), 7.31 (t, $J = 8.2$ Hz, 1H), 6.88 (ddd, $J = 8.4, 2.5, 0.9$ Hz, 1H), 6.77 (t, $J = 2.3$ Hz, 1H), 6.76 – 6.75 (m, 1H), 5.25 (s, 2H), 2.30 (s, 3H).

^{13}C NMR (176 MHz, cdCl_3) δ 169.63, 159.27, 152.01, 140.56, 133.45, 133.21, 130.38, 128.79, 128.68, 117.31, 115.14, 112.70, 111.37, 109.11, 67.96, 21.47.

2-((2-cyanobenzyl)oxy)phenyl acetate (2-3j-std-ortho) (authentic standard)

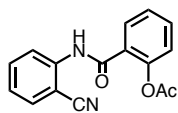


To an oven-dried round-bottom flask with stir bar was added catechol (220.2 mg, 2.0 mmol), 2-bromomethyl-benzonitrile (431.3 mg, 2.2 mmol), cesium carbonate (776.2 mg, 2.2 mmol) and 40 mL acetonitrile. The mixture was stirred at room temperature for overnight, under nitrogen. The reaction mixture was extracted with ethyl acetate, and chromatographed using Biotage isolera, to afford 114.0 mg (51%) of 2-((2hydroxyphenoxy)methyl)benzonitrile. Then, 2-((2hydroxyphenoxy)methyl)benzonitrile, acetic anhydride (0.07 mL, 0.735 mmol), triethyl amine (0.34 mL, 2.45 mmol) and DMAP (29.9 mg, 0.245 mmol) were dissolved in DCM (1.0 mL). The mixture was allowed to stir overnight at room temperarue. The reaction mixture was diluted with ethyl acetate, extracted with sodium bicarbonate, and washed with water and brine. The mixture was concentrated and chromatographed using Biotage isolera, to afford 112.6 mg (86%) of the ether standard.

$^1\text{H NMR}$ (700 MHz, cdcl_3) δ 7.70 – 7.69 (m, 1H), 7.65 – 7.60 (m, 2H), 7.42 (td, $J = 7.4, 1.7$ Hz, 1H), 7.21 – 7.18 (m, 1H), 7.08 (dd, $J = 7.8, 1.7$ Hz, 1H), 7.03 – 6.99 (m, 2H), 5.32 (s, 2H), 2.31 (s, 3H).

$^{13}\text{C NMR}$ (176 MHz, cdcl_3) δ 169.33, 149.84, 140.67, 140.60, 133.47, 133.11, 128.71, 128.45, 127.30, 123.45, 122.28, 117.24, 114.50, 111.08, 68.36, 21.01.

2-((2-cyanophenyl)carbamoyl)phenyl acetate (2-3k)



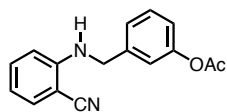
Following general procedure C for the distal *meta*-acetoxylation of biaryl substrates, N-(2-cyanophenyl)benzamide (44.5 mg, 0.2 mmol), palladium acetate (8.9 mg, 0.04 mmol), silver trifluoroacetic acid (8.8 mg, 0.04 mmol), *N*-Acetylglycine (5.0 mg, 0.04 mmol), (diacetoxyiodo)benzene (193.3 mg, 0.6 mmol), acetic anhydride (0.13 mL, 1.4 mmol), and 1 mL (x2) hexafluoroisopropanol (HFIP) were used to produce, after purification on silica gel (9:1 hexanes: ethyl acetate), 42.5 mg (76%) of the acetoxyated product as a yellow solid.

¹H NMR (700 MHz, Benzene-*d*₆) δ 8.82 (d, *J* = 1.6 Hz, 2H), 8.02 (dt, *J* = 7.8, 1.4 Hz, 1H), 6.95 (td, *J* = 7.8, 1.7 Hz, 2H), 6.89 (dd, *J* = 7.7, 1.6 Hz, 1H), 6.86 (dd, *J* = 8.2, 1.2 Hz, 1H), 6.81 (td, *J* = 7.5, 1.1 Hz, 1H), 6.42 (td, *J* = 7.6, 1.1 Hz, 1H), 2.05 (s, 3H).

¹³C NMR (176 MHz, cdcl₃) δ 169.15, 163.87, 148.48, 141.03, 134.77, 133.44, 132.78, 131.05, 127.10, 126.92, 124.68, 124.03, 121.58, 116.81, 102.11, 21.77.

MS(ESI+) calc'd for C₁₆H₁₂N₂O₃: 303.0746, found: 303.0704 [M+Na]⁺

3-(((2-cyanophenyl)amino)methyl)phenyl acetate (2-3m)



Following general procedure C for the distal *meta*-acetoxylation of biaryl substrates, *tert*-butyl benzyl(2-cyanophenyl)carbamate (61.7 mg, 0.2 mmol), palladium acetate (8.9 mg, 0.04 mmol), silver trifluoroacetic acid (8.8 mg, 0.04 mmol), *N*-Acetylglycine (5.0 mg, 0.04 mmol), (diacetoxyiodo)benzene (193.3 mg, 0.6 mmol), acetic anhydride (0.13 mL, 1.4 mmol), and 1 mL (x2) hexafluoroisopropanol (HFIP) were used to produce, after purification by biotage, 8.0 mg (19%) of overall acetoxyated product a colorless, viscous oil. Product was isolated as a mixture

of major *meta*-product, with a small amount of a minor regioisomer (2.3 : 1.0). The *meta* regioisomer is characterized below.

¹H NMR (700 MHz, cdcl₃) δ 7.43 – 7.41 (m, 1H), 7.37 (t, *J* = 7.6 Hz, 1H), 7.35 – 7.32 (m, 1H), 7.21 (d, *J* = 7.7 Hz, 1H), 7.08 (d, *J* = 2.6 Hz, 1H), 7.03 (d, *J* = 8.0 Hz, 1H), 6.70 (t, *J* = 7.6 Hz, 1H), 6.59 (d, *J* = 8.5 Hz, 1H), 5.05 (s, 1H), 4.46 (d, *J* = 5.7 Hz, 2H), 2.30 (s, 3H).

¹³C NMR (176 MHz, cdcl₃) δ 169.37, 151.10, 149.83, 139.64, 134.31, 132.75, 129.87, 128.78, 124.29, 120.82, 117.76, 117.11, 111.06, 96.32, 47.03, 21.12.

MS(ESI+) calc'd for C₁₆H₁₄N₂O₂: 267.1128, found: 267.1130 [M+H]⁺

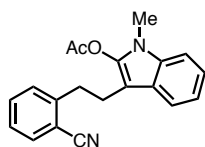
The meta-acetylated authentic standard was synthesized by literature protocol, and is characterized below.(2-3m-std-meta)

To an oven-dried round-bottom flask with stir bar, was added 2-amino benzonitrile (0472.6 mg, 4.0 mmol), and 3-acetoxy benzaldehyde (656.6 mg, 4.0 mmol). The reagents were dissolved in dichloroethane (14 mL), under nitrogen. To the mixture, was added sodium triacetoxyborohydride (NaBH(OAc)₃) (1.187 g) and AcOH (0.23 mL). The mixture was stirred at room temperature, under nitrogen, overnight. The reaction mixture was quenched with 1 N NaOH, and the product was extracted with ether. The extract was washed with brine, dried with magnesium sulfate, concentrated, chromatographed on silica gel (biotage), to afford the corresponding imine (3-(((2-cyanophenyl)imino)methyl)phenyl acetate 488.5 mg (46%). The imine was subsequently dissolved in methanol (6 mL), at 0 °C, sodium borohydride (NaBH₄) (34.4 mg, 0.91 mmol) was added in portion, and the mixture was stirred for 30 minutes, warming to room temperature. The product was extracted with ether, washed with brine, dried with magnesium sulfate, concentrated, chromatographed on silica gel (biotage), to afford 181.2 mg (37%) of the *meta*-acetylation standard for **2-3m**.

¹H NMR (700 MHz, cdcl₃) δ 7.42 (dd, *J* = 7.7, 1.6 Hz, 1H), 7.37 (t, *J* = 7.9 Hz, 1H), 7.33 (t, *J* = 7.9 Hz, 1H), 7.21 (d, *J* = 7.6 Hz, 1H), 7.07 (s, 1H), 7.04 – 7.02 (m, 1H), 6.71 (t, *J* = 7.5 Hz, 1H), 6.59 (d, *J* = 8.5 Hz, 1H), 5.05 (s, 1H), 4.46 (d, *J* = 5.7 Hz, 2H), 2.30 (s, 3H).

¹³C NMR (176 MHz, cdcl₃) δ 169.36, 151.10, 149.82, 139.64, 134.30, 132.74, 129.87, 124.28, 120.81, 120.09, 117.76, 117.10, 111.05, 96.08, 47.03, 21.11.

3-(2-cyanophenethyl)-1-methyl-1H-indol-2-yl acetate (2-3p)



Following a modified general procedure C for the distal *meta*-acetoxylation of biaryl substrates, 2-(2-(1-methyl-1H-indol-3-yl)ethyl)benzotrile (52.1 mg, 0.2 mmol), *N*-Acetylglycine (5.0 mg, 0.04 mmol), and (diacetoxyiodo)benzene (193.3 mg, 0.6 mmol), acetic anhydride (0.13 mL, 1.4 mmol), and 1 mL (x2) hexafluoroisopropanol (HFIP) were used to produce, after purification on silica gel (9:1 hexanes: ethyl acetate), 15.9 mg (35%) of the acetoxyated product as a viscous, yellow oil.

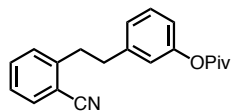
¹H NMR (500 MHz, cdcl₃) δ 7.57 (d, *J* = 7.7 Hz, 1H), 7.47 (t, *J* = 7.9 Hz, 1H), 7.34 (t, *J* = 7.8 Hz, 1H), 7.31 – 7.27 (m, 3H), 7.07 (t, *J* = 7.5 Hz, 1H), 6.87 (d, *J* = 7.8 Hz, 1H), 3.26 (s, 3H), 2.90 (ddd, *J* = 10.0, 6.5, 2.7 Hz, 2H), 2.31 (dt, *J* = 8.8, 6.4 Hz, 2H), 2.05 (s, 3H).

¹³C NMR (126 MHz, cdcl₃) δ 174.73, 169.30, 145.12, 144.20, 133.28, 133f.23, 130.41, 129.94, 127.47, 127.20, 123.34, 123.22, 118.04, 112.76, 108.95, 79.65, 37.63, 27.83, 26.90, 21.02.

MS(ESI+) calc'd for C₂₀H₁₈N₂O₂: 357.1005, found: 357.1215 [M+K]⁺

6.2.5 Spectral Characterization of Miscellaneous Transformations

3-(2-cyanophenethyl)phenyl pivalate (2-7)



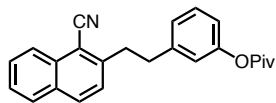
Following general procedure D for the distal *meta*-pivalation of biaryl substrates, 2-phenylbenzotrile (41.5 mg, 0.2 mmol), palladium acetate (8.9 mg, 0.04 mmol), *N*-Acetylglycine (5.0 mg, 0.04 mmol), di-(pivaloyloxy)iodobenzene (243.8 mg, 0.6 mmol), pivalic anhydride (0.284 mL, 1.4 mmol), and 2 mL hexafluorosopropanol (HFIP). Were used to produce 40.7 mg (70%) of the pivalated products in a 7.0 : 1.0 *meta* : other ratio.

¹H NMR (500 MHz, cdcl₃) δ 7.63 (dd, *J* = 7.7, 1.4 Hz, 1H), 7.50 – 7.46 (m, 1H), 7.32 – 7.27 (m, 2H), 7.24 (d, *J* = 7.8 Hz, 1H), 7.04 (dt, *J* = 7.7, 1.3 Hz, 1H), 6.93 – 6.88 (m, 2H), 3.16 – 3.12 (m, 2H), 2.97 (dd, *J* = 9.6, 6.5 Hz, 2H), 1.36 (s, 9H).

¹³C NMR (126 MHz, cdcl₃) δ 177.28, 151.35, 145.34, 142.24, 133.04, 132.93, 129.94, 129.51, 126.88, 126.01, 121.70, 119.59, 118.15, 112.49, 39.21, 37.01, 36.65, 27.30.

MS(ESI+) calc'd for C₂₀H₂₁NO₂: 325.1910, found: 325.1911 [M+NH₄⁺]⁺

3-(2-(1-cyanonaphthalen-2-yl)ethyl)phenyl pivalate (2-7b)



Following general procedure D for the distal *meta*-pivalation of biaryl substrates, 2-phenethyl-1-naphthonitrile (52.5 mg, 0.2 mmol), palladium acetate (8.9 mg, 0.04 mmol), *N*-Acetylglycine (5.0 mg, 0.04 mmol), di-(pivaloyloxy)iodobenzene (243.8 mg, 0.6 mmol), pivalic anhydride (0.284

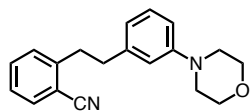
mL, 1.4 mmol), and 2 mL hexafluoroisopropanol (HFIP). Were used to produce 40.4 mg (57%) of the pivalated product as a colorless, viscous oil.

¹H NMR (700 MHz, cdcl₃) δ 8.23 (d, *J* = 8.4 Hz, 1H), 7.96 (d, *J* = 8.5 Hz, 1H), 7.88 (d, *J* = 8.1 Hz, 1H), 7.68 (dd, *J* = 8.4, 6.8 Hz, 1H), 7.59 – 7.55 (m, 1H), 7.33 (dd, *J* = 8.5, 1.5 Hz, 1H), 7.30 – 7.27 (m, 1H), 7.07 (d, *J* = 7.6 Hz, 1H), 6.93 – 6.91 (m, 2H), 3.35 (td, *J* = 7.9, 1.5 Hz, 2H), 3.05 (dd, *J* = 9.2, 7.2 Hz, 2H), 1.35 (d, *J* = 1.6 Hz, 9H).

¹³C NMR (176 MHz, cdcl₃) δ 177.45, 151.58, 146.50, 142.37, 133.20, 133.16, 131.83, 129.73, 128.93, 128.73, 127.33, 127.18, 126.21, 125.44, 121.91, 119.83, 117.18, 109.40, 37.61, 37.37, 27.48, 27.34.

MS(ESI+) calc'd for C₂₄H₂₃NO₂: 380.1626, found: 380.1598 [M+Na]⁺

2-(3-morpholinophenethyl)benzonitrile (2-8)



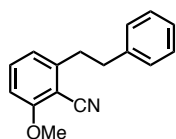
To an oven-dried 8 mL culture tube with stir bar was added under Nitrogen atmosphere, Ni(COD)₂ (11.0 mg, 0.04 mmol), IPrHCl (17.1 mg, 0.04 mmol), and sodium *tert*-butoxide (28.8 mg, 0.3 mmol), and toluene (1.0 mL). The reaction mixture was allowed to stir, under nitrogen, for 10 minutes. Morpholine (0.035 mL, 0.4 mmol) and 3-(2-cyanophenethyl)phenyl pivalate (61.5 mg, 0.2 mmol) were added via syringe, and the reaction mixture was allowed to stir at 80 °C for 16h. After cooled to room temperature, the reaction mixture was filtered through a pad of silica, concentrated, and chromatographed on silica gel (9:1 hexanes: ethyl acetate), to afford 29.1 mg (50%) of the amination product as a viscous, yellow oil.

¹H NMR (500 MHz, cdcl₃) δ 7.63 (d, *J* = 7.7 Hz, 1H), 7.48 (t, *J* = 7.7 Hz, 1H), 7.30 (t, *J* = 7.8 Hz, 1H), 7.26 (s, 1H), 7.20 (t, *J* = 7.9 Hz, 1H), 6.77 (dd, *J* = 8.2, 2.4 Hz, 1H), 6.75 – 6.71 (m, 2H), 3.85 (t, *J* = 4.8 Hz, 4H), 3.13 (dd, *J* = 5.8, 3.7 Hz, 6H), 2.93 (dd, *J* = 9.5, 6.8 Hz, 2H).

¹³C NMR (176 MHz, cdcl₃) δ 151.44, 145.58, 141.53, 132.81, 132.65, 129.69, 129.24, 126.58, 120.28, 118.02, 115.98, 113.65, 112.38, 66.91, 49.37, 37.50, 36.77.

MS(ESI+) calc'd for C₁₉H₂₀N₂O: 293.1609, found: 293.1648 [M+H]⁺

2-methoxy-6-phenethylbenzonitrile (2-11)



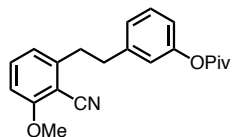
Following general procedure E for the proximal *ortho*-methoxylation of biaryl substrates, 2-phenylbenzonitrile (41.5 mg, 0.2 mmol), hydroxyl(tosyloxy)iodobenzene (392.2 mg, 1.0 mmol), palladium acetate (8.9 mg, 0.04 mmol), methanol (0.3 mL) and hexafluoroisopropanol (0.3 mL) were used to produce 34.3 mg (73%) of the methoxylated product as a colorless oil.

¹H NMR (400 MHz cdcl₃) δ 7.40 (t, *J* = 8.1 Hz, 1H), 7.29 (ddd, *J* = 7.4, 6.1, 2.1 Hz, 2H), 7.21 (d, *J* = 7.1 Hz, 3H), 6.82 (d, *J* = 1.5 Hz, 1H), 6.80 (d, *J* = 2.4 Hz, 1H), 3.93 (s, 3H), 3.14 – 3.06 (m, 2H), 2.96 (dd, *J* = 9.8, 6.3 Hz, 2H).

¹³C NMR (176 MHz, cdcl₃) δ 161.73, 147.41, 140.61, 133.58, 128.49, 128.40, 126.17, 121.46, 115.51, 108.58, 101.87, 56.01, 36.93, 36.78.

MS(ESI+) calc'd for C₁₆H₁₅NO: 238.1132, found: 238.1223 [M+H]⁺

3-(2-cyano-3-methoxyphenethyl)phenyl pivalate (2-12)



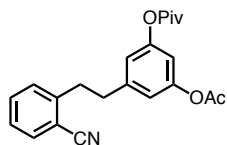
Following general procedure E for the proximal *ortho*-methoxylation of biaryl substrates, 3-(2-cyanophenethyl)phenyl pivalate) (61.5 mg, 0.2 mmol), hydroxyl(tosyloxy)iodobenzene (392.2 mg, 1.0 mmol), palladium acetate (8.9 mg, 0.04 mmol), methanol (0.3 mL) and hexafluoroisopropanol (0.3 mL) were used to produce 34.3 mg (73%) of the methoxylated product as a colorless oil.

¹H NMR (700 MHz, cdCl_3) δ 7.40 (dd, $J = 8.5, 7.7$ Hz, 1H), 7.28 (dd, $J = 8.9, 7.6$ Hz, 1H), 7.07 – 7.05 (m, 1H), 6.90 (dd, $J = 6.5, 1.2$ Hz, 2H), 6.81 (dd, $J = 8.1, 4.7$ Hz, 2H), 3.93 (s, 3H), 3.11 – 3.08 (m, 2H), 2.97 – 2.94 (m, 2H), 1.36 (s, 9H).

¹³C NMR (176 MHz, cdCl_3) δ 177.08, 161.79, 151.16, 147.11, 142.23, 133.67, 129.29, 125.82, 121.54, 121.48, 119.34, 115.47, 108.70, 101.86, 56.03, 39.03, 36.63, 36.51, 27.13.

MS(ESI+) calc'd for $\text{C}_{21}\text{H}_{23}\text{NO}_3$: 360.1576, found: 360.1457 [M+Na]⁺

3-acetoxy-5-(2-cyanophenethyl)phenyl pivalate (2-21)



Following a time/temperature modified general procedure C for the distal *meta*-acetoxylation of biaryl substrates, to an oven-dried 8 mL culture tube with stir bar was added palladium acetate (8.9 mg, 0.04 mmol), *N*-Acetylglycine (5.0 mg, 0.04 mmol), and (diacetoxyiodo)benzene (193.3 mg, 0.6 mmol) and 1 mL hexafluoroisopropanol (HFIP). The mixture was stirred at room temperature for 10 minutes. Acetic anhydride (0.13 mL, 1.4 mmol), the pivalated biaryl substrate (61.5 mg, 0.2 mmol), and another 1 mL hexafluoroisopropanol were then added. The tube was capped and the

reaction was stirred at 100 °C for 48h. After cooled to room temperature, the reaction mixture was filtered through a pad of silica, concentrated, and chromatographed on silica gel (9:1 hexanes: ethyl acetate), to afford 48.0 mg (66 %) of the pivalated product as a yellow oil. The product was isolated as a mixture of *meta*- and *para*-pivalated products with a 1.0 :1.0 *meta* : *para* ratio.

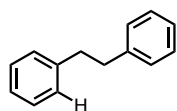
¹H NMR (401 MHz, cdcl₃) δ 7.64 (dd, *J* = 7.7, 1.4 Hz, 2H), 7.52 – 7.47 (m, 2H), 7.31 (tt, *J* = 7.6, 1.3 Hz, 2H), 7.24 (d, *J* = 7.9 Hz, 2H), 7.10 – 7.02 (m, 2H), 6.99 (d, *J* = 1.8 Hz, 1H), 6.82 – 6.79 (m, 2H), 6.76 (t, *J* = 2.1 Hz, 1H), 3.13 (dd, *J* = 9.7, 6.4 Hz, 4H), 2.99 – 2.92 (m, 4H), 2.27 (s, 2H), 2.26 (s, 2H), 1.35 (s, 9H), 1.34 (s, 9H).

¹³C NMR (176 MHz, cdcl₃) δ 176.60, 175.86, 169.02, 168.27, 151.50, 151.03, 144.99, 144.81, 142.78, 142.27, 140.48, 139.31, 132.89, 132.88, 132.84, 132.80, 129.76, 126.80, 126.76, 126.44, 123.33, 123.22, 119.05, 118.89, 117.93, 117.91, 113.41, 112.29, 112.27, 39.11, 39.08, 36.75, 36.48, 36.47, 36.21, 27.10, 27.06, 21.05, 20.65.

MS(ESI+) calc'd for C₂₂H₂₃NO₄: 388.1525, found: 388.1517 [M+Na]⁺

6.2.6 Spectral Characterization of Decyanation Compounds

1,2-diphenylethane (2-9)



Following general procedure F for the decyanation of bibenzyl benzonitriles, 2-phenylbenzonitrile (41.5 mg, 0.2 mmol), Ni(COD)₂ (11.0 mg, 0.04 mmol), tricyclohexylphosphine (16.8 mg, 0.06 mmol), sodium *tert*-butoxide (96.1 mg, 1.0 mmol), 0.4 mL toluene, and Ti(*o*-*i*-pr)₄ (0.065 mL, 0.22 mmol) were used to produce, after chromatographed with biotage isolera, 23.5 mg (64%) of the decyanated product as a white solid. All spectra match published data.⁵

3-phenethylphenol (2-13) and 2-(3-hydroxyphenethyl)benzotrile (2-14)



Following general procedure F for the decyanation of bibenzyl benzonitriles, 3-(2-cyanophenethyl)phenyl pivalate) (61.5 mg, 0.2 mmol), Ni(COD)₂ (11.0 mg, 0.04 mmol), tricyclohexylphosphine (16.8 mg, 0.06 mmol), sodium *tert*-butoxide (96.1 mg, 1.0 mmol), 0.4 mL toluene, and Ti(*o-i*-pr)₄ (0.065 mL, 0.22 mmol) were used to produce, after chromatographed by biotage, 24.8 mg (63%) of the decyanated product as a white solid and 5.6 mg (13%) of the deprotected product as a viscous, colorless oil.

3-phenethylphenol (2-13)

¹H NMR (700 MHz, cdcl₃) δ 7.29 (t, *J* = 7.6 Hz, 2H), 7.22 – 7.17 (m, 3H), 7.15 (dd, *J* = 8.8, 7.5 Hz, 1H), 6.77 (d, *J* = 7.5 Hz, 1H), 6.70 – 6.64 (m, 2H), 4.68 (s, 1H), 2.91 (ddd, *J* = 9.3, 5.7, 2.2 Hz, 2H), 2.88 (ddd, *J* = 10.1, 5.7, 2.2 Hz, 2H).

¹³C NMR (176 MHz, cdcl₃) δ 155.46, 143.71, 141.63, 129.49, 128.40, 128.31, 125.92, 120.95, 115.34, 112.80, 37.71, 37.66.

MS(ESI+) calc'd for C₁₄H₁₄O: 198.1045, found: 198.1045 (M⁺)

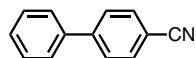
2-(3-hydroxyphenethyl)benzotrile (2-14)

¹H NMR (500 MHz, cdcl₃) δ 7.63 (dd, *J* = 7.7, 1.4 Hz, 1H), 7.49 (td, *J* = 7.6, 1.4 Hz, 1H), 7.30 (td, *J* = 7.7, 1.2 Hz, 1H), 7.25 (s, 1H), 7.15 (dd, *J* = 8.9, 7.5 Hz, 1H), 6.77 (dd, *J* = 7.5, 1.5 Hz, 1H), 6.71 – 6.66 (m, 2H), 4.72 (d, *J* = 8.0 Hz, 1H), 3.15 – 3.11 (m, 2H), 2.92 (dd, *J* = 9.5, 6.6 Hz, 2H).

^{13}C NMR (126 MHz, cdcl_3) δ 156.02, 145.82, 142.78, 133.26, 133.15, 130.10, 127.09, 121.43, 118.42, 115.84, 113.66, 112.76, 37.38, 36.97.

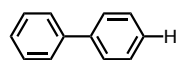
MS(ESI+) calc'd for $\text{C}_{15}\text{H}_{13}\text{NO}$: 222.1277, found: 222.1276 (M+H)

[1,1'-biphenyl]-4-carbonitrile (2-16)



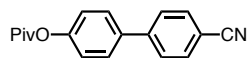
Purchased, and used as received.

Biphenyl (2-17)



Following general procedure G for the decyanation of biphenyl benzonitriles, 4-phenylbenzonitrile (35.8 mg, 0.2 mmol), $\text{Ni}(\text{acac})_2$ (10.3 mg, 0.03 mmol), tricyclohexylphosphine (16.8 mg, 0.06 mmol), potassium *tert*-butoxide (56.1 mg, 0.5 mmol), 0.4 mL toluene, and $\text{Ti}(\text{o-}i\text{-pr})_4$ (0.065 mL, 0.22 mmol) were used to produce, after chromatographed by biotage, 26.8 mg (87%) of the decyanated product as a white solid. All spectra match published data.⁸

4'-cyano-[1,1'-biphenyl]-4-yl pivalate (2-18)



In an oven-dried round-bottom flask with stir bar, 4-hydroxybiphenyl (585.7 mg, 3.0 mmol), pivalic anhydride (0.61 mL, 3.0 mmol), trimethylamine (0.42 mL, 3.0 mL), and DMAP (183.3 mg, 1.5 mmol) were dissolved in dichloromethane (5.0 mL), and the reaction mixture was allowed to stir overnight at room temperature. The mixture was diluted with ethyl acetate, extracted with sodium bicarbonate, water, washed with brine, dried over magnesium sulfate, filtered, and

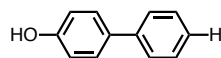
concentrated. The concentrate was chromatographed using Biotage isolera to afford 786.6 mg (94%) pivalated starting material as a clear oil.

$^1\text{H NMR}$ (500 MHz, cdcl_3) δ 7.73 (d, $J = 8.3$ Hz, 2H), 7.66 (d, $J = 8.3$ Hz, 2H), 7.59 (d, $J = 8.6$ Hz, 2H), 7.18 (d, $J = 8.5$ Hz, 2H), 1.38 (s, 9H).

$^{13}\text{C NMR}$ (176 MHz, cdcl_3) δ 177.35, 151.91, 145.16, 136.95, 132.96, 128.60, 128.00, 122.59, 119.22, 111.29, 39.48, 27.45.

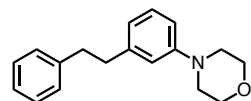
MS(ESI+) calc'd for $\text{C}_{18}\text{H}_{17}\text{NO}_2$: 280.1332, found: 280.1337 $[\text{M}+\text{H}]^+$

4-Hydroxybiphenyl (2-19)



Following general procedure G for the decyanation of biphenyl benzonitriles, 4'-cyano-[1,1'-biphenyl]-4-yl pivalate (55.9 mg, 0.2 mmol), $\text{Ni}(\text{acac})_2$ (10.3 mg, 0.03 mmol), tricyclohexylphosphine (16.8 mg, 0.06 mmol), potassium *tert*-butoxide (56.1 mg, 0.5 mmol), 0.8 mL toluene, and $\text{Ti}(\text{o-}i\text{-pr})_4$ (0.065 mL, 0.22 mmol) were used to produce, after chromatographed by biotage, 28.7 mg (84%) of the decyanated product as a white solid. All spectra match published data.⁹

4-(3-phenethylphenyl)morpholine (2-20)



Following general procedure F for the decyanation of bibenzyl benzonitriles, 2-(3-morpholinophenethyl)benzonitrile (75.0 mg, 0.25 mmol), $\text{Ni}(\text{COD})_2$ (13.8 mg, 0.05 mmol), tricyclohexylphosphine (13.8 mg, 0.1 mmol), sodium *tert*-butoxide (120.1 mg, 1.25 mmol), 0.5

mL toluene, 2-(3-morpholinophenethyl)benzonitrile) (75.0 mg, 0.25 mmol), and $\text{Ti}(\text{o-}i\text{-pr})_4$ (0.081 mL, 0.275 mmol) were used to produce, after chromatographed by biotage, 48.8 mg (73%) of the decyanated product as a yellow oil.

$^1\text{H NMR}$ (500 MHz, cdcl_3) δ 7.31 – 7.27 (m, 2H), 7.20 (td, $J = 7.8, 3.4$ Hz, 4H), 6.80 – 6.73 (m, 2H), 6.71 (s, 1H), 3.87 – 3.83 (m, 4H), 3.15 – 3.11 (m, 4H), 2.96 – 2.85 (m, 4H).

$^{13}\text{C NMR}$ (176 MHz, cdcl_3) δ 151.71, 143.17, 142.19, 129.46, 128.81, 128.66, 126.22, 120.65, 116.46, 113.74, 67.31, 49.84, 38.64, 38.31.

$\text{MS}(\text{ESI}^+)$ calc'd for $\text{C}_{18}\text{H}_{21}\text{NO}$: 267.1623, found: 268.1696 $[\text{M}+\text{H}]^+$

6.2.7 General Procedure for Authentic Standard Synthesis (and Characterization)

This procedure follows general procedure A for the synthesis of biaryl substrates (via cyanoborylation/Suzuki). These authentic standards were used to verify NMR data, and were used as standards for creating GC-FID curves which could then be used to acquire yields and regioisomeric ratios, based on the product peak integration (for initial screening). They were also used to confirm regioselectivity of the isolated reaction products. This information can also be

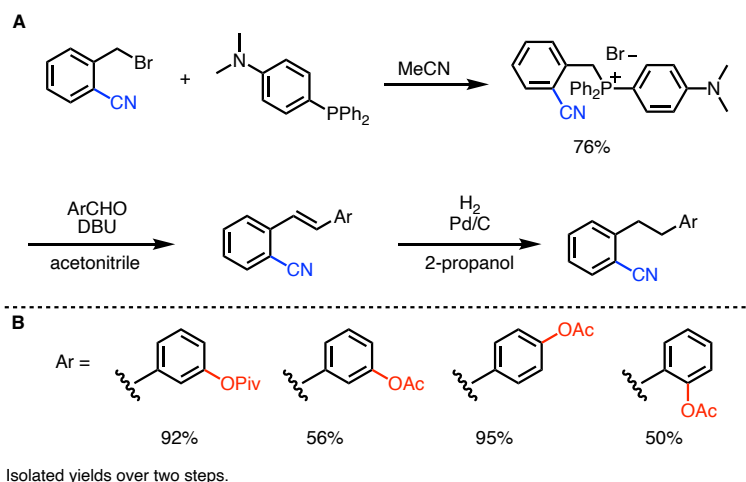
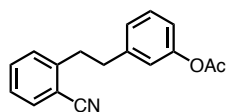


Figure 6-6 Acetoxylation standard synthesis.

found in Chapter 2.2 (Figure 2-3), and corresponds to compounds **2-3**, **2-5**, **2-6**, and **2-7** (Figure 6-6).

3-(2-cyanophenethyl)phenyl acetate (**2-3-std-meta**)

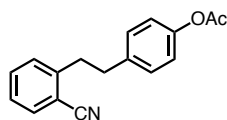


¹H NMR (700 MHz, CDCl₃) δ 7.63 (dd, *J* = 7.8, 1.4 Hz, 1H), 7.51 – 7.46 (m, 1H), 7.30 (q, *J* = 7.8 Hz, 2H), 7.24 (d, *J* = 7.8 Hz, 1H), 7.06 (dd, *J* = 7.4, 1.6 Hz, 1H), 6.96 – 6.91 (m, 2H), 3.14 (dd, *J* = 9.5, 6.7 Hz, 2H), 2.97 (dd, *J* = 9.5, 6.7 Hz, 2H), 2.29 (d, *J* = 0.9 Hz, 3H).

¹³C NMR (176 MHz, cdcl₃) δ 169.81, 151.11, 145.45, 142.50, 133.21, 133.11, 130.07, 129.76, 127.08, 126.40, 121.97, 119.85, 118.29, 112.69, 37.18, 36.80, 21.48.

MS(ESI+) calc'd for C₁₇H₁₅NO₂: 266.1136, found: 266.1176 [M+H]⁺

4-(2-cyanophenethyl)phenyl acetate (**2-5**)



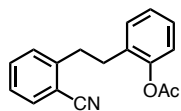
*This compound also served as the para acetoxylation substrate (**2-2f**).*

¹H NMR (700 MHz, cdcl₃) δ 7.63 (dd, *J* = 7.8, 1.8 Hz, 1H), 7.49 (tt, *J* = 7.6, 1.5 Hz, 1H), 7.32 – 7.29 (m, 1H), 7.25 (d, *J* = 7.9 Hz, 1H), 7.20 (dd, *J* = 8.3, 1.6 Hz, 2H), 7.00 (dd, *J* = 8.4, 1.7 Hz, 2H), 3.13 (dd, *J* = 9.1, 7.3 Hz, 2H), 2.96 (dd, *J* = 9.3, 7.1 Hz, 2H), 2.29 (s, 3H).

¹³C NMR (176 MHz, cdcl₃) δ 169.55, 149.09, 145.25, 138.04, 132.85, 132.72, 129.45, 126.70, 121.50, 117.95, 112.37, 36.71, 36.51, 21.11.

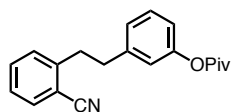
MS(ESI+) calc'd for C₁₇H₁₅NO₂: 266.1176, found: 266.1176 [M+H]⁺

2-(2-cyanophenethyl)phenyl acetate (2-6)



$^1\text{H NMR}$ (500 MHz, cdCl_3) δ 7.63 (dt, $J = 7.7, 1.5$ Hz, 1H), 7.47 (tt, $J = 7.8, 1.6$ Hz, 1H), 7.30 (tt, $J = 7.7, 1.4$ Hz, 1H), 7.25 – 7.14 (m, 4H), 7.04 (dd, $J = 8.1, 1.4$ Hz, 1H), 3.09 (td, $J = 7.6, 1.4$ Hz, 2H), 2.89 (td, $J = 7.8, 1.4$ Hz, 2H), 2.35 (d, $J = 1.5$ Hz, 3H).

3-(2-cyanophenethyl)phenyl pivalate) (2-7-std-*meta*)



$^1\text{H NMR}$ (500 MHz, cdCl_3) δ 7.63 (d, $J = 6.9$ Hz, 1H), 7.48 (t, $J = 7.7$ Hz, 1H), 7.29 (q, $J = 8.0$ Hz, 3H), 7.24 (d, $J = 7.8$ Hz, 2H), 7.04 (d, $J = 7.7$ Hz, 2H), 6.90 (d, $J = 13.6$ Hz, 2H), 3.14 (dd, $J = 9.5, 6.6$ Hz, 2H), 2.97 (dd, $J = 9.5, 6.6$ Hz, 2H), 1.36 (s, 9H).

$^{13}\text{C NMR}$ (176 MHz, cdCl_3) δ 177.08, 151.19, 145.16, 142.06, 132.86, 132.74, 129.76, 129.33, 126.69, 125.82, 121.52, 119.41, 117.96, 112.33, 39.03, 36.83, 36.47, 27.13.

MS(ESI+) calc'd for $\text{C}_{20}\text{H}_{21}\text{NO}_2$: 325.1910, found: 325.1911 $[\text{M}+\text{NH}_4^+]^+$

6.2.8 Calibration Curve for *meta*-Acetoxylation GC-FID Analysis

Solutions containing a constant concentration of an internal standard (tridecane (0.164 M) and varying concentrations of the desired product (approximately, 0.05, 0.075, 0.15 and 0.20 M) were prepared in ethyl acetate. Each was analyzed by GC-FID and the response factor (F) calculated by solving equation Eq. 1 for the area of product to give equation Eq. 2, where the response factor (F) is the slope. Yields of crude reactions mixtures, containing a known amount

of internal standard, were then determined by solving Eq. 1 for the concentration of the product to give Eq. 3 and filling in the known data from a crude reaction. This information was used to generate a calibration curve for regioisomer analysis (Figure 6-7).

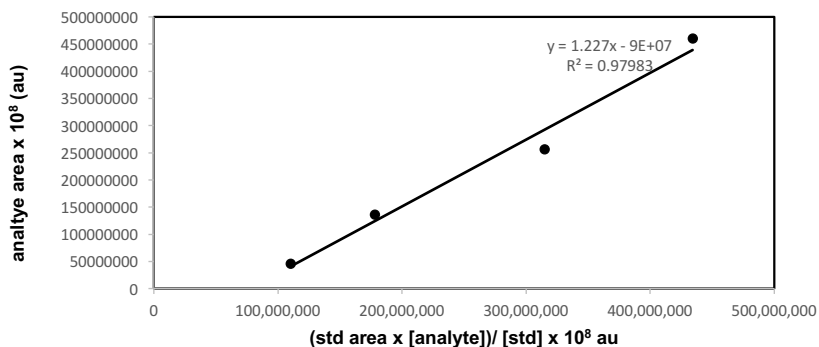
Equations:

$$\text{Eq. 1} \quad \frac{\text{Area of Product}}{\text{Concentration of Product}} = F \left(\frac{\text{Area of Standard}}{\text{Concentration of Standard}} \right)$$

$$\text{Eq. 2} \quad \text{Area of Product} = F \left(\frac{(\text{Area of Standard})(\text{Concentration of Product})}{\text{Concentration of Standard}} \right)$$

$$\text{Eq. 3} \quad \text{Concentration of Product} = \left(\frac{(\text{Concentration of Standard})(\text{Area of Product})}{F(\text{Area of Standard})} \right)$$

Calibration Curve for *meta*-Acetoxylation Product (2-3a):



Plot of analyte area versus (std area x [2-3a]) / [standard]

Fitted to $y = mx + b$ where $m = 1.227$ and $b = 9 \times 10^7$ with an R^2 of 0.97983

Concentration of Product (2-3a)	Area of Product (2-3a)	Area of Standard (tridecane)	(Std Area x Prod Conc.)/(Std. Conc.)
0.050808	45646441	356154781	110320390.6
0.076212	136635681	383699890	178278900.1
0.12702	255922806	406847842	315056930.7
0.20323	459710359	350525856	434302959

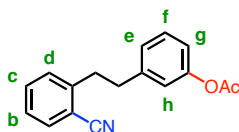
Figure 6-7 Calibration curve for *meta*-acetoxylation GC-FID analysis.

6.2.9 General Explanation for Regioselectivity Determination and Sample Characterization

meta-Acetoxylated Substrates

Proton shift (ppm) and splitting for each proton a - h								
Product #	a	b	c	d	e	f	g	h
2-3a ^a	7.63 (d)	7.3 L	7.48 (t)	7.23	7.06 (d)	7.3 R	6.94 (d)	6.93 (s)
2-3b	7.42 (s)	-	7.28 (d)	7.12 (d)	7.06 (d)	7.28 (t)	6.94 (d)	6.93 (s)
2-3c	7.6 (s)	-	7.45 (d)	7.15 (d)	7.03 (d)	7.3 (t)	6.95 (d)	6.90 (s)
2-3d	7.32 (dd ^b)	-	7.18 L	7.18 R	7.03 (d)	7.29 (t)	6.95 (d)	6.90 (s)
2-3e	7.62 (d)	7.3 (t)	7.48 (t)	7.23 (d)	7.01 (d)	6.88 (d)	-	6.89 (s)
2-3f	7.63 (d)	7.3 (t)	7.49 (t)	7.25 (d)	7.08 (d)	7.09 (d)	-	7.03 (s)
2-3g	-	-	-	-	7.1 (d)	7.29 (t)	6.95 (d)	6.98 (s)
2-3h	7.84 (s)	-	7.7 (d)	7.3 (m ^c)	7.1 (d)	7.23 (m ^c)	6.98 (d)	6.95 (s)
2-3i	7.62 (d)	7.3 (t)	7.5 (t)	7.28 (d)	7.07 (d)	7.3 (m)	6.92 (d)	6.92 (s)
Pivalation (2-7)	7.63 (d)	7.29 (m)	7.48 (t)	7.24 (d)	7.04 (d)	7.29 (m)	6.91 (d)	6.90 (s)
Authentic Ac. Std.	7.6 (d)	7.3 L (t)	7.48 (t)	7.23 (d)	7.06 (d)	7.3 R (t)	6.94 (d)	6.92 (s)
Authentic Piv. Std.	7.63 (d)	7.29 (t)	7.48 (t)	7.23 (d)	7.04 (d)	7.3 (t)	6.92 (d)	6.89 (s)

¹H NMR shifts in Chloroform-*d*. ^aScaled-up (1.0 mmol) acetoxylation and isolated as a mixture. ^bSplitting due to *meta*-aromatic proton coupling and *ortho*-fluorine (based on J-values). ^cDue to overlap with minor regioisomer.



s = singlet
d = doublet
t = triplet
m = multiplet
R = right side of an overlapping signal
L = left side of an overlapping signal

Product numbering follows numbering system in Chapter 2.3 scope.

Table 6-3 Acetoxylation ¹H NMR analysis.

In general, the acetoxyated compounds were analyzed and assigned by both 2D and 1D NMR. One of the main features that points towards the *meta* selectivity is the signal for the proton between the connecting chain and the acetoxy or pivaloxy group, which typically overlaps with the doublet around 6.94 ppm. Additionally, this signal has J-value of <2 Hz in cases where it is resolved, and in some cases appears as a singlet. This appearance is very diagnostic of the *meta* oxidation product, and authentic standards of the *ortho*- and *para*-oxidation products displayed much larger J-values due to vicinal coupling. Further, by COSY, two very clear spin systems are apparent (see sample below). While the system with four protons corresponds to unchanged protons from the bibenzyl starting material, and can be identified by a four signal spin-system, the three protons make up the second (distal, functionalized ring) can be identified

as a second distinct spin system, and weakly correlate to the singlet. NOE analysis also revealed long-range coupling of the acetoxy CH₃ protons coupling to **h** and **g** protons (on either side of the *meta* functionalization).

The *meta*-acetylated products result in a set of ¹H NMR signals which follow the same general splitting and shift pattern on the distal ring. When compared to the starting material, the benzonitrile ring (protons **a-d**) appears relatively unchanged, while the distal ring proton signals are shifted and splitting changes (protons **e-g** and **h**) with acetoxylation. Although overlap does occur in some cases due to the electronically similar arene, the signals are usually distinct. Table 6-3, which was made over time as the compounds were analyzed, demonstrates this pattern very clearly.

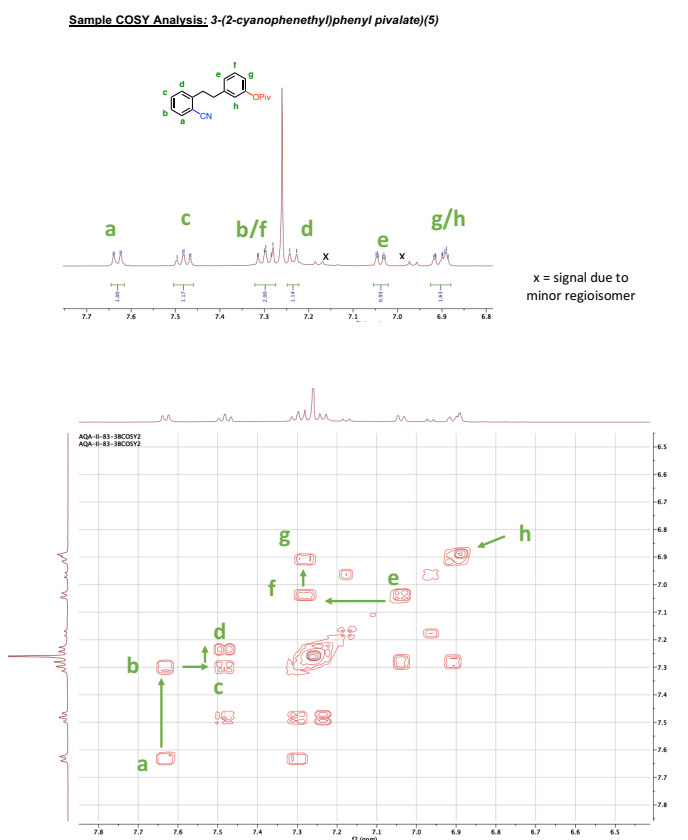


Figure 6-8 Sample COSY analysis for C–H acetoxylation.

The acetoxyated compounds in the substrate table were also analyzed by COSY. Although overlap does occur, there are usually two distinct ring systems identified by the ^1H - ^1H correlations: 4 protons (a-d), 3 protons (e-g), and 1 proton(h). Further, the splitting J-values taken from the 1D spectra confirmed these observations. Both *ortho* and *meta* J-values, allow for identifying the adjacent and more remote protons on the arenes. A sample COSY analysis for compound is provided in Figure 6-8.

6.3 Chapter 4 Experimental

6.3.1 General Procedures for Chapter 4 (A-H)

6.3.1.1 General Procedure (A) for the Fluorination of Monosaccharides

To an oven-dried round-bottom flask with stir bar, was added monosaccharide (1.0 equiv.). The flask was evacuated and filled with nitrogen (3x). Anhydrous DCM (0.15 M) was then added to the flask. The mixture was cooled to 0 °C, and to the solution was added diethylaminosulfur trifluoride (DAST) (1.5 equiv.) dropwise. The mixture was stirred under nitrogen, at 0°C for 30 minutes, and then room temperature for 2 hours, or until complete by thin layer chromatography (TLC). The reaction mixture was quenched with NaHCO_3 . The organic layer was extracted with DCM (2x), washed with water and brine, dried with Na_2SO_4 , filtered, and concentrated. The crude mixture was purified by biotage (ethyl acetate/hexanes) to give the fluorinated product.

6.3.1.2 General Procedure (B) for the Trimethylsilyl Protection of Acceptors

To an oven-dried round-bottom flask with stir bar, was added monosaccharide (1.0 equiv.). The flask was evacuated and filled with nitrogen (3x). Anhydrous DCM (~0.10 M) was then added to the flask. To the solution of the alcohol was added trimethylamine (2.0 equiv.) dropwise, and

chlorotrimethylsilane (1.5 equiv.) at 0°C. The mixture was stirred at room temperature for 2 hours, under nitrogen, and monitored by TLC. The final mixture was diluted with DCM, quenched with water, washed NaHCO₃, water (2x) and brine. The organic layer was dried with Na₂SO₄, filtered, and concentrated. The crude mixture was purified by biotage isolaera (ethyl acetate/hexanes) to give the TMS ether product.

6.3.1.3 General Procedure (C) for the Tributylsilyl Protection of Acceptors

To an oven-dried round-bottom flask with stir bar, was added monosaccharide (1.0 equiv.). The flask was evacuated and filled with nitrogen (3x). Anhydrous DMF (DCM in indicated cases) (~0.10 M) was then added to the flask. To the solution of the alcohol was added imidazole (3.0 equiv.), and chlorotributylsilane (1.5 equiv.). The mixture was stirred at room temperature overnight, under nitrogen, and monitored by TLC. The final mixture was diluted with ethyl acetate (DCM if the solvent used in the reaction is DCM), quenched with water, washed NaHCO₃, water (2x) and brine. The organic layer was dried with Na₂SO₄, filtered, and concentrated. The crude mixture was purified by biotage isolera (ethyl acetate/hexanes) to give the tributylsilyl ether product.

6.3.1.4 General Procedure (D) for the Triethylsilyl Protection of Acceptors

To an oven-dried round-bottom flask with stir bar, was added monosaccharide (1.0 equiv.). The flask was evacuated and filled with nitrogen (3x). Anhydrous DMF was then added to the flask. To the solution of the alcohol was added imidazole (3.0 equiv.), and chlorotriethylsilane (2.0 equiv.). The mixture was stirred at room temperature overnight, under nitrogen, and monitored by TLC. The final mixture was quenched with water, washed NaHCO₃, water (2x) and brine. The

organic layer was dried with Na₂SO₄, filtered, and concentrated. The crude mixture was purified by biotage isolera (ethyl acetate/hexanes) to give the TES ether product.

6.3.1.5 General Procedure (E) for the Tris(pentafluoropenyl) Borane-Catalyzed Polysaccharide Synthesis (Cap included, No Slow Addition)

To an oven-dried round-bottom flask with stir bar, was added silyl ether acceptor monosaccharide (1.0 equiv.) and donor/acceptor silyl ether glycosyl fluoride (5.0 or 20.0 equiv.). The flask was evacuated and filled with nitrogen (3x). anhydrous DCM was then added to the flask. Tris(pentafluoropenyl) borane (5.0, 10. 0 or 20.0 mol%) was weighed out in an inert atmosphere glovebox, and added as a solution in anhydrous DCM. The overall resulting solution concentration was 0.04 M (relative to the silyl ether glycosyl fluoride). The reaction was stirred under nitrogen, at room temperature. The glycosylation mixture was concentrated under reduced pressure to give the glycosylation product, and purified via biotage (ethyl acetate/hexanes), or analyzed in the crude by NMR, MALDI, and mass spectrometry. This procedure was carried out in experiments described in Figures 4-4 and 4-13, and Table 4-4 (unless otherwise noted).

6.3.1.6 General Procedure (F) for the Tris(pentafluoropenyl) Borane-Catalyzed Polysaccharide Synthesis (Cap Included, Slow Addition)



Figure 6-9 Polymerization slow addition setup.

To an oven-dried round-bottom flask with stir bar, was added silyl ether acceptor monosaccharide (1.0 equiv.). The flask was evacuated and filled with nitrogen (3x). anhydrous DCM was then added to the flask. Tris(pentafluoropenyl) borane (5.0, 10. 0 or 20.0 mol%) was weighed out in an inert atmosphere glovebox, and added as a solution in anhydrous DCM. The mixture was stirred under nitrogen, at room temperature. The donor/acceptor silyl ether glycosyl fluoride (5.0 or 20.0 equiv.) was then added dropwise in a solution of anhydrous DCM or toluene (0.05 M relative to the silyl ether glycosyl fluoride), via syringe pump addition, over a rate of 2 mL per hour, and the reaction was stirred until complete by TLC. The overall resulting solution concentration was 0.025 M (relative to the silyl ether glycosyl fluoride). The glycosylation mixture was quenched with a drop of pyridine, concentrated under reduced pressure to give the glycosylation product, and purified via biotage (ethyl acetate/hexanes), or analyzed in the crude by NMR, MALDI, and mass spectrometry. This procedure was carried out in experiments described in Figures 4-5, 4-10, 4-11, 4-12, and 4-14 and Table 4-1, 4-2, 4-3 and 4-4 (unless otherwise noted).

6.3.1.7 General Procedure (G) for the Triarylborane-Catalyzed Polysaccharide Synthesis (No Cap Included, No Slow Addition)

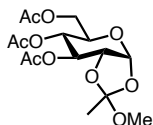
Tris(pentafluorophenyl) borane (5.0, 10.0 or 20.0 mol%) was weighed out in an inert atmosphere glovebox to an oven-dried round-bottom flask with stir bar. Silyl ether glycosyl fluoride (1.0 equiv.) was added as a solution in anhydrous DCM. The overall resulting solution concentration was 0.033 M (relative to the silyl ether glycosyl fluoride). The reaction was stirred under nitrogen, at room temperature. The glycosylation mixture was quenched with a drop of pyridine, concentrated under reduced pressure to give the glycosylation product, and purified via biotage (ethyl acetate/hexanes), or analyzed in the crude by NMR, MALDI, and mass spectrometry. This procedure was carried out in experiments described in Table 4-5 (unless otherwise noted).

6.3.1.7 General Procedure (H) For the Tris(pentafluorophenyl) Borane-Catalyzed Glycosylation Using Glycosyl Fluorides and TMS Ethers Under Inert Conditions

Tris(pentafluorophenyl) borane was weighed out in an inert atmosphere glovebox, and added as a solution in anhydrous DCM to a stirring solution of glycosyl fluoride donor and silyl ether acceptor in anhydrous DCM, at room temperature, under nitrogen. The reaction was monitored by TLC, and stirred until complete. The mixture was quenched with a drop of pyridine, concentrated under reduced pressure, and purified by biotage (ethyl acetate/hexanes) to give the glycosylation product.

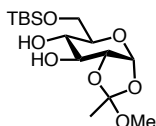
6.3.2 Spectral Characterization of Compounds in Chapter 4

1,2-*O*-(*exo*-Methoxyethylidene)-3, 4, 6-tri-*O*-acetyl- α -D-glucopyranoside (4-1)



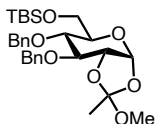
This compound was prepared according to literature procedure, and all spectra match published data.^{10,11}

1,2-*O*-(*exo*-Methoxyethylidene)-6-*O*-*tert*-butyldimethylsilyl- α -D-glucopyranoside (4-2)



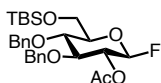
This compound was prepared according to literature procedure, and all spectra match published data.^{11,12}

1,2-*O*-(*exo*-Methoxyethylidene)-2,3-di-*O*-benzyl-6-*O*-*tert*-butyldimethylsilyl- α -D-glucopyranoside (4-3)



This compound was prepared according to literature procedure, and all spectra match published data.^{11,12}

2-*O*-Acetyl-3,4-di-*O*-benzyl-6-*O*-*tert*-butyldimethylsilyl- β -D-glucopyranosyl fluoride (4-4)



Following the general procedure A for the fluorination of monosaccharides, 1,2-*O*-(Methoxyethylidene)-2,3-di-*O*-benzyl-6-*O*-*tert*-butyldimethylsilyl- α -D-

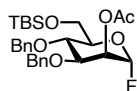
Glucopyranoside (100 mg, 0.18 mmol), DAST (0.024 mL, 0.18 mmol), and DCM (1.5 mL), were used to produce desired product **4-4**, 82.4 mg (88%), as a colorless, viscous oil.

¹H NMR (500 MHz, cdcl₃) δ 7.37 – 7.27 (m, 10H), 5.29 (d, *J* = 6.1 Hz, 1H), 5.18 (d, *J* = 6.0 Hz, 1H), 5.06 (ddd, *J* = 10.1, 7.6, 6.0 Hz, 1H), 4.79 (dd, *J* = 13.3, 11.2 Hz, 2H), 4.72 (d, *J* = 3.3 Hz, 1H), 4.69 (d, *J* = 4.1 Hz, 1H), 3.93 – 3.88 (m, 3H), 3.67 (t, *J* = 8.2 Hz, 1H), 3.53 – 3.50 (m, 1H), 2.01 (s, 3H), 0.91 (s, 9H), 0.08 (d, *J* = 6.8 Hz, 6H).

¹³C NMR (176 MHz, cdcl₃) δ 169.40, 137.94, 137.83, 128.47, 128.44, 127.95, 127.92, 127.89, 127.83, 106.71 (d, *J* = 216.8 Hz), 81.48 (d, *J* = 7.5 Hz), 76.31, 75.91 (d, *J* = 2.6 Hz), 74.91, 74.42, 72.68 (d, *J* = 27.6 Hz), 61.63, 25.86, 20.80, 18.30, -5.17, -5.45.

MS (ESI+) calc'd for C₂₈H₃₉FO₆Si: 536.2836, found: 536.2838 [M+NH₄]⁺

2-*O*-Acetyl-3,4-di-*O*-benzyl-6-*O*-*tert*-butyldimethylsilyl- α -D-mannopyranosyl fluoride (4-5)



Following the general procedure A for the fluorination of monosaccharides, 1,2-*O*-(Methoxyethylidene)-2,3-di-*O*-benzyl-6-*O*-*tert*-butyldimethylsilyl- α -D-

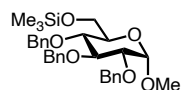
mannopyranoside (240 mg, 0.45 mmol), DAST (0.055 mL, 0.45 mmol), and DCM (6.0 mL), were used to produce desired product **4-5**, 9.7 mg (4%), as a colorless, viscous oil.

¹H NMR (700 MHz, cdcl₃) δ 7.37 – 7.28 (m, 10H), 5.59 – 5.56 (m, 1H), 5.36 (dd, *J* = 50.0, 1.5 Hz, 1H), 4.82 (d, *J* = 11.0 Hz, 1H), 4.71 (d, *J* = 11.5 Hz, 1H), 4.64 (d, *J* = 10.9 Hz, 1H), 4.55 (d, *J* = 11.5 Hz, 1H), 3.99 – 3.91 (m, 3H), 3.71 (dd, *J* = 8.4, 3.3 Hz, 1H), 3.47 (dt, *J* = 7.5, 3.5 Hz, 1H), 2.17 (s, 3H), 0.91 (s, 9H), 0.10 (s, 3H), 0.07 (s, 3H).

^{13}C NMR (176 MHz, cdCl_3) δ 170.65, 138.50, 137.71, 128.80, 128.77, 128.45, 128.27, 128.16, 105.76(d, $J = 217.4$ Hz), 78.12(d, $J = 6.2$ Hz), 76.42(d, $J = 3.7$ Hz), 75.00, 73.26, 72.23, 67.50, (d, $J = 18.2$ Hz), 62.23, 26.18, 21.18, 18.60, -4.88, -5.05.

MS (ESI+) calc'd for $\text{C}_{22}\text{H}_{24}\text{O}_6$: 541.2398, found: 541.2376 $[\text{M}+\text{Na}]^+$

Methyl-2,3,4-tri-*O*-benzyl-6-*O*-trimethylsilyl- α -D-glucopyranoside (4-6)

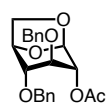


Following the general procedure B for the trimethylsilyl protection of acceptors, methyl-2,3,4-tri-*O*-benzyl- α -D-glucopyranoside (50 mg, 0.11 mmol), trimethylamine (0.031 mL, 0.22 mmol), chlorotrimethylsilane (0.021 mL, 0.165 mmol), and DCM (0.5 mL) were used to produce desired product **4-6**, 66.9 mg (95%), as a colorless, viscous oil. All spectra match published data.^{11,13}

^1H NMR (500 MHz, cdCl_3) δ 7.37 – 7.27 (m, 15H), 4.98 (d, $J = 10.8$ Hz, 1H), 4.89 (d, $J = 11.0$ Hz, 1H), 4.83 – 4.77 (m, 2H), 4.69 – 4.60 (m, 3H), 4.00 (dd, $J = 9.7, 8.7$ Hz, 1H), 3.81 – 3.74 (m, 2H), 3.65 – 3.61 (m, 1H), 3.59 – 3.56 (m, 1H), 3.55 – 3.51 (m, 1H), 3.37 (s, 3H), 0.10 (s, 9H).

All spectra match published data.^{11,13}

1,6-Anhydro-2-*O*-acetyl-3,4-di-*O*-benzyl- β -D-glucopyranoside (4-7)



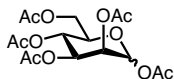
Following general procedure F for the tris(pentafluorophenyl) borane-catalyzed polysaccharide synthesis, **1**, (2-*O*-(Methoxyethylidene)-6-*O*-*tert*-butyldimethylsilyl- α -D-glucopyranoside (49.0 mg, 0.094 mmol), Methyl-2,3,4-tri-*O*-benzyl-6-*O*-trimethylsilyl- α -D-glucopyranoside (10.1 mg,

0.0188 mmol), tris(pentafluoropentyl) borane (9.6 mg, 0.0188 mmol), and DCM (1.88 mL) were used to produce anhydrosugar **4-7**, 37.8 mg (>90%), as a colorless, viscous oil, as the major product. All spectra match published data.¹⁴

¹H NMR (400 MHz, CDCl_3) δ 7.37 – 7.26 (m, 9H), 7.25 (s, 1H), 5.45 (t, $J = 1.7$ Hz, 1H), 4.76 – 4.71 (m, 2H), 4.60 (dd, $J = 6.0, 1.6$ Hz, 1H), 4.56 – 4.50 (m, 2H), 4.43 (d, $J = 12.5$ Hz, 1H), 4.05 (dd, $J = 7.2, 1.2$ Hz, 1H), 3.72 (dd, $J = 7.2, 5.9$ Hz, 1H), 3.53 – 3.52 (m, 1H), 3.33 (d, $J = 1.6$ Hz, 1H), 2.11 (s, 3H).

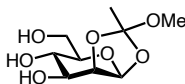
MS (ESI+) calc'd for $\text{C}_{22}\text{H}_{24}\text{O}_6$: 407.1471, found: 407.1461 $[\text{M}+\text{Na}]^+$

Penta-*O*-acetyl- β -D-mannopyranoside (**4-8**)



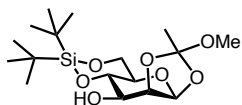
This compound was prepared according to literature procedure, and all spectra match published data.^{11,15}

1,2-*O*-(*exo*-Methoxyethylidene)- β -D-mannopyranoside (**4-9**)



This compound was prepared according to literature procedure, and all spectra match published data.^{11,16}

1,2-*O*-(*exo*-Methoxyethylidene)-4,6-*O*-di-*tert*-butylsilylene- β -D-mannopyranoside (**4-10**)

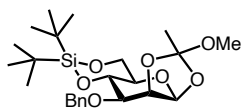


To a solution of 1,2-*O*-(*exo*-methoxyethylidene)- β -D-mannopyranoside (1.0 g, 4.24 mmol) in *N,N*-dimethylformamide (20 mL), under nitrogen, was added 2,6-lutidine (1.5 mL, 12.71 mmol) and di-*tert*-butylsilyl bis(trifluoromethanesulfonate) (1.6 mL, 5.08 mmol) dropwise, at 0 °C. The reaction was allowed to warm to room temperature, and was stirred overnight. The reaction mixture was diluted with ethyl acetate, washed with water (2x) and brine, dried with Na₂SO₄, filtered, and concentrated. The crude mixture was purified by biotage (ethyl acetate/hexanes) to give the desired product **4-10**, 476.0 mg (30%), as a white foam. All spectra match published data.¹¹

¹H NMR (500 MHz, cdCl₃) δ 5.44 (d, *J* = 2.3 Hz, 1H), 4.57 (dd, *J* = 4.1, 2.3 Hz, 1H), 4.16 (dd, *J* = 10.4, 5.1 Hz, 1H), 3.98 (t, *J* = 9.3 Hz, 1H), 3.88 (t, *J* = 10.2 Hz, 1H), 3.79 (dt, *J* = 8.9, 4.2 Hz, 1H), 3.33 (s, 3H), 2.71 (d, *J* = 4.3 Hz, 1H), 1.68 (s, 3H), 1.07 (s, 9H), 0.99 (s, 9H).

MS (ESI+) calc'd for C₁₇H₃₂O₇Si: 399.1815, found: 399.1775 [M+Na]⁺

1,2-*O*-(*exo*-Methoxyethylidene)-3-*O*-benzyl-4,6-*O*-di-*tert*-butylsilylene- β -D-mannopyranoside (4-11)



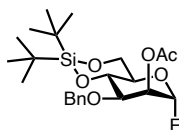
To a solution of 1,2-*O*-(*exo*-methoxyethylidene)-4,6-*O*-di-*tert*-butylsilylene- β -D-mannopyranoside (660 mg, 1.75 mmol) in *N,N*-dimethylformamide (10 mL), under nitrogen, was added sodium hydride (60 % suspension in mineral oil, portion-wise, at 0 °C). The reaction was stirred at 0°C for 15 minutes, before benzyl bromide (0.31 mL, 2.63 mmol) was added. The reaction mixture was allowed to warm to room temperature, and was stirred overnight. The mixture was diluted with ethyl acetate, washed with water (2x) and brine, dried with Na₂SO₄, filtered, and

concentrated. The crude mixture was purified by biotage (ethyl acetate/hexanes) to give the desired product **4-11**, 531.6 mg (82%), as a white foam. All spectra match published data.¹¹

¹H NMR (500 MHz, cdcl₃) δ 7.43 – 7.41 (m, 1H), 7.35 (t, *J* = 7.3 Hz, 2H), 7.32 – 7.28 (m, 1H), 5.31 (d, *J* = 2.2 Hz, 1H), 4.97 (d, *J* = 12.7 Hz, 1H), 4.90 (d, *J* = 12.7 Hz, 1H), 4.38 (dd, *J* = 4.2, 2.2 Hz, 1H), 4.23 (t, *J* = 9.3 Hz, 1H), 4.16 – 4.13 (m, 1H), 3.89 (t, *J* = 10.3 Hz, 1H), 3.57 (dd, *J* = 9.1, 4.2 Hz, 1H), 3.31 (s, 3H), 1.67 (s, 3H), 1.10 (s, 9H), 1.00 (s, 9H).

MS (ESI+) calc'd for C₂₄H₃₈O₇Si: 489.2284, found: 489.2270 [M+Na]⁺

2-*O*-Acetyl-3-*O*-benzyl-4,6-*O*-di-*tert*-butylsilylene- α -D-mannopyranosyl fluoride (**4-12**)

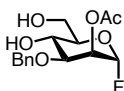


Following the general procedure A for the fluorination of monosaccharides, 1,2-*O*-(*exo*-Methoxyethylidene)-3-*O*-benzyl-4,6-*O*-di-*tert*-butylsilylene- β -D-mannopyranoside

(370 mg, 0.79 mmol), DAST (0.125 mL, 0.948 mmol), and DCM (10 mL), were used to produce desired product **4-12**, 339.1 mg (94%), as a colorless, viscous oil. All spectra match published data.¹¹

¹H NMR (500 MHz, Chloroform-*d*) δ 7.41 – 7.38 (m, 2H), 7.37 – 7.33 (m, 2H), 7.30 (d, *J* = 7.2 Hz, 1H), 5.52 (d, *J* = 1.7 Hz, 1H), 5.42 – 5.41 (m, 1H), 4.78 (s, 1H), 4.24 (t, *J* = 9.6 Hz, 1H), 4.17 (dd, *J* = 9.9, 4.8 Hz, 1H), 3.98 (td, *J* = 10.1, 1.2 Hz, 1H), 3.88 (td, *J* = 10.0, 4.8 Hz, 1H), 3.76 (ddd, *J* = 9.5, 3.6, 1.8 Hz, 1H), 2.16 (s, 3H), 1.12 (s, 5H), 1.02 (s, 9H).

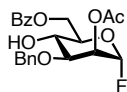
2-*O*-Acetyl-3-*O*-benzyl- α -D-mannopyranosyl fluoride (**4-13**)



To a stirring solution of 2-*O*-Acetyl-3-*O*-benzyl-4,6-*O*-di-*tert*-butylsilylene- α -D-mannopyranosyl fluoride in THF (5.0 mL), was added glacial acetic acid (0.2 mL, 3.5 mmol) at room temperature, followed by tetrabutylammoniumfluoride (1.0 M in tetrahydrofuran, 2.8 mL, 2.8 mmol). The reaction was stirred at room temperature, and when complete by TLC, after 5 hours, the mixture was diluted with ethyl acetate, washed with water (2x) and brine, dried with Na₂SO₄, filtered, and concentrated. The crude mixture was purified by biotage (ethyl acetate/hexanes) to give the desired diol **4-13**, 212.3 mg (96%), as a white foam. All spectra match published data.¹¹

¹H NMR (500 MHz, cdcl₃) δ 7.39 – 7.34 (m, 2H), 7.34 – 7.31 (m, 3H), 5.58 (dd, $J = 48.8, 1.9$ Hz, 1H), 5.48 – 5.47 (m, 1H), 4.74 (d, $J = 11.2$ Hz, 1H), 4.47 (d, $J = 11.2$ Hz, 1H), 3.98 (t, $J = 9.7$ Hz, 1H), 3.94 – 3.83 (m, 3H), 3.78 (ddd, $J = 9.5, 3.3, 2.1$ Hz, 1H), 2.44 (s, 1H), 2.13 (s, 3H), 1.92 (d, $J = 10.5$ Hz, 1H).

2-*O*-Acetyl-3-*O*-benzyl-6-*O*-benzoyl- α -D-mannopyranosyl fluoride (**4-14**)

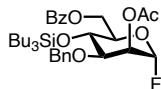


To a stirred solution of 2-*O*-Acetyl-3-*O*-benzyl- α -D-mannopyranosyl fluoride (200 mg, 0.64 mmol), in anhydrous acetonitrile (4.0 mL), was added trimethylamine (0.27 mL, 1.92 mmol), followed dropwise addition of a solution of benzoyl cyanide (88.1 mg, 0.67 mmol) in anhydrous acetonitrile (1.0 mL) at 0 °C. The reaction was stirred for 2 hours at 0 °C, and after complete by TLC, was quenched with methanol. The mixture concentrated under reduced pressure and purified via biotage (ethyl acetate/hexanes), to give the desired alcohol **4-14**, 259.1 mg (97%), as a white foam. All spectra match published data.¹¹

¹H NMR (400 MHz, cdcl₃) δ 8.09 – 8.06 (m, 2H), 7.61 – 7.54 (m, 1H), 7.44 (t, $J = 7.8$ Hz, 2H), 7.40 – 7.29 (m, 5H), 5.60 (dd, $J = 48.8, 2.0$ Hz, 1H), 5.47 (s, 1H), 4.75 (d, $J = 11.2$ Hz, 1H), 4.70

(dd, $J = 12.2, 4.3$ Hz, 1H), 4.62 (dd, $J = 12.2, 2.2$ Hz, 1H), 4.52 (d, $J = 11.2$ Hz, 1H), 4.11 – 4.06 (m, 1H), 3.99 (td, $J = 9.7, 2.7$ Hz, 1H), 3.84 (dt, $J = 9.4, 2.8$ Hz, 1H), 2.63 (d, $J = 2.7$ Hz, 1H), 2.09 (s, 3H).

2-*O*-Acetyl-3-*O*-benzyl-4-*O*-tributylsilyl-6-*O*-benzoyl- α -D-mannopyranosyl fluoride (4-15)



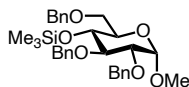
Following the general procedure C for the tributylsilyl protection of acceptors, 2-*O*-acetyl-3-*O*-benzyl-6-*O*-benzoyl- α -D-mannopyranosyl fluoride (17 mg, 0.035 mmol), imidazole (7.1 mg, 0.105 mmol), chlorotributylsilane (0.014 mL, 0.053 mmol), and DCM (0.5 mL) were used to produce desired product **4-15**, 20.4 mg (90%), as a colorless, viscous oil.

¹H NMR (500 MHz, cdcl₃) δ 8.10 – 8.07 (m, 2H), 7.59 – 7.55 (m, 1H), 7.44 (t, $J = 7.8$ Hz, 2H), 7.35 – 7.27 (m, 5H), 5.62 (d, $J = 2.0$ Hz, 1H), 5.46 (t, $J = 2.6$ Hz, 1H), 4.71 (d, $J = 11.1$ Hz, 1H), 4.67 (dd, $J = 12.0, 2.1$ Hz, 1H), 4.47 (dd, $J = 11.7, 3.7$ Hz, 2H), 4.21 (t, $J = 9.4$ Hz, 1H), 4.05 (ddd, $J = 9.8, 4.1, 2.1$ Hz, 1H), 3.78 (dt, $J = 9.3, 2.6$ Hz, 1H), 2.10 (s, 3H), 1.23 – 1.18 (m, 12H), 0.80 (t, $J = 6.9$ Hz, 9H), 0.58 – 0.53 (m, 6H).

¹³C NMR (176 MHz, cdcl₃) δ 169.98, 166.44, 137.84, 133.41, 130.01, 128.65, 128.58, 128.00, 105.02 (d, $J = 220.6$ Hz), 74.13, 71.73 (d, $J = 802.3$ Hz), 66.90, (d, $J = 39.6$ Hz), 63.36, 26.88, 25.73, 20.93, 14.27, 14.03.

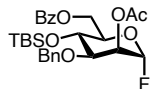
MS (ESI+) calc'd for C₃₄H₄₉FO₇Si: 639.3129, found: 639.3150 [M+Na]⁺

Methyl-2,3,6,-tri-*O*-benzyl-4-*O*-trimethylsilyl- α -D-glucopyranoside (4-16)



This compound was prepared according to literature procedure, and all spectra match published data.^{11,17}

2-*O*-Acetyl-3-*O*-benzyl-4-*O*-*tert*-butyldimethylsilyl-6-*O*-benzoyl- α -D-mannopyranosyl fluoride (4-17)

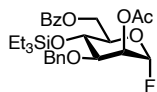


To an oven-dried round-bottom flask with stir bar, was added 2-*O*-acetyl-3-*O*-benzyl-6-*O*-benzoyl- α -D-mannopyranosyl fluoride (259.1 mg, 0.619 mmol). The flask was evacuated and filled with nitrogen (3x). Anhydrous DMF (5.0 mL) was then added to the flask. To the solution of the alcohol was added imidiazole (89 mg, 1.238 mmol), and *tert*-butyldimethylsilyl chloride (112 mg, 0.743 mmol). The mixture was stirred at room temperature overnight, under nitrogen, and monitored by TLC. The final mixture was quenched with water, washed NaHCO₃, water and brine. The organic layer was dried with Na₂SO₄, filtered, and concentrated. The crude mixture was purified by biotage (ethyl acetate/hexanes) to give the desired TBS ether product **4-17**, 220.4 mg (69%), as a colorless, viscous oil.

¹H NMR (500 MHz, cdcl₃) δ 8.09 – 8.06 (m, 2H), 7.60 – 7.55 (m, 1H), 7.45 (t, J = 7.8 Hz, 2H), 7.36 – 7.28 (m, 5H), 5.56 (dd, J = 49.3, 2.1 Hz, 1H), 5.44 (t, J = 2.6 Hz, 1H), 4.73 (dd, J = 12.0, 2.1 Hz, 1H), 4.67 (d, J = 11.1 Hz, 1H), 4.50 (d, J = 11.1 Hz, 1H), 4.43 (dd, J = 12.0, 4.4 Hz, 1H), 4.14 (t, J = 9.3 Hz, 1H), 2.11 (s, 3H), 0.86 (s, 9H), 0.03 (s, 3H), 0.02 (s, 3H).

MS (ESI+) calc'd for C₂₈H₃₇FO₇Si: 555.2190, found: 555.2184 [M+Na]⁺

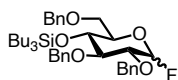
2-*O*-Acetyl-3-*O*-benzyl-4-*O*-triethylsilyl-6-*O*-benzoyl- α -D-mannopyranosyl fluoride (4-18)



Following the general procedure D for the triethylsilyl protection of acceptors, 2-*O*-acetyl-3-*O*-benzyl-6-*O*-benzoyl- α -D-mannopyranosyl fluoride (350 mg, 0.84 mmol), imidazole (171.6 mg, 2.52 mmol), chlorotributylsilane (0.28 mL, 1.68 mmol), and DMF (3.0 mL) were used to produce desired product **4-18**, 398.5 mg (89%), as a colorless, viscous oil. All spectra match published data.¹¹

¹H NMR (500 MHz, cdcl₃) δ 8.08 (dd, $J = 8.3, 1.4$ Hz, 2H), 7.59 – 7.55 (m, 1H), 7.44 (t, $J = 7.8$ Hz, 2H), 7.36 – 7.28 (m, 5H), 5.57 (dd, $J = 49.3, 2.1$ Hz, 1H), 5.46 – 5.44 (m, 1H), 4.72 – 4.68 (m, 2H), 4.49 (d, $J = 11.3$ Hz, 1H), 4.47 – 4.44 (m, 1H), 4.16 (t, $J = 9.4$ Hz, 1H), 4.06 (ddd, $J = 9.8, 4.7, 2.0$ Hz, 1H), 3.79 (dt, $J = 9.2, 2.6$ Hz, 1H), 2.10 (s, 3H), 0.88 (t, $J = 7.9$ Hz, 9H), 0.65 – 0.50 (m, 6H).

2,3,6-tri-*O*-benzyl-4-*O*-tributylsilyl-D-mannopyranosyl fluoride (4-19)



Following the general procedure C for the tributylsilyl protection of acceptors, 2,3,6-tri-*O*-benzyl-D-glucopyranosyl fluoride (239.4 mg, 0.52 mmol), imidazole (106.2 mg, 1.56 mmol), chlorotributylsilane (0.21 mL, 0.78 mmol), and DMF (3 mL) were used to produce desired product **4-19** as a mixture of anomers, 310.8 mg (92%) approximately 2.6 : 1.0 (β : α), as a colorless, viscous oil. The mixture of anomers is characterized below.

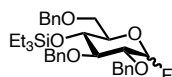
¹H NMR (700 MHz, cdcl₃) δ 7.37 – 7.27 (m, 29H), 7.24 (s, 1H), 5.55 (dd, $J = 53.3, 2.6$ Hz, 1H), 5.29 (dd, $J = 53.1, 6.7$ Hz, 2H), 5.07 (d, $J = 11.6$ Hz, 1H), 4.99 (d, $J = 11.5$ Hz, 3H), 4.80 (d, $J = 11.0$ Hz, 3H), 4.73 (d, $J = 11.6$ Hz, 1H), 4.68 – 4.53 (m, 14H), 3.87 (d, $J = 9.8$ Hz, 1H), 3.79 (dt,

$J = 14.1, 8.9$ Hz, 4H), 3.76 – 3.72 (m, 4H), 3.69 – 3.63 (m, 4H), 3.60 – 3.51 (m, 4H), 3.44 (t, $J = 8.4$ Hz, 3H), 1.35 – 1.30 (m, 12H), 1.22 – 1.18 (m, 31H), 0.89 (t, $J = 6.9$ Hz, 9H), 0.83 – 0.79 (m, 23H), 0.62 – 0.58 (m, 6H), 0.53 (tt, $J = 10.4, 5.9$ Hz, 15H).

^{13}C NMR (126 MHz, cdCl_3) δ 132.89, 129.57, 128.39, 128.29, 128.24, 128.04, 128.02, 128.00, 127.89, 127.75, 127.63, 127.54, 127.53, 127.04, 126.69, 126.68, 74.74, 74.37, 74.09, 73.83, 73.53, 73.44, 70.09, 69.12, 68.88, 63.91, 26.54, 26.50, 25.38, 25.35, 13.95, 13.88, 13.66, 13.64.

MS (ESI+) calc'd for $\text{C}_{39}\text{H}_{55}\text{FO}_5\text{Si}$: 673.3700, found: 673.3690 $[\text{M}+\text{Na}]^+$

2,3,6-tri-*O*-benzyl-4-*O*-triethylsilyl-D-mannopyranosyl fluoride (4-20)

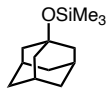


Following the general procedure D for the triethylsilyl protection of acceptors, 2,3,6-tri-*O*-benzyl-D-glucopyranosyl fluoride (88.5 mg, 0.196 mmol), imidazole (60.0 mg, 0.392 mmol), chlorotributylsilane (0.045 mL, 0.588 mmol), and DMF (3.0 mL) were used to produce desired product **4-20** as a mixture of anomers, 41.9 mg (38%) approximately 2.4 : 1.0 (β : α), as a colorless, viscous oil. The mixture of anomers is characterized below.

^1H NMR (500 MHz, cdCl_3) δ 7.38 – 7.27 (m, 45H), 7.24 (d, $J = 4.4$ Hz, 6H), 5.54 (dd, $J = 53.4, 2.7$ Hz, 1H), 5.29 (dd, $J = 53.1, 6.7$ Hz, 2H), 5.04 (d, $J = 11.4$ Hz, 1H), 4.96 (d, $J = 11.5$ Hz, 3H), 4.80 (dd, $J = 11.1, 1.1$ Hz, 3H), 4.74 (d, $J = 11.6$ Hz, 1H), 4.69 – 4.53 (m, 14H), 3.79 – 3.71 (m, 8H), 3.68 – 3.63 (m, 4H), 3.56 (dtd, $J = 8.9, 4.9, 4.5, 1.7$ Hz, 6H), 3.45 (t, $J = 8.4$ Hz, 2H), 0.86 (dt, $J = 10.0, 8.0$ Hz, 30H), 0.57 – 0.47 (m, 20H).

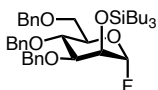
MS (ESI+) calc'd for $\text{C}_{33}\text{H}_{43}\text{FO}_5\text{Si}$: 589.2761, found: 589.2766 $[\text{M}+\text{Na}]^+$

1-((trimethylsilyl)oxy)adamantine (4-21)



This compound was prepared according to literature procedure (following the general procedure B for the trimethylsilyl protection of acceptors), and all spectra match published data.¹⁸

2-*O*-tributylsilyl-3,4,6-tri-*O*-benzyl- α -D-mannopyranosyl fluoride (4-22)



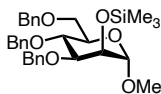
Following the general procedure C for the tributylsilyl protection of acceptors, 3,4,6-tri-*O*-benzyl- α -D-mannopyranosyl fluoride (452.5 mg, 1.0 mmol), imidazole (204.2 mg, 3.0 mmol), chlorotributylsilane (0.4 mL, 1.5 mmol), and DMF (10 mL) were used to produce desired product **4-22**, 620.4 mg (95%) as a colorless, viscous oil.

¹H NMR (500 MHz, cdcl₃) δ 7.40 – 7.25 (m, 13H), 7.18 (dd, J = 7.2, 2.4 Hz, 2H), 5.49 (dd, J = 51.5, 2.2 Hz, 1H), 4.84 (d, J = 10.8 Hz, 1H), 4.73 (s, 2H), 4.67 (d, J = 12.2 Hz, 1H), 4.55 (dd, J = 11.5, 5.8 Hz, 2H), 4.16 (t, J = 2.5 Hz, 1H), 4.01 (t, J = 9.5 Hz, 1H), 3.95 – 3.90 (m, 1H), 3.81 – 3.70 (m, 3H), 1.35 – 1.25 (m, 12H), 0.89 – 0.83 (m, 9H), 0.64 – 0.59 (m, 6H).

¹³C NMR (176 MHz, cdcl₃) δ 138.30, 138.21, 138.16, 128.31, 128.25, 127.98, 127.65, 127.63, 127.53, 127.44, 109.08 (d, J = 222.2 Hz), 79.06, 74.93, 74.57, 73.91, 73.24, 72.84, 68.94, 68.74, 26.51, 25.31, 13.74.

MS (ESI+) calc'd for C₃₉H₅₅FO₅Si: 673.3700, found: 673.3700 [M+Na]⁺

Methyl-2-*O*-trimethylsilyl-3,4,6-tri-*O*-benzyl- α -D-mannopyranoside (4-23)



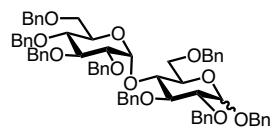
Following the general procedure B for the trimethylsilyl protection of acceptors, methyl-3,4,6-tri-*O*-benzyl- α -D-mannopyranoside (1.4313 g, 3.08 mmol), imidazole (629.0 mg, 9.24 mmol), chlorotrimethylsilane (0.6 mL, 4.62 mmol), and DMF (10 mL) were used to produce desired product **4-23**, 1.1055 g (68%), as a colorless, viscous oil.

$^1\text{H NMR}$ (500 MHz, cdCl_3) δ 7.37 – 7.24 (m, 13H), 7.17 – 7.14 (m, 2H), 4.83 (d, $J = 10.9$ Hz, 1H), 4.73 – 4.60 (m, 4H), 4.55 (d, $J = 12.1$ Hz, 1H), 4.49 (d, $J = 10.9$ Hz, 1H), 4.06 (t, $J = 1.8$ Hz, 1H), 3.90 (t, $J = 9.1$ Hz, 1H), 3.81 – 3.71 (m, 4H), 3.36 (d, $J = 1.2$ Hz, 3H), 0.14 (d, $J = 1.2$ Hz, 9H).

$^{13}\text{C NMR}$ (126 MHz, cdCl_3) δ 138.44, 138.41, 128.16, 128.14, 127.79, 127.58, 127.52, 127.39, 127.32, 127.28, 101.56, 80.01, 74.76, 74.52, 73.12, 72.31, 71.90, 69.46, 69.24, 54.59, 0.29.

MS (ESI+) calc'd for $\text{C}_{31}\text{H}_{40}\text{O}_6\text{Si}$: 559.2492, found: 559.2494 $[\text{M}+\text{Na}]^+$

Benzyl 2,3,6-tri-*O*-benzyl-4-*O*-(2,3,4,6-tetra-*O*-benzyl-D-glucopyranosyl)- α -D-glucopyranoside (4-24)



Following literature procedure,^{19–21} maltose was added to a oven-dried round-bottom flask, and dissolved in anhydrous DMF. The reaction was stirred under nitrogen and 0 °C, and sodium hydride (6.67 g, 166.8 mmol)(60 % suspension in mineral oil) was added in portion. The reaction was kept at 0 °C, and benzyl bromide (25 mL, 208.5 mmol) was added dropwise. The mixture was allowed to warm to room temperature, and to stirred for 36 hours, under nitrogen, and monitored by TLC. When the reaction was complete, it was quenched by pouring the mixture into a large flask with ice and water. The mixture was extracted with ethyl acetate and washed with brine,

dried with Na₂SO₄, filtered, concentrated, dried under vacuum, and purified as a white powder (full conversion), and carried on to the next step. All spectra match published data.¹⁹⁻²¹

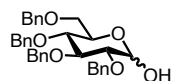
¹H NMR (500 MHz, cdcl₃) δ 7.45 – 7.27 (m, 18H), 7.24 – 7.08 (m, 22H), 5.67 (d, *J* = 3.7 Hz, 1H), 4.98 – 4.57 (m, 12H), 4.57 – 4.42 (m, 9H), 4.07 (t, *J* = 9.1 Hz, 1H), 3.92 – 3.73 (m, 6H), 3.67 – 3.54 (m, 5H), 3.51 – 3.42 (m, 2H).

MS (ESI+) calc'd for C₆₈H₇₀O₁₁: 1080.5262, found: 1080.5248 [M+NH₄]⁺

2,3,4,6-tetra-*O*-benzyl-D-glucopyranoside (4-25) and 2,3,6-tri-*O*-benzyl-D-glucopyranoside (4-26)

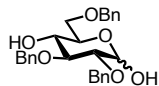
Following literature procedure,¹⁹⁻²¹ to an oven-dried round bottom flask, with stir bar, was added, benzyl 2,3,6-tri-*O*-benzyl-4-*O*-(2,3,4,6-tetra-*O*-benzyl-D-glucopyranosyl)- α-D-glucopyranoside (1.13 g, 1.1 mmol), followed by acetic acid (12 mL). To the dissolved disaccharide was added sulfuric acid (10 M solution, 1.5 mL). The reaction was heated to 85 °C for 5 hours, then stirred at room temperature overnight. When complete by TLC, the mixture was concentrated, quenched with sodium bicarbonate and water, extracted with ethyl acetate and washed with brine, dried with Mg₂SO₄, filtered, concentrated, dried under vacuum, and purified by biotage (ethyl acetate/hexanes). The reaction yielded the monosaccharides **4-25** and **4-26**, 80% yield overall, (characterized, below) as well as other hydrolysis products.

Product 1 (4-25)



Isolated as a white powder 194.4 mg (33%), as a mixture of anomers, approximately 1.0 : 0.3 (α : β). This product was not carried forward. All spectra match published data.¹⁹⁻²¹

Product 2 (4-26)

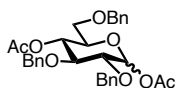


Isolated as a white powder 237.8 mg (47%), as a mixture of anomers, approximately 1.5 : 1.0 (α : β). The mixture of anomers is characterized below. This desired product, **4-26**, was moved forward to the next step in the synthesis. All spectra match published data.¹⁹⁻²¹

¹H NMR (500 MHz, cdCl_3) δ 7.41 – 7.25 (m, 38H), 5.24 (d, $J = 3.5$ Hz, 1H), 5.01 – 4.94 (m, 3H), 4.81 – 4.69 (m, 6H), 4.64 – 4.52 (m, 6H), 4.01 (dt, $J = 9.3, 4.1$ Hz, 1H), 3.83 – 3.74 (m, 2H), 3.71 – 3.46 (m, 9H), 3.39 (dd, $J = 9.1, 7.6$ Hz, 1H), 3.15 (s, 1H), 2.87 (s, 1H), 2.40 (d, $J = 13.4$ Hz, 2H), 2.19 (s, 1H), 2.11 (s, 1H).

MS (ESI+) calc'd for $\text{C}_{27}\text{H}_{30}\text{O}_6$: 473.1940, found: 473. 3364 [$\text{M} + \text{NH}_4$]⁺

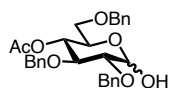
1,4-di-*O*-Acetyl-2,3,6-tri-*O*-benzyl-D-glucopyranoside (4-27)



Following literature procedure,²² to an oven-dried round bottom flask, with stir bar, was added under nitrogen, 2,3,6-tri-*O*-benzyl-D-glucopyranoside (230.0 mg, 0.5 mmol), followed by pyridine (2 mL) and acetic anhydride (2 mL). The reaction was stirred at room temperature for 3 hours. When complete by TLC, the mixture was quenched with hydrochloric acid (1.0 M), extracted with ethyl acetate and washed with brine, dried with Na_2SO_4 , filtered, concentrated, dried under vacuum, and purified by biotage (ethyl acetate/hexanes), to give the desired product **4-27**, 266.0 mg (99%), a mixture of anomers, approximately 1.0 : 1.0 (α : β), as a colorless, viscous oil. The mixture of anomers is characterized below. All spectra match published data.^{22,23}

¹H NMR (500 MHz, cdcl₃) δ 7.35 – 7.27 (m, 28H), 7.24 (d, *J* = 1.3 Hz, 2H), 6.34 (d, *J* = 3.5 Hz, 1H), 5.63 (d, *J* = 7.8 Hz, 1H), 5.11 (ddd, *J* = 10.0, 9.2, 3.0 Hz, 2H), 4.87 (d, *J* = 11.5 Hz, 1H), 4.83 – 4.61 (m, 8H), 4.54 – 4.45 (m, 4H), 3.93 (ddd, *J* = 10.3, 4.6, 3.1 Hz, 1H), 3.86 (t, *J* = 9.5 Hz, 1H), 3.74 – 3.60 (m, 4H), 3.57 – 3.43 (m, 4H), 2.17 (s, 3H), 2.06 (s, 3H), 1.84 (s, 3H), 1.82 (s, 3H).

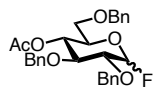
2,3,6-tri-*O*-benzyl-4-*O*-acetyl-D-glucopyranoside (4-28)



Following literature procedure,²² to an oven-dried round bottom flask, with stir bar, was added under nitrogen, 1,4-*O*-acetyl-2,3,6-tri-*O*-benzyl-D-glucopyranoside (260.0 mg, 0.48 mmol), followed by anhydrous THF (2.5 mL). 3-(Dimethylamino)-1-propylamine (0.3 mL, 2.4 mmol) was added, and the reaction was stirred at room temperature for 5 hours. When complete by TLC, the mixture was diluted with DCM, washed with hydrochloric acid (1.0 M) and brine, and the organic layer was dried with Na₂SO₄, filtered, concentrated, dried under vacuum, and purified by biotage (ethyl acetate/hexanes), to give the desired product **4-28**, 226.7 mg (96%), as a colorless, viscous oil. The mixture of anomers is characterized below. All spectra match published data.²²

¹H NMR (500 MHz, cdcl₃) δ 7.38 – 7.27 (m, 28H), 7.25 – 7.22 (m, 2H), 5.20 (d, *J* = 3.5 Hz, 1H), 5.06 – 4.91 (m, 2H), 4.88 – 4.73 (m, 4H), 4.69 – 4.60 (m, 3H), 4.54 – 4.46 (m, 3H), 4.10 – 4.06 (m, 1H), 3.92 (t, *J* = 9.4 Hz, 1H), 3.61 (ddt, *J* = 10.0, 6.5, 3.3 Hz, 2H), 3.55 – 3.41 (m, 4H), 1.84 (s, 3H), 1.83 (s, 3H), 1.54 (s, 2H).

2,3,6-tri-*O*-benzyl-4-*O*-acetyl-D-mannopyranosyl fluoride (4-29)



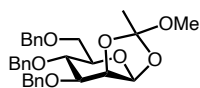
Following the general procedure A for the fluorination of monosaccharides, 2,3,6-tri-*O*-benzyl-4-*O*-acetyl-D-glucopyranoside (220 mg, 0.45 mmol), DAST (0.09 mL, 0.675 mmol), and DCM (3.0 mL), were used to produce desired product **4-29**, 187.4 mg (84%), a mixture of anomers, approximately 1.0 : 2.5 (α : β), as a colorless, viscous oil. The mixture of anomers is characterized below.

$^1\text{H NMR}$ (500 MHz, cdCl_3) δ 7.37 – 7.29 (m, 48H), 7.26 – 7.24 (m, 5H), 5.55 (dd, $J = 52.9, 2.7$ Hz, 1H), 5.35 – 5.22 (m, 2H), 5.15 (t, $J = 9.9$ Hz, 1H), 5.10 – 5.06 (m, 2H), 4.91 – 4.79 (m, 7H), 4.72 – 4.61 (m, 8H), 4.52 (d, $J = 23.3$ Hz, 7H), 4.02 (ddd, $J = 10.4, 4.5, 2.8$ Hz, 1H), 3.93 (t, $J = 9.5$ Hz, 1H), 3.66 – 3.56 (m, 11H), 3.53 (dd, $J = 10.9, 2.8$ Hz, 1H), 3.46 (dd, $J = 10.9, 4.5$ Hz, 1H), 1.85 (d, $J = 2.0$ Hz, 10H).

$^{19}\text{F NMR}$ (377 MHz, cdCl_3) δ -138.05, -150.10.

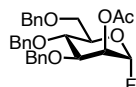
MS (ESI+) calc'd for $\text{C}_{29}\text{H}_{31}\text{FO}_6$: 517.2002, found: 517.2025 $[\text{M}+\text{Na}]^+$

1,2-*O*-(*exo*-Methoxyethylidene)-3,4,6-tri-*O*-benzyl- β -D-mannopyranoside (**4-30**)



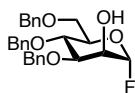
This compound was prepared according to literature procedure, and all spectra match published data.^{10,11,24}

2-*O*-Acetyl-3,4,6-tri-*O*-benzyl- α -D-mannopyranosyl fluoride (**4-31**)



This compound was prepared according to literature procedure, and all spectra match published data.^{10,11,24}

3,4,6-tri-*O*-benzyl- α -D-mannopyranosyl fluoride (4-32)

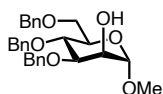


Following literature procedure,¹⁰ to an oven-dried round bottom flask, with stir bar, was added under nitrogen, 2-*O*-Acetyl-3,4,6-tri-*O*-benzyl- α -D-mannopyranosyl fluoride (1.1692 g, 2.36 mmol), followed by anhydrous THF (6.0 mL) and MeOH (3.0 mL). To the solution was added *n*-propylamine (3.0 mL) dropwise (giving a ratio of 2:1:1 THF : MeOH : ⁿPrNH₂), and the reaction was refluxed overnight. When complete by TLC, and cooled to room temperature, the mixture was concentrated, and purified by biotage (ethyl acetate/hexanes), to give the desired product **4-32**, 914.3 mg (86%), as a colorless, viscous oil. All spectra match published data.²⁵

¹H NMR (401 MHz, cdcl₃) δ 7.37 – 7.27 (m, 13H), 7.18 (dd, *J* = 7.3, 2.2 Hz, 2H), 5.68 (dd, *J* = 49.4, 1.8 Hz, 1H), 4.83 (d, *J* = 10.8 Hz, 1H), 4.76 – 4.64 (m, 3H), 4.54 (dd, *J* = 11.5, 3.4 Hz, 2H), 4.15 – 4.09 (m, 1H), 4.00 – 3.85 (m, 3H), 3.77 (dd, *J* = 10.9, 3.4 Hz, 1H), 3.70 (dd, *J* = 10.9, 1.6 Hz, 1H), 2.52 (dd, *J* = 4.4, 2.0 Hz, 1H).

MS (ESI+) calc'd for C₂₇H₂₉FO₅: 475.1897, found: 475.1892 [M+Na]⁺

Methyl-3,4,6-tri-*O*-benzyl- α -D-mannopyranoside (4-33)



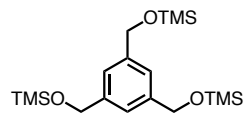
To an oven-dried round bottom flask, with stir bar, was added under nitrogen, 2-*O*-Acetyl-3,4,6-tri-*O*-benzyl- α -D-mannopyranosyl fluoride (2.8704 g, 5.8 mol). The flask was evacuated and filled with nitrogen (3x). Anhydrous Methanol (40 mL) was then added to the flask. To the stirring solution was quickly added a small, towel-dried, cube of sodium metal (in mineral oil). The

reaction was stirred under nitrogen for 3 hours. When complete by TLC, the mixture was diluted with DCM, washed with a minimal amount of saturated sodium bicarbonate, water, and brine. The organic layer was dried with Na₂SO₄, filtered, concentrated, dried under vacuum, and purified by biotage (ethyl acetate/hexanes), to give the product **4-33**, 1.4313 g (53%), as a colorless, viscous oil (other unidentified decomposition products were also isolated/observed by NMR and HRMS). All spectra of **4-33** match published data.²⁶

¹H NMR (700 MHz, cdcl₃) δ 7.38 – 7.26 (m, 13H), 7.19 – 7.16 (m, 2H), 4.82 (d, *J* = 10.8 Hz, 1H), 4.80 (s, 1H), 4.71 – 4.64 (m, 3H), 4.55 (d, *J* = 12.2 Hz, 1H), 4.51 (d, *J* = 10.8 Hz, 1H), 4.04 – 4.02 (m, 1H), 3.88 – 3.82 (m, 2H), 3.77 – 3.70 (m, 3H), 2.44 – 2.41 (m, 1H).

MS (ESI+) calc'd for C₂₈H₃₂O₆: 482.2543, found: 482.2531 [M+NH₄]⁺

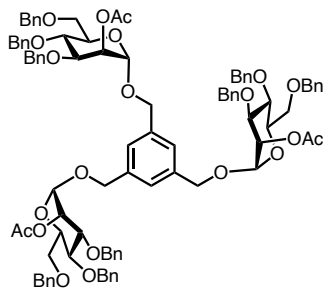
1,3,5-tris(((trimethylsilyl)oxy)methyl)benzene (4-34)



Following the general procedure B for the trimethylsilyl protection of acceptors, benzene-1,3,5-triyltrimethanol (400 mg, 2.3 mmol), trimethylamine (1.28 mL, 9.2 mmol), chlorotrimethylsilane (1.16 mL, 9.2 mmol), and DCM (20 mL) were used to produce desired product **4-34**, 838.9 mg (95%), as a colorless, viscous oil. All spectra match published data.²⁷

¹H NMR (500 MHz, cdcl₃) δ 7.17 (s, 3H), 4.69 (s, 6H), 0.15 (s, 27H).

1,3,5-tris(2-*O*-Acetyl-3,4,6-tri-*O*-benzyl- α -D-mannopyranosyl-methylene)benzene (4-35)



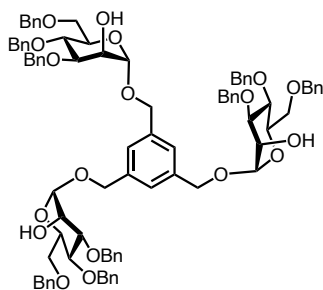
Following the general procedure H for the tris(pentafluorophenyl) borane-catalyzed glycosylation using glycosyl fluorides and TMS ethers, 2-*O*-Acetyl-3,4,6-tri-*O*-benzyl- α -D-mannopyranosyl fluoride (148.4 mg, 0.3 mmol), 1,3,5-tris(((trimethylsilyl)oxy)methyl)benzene (38.5 mg, 0.1 mmol), tris(pentafluorophenyl) borane (5.1 mg, 0.01 mmol), and DCM (3 mL) were used to produce desired dendrimer **4-36**, 153.4 mg (97%), as a light yellow, viscous oil.

$^1\text{H NMR}$ (700 MHz, cdCl_3) δ 7.35 (d, $J = 7.4$ Hz, 6H), 7.29 (q, $J = 8.1, 7.4$ Hz, 21H), 7.25 (d, $J = 2.2$ Hz, 12H), 7.19 (d, $J = 2.3$ Hz, 3H), 7.13 (d, $J = 6.8$ Hz, 6H), 5.44 (d, $J = 3.1$ Hz, 3H), 4.94 (s, 3H), 4.84 (dd, $J = 10.9, 2.1$ Hz, 3H), 4.69 (t, $J = 10.9$ Hz, 9H), 4.53 – 4.45 (m, 12H), 4.03 (d, $J = 9.3$ Hz, 3H), 3.93 (t, $J = 9.2$ Hz, 3H), 3.84 (t, $J = 11.6$ Hz, 6H), 3.72 (d, $J = 10.5$ Hz, 3H), 2.12 (t, $J = 1.9$ Hz, 9H).

$^{13}\text{C NMR}$ (176 MHz, cdCl_3) δ 170.46, 138.47, 138.33, 138.10, 137.47, 128.47, 128.44, 128.42, 128.22, 128.03, 127.93, 127.80, 127.72, 127.61, 97.34, 78.48, 75.35, 74.36, 73.59, 72.00, 71.74, 69.05, 68.87, 68.82, 21.22.

MS (ESI+) calc'd for $\text{C}_{96}\text{H}_{102}\text{O}_{21}$: 1608.7257, found: 1608.7238 $[\text{M}+\text{NH}_4]^+$

1,3,5-tris(3,4,6-tri-*O*-benzyl- α -D-mannopyranosyl-methylene)benzene (4-36)



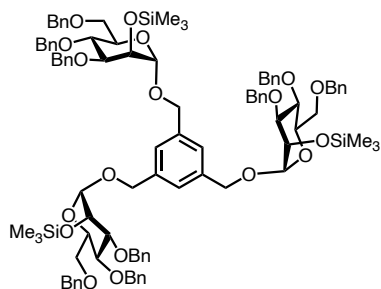
To an oven-dried round-bottom flask with stir bar, was added 1,3,5-tris(2-*O*-Acetyl-3,4,6-tri-*O*-benzyl- α -D-mannopyranosyl-methylene)benzene (108.6 mg, 0.068 mmol). The flask was evacuated and filled with nitrogen (3x). Anhydrous methanol (10.0 mL) was then added to the flask, and the solution was cooled to 0 °C. To the solution was added sodium methoxide (12.1 mg, 0.224 mmol), and the reaction was let stir overnight. After 18 hours to the reaction was not complete, and to solution was added additional sodium methoxide (12.1 mg, 0.224 mmol). The mixture continued to stir at room temperature for 6 hours, under nitrogen, and monitored by TLC. When the reaction was complete, it was quenched with DOWEX exchange resin, filtered, concentrated, dried under vacuum, and collected as a white powder (full conversion, clean by NMR), and carried on to the next step assuming 100% yield.

^1H NMR (700 MHz, cdCl_3) δ 7.37 – 7.23 (m, 39H), 7.20 (d, J = 2.4 Hz, 3H), 7.16 (d, J = 6.8 Hz, 6H), 4.98 (s, 3H), 4.81 (dd, J = 10.7, 2.4 Hz, 3H), 4.71 – 4.63 (m, 12H), 4.54 (dd, J = 12.2, 2.4 Hz, 3H), 4.50 (dt, J = 11.6, 3.8 Hz, 6H), 4.09 (s, 3H), 3.93 (d, J = 8.5 Hz, 3H), 3.90 – 3.83 (m, 6H), 3.77 (dt, J = 10.8, 3.2 Hz, 3H), 3.72 (d, J = 10.7 Hz, 3H), 2.49 (s, 3H).

^{13}C NMR (176 MHz, cdCl_3) δ 138.25, 137.90, 137.61, 128.50, 128.35, 128.33, 127.96, 127.89, 127.82, 127.79, 127.68, 127.57, 127.52, 98.32, 80.26, 75.18, 74.27, 73.46, 71.99, 71.34, 68.90, 68.64, 68.30.

MS (ESI+) calc'd for $\text{C}_{90}\text{H}_{96}\text{O}_{18}$: 1482.6940, found: 1482.6922 $[\text{M}+\text{NH}_4]^+$

1,3,5-tris(2-*O*-trimethylsilyl-3,4,6-tri-*O*-benzyl- α -D-mannopyranosyl-methylene)benzene (4-37)



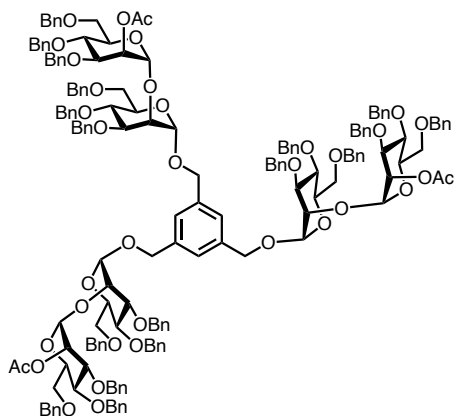
Following literature conditions,^{11,28} to an oven-dried round-bottom flask with stir bar, was added 1,3,5-tris(3,4,6-tri-*O*-benzyl- α -D-mannopyranosyl-methylene)benzene (20.3 mg, 0.0138 mmol). To the flask was added DCM (2 mL), catalytic iodine (2.0 mg, 0.0014 mmol), and hexamethyldisilazane (0.014 mL, 0.069 mmol). The reaction was stirred overnight, and after complete by TLC, the solution was cooled to 0 °C, quenched with Na₂S₂O₃, diluted with ethyl acetate, washed with water (2x) and brine, dried with Na₂SO₄, filtered, and concentrated. The crude mixture was purified by biotage (ethyl acetate/hexanes) to give the desired protected dendrimer **4-38**, 21.6 mg (93%), as a colorless, viscous oil. In cases in which **4-37** was carried forward without purification (as a pure white powder), the desired protected dendrimer **4-38** was obtained in 86% yield over two steps.

¹H NMR (700 MHz, cdcl₃) δ 7.31 (ddd, J = 35.5, 16.8, 7.9 Hz, 24H), 7.25 – 7.21 (m, 15H), 7.19 (s, 3H), 7.12 (d, J = 6.4 Hz, 6H), 4.82 – 4.80 (m, 6H), 4.73 – 4.67 (m, 9H), 4.64 (d, J = 11.4 Hz, 3H), 4.52 (d, J = 12.1 Hz, 3H), 4.47 (t, J = 11.6 Hz, 6H), 4.09 (d, J = 2.6 Hz, 3H), 3.97 (t, J = 9.4 Hz, 3H), 3.87 – 3.77 (m, 9H), 3.73 (d, J = 10.6 Hz, 3H), 0.09 (d, J = 2.1 Hz, 27H).

¹³C NMR (176 MHz, cdcl₃) δ 138.64, 138.63, 138.57, 138.00, 128.44, 128.41, 128.38, 128.14, 127.86, 127.80, 127.70, 127.58, 127.57, 127.14, 100.17, 80.33, 75.14, 74.81, 73.43, 72.75, 72.56, 69.96, 69.36, 68.86, 0.55.

MS (ESI+) calc'd for C₉₉H₁₂₀O₁₈Si₃: 1698.8126, found: 1698.8088 [M+NH₄]⁺

1,3,5-tris(2-*O*-(2-*O*-acetyl-3,4,6-tri-*O*-benzyl- α -D-mannopyranosyl)-3,4,6-tri-*O*-benzyl- α -D-mannopyranosyl-methylene)benzene (4-38)



Following the general procedure H for the tris(pentafluorophenyl) borane-catalyzed glycosylation using glycosyl fluorides and TMS ethers, 2-*O*-Acetyl-3,4,6-tri-*O*-benzyl-D-mannopyranosyl fluoride (18.0 mg, 0.0363 mmol), 1,3,5-tris(2-*O*-trimethylsilyl-3,4,6-tri-*O*-benzyl- α -D-mannopyranosyl-methylene)benzene (17.9 mg, 0.011 mmol), tris(pentafluorophenyl) borane (1.1 mg, 0.0022 mmol), and DCM (3 mL) were used to produce desired dendrimer **4-38**, 15.3 mg (48%), as a colorless, viscous oil. The product was isolated (coeluted) with as a mixture with remaining glycosyl fluoride **4-31** in a 4.9 : 1.0 ratio). The dendrimer **4-38** is characterized below.

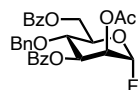
¹H NMR (700 MHz, cdcl₃) δ 7.38 – 7.09 (m, 90H), 7.05 (s, 3H), 5.54 (t, J = 2.6 Hz, 3H), 5.08 – 5.07 (m, 3H), 5.02 (d, J = 1.8 Hz, 3H), 4.83 (dd, J = 10.8, 3.8 Hz, 6H), 4.69 – 4.60 (m, 18H), 4.55 (d, J = 10.8 Hz, 3H), 4.50 (d, J = 12.1 Hz, 3H), 4.40 (d, J = 12.1 Hz, 3H), 4.37 (d, J = 10.9 Hz, 3H), 4.29 (d, J = 11.6 Hz, 3H), 4.06 (d, J = 2.5 Hz, 3H), 4.00 – 3.93 (m, 9H), 3.91 (t, J = 9.3 Hz,

3H), 3.85 (t, $J = 9.7$ Hz, 3H), 3.79 – 3.74 (m, 9H), 3.71 – 3.67 (m, 3H), 3.65 – 3.62 (m, 3H), 2.10 (s, 9H).

^{13}C NMR (176 MHz, cdCl_3) δ 170.40, 138.82, 138.80, 138.66, 138.64, 138.50, 138.34, 137.92, 128.73, 128.67, 128.64, 128.63, 128.61, 128.58, 128.50, 128.44, 128.23, 128.11, 127.96, 127.93, 127.91, 127.84, 127.82, 127.80, 127.77, 127.73, 126.98, 100.02, 99.00, 80.09, 78.50, 75.58, 75.43, 75.39, 74.83, 74.61, 73.69, 73.66, 72.42, 72.23, 72.21, 69.46, 69.41, 69.26, 69.03, 65.39, 21.45.

MS (ESI+) calc'd for $\text{C}_{177}\text{H}_{186}\text{O}_{36}$: 2905.3068, found: 2905.3039 $[\text{M}+\text{NH}_4]^+$

2-*O*-Acetyl-3,6-di-*O*-benzoyl-4-*O*-benzyl- α -D-mannopyranosyl fluoride (4-39)



Following the general procedure A for the fluorination of monosaccharides, 1,2-*O*-(*exo*-Methoxyethylidene)-3,6-di-*O*-benzoyl-4-*O*-benzyl- β -D-mannopyranoside

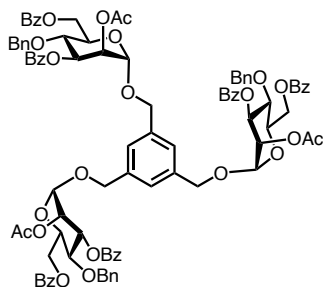
(418 mg, 0.78 mmol), DAST (0.15 mL, 1.17 mmol), and DCM (10 mL), were used to produce desired product **4-40**, 184 mg (45%), as a colorless, viscous oil.

^1H NMR (500 MHz, cdCl_3) δ 8.07 (dd, $J = 7.3, 1.2$ Hz, 2H), 8.04 – 7.98 (m, 2H), 7.63 – 7.57 (m, 2H), 7.46 (t, $J = 7.4$ Hz, 4H), 7.21 – 7.15 (m, 5H), 5.72 – 5.58 (m, 2H), 5.54 (t, $J = 2.2$ Hz, 1H), 4.76 (d, $J = 10.8$ Hz, 1H), 4.68 – 4.58 (m, 3H), 4.30 – 4.26 (m, 1H), 4.20 (t, $J = 9.5$ Hz, 1H), 2.12 (d, $J = 0.9$ Hz, 3H).

^{13}C NMR (126 MHz, cdCl_3) δ 169.78, 166.43, 165.57, 137.30, 133.90, 133.63, 130.13, 130.05, 129.01, 128.89, 128.82, 128.55, 128.51, 106.11 (d, $J = 223.1$ Hz), 75.55, 72.62, 71.72, 69.17, 68.85, 63.11, 21.00.

MS (ESI+) calc'd for $\text{C}_{29}\text{H}_{27}\text{FO}_8$: 545.1588, found: 545.1577 $[\text{M}+\text{Na}]^+$

1,3,5-tris(2-*O*-Acetyl-3,6-di-*O*-benzoyl-4-*O*-benzyl- α -D-mannopyranosyl-methylene)benzene (4-40)



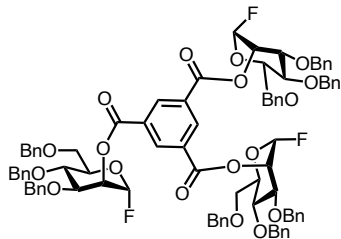
Following the general procedure H for the tris(pentafluorophenyl) borane-catalyzed glycosylation using glycosyl fluorides and TMS ethers, 2-*O*-Acetyl-3,6-di-*O*-benzoyl-4-*O*-benzyl- α -D-mannopyranosyl fluoride (172.4 mg, 0.33 mmol), 1,3,5-tris(((trimethylsilyl)oxy)methyl)benzene (38.5 mg, 0.1 mmol), tris(pentafluorophenyl) borane (5.1 mg, 0.01 mmol), and DCM (10 mL) were used to produce desired dendrimer **4-40**, 87.3 mg (52%), as a light yellow, viscous oil.

$^1\text{H NMR}$ (700 MHz, cdCl_3) δ 8.09 (dd, $J = 8.3, 1.4$ Hz, 6H), 8.01 (dd, $J = 8.3, 1.3$ Hz, 6H), 7.60 – 7.56 (m, 6H), 7.48 – 7.42 (m, 12H), 7.34 – 7.32 (m, 3H), 7.20 – 7.13 (m, 15H), 5.74 (dd, $J = 9.0, 3.7$ Hz, 3H), 5.43 (dd, $J = 3.4, 1.9$ Hz, 3H), 4.93 (d, $J = 2.0$ Hz, 3H), 4.76 (d, $J = 12.1$ Hz, 3H), 4.72 – 4.70 (m, 6H), 4.61 – 4.57 (m, 12H), 4.14 (d, $J = 6.8$ Hz, 5H), 2.09 (s, 7H).

$^{13}\text{C NMR}$ (176 MHz, cdCl_3) δ 170.06, 166.51, 165.56, 142.28, 137.51, 133.59, 133.52, 130.38, 130.08, 130.02, 129.94, 128.84, 128.76, 128.42, 128.32, 127.35, 126.72, 96.98, 75.44, 73.62, 72.65, 70.81, 70.46, 69.75, 65.34, 63.64, 21.11.

MS (ESI $^+$) calc'd for $\text{C}_{96}\text{H}_{90}\text{O}_{27}$: 1692.6013, found: 1692.6008 $[\text{M}+\text{NH}_4]^+$

1,3,5-tris(3,4,6-tri-*O*-benzyl- α -D-mannopyranosyl fluoride)benzene carboxylate (4-41)



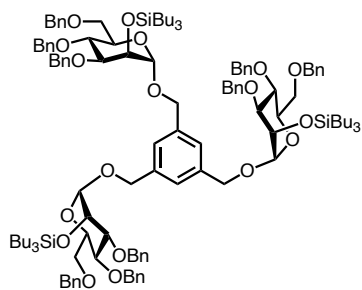
Following literature procedure,²⁹ to an oven-dried round bottom flask, with stir bar, was added under nitrogen, benzene-1,3,5 tricarboxyl trichloride (26.3 mg, 0.099 mmol), followed by pyridine (20 mL) and 3,4,6-tri-*O*-benzyl- α -D-mannopyranosyl fluoride (268.8 mg, 0.594 mmol). The reaction was stirred at room temperature overnight. When complete by TLC, the mixture was quenched by pouring it into a large flask of ice water, and was extracted with DCM. The combined organic layer was washed with CuSO₄ (2x) and brine, dried with Na₂SO₄, filtered, concentrated, dried under vacuum, and purified by biotage (ethyl acetate/hexanes), to give the desired dendrimer **4-41**, 77.9 mg (52%), as a colorless, viscous oil.

¹H NMR (700 MHz, cdcl₃) δ 9.00 (s, 3H), 7.38 – 7.36 (m, 6H), 7.28 (dd, J = 9.3, 2.2 Hz, 15H), 7.24 (d, J = 7.0 Hz, 9H), 7.20 (t, J = 7.5 Hz, 6H), 7.15 – 7.09 (m, 9H), 5.66 (d, J = 51.7 Hz, 6H), 4.82 (d, J = 10.8 Hz, 3H), 4.78 (d, J = 11.4 Hz, 3H), 4.74 (d, J = 12.3 Hz, 3H), 4.61 (d, J = 11.4 Hz, 3H), 4.56 (d, J = 12.3 Hz, 3H), 4.45 (d, J = 10.8 Hz, 3H), 4.11 – 4.06 (m, 6H), 4.02 (s, 3H), 3.78 (dd, J = 10.9, 4.3 Hz, 3H), 3.72 (dd, J = 10.9, 2.0 Hz, 3H).

¹³C NMR (176 MHz, cdcl₃) δ 163.62, 138.05, 137.86, 137.38, 135.58, 130.93, 128.43, 128.33, 128.32, 128.01, 128.01, 127.96, 127.87, 127.73, 127.62, 105.82(d, J = 220.2 Hz),, 75.25(d, J = 311.0 Hz),, 73.33(d, J = 218.2 Hz),, 67.96, 34.64, 29.03, 25.26, 21.03, 11.40.

MS (ESI+) calc'd for C₉₀H₈₇F₃O₁₈: 1530.6188, found: 1530.6183 [M+NH₄]⁺

1,3,5-tris(2-*O*-tributylsilyl-3,4,6-tri-*O*-benzyl-D-mannopyranosyl-methylene)benzene (4-42)



Following the general procedure H for the tris(pentafluorophenyl) borane-catalyzed glycosylation using glycosyl fluorides and TMS ethers, 2-*O*-tributylsilyl-3,4,6-tri-*O*-benzyl- α -D-mannopyranosyl fluoride (128.9 mg, 0.198 mmol), 1,3,5-tris(((trimethylsilyl)oxy)methyl)benzene (23.1 mg, 0.06 mmol), tris(pentafluorophenyl) borane (3.1 mg, 0.006 mmol), and DCM (10 mL) were used to produce desired dendrimer **4-42**, 4.8 mg (4%), as a colorless, viscous oil. Monoglycosylation of core was isolated as the α -anomer, which is characterized below.

^1H NMR (500 MHz, cdCl_3) δ 7.38 – 7.27 (m, 39H), 7.24 (d, $J = 1.7$ Hz, 3H), 7.17 – 7.14 (m, 6H), 4.86 – 4.65 (m, 18H), 4.56 (d, $J = 12.2$ Hz, 3H), 4.50 (t, $J = 11.9$ Hz, 6H), 4.09 (t, $J = 2.4$ Hz, 3H), 3.95 (t, $J = 9.5$ Hz, 3H), 3.83 (ddd, $J = 12.7, 7.2, 2.3$ Hz, 6H), 3.74 (qd, $J = 10.8, 3.4$ Hz, 5H), 1.28 – 1.24 (m, 36H), 0.84 – 0.80 (m, 27H), 0.58 (dddd, $J = 21.3, 10.4, 6.0, 2.8$ Hz, 18H).

^{13}C NMR (176 MHz, cdCl_3) δ 139.01, 138.96, 138.79, 137.89, 128.72, 128.64, 128.57, 128.51, 128.42, 128.23, 128.05, 127.91, 127.69, 127.66, 100.23, 80.62, 75.33, 75.18, 73.55, 72.93, 72.85, 70.37, 69.71, 69.18, 26.89, 25.72, 14.16, 14.12.

6.3.3 Spectral Data for Polysaccharide Optimization

All triarylborane-catalyzed experiments were analyzed by MALDI-TOF, as well as select experiments analyzed by HRMS and/or ^1H NMR (See Chapter 6.1 General Considerations for experimental details).

The table number (and entry number), or figure number from Chapter 4 is listed above the corresponding spectra and analyses. Each MALDI-TOF spectra was analyzed by determining the exact mass (g/mol) of the expected oligosaccharide products, as pictured in Chapter 4. Major products were determined by peak height, and maximum length oligomer was determined by the largest identifiable oligosaccharide mass on the spectrum (m/z). The presence of smaller oligosaccharide products were determined by HRMS if not observed in the MALDI spectrum (1-10 kDa).

Figure 4-4: Initial C6 monomer polymerization results.

Following general procedure E for the tris(pentafluoropenyl) borane-catalyzed polysaccharide synthesis, the following products (A, C, D) were observed.

Timer (product A)

MS (ESI+) calc'd for $C_{78}H_{94}O_{18}Si$: 1369.6107, found: 1369.6076 [M+Na]⁺

Cyclic trimer (product C)

MS (ESI+) calc'd for $C_{66}H_{73}O_{18}$: 1176.4695, found: 1176.4610 [M+Na]⁺

Major product (product D) anhydrosugar (**4-7**)

MS (ESI+) calc'd for $C_{22}H_{24}O_6$: 407.1471, found: 407.1461 [M+Na]⁺

Figure 4-5: Initial C6 monomer polymerization with slow addition.

Following general procedure F for the tris(pentafluoropenyl) borane-catalyzed polysaccharide synthesis, the following products (A, B, C) were observed.

Timer (product A)

MS (ESI+) calc'd for $C_{78}H_{94}O_{18}Si$: 1369.6107, found: 1369.6052 [M+Na]⁺

Dimer (product B)

¹H NMR (400 MHz, cdcl₃) δ 7.31 (dtd, *J* = 13.5, 6.9, 2.9 Hz, 23H), 7.24 (d, *J* = 6.1 Hz, 2H), 5.01 – 4.93 (m, 2H), 4.86 – 4.74 (m, 6H), 4.65 (dd, *J* = 11.4, 9.3 Hz, 3H), 4.58 – 4.49 (m, 3H), 4.35 (d, *J* = 8.0 Hz, 1H), 4.08 – 4.03 (m, 1H), 3.96 (t, *J* = 9.3 Hz, 1H), 3.84 – 3.57 (m, 7H), 3.50 (dd, *J* = 9.6, 3.5 Hz, 1H), 3.42 (t, *J* = 9.5 Hz, 1H), 3.33 (s, 3H), 1.85 (s, 3H), 0.87 (s, 9H), 0.04 (s, 3H), 0.03 (s, 3H).

MS (ESI+) calc'd for C₅₆H₇₀O₁₂Si: 985.5434, found: 985.4519 [M+Na]⁺

Major product (product C) anhydrosugar

MS (ESI+) calc'd for C₂₂H₂₄O₆: 407.1471, found: 407.1461 [M+Na]⁺

(4-7) 1,6-Anhydro-2-*O*-acetyl-3,4-di-*O*-benzyl-β-D-glucopyranoside also isolated and analyzed by NMR (>90%). See characterization above.

Table 4-1 (entry 1)

Following general procedure E for the tris(pentafluoropenyl) borane-catalyzed polysaccharide synthesis, the maximum oligosaccharide observed was a hexamer (n=4).

MS (ESI+) calc'd for C₁₅₀H₁₆₈O₄₁Si: 2671.1174, found: 2672.1054 [M+NH₄]⁺

Table 4-1 (entry 2)

Following general procedure F for the tris(pentafluoropenyl) borane-catalyzed polysaccharide synthesis, the maximum oligosaccharide observed was an octomer (n=6).

MS (MALDI-TOF) calc'd for C₁₉₄H₂₁₂O₅₅Si: 3640.3882, found: 3645.350 [M+Na+matrix]⁺

(matrix is 2,4,6-Trihydroxyacetophenone with exact mass = 168.0432 g/mol)

Table 4-1 (entry 3)

Following general procedure F for the tris(pentafluoropenyl) borane-catalyzed polysaccharide synthesis, the maximum oligosaccharide (without cap, no silyl) observed was a tetramer (n=2).

MS (ESI+) calc'd for $C_{88}H_{90}O_{29}$: 1628.5912, found: 1629.5894 $[M+NH_4]^+$

Table 4-1 (entry 4)

Following general procedure F for the tris(pentafluoropenyl) borane-catalyzed polysaccharide synthesis, the maximum oligosaccharide observed was a trimer (n=1).

MS (MALDI-TOF) calc'd for $C_{78}H_{90}O_{20}Si$: 1397.5692, found: 1399.155 $[M+Na]^+$

Table 4-1 (entry 5)

Following general procedure F for the tris(pentafluoropenyl) borane-catalyzed polysaccharide synthesis, the maximum oligosaccharide observed (with cap, as pictured in table) was a tetramer (n=2).

MS (MALDI-TOF) calc'd for $C_{100}H_{112}O_{27}Si$: 1795.7058, found: 1793.795 $[M+Na]^+$

Table 4-1 (entry 6)

Following general procedure F for the tris(pentafluoropenyl) borane-catalyzed polysaccharide synthesis, the maximum oligosaccharide observed (with cap, as pictured in table) was a dimer (n=0).

MS (MALDI-TOF) calc'd for $C_{56}H_{68}O_{13}Si$: 999.4327, found: 999.936 $[M+Na]^+$

MS (ESI+) calc'd for $C_{56}H_{68}O_{13}Si$: 994.4773, found: 994.3648 $[M+NH_4]^+$

Table 4-2 (entry 1)

Following general procedure F for the tris(pentafluoroperyl) borane-catalyzed polysaccharide synthesis, the maximum oligosaccharide observed was a dimer (n=0).

MS (ESI+) calc'd for C₅₆H₆₈O₁₃Si: 994.4773, found: 994.4756 [M+NH₄]⁺

Table 4-2 (entry 2)

Following general procedure F for the tris(pentafluoroperyl) borane-catalyzed polysaccharide synthesis, the maximum oligosaccharide observed was a dimer (n=0).

MS (ESI+) calc'd for C₅₆H₆₈O₁₃Si: 994.4773, found: 994.3019 [M+NH₄]⁺

Table 4-2 (entry 3)

Following general procedure F for the tris(pentafluoroperyl) borane-catalyzed polysaccharide synthesis, the maximum oligosaccharide observed (with cap, as pictured in table) was a trimer (n=1).

MS (ESI+) calc'd for C₆₂H₈₀O₁₃Si: 1078.5712, found: 1078.5695 [M+NH₄]⁺ (dimer)

MS (MALDI-TOF) calc'd for C₈₄H₁₀₂O₂₀Si: 1481.6631, found: 1481.479 [M+Na]⁺ (trimer)

Table 4-3 (entry 1)

Following general procedure F for the tris(pentafluoroperyl) borane-catalyzed polysaccharide synthesis, the major oligosaccharide observed (with cap, as pictured in table) was a dimer (n=0), while maximum oligosaccharide observed (with cap, as pictured in table) was a trimer (n=1).

MS (ESI+) calc'd for C₆₇H₈₆O₁₁Si: 1095.6018, found: 1098.6115 [M+H]⁺ (dimer)

MS (ESI+) calc'd for C₉₄H₁₁₄O₁₆Si: 1527.7954, found: 1531.8051 [M+H]⁺ (trimer)

Table 4-3 (entry 2)

Following general procedure F for the tris(pentafluoropenyl) borane-catalyzed polysaccharide synthesis, the major oligosaccharide observed (with cap, as pictured in table) was a dimer (n=0) while maximum oligosaccharide observed (with no cap, as pictured in table) was a tetramer (n=2).

MS (MALDI-TOF) calc'd for C₆₇H₈₆O₁₁Si: 1095.6018, found: 1097.1079 [M+H]⁺ (dimer)

MS (MALDI-TOF) calc'd for C₁₀₈H₁₁₄O₂₁: 1747.7931, found: 1748.135 [M+H]⁺ (tetramer)

Figure 4-10: Iterative addition polymerization experiment.

Following general procedure F for the tris(pentafluoropenyl) borane-catalyzed polysaccharide synthesis, the following products (A, B, C, D) were observed.

Tributyl silyl ether dimer (product A)

MS (MALDI-TOF) calc'd for C₆₇H₈₆O₁₁Si: 1117.58, found: 1118.731 [M+Na]⁺

MS (ESI⁺) calc'd for C₆₇H₈₆O₁₁Si: 1095.6018, found: 1098.6112 [M+H]⁺

Trisilyl silyl ether dimer (product B)

MS (MALDI-TOF) calc'd for C₆₁H₇₄O₁₁Si: 1033.4898, found: 1034.273 [M+Na]⁺

Tributyl silyl ether trimer (product C)

MS (MALDI-TOF) calc'd for C₉₄H₁₁₄O₁₆Si: 1549.7774, found: 1552.321 [M+Na]⁺

Hydrolyzed (no silyl ether or cap) trimer (product D)

MS (MALDI-TOF) calc'd for C₈₁H₈₆O₁₆: 1315.5994, found: 1317.288 [M+H]⁺

Figure 4-11: Follow up iterative addition polymerization experiment.

Following general procedure F for the tris(pentafluoropenyl) borane-catalyzed polysaccharide

synthesis, the following products (A, B, C) were observed.

tert-butyldimethyl silyl ether trimer (product A)

MS (MALDI-TOF) calc'd for C₇₈H₉₀O₂₀Si: 1392.6138, found: 1397.312 [M+NH₄]⁺

tert-butyldimethyl silyl ether dimer (product B)

MS (MALDI-TOF) calc'd for C₅₆H₆₈O₁₃Si: 1015.4066, found: 1015.055 [M+K]⁺

Tributyl silyl ether dimer (product C)

MS (MALDI-TOF) calc'd for C₆₂H₈₀O₁₃Si: 1083.340, found: 1083.091 [M+Na]⁺

Figure 4-12: Polymerization experiment with adamantol acceptor: slow addition, extended stir.

Following general procedure F for the tris(pentafluoropenyl) borane-catalyzed polysaccharide synthesis, the following products (A, B, C, D, E) were observed.

Tributyl silyl ether dimer/no adamantol (product A)

MS (MALDI-TOF) calc'd for C₆₆H₈₄O₁₁Si: 1103.5681, found: 1103.803 [M+Na]⁺

MS (ESI⁺) calc'd for C₆₆H₈₄O₁₁Si: 1098.6127, found: 1098.6116 [M+NH₄]⁺

Tributyl silyl ether dimer/with adamantol (product B)

MS (MALDI-TOF) calc'd for C₇₆H₉₈O₁₁Si: 1237.6776, found: 1238.437 [M+Na]⁺

Tributyl silyl ether trimer/no adamantol (product C)

MS (MALDI-TOF) calc'd for C₉₃H₁₁₂O₁₆Si: 1535.7617, found: 1536.679 [M+Na]⁺

Hydrolyzed (no silyl ether or adamantol) trimer (product D)

MS (MALDI-TOF) calc'd for C₈₁H₈₆O₁₆: 1315.5994, found: 1317.494 [M+H]⁺

Hydrolyzed (no silyl ether or adamantol) tetramer (product E)

MS (MALDI-TOF) calc'd for C₁₀₈H₁₁₄O₂₁: 1747.7931, found: 1749.556 [M+H]⁺

Figure 4-13: Polymerization experiment with adamantol acceptor: no slow addition, two hour stir.

Following general procedure F for the tris(pentafluoropenyl) borane-catalyzed polysaccharide synthesis, the following products (A, B, C, D, E) were observed.

Tributyl silyl ether dimer/no adamantol (product A)

MS (MALDI-TOF) calc'd for $C_{66}H_{84}O_{11}Si$: 1103.5681, found: 1103.353 [M+Na]⁺

MS (ESI⁺) calc'd for $C_{66}H_{84}O_{11}Si$: 1103.5681, found: 1103.5661 [M+Na]⁺

Tributyl silyl ether dimer/with adamantol (product B)

MS (MALDI-TOF) calc'd for $C_{76}H_{98}O_{11}Si$: 1237.6776, found: 1238.494 [M+Na]⁺

Hydrolyzed (no silyl ether or adamantol) trimer (product C)

MS (MALDI-TOF) calc'd for $C_{81}H_{86}O_{16}$: 1315.5994, found: 1317.418 [M+H]⁺

Hydrolyzed (no silyl ether or adamantol) dimer (product D)

MS (ESI⁺) calc'd for $C_{54}H_{58}O_{11}$: 921.3616, found: 922.0098 [M+K]⁺

Tributyl silyl ether monosaccharide with adamantol (product D)

MS (ESI⁺) calc'd for $C_{49}H_{70}O_6$: 800.5285, found: 800.5274 [M+K]⁺

Figure 4-14: Polymerization experiment with adamantol acceptor: slow addition, one hour stir.

Following general procedure F for the tris(pentafluoropenyl) borane-catalyzed polysaccharide synthesis, the following products (A, B, and up to hexamers) were observed.

Triethyl silyl ether dimer/no adamantol (product A)

MS (MALDI-TOF) calc'd for $C_{60}H_{72}O_{11}Si$: 1019.4742, found: 1020.574 [M+Na]⁺

Triethyl silyl ether dimer/with adamantol (product B)

MS (MALDI-TOF) calc'd for $C_{70}H_{86}O_{11}Si$: 1153.5837, found: 1153.104 [M+Na]⁺

Tributyl silyl ether hexamer/no adamantol

MS (MALDI-TOF) calc'd for $C_{168}H_{184}O_{31}Si$: 2748.2489, found: 2747.482 [M+Na]⁺

Tributyl silyl ether hexamer/with adamantol

MS (MALDI-TOF) calc'd for $C_{178}H_{198}O_{31}Si$: 2877.4030, found: 2879.624 [M+NH₄]⁺

Figure 4-15: Adamantol oligosaccharides: deglycosylation experiment

Following general procedure H for the tris(pentafluoropenyl) borane-catalyzed polysaccharide synthesis, the mixture from **Figure 4-14** was resubjected to BCF catalysis, and MALDI was monitored. No observable change in oligomer profile (see above).

Table 4-4 (entry 1)

Following general procedure F for the tris(pentafluoropenyl) borane-catalyzed polysaccharide synthesis, the major oligosaccharide observed (with cap, as pictured in table, A) was a dimer (n=0), while maximum oligosaccharides observed (with cap, as pictured in table, B) was a heptamer (n=5), and (with no cap, as pictured in table, C) an octomer (n=6).

Dimer (including cap, A)

MS (MALDI-TOF) calc'd for $C_{67}H_{86}O_{11}Si$: 1094.5939, found: 1094.365 [M]⁺

Heptamer (including cap, B)

MS (MALDI-TOF) calc'd for $C_{190}H_{200}O_{36}$: 3080.3717, found: 3082.232 [M+Na]⁺

Octomer (no cap, C)

MS (MALDI-TOF) calc'd for $C_{216}H_{226}O_{41}$: 3498.5497, found: 3500.906 [M+Na]⁺

Table 4-4 (entry 2)

Following general procedure E for the tris(pentafluoropenyl) borane-catalyzed polysaccharide synthesis, the major oligosaccharide observed (with cap, as pictured in table, B) was a trimer (n=1), while maximum oligosaccharides observed (with cap, as pictured in table, B) was an octomer (n=6), and (with no cap, as pictured in table, C) a nonomer (n=7).

Trimer (including cap, B)

MS (MALDI-TOF) calc'd for C₈₂H₈₈O₁₆: 1351.5970, found: 1351.907 [M+Na]⁺

Octomer (including cap, B)

MS (MALDI-TOF) calc'd for C₂₁₇H₂₂₈O₄₁: 3512.5654, found: 3513.325 [M+Na]⁺

Nonomer (no cap, B)

MS (MALDI-TOF) calc'd for C₂₄₃H₂₅₄O₄₆: 3930.7434, found: 3930.393 [M+Na]⁺

Table 4-4 (entry 3)

Following general procedure E for the tris(pentafluoropenyl) borane-catalyzed polysaccharide synthesis, the major oligosaccharide observed (with cap, as pictured in table, B) was a trimer (n=1), while maximum oligosaccharides observed (with cap, as pictured in table, B) was an octomer (n=6), and (with no cap, as pictured in table, C) an octomer (n=6).

Trimer (including cap, B)

MS (MALDI-TOF) calc'd for C₈₂H₈₈O₁₆: 1351.5970, found: 1353.191 [M+Na]⁺

Octomer (including cap, B)

MS (MALDI-TOF) calc'd for C₂₁₇H₂₂₈O₄₁: 3512.5654, found: 3513.325 [M+Na]⁺

Octomer (no cap, C)

MS (MALDI-TOF) calc'd for $C_{216}H_{226}O_{41}$: 3498.5497, found: 3502.173 [M+Na]⁺

Table 4-4 (entry 4)

Following general procedure G for the tris(pentafluoropenyl) borane-catalyzed polysaccharide synthesis, the major oligosaccharide observed (as pictured in table, C) was a trimer (n=1), while maximum oligosaccharide observed (as pictured in table, C) was an heptamer (n=5).

Trimer (C)

MS (MALDI-TOF) calc'd for $C_{81}H_{86}O_{16}$: 1337.5814, found: 1337.728 [M+Na]⁺

Heptamer (C)

MS (MALDI-TOF) calc'd for $C_{189}H_{198}O_{36}$: 3066.3561, found: 3066.190 [M+Na]⁺

Table 4-4 (entry 5)

Following general procedure G for the tris(pentafluoropenyl) borane-catalyzed polysaccharide synthesis, the major oligosaccharide observed (with silyl) was a dimer (n=0), while maximum oligosaccharide observed (with silyl) was an trimer (n=1).

Dimer (C)

MS (MALDI-TOF) calc'd for $C_{66}H_{84}O_{11}Si$: 1103.5681, found: 1103.308 [M+Na]⁺

Trimer (C)

MS (MALDI-TOF) calc'd for $C_{93}H_{112}O_{16}Si$: 1535.7617, found: 1535.761 [M+Na]⁺

Table 4-5 (entry 1)

Following general procedure E for the tris(pentafluoropenyl) borane-catalyzed polysaccharide synthesis, the major oligosaccharide observed (with cap, as pictured in table 4-4, B) was a trimer

(n=1), while maximum oligosaccharides observed was (with no cap, as pictured in table 4-5, A) an octomer (n=6).

Trimer (including cap, 4-4 B)

MS (MALDI-TOF) calc'd for $C_{82}H_{88}O_{16}$: 1351.5970, found: 1353.191 [M+Na]⁺

Octomer (no cap, 4-5 A)

MS (MALDI-TOF) calc'd for $C_{216}H_{226}O_{41}$: 3498.5497, found: 3502.173 [M+Na]⁺

Table 4-5 (entry 2)

Following general procedure G for the tris(pentafluoropenyl) borane-catalyzed polysaccharide synthesis, the major oligosaccharide observed (as pictured in table, A) was a trimer (n=1), while maximum oligosaccharide observed was (as pictured in table, A) a heptamer (n=5).

Trimer (A)

MS (MALDI-TOF) calc'd for $C_{81}H_{86}O_{16}$: 1337.5814, found: 1337.600 [M+Na]⁺

Hexamer (A)

MS (MALDI-TOF) calc'd for $C_{162}H_{170}O_{31}$: 2634.1624, found: 2635.894 [M+Na]⁺

Heptamer (A)

MS (MALDI-TOF) calc'd for $C_{189}H_{198}O_{36}$: 3082.3300, found: 3195.317 [M+Na]⁺

Table 4-5 (entry 3)

Following general procedure G for the tris(pentafluoropenyl) borane-catalyzed polysaccharide synthesis, the major oligosaccharide observed (as pictured in table, A) was a trimer (n=1), while maximum oligosaccharide observed was (as pictured in table, A) a pentamer (n=3).

Trimer (A)

MS (MALDI-TOF) calc'd for $C_{81}H_{86}O_{16}$: 1337.5814, found: 1338.725 [M+Na]⁺

Pentamer (A)

MS (MALDI-TOF) calc'd for $C_{135}H_{142}O_{26}$: 2201.9687, found: 2204.061 [M+Na]⁺

Table 4-5 (entry 4)

Following general procedure G for the tris(pentafluoropenyl) borane-catalyzed polysaccharide synthesis, the major oligosaccharide observed (using monomer 4-15) was recovered monosaccharide, while the maximum oligosaccharide observed was a trimer (n=1).

Recovered monosaccharide silyl-ether protected glycosyl fluoride (**4-15**)

MS (MALDI-TOF) calc'd for $C_{34}H_{49}FO_7Si$: 639.3129, found: 639.602 [M+Na]⁺

Dimer (B)

MS (MALDI-TOF) calc'd for $C_{56}H_{72}O_{15}Si$: 1030.4984, found: 1030.00 [M+NH₄]⁺

Trimer (A)

MS (MALDI-TOF) calc'd for $C_{66}H_{68}O_{22}$: 1230.4546, found: 1233.927 [M+NH₄]⁺

Figure 4-24: Poly-glycosylation of silyl-protected dendrimer core with a bifunctional monosaccharide.

Following general procedure H for the tris(pentafluoropenyl) borane-catalyzed polysaccharide synthesis, the following products (A, B, and C) were observed.

Mono-glycosylation of core (product A)

MS (MALDI-TOF) calc'd for $C_{90}H_{96}O_{18}$: 1487.6494, found: 1488.469 [M+Na]⁺

Mono-glycosylation of core (But one silyl group on product A)

MS (MALDI-TOF) calc'd for $C_{102}H_{122}O_{18}Si$: 1685.8298, found: 1686.994 [M+Na]⁺

Di-glycosylation of core (product B)

MS (MALDI-TOF) calc'd for C₁₇₁H₁₈₀O₃₃: 2762.2485, found: 2750.424 [M+Na]⁺

Di-glycosylation of core (But two silyl groups on product B)

MS (MALDI-TOF) calc'd for C₁₉₅H₂₃₂O₃₃Si₂: 1153.5837, found: 1153.104 [M+Na]⁺

Disaccharide (product C)

MS (MALDI-TOF) calc'd for C₆₆H₈₄O₁₁Si: 1103.5681, found: 1103.561 [M+Na]⁺

Figure 4-25: Mono-glycosylation of silyl-protected dendrimer core with a bifunctional monosaccharide.

Following general procedure H for the tris(pentafluoropentyl) borane-catalyzed polysaccharide synthesis, the following products A and a large mixture of glycosylation products were observed.

Mono-glycosylation of core (product A: **4-42**, see above) was isolated as the α -anomer.

¹H NMR (500 MHz, cdCl₃) δ 7.38 – 7.27 (m, 39H), 7.24 (d, J = 1.7 Hz, 3H), 7.17 – 7.14 (m, 6H), 4.86 – 4.65 (m, 18H), 4.56 (d, J = 12.2 Hz, 3H), 4.50 (t, J = 11.9 Hz, 6H), 4.09 (t, J = 2.4 Hz, 3H), 3.95 (t, J = 9.5 Hz, 3H), 3.83 (ddd, J = 12.7, 7.2, 2.3 Hz, 6H), 3.74 (qd, J = 10.8, 3.4 Hz, 5H), 1.28 – 1.24 (m, 36H), 0.84 – 0.80 (m, 27H), 0.58 (dddd, J = 21.3, 10.4, 6.0, 2.8 Hz, 18H).

¹³C NMR (176 MHz, cdCl₃) δ 139.01, 138.96, 138.79, 137.89, 128.72, 128.64, 128.57, 128.51, 128.42, 128.23, 128.05, 127.91, 127.69, 127.66, 100.23, 80.62, 75.33, 75.18, 73.55, 72.93, 72.85, 70.37, 69.71, 69.18, 26.89, 25.72, 14.16, 14.12.

6.3.4 Sample MALDI Analysis of Polysaccharide Products

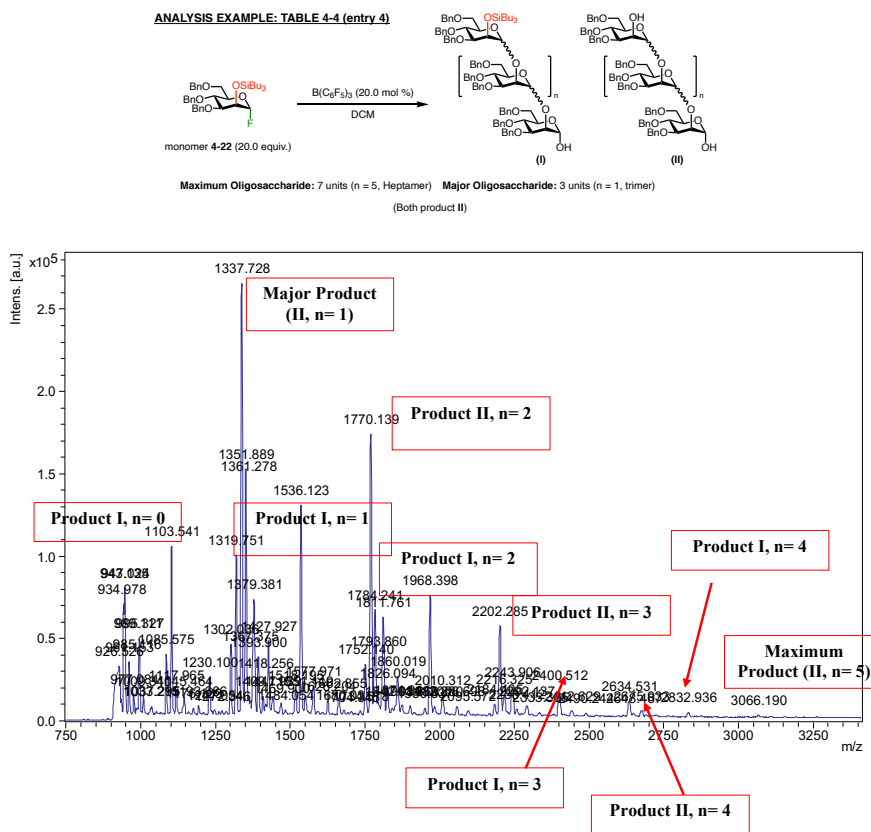


Figure 6-10 Sample MALDI-TOF analysis for polymerization results.

Each MALDI-TOF spectra was analyzed by determining the exact mass (g/mol) of the expected oligosaccharide products, as pictured in Chapter 4. This includes products with and without capping monosaccharides and silyl-protecting groups, which could be identified by their corresponding masses. Major products were determined by peak height, and maximum length oligomer was determined by the largest identifiable oligosaccharide mass on the spectrum (m/z). The presence of smaller oligosaccharide products were determined by HRMS if not observed in the MALDI spectrum (1-10 kDa). Above is a sample spectra with all major products labeled (Figure 6-10).

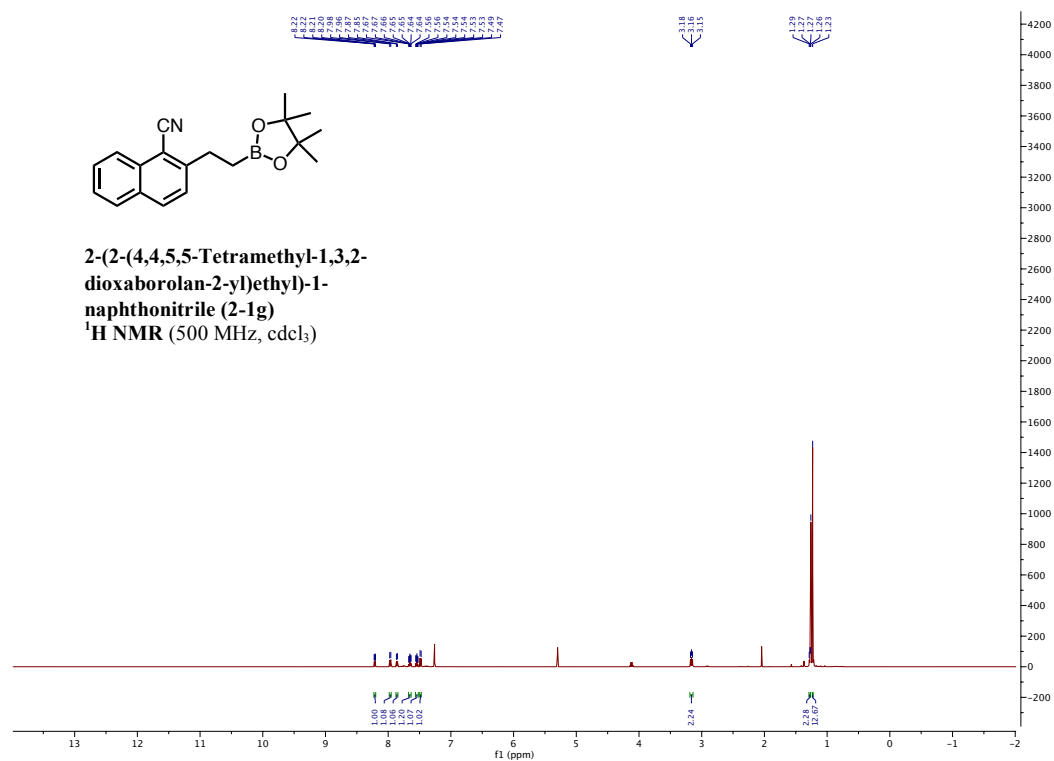
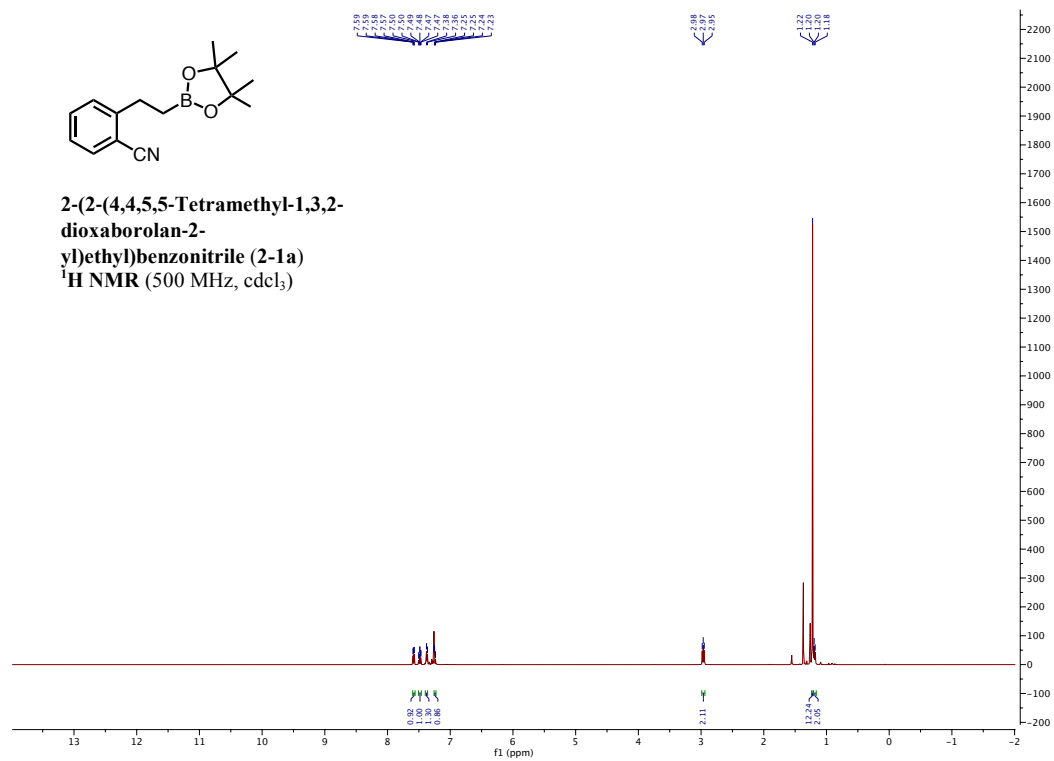
6.4 References

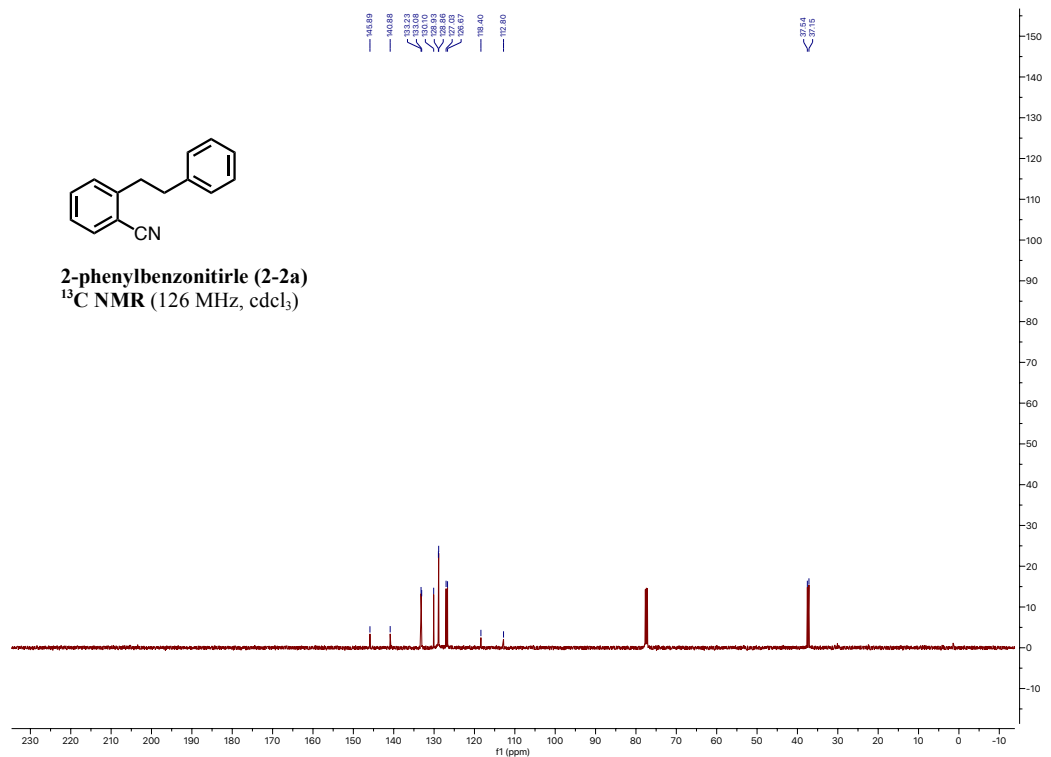
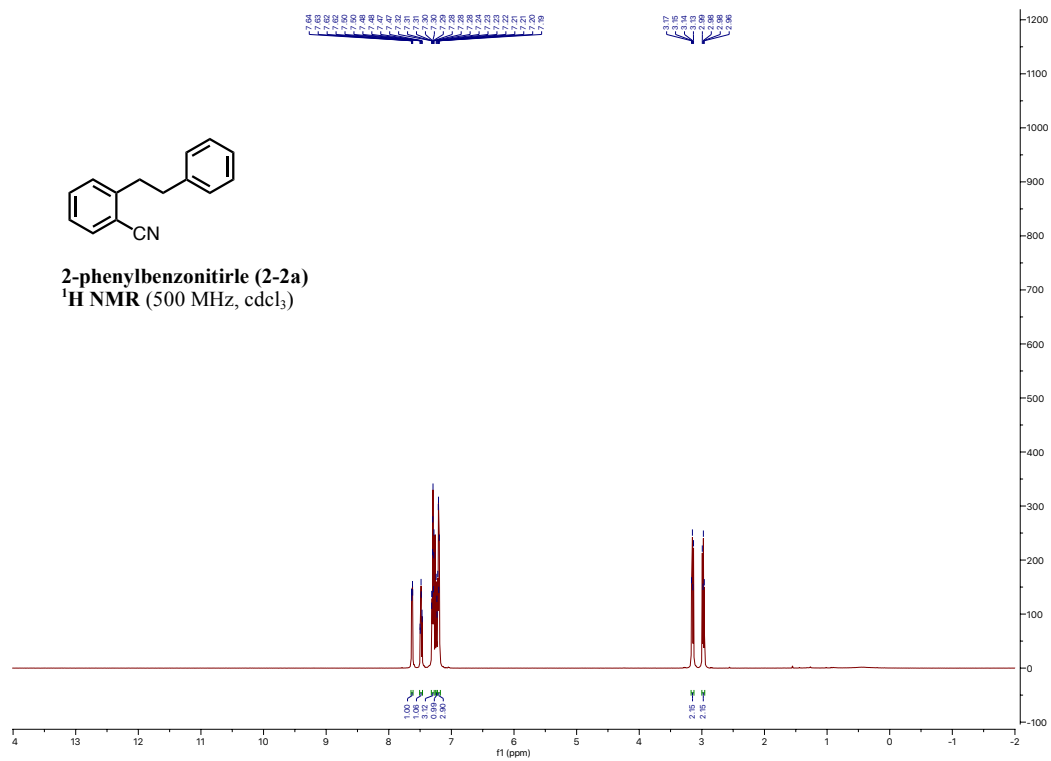
- (1) Shen, P.-X.; Wang, X.-C.; Wang, P.; Zhu, R.-Y.; Yu, J.-Q. Ligand-Enabled Meta-C-H Alkylation and Arylation Using a Modified Norbornene. *J. Am. Chem. Soc.* **2015**, *137* (36), 11574–11577. <https://doi.org/10.1021/jacs.5b08914>.
- (2) Shimasaki, T.; Tobisu, M.; Chatani, N. Nickel-Catalyzed Amination of Aryl Pivalates by the Cleavage of Aryl C–O Bonds. *Angew. Chem. Int. Ed.* **2010**, *49* (16), 2929–2932. <https://doi.org/10.1002/anie.200907287>.
- (3) Zhao, W.; Montgomery, J. Functionalization of Styrenes by Copper-Catalyzed Borylation/Ortho-Cyanation and Silver-Catalyzed Annulation Processes. *Angew. Chem. Int. Ed.* **2015**, *54* (43), 12683–12686. <https://doi.org/10.1002/anie.201507303>.
- (4) Mlynarski, S. N.; Schuster, C. H.; Morken, J. P. Asymmetric Synthesis from Terminal Alkenes by Cascades of Diboration and Cross-Coupling. *Nature* **2014**, *505* (7483), 386–390. <https://doi.org/10.1038/nature12781>.
- (5) Husemoen, G.; Olsson, R.; Andersson, C.-M.; Harvey, S. C.; Hansen, H. C. Solution-Phase Parallel Wittig Olefination: Synthesis of Substituted 1,2-Diarylethanes. *J. Comb. Chem.* **2003**, *5* (5), 606–609. <https://doi.org/10.1021/cc0300210>.
- (6) Elangovan, A.; Wang, Y.-H.; Ho, T.-I. Sonogashira Coupling Reaction with Diminished Homocoupling. *Org. Lett.* **2003**, *5* (11), 1841–1844. <https://doi.org/10.1021/ol034320+>.
- (7) Wang, P.; Chen, B.-Z.; Guo, Y.-C.; Rao, W.; Shen, Z.-L. Copper(II)-Catalyzed Preparation of Alkylindium Compounds and Applications in Cross-Coupling Reactions Both in Aqueous Media. *Tetrahedron Lett.* **2019**, *60* (49), 151288. <https://doi.org/10.1016/j.tetlet.2019.151288>.
- (8) Wiensch, E. M.; Todd, D. P.; Montgomery, J. Silyloxyarenes as Versatile Coupling Substrates Enabled by Nickel-Catalyzed C–O Bond Cleavage. *ACS Catal.* **2017**, *7* (9), 5568–5571. <https://doi.org/10.1021/acscatal.7b02025>.
- (9) Riemer, N.; Coswig, C.; Shipman, M.; Schmidt, B. Palladium-Catalyzed Cross-Coupling of Arenediazonium Salts with Organoindium or Organobismuth Reagents. *Synlett* **2018**, *29* (18), 2427–2431. <https://doi.org/10.1055/s-0037-1611001>.
- (10) Cumpstey, I.; Fairbanks, A. J.; Redgrave, A. J. Stereospecific Synthesis of 1,2- *Cis* Glycosides by Allyl-Mediated Intramolecular Aglycon Delivery. 2. The Use of Glycosyl Fluorides. *Org. Lett.* **2001**, *3* (15), 2371–2374. <https://doi.org/10.1021/ol016175a>.
- (11) Sati, G. C.; Martin, J. L.; Xu, Y.; Malakar, T.; Zimmerman, P. M.; Montgomery, J. Fluoride Migration Catalysis Enables Simple, Stereoselective, and Iterative Glycosylation. *J. Am. Chem. Soc.* **2020**, *jacs.0c03165*. <https://doi.org/10.1021/jacs.0c03165>.
- (12) Access to Molecular Diversity in Glycosaminoglycans: Combinatorial Synthesis of Eight Chondroitin Sulfate Disaccharides - Lubineau - 1999 - European Journal of Organic Chemistry - Wiley Online Library [https://chemistry-europe.onlinelibrary.wiley.com/doi/abs/10.1002/\(SICI\)1099-0690\(199910\)1999:10%3C2523::AID-EJOC2523%3E3.0.CO%3B2-Q](https://chemistry-europe.onlinelibrary.wiley.com/doi/abs/10.1002/(SICI)1099-0690(199910)1999:10%3C2523::AID-EJOC2523%3E3.0.CO%3B2-Q) (accessed Jun 24, 2020).
- (13) Hashimoto, S.; Hayashi, M.; Noyori, R. Glycosylation Using Glucopyranosyl Fluorides and Silicon-Based Catalysts. Solvent Dependency of the Stereoselection. *Tetrahedron Lett.* **1984**, *25* (13), 1379–1382. [https://doi.org/10.1016/S0040-4039\(01\)80163-5](https://doi.org/10.1016/S0040-4039(01)80163-5).
- (14) Zhu, X.; Dere, R. T.; Jiang, J.; Zhang, L.; Wang, X. Synthesis of α -Glycosyl Thiols by Stereospecific Ring-Opening of 1,6-Anhydrosugars. *J. Org. Chem.* **2011**, *76* (24), 10187–10197. <https://doi.org/10.1021/jo202069y>.

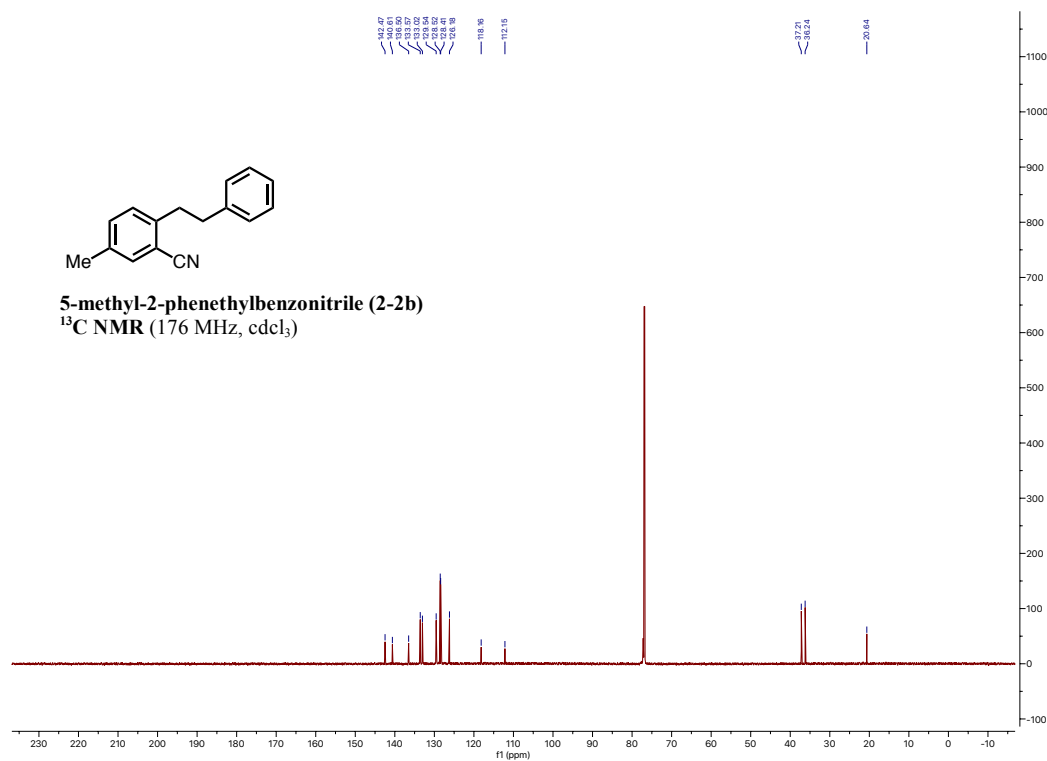
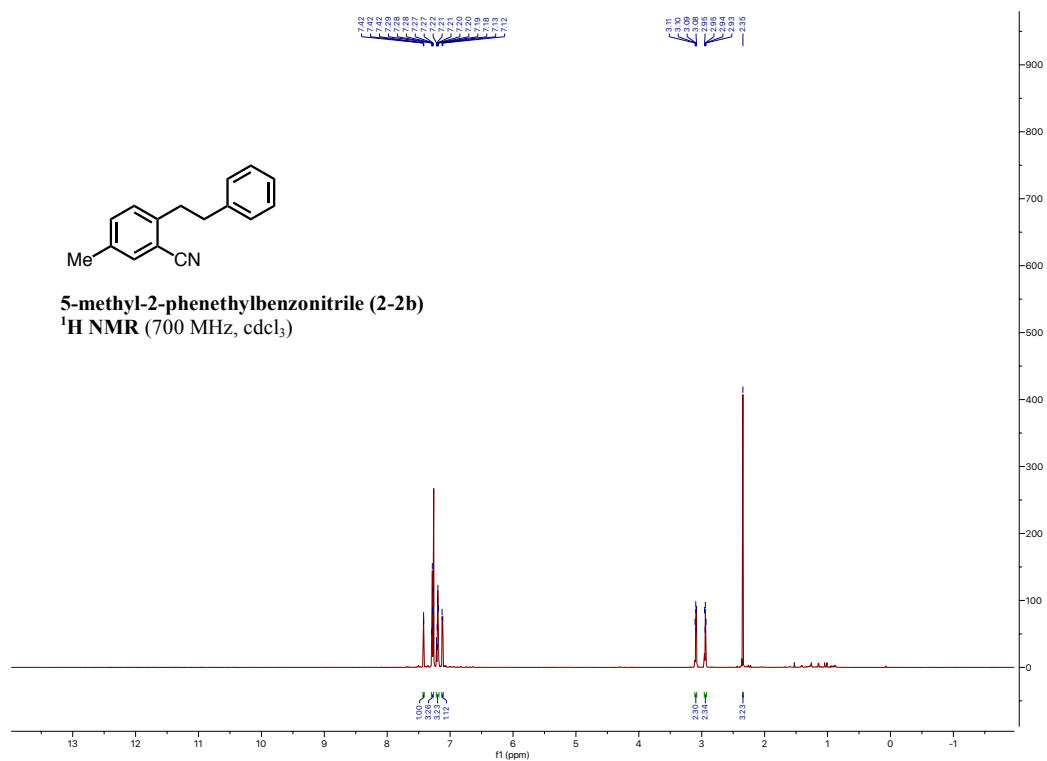
- (15) Wang, J.; Qi, W.; Chen, G. The Effect of Monosaccharides on Self-Assembly of Benzenetricarboxamides. *Chin. Chem. Lett.* **2019**, *30* (3), 587–591. <https://doi.org/10.1016/j.ccllet.2018.12.014>.
- (16) Baeschlin, D. K.; Green, L. G.; Hahn, M. G.; Hinzen, B.; Ince, S. J.; Ley, S. V. Rapid Assembly of Oligosaccharides: 1,2-Diacetal-Mediated Reactivity Tuning in the Coupling of Glycosyl Fluorides. *Tetrahedron Asymmetry* **2000**, *11* (1), 173–197. [https://doi.org/10.1016/S0957-4166\(99\)00519-4](https://doi.org/10.1016/S0957-4166(99)00519-4).
- (17) Mukaiyama, T.; Takashima, T.; Katsurada, M.; Aizawa, H. A Highly Stereoselective Synthesis of α -Glucosides from 1-O-Acetyl Glucose by Use of Tin(IV) Chloride–Silver Perchlorate Catalyst System. *Chem. Lett.* **1991**, *20* (4), 533–536. <https://doi.org/10.1246/cl.1991.533>.
- (18) Saito, T.; Nishimoto, Y.; Yasuda, M.; Baba, A. InCl₃/I₂-Catalyzed Cross-Coupling of Alkyl Trimethylsilyl Ethers and Allylsilanes via an in Situ Derived Combined Lewis Acid of InCl₃ and Me₃SiI. *J. Org. Chem.* **2007**, *72* (22), 8588–8590. <https://doi.org/10.1021/jo7015289>.
- (19) Micheel, F.; Kreutzer, U. Synthese des kristallinen D-Glucose-anhydrids- α . β . *Justus Liebigs Ann. Chem.* **1969**, *722* (1), 228–231. <https://doi.org/10.1002/jlac.19697220124>.
- (20) Sato, T.; Nakamura, H.; Ohno, Y.; Endo, T. Synthesis of 1,4-Anhydro-2,3,6-Tri-O-Benzyl- α -D-Glucopyranose by Cis-Ring-Closure of a Glycosyl Chloride. *Carbohydr. Res.* **1990**, *199* (1), 31–35. [https://doi.org/10.1016/0008-6215\(90\)84090-H](https://doi.org/10.1016/0008-6215(90)84090-H).
- (21) Hanashima, S.; Yamaguchi, Y.; Ito, Y.; Sato, K. Synthesis of the Starfish Ganglioside AG2 Pentasaccharide. *Tetrahedron Lett.* **2009**, *50* (45), 6150–6153. <https://doi.org/10.1016/j.tetlet.2009.08.071>.
- (22) Andersen, S. M.; Heuckendorff, M.; Jensen, H. H. 3-(Dimethylamino)-1-Propylamine: A Cheap and Versatile Reagent for Removal of Byproducts in Carbohydrate Chemistry. *Org. Lett.* **2015**, *17* (4), 944–947. <https://doi.org/10.1021/acs.orglett.5b00041>.
- (23) Haque, W.; Diakur, J. CYCLODEXTRIN—A CARRIER OR SYNTHON? SYNTHESIS OF PER-O-METHYL- β -CYCLODEXTRIN-GM3. *J. Carbohydr. Chem.* **2001**, *20* (1), 17–29. <https://doi.org/10.1081/CAR-100102540>.
- (24) Elie, C. J. J.; Dreef, C. E.; Verduyn, R.; Van Der Marel, G. A.; Van Boom, J. H. Synthesis of 1-O-(1,2-Di-O-Palmitoyl-SN-Glycero-3-Phosphoryl)-2-O- α -D-Mannopyranosyl-D-MYO-Inositol: A Fragment of Mycobacterial Phospholipids. *Tetrahedron* **1989**, *45* (11), 3477–3486. [https://doi.org/10.1016/S0040-4020\(01\)81026-7](https://doi.org/10.1016/S0040-4020(01)81026-7).
- (25) Fraser-Reid, B.; Lopez, J. C.; Bernal-Albert, P.; Gomez, A. M.; Uriel, C.; Ventura, J. Glycosyl Fluorides from N-Pentenyl-Related Glycosyl Donors - Application to Glycosylation Strategies. *Can. J. Chem.* **2013**, *91* (1), 51–65. <https://doi.org/10.1139/cjc-2012-0285>.
- (26) Nestor, G.; Anderson, T.; Oscarson, S.; Gronenborn, A. M. Exploiting Uniformly ¹³C-Labeled Carbohydrates for Probing Carbohydrate–Protein Interactions by NMR Spectroscopy. *J. Am. Chem. Soc.* **2017**, *139* (17), 6210–6216. <https://doi.org/10.1021/jacs.7b01929>.
- (27) Öztürk, B. Ö.; Karabulut, S.; İmamoğlu, Y. Activity of Homobimetallic Ruthenium Alkylidene Complexes on Intermolecular [2+2+2] Cyclotrimerisation Reactions of Terminal Alkynes. *Inorganica Chim. Acta* **2011**, *378* (1), 257–263. <https://doi.org/10.1016/j.ica.2011.09.023>.

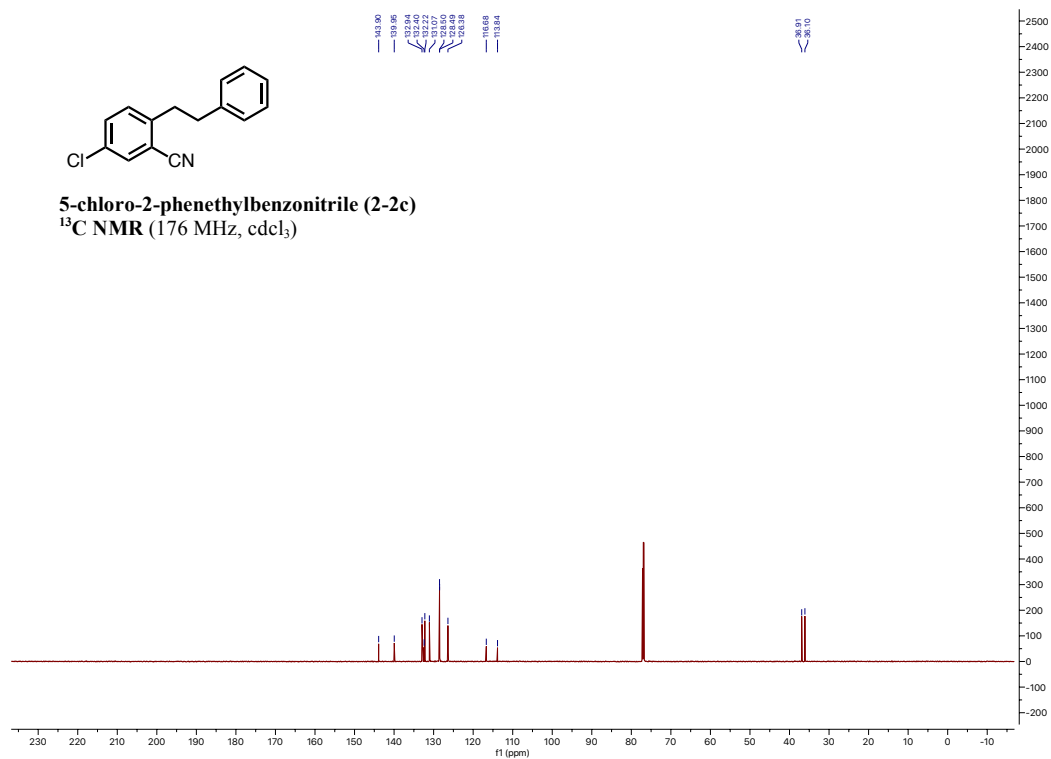
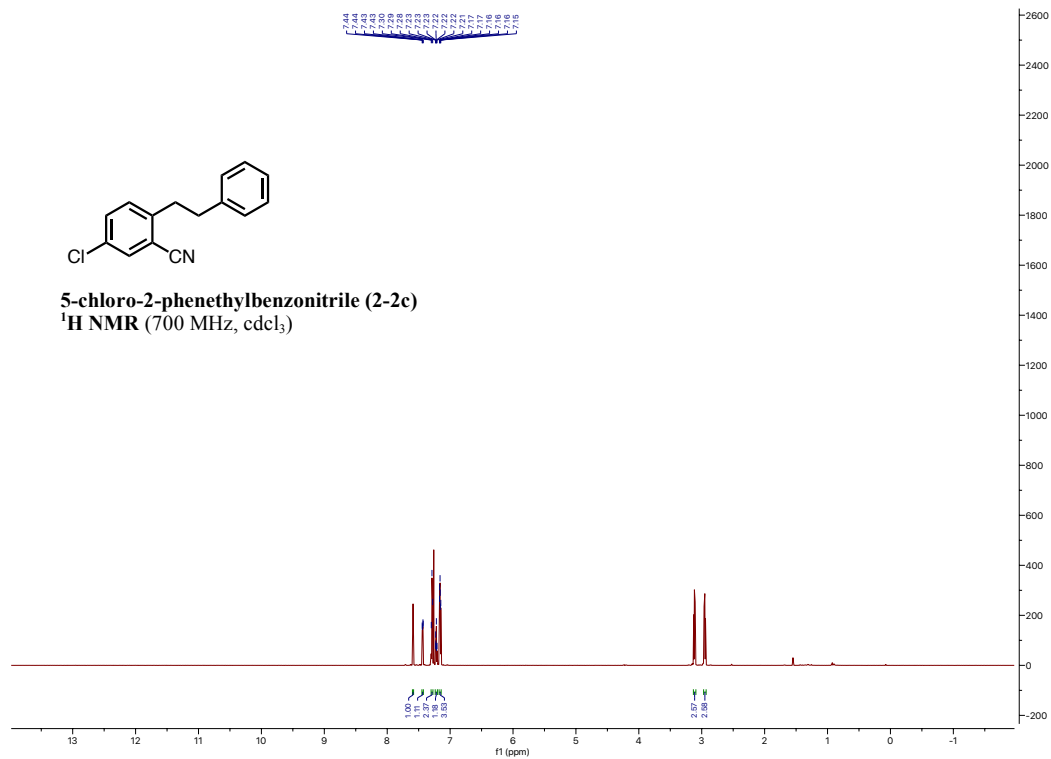
- (28) Karimi, B.; Golshani, B. Mild and Highly Efficient Method for the Silylation of Alcohols Using Hexamethyldisilazane Catalyzed by Iodine under Nearly Neutral Reaction Conditions. *J. Org. Chem.* **2000**, *65* (21), 7228–7230. <https://doi.org/10.1021/jo005519s>.
- (29) Ma, T.; Li, C.; Zhang, Z.; Wang, Z.; Yu, L.; Xue, W. Indium(III) Iodide-Catalyzed Stereoselective Synthesis of β -Glucopyranosides by Using a Glucosyl Fluoride Donor with 2-O-Benzoyl-3,4,6-Tri-O-Benzyl Protection. *Synlett* **2017**, *28* (19), 2633–2636. <https://doi.org/10.1055/s-0036-1589121>.

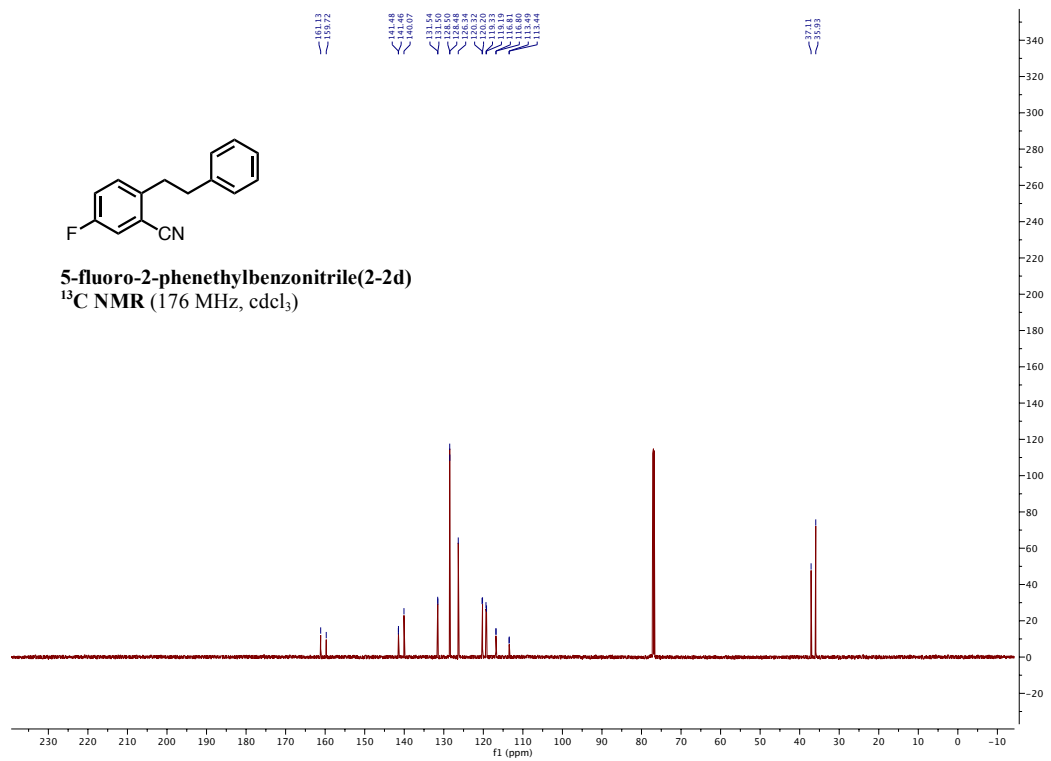
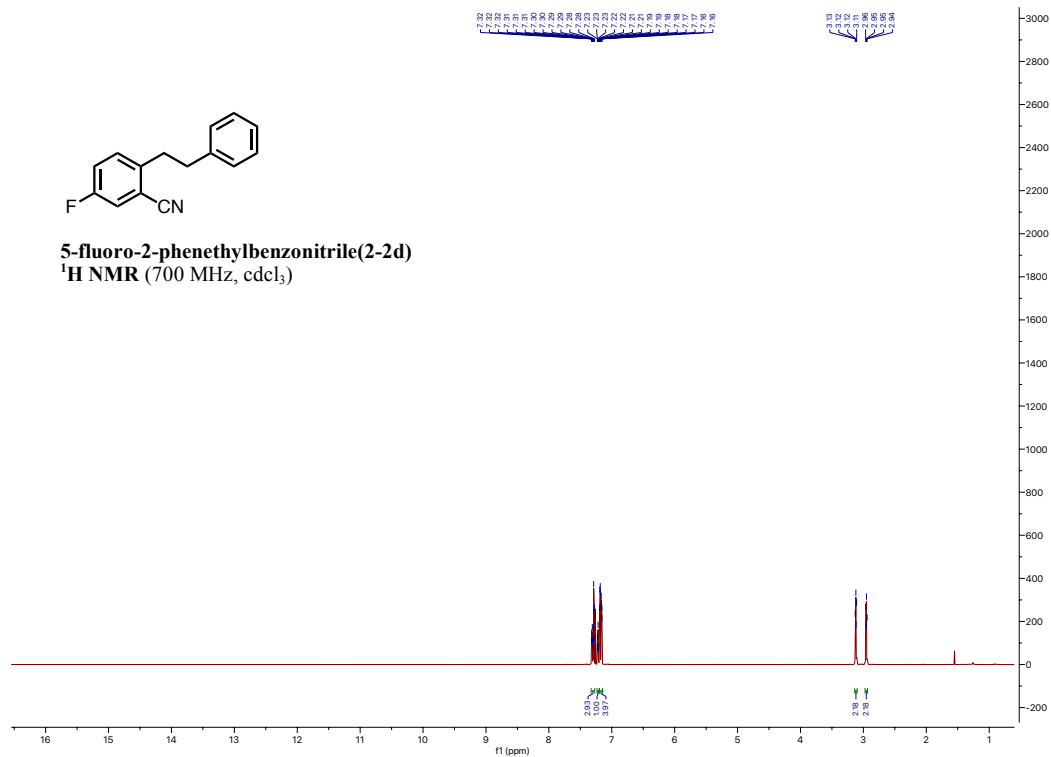
6.6 NMR Spectra of New Compounds

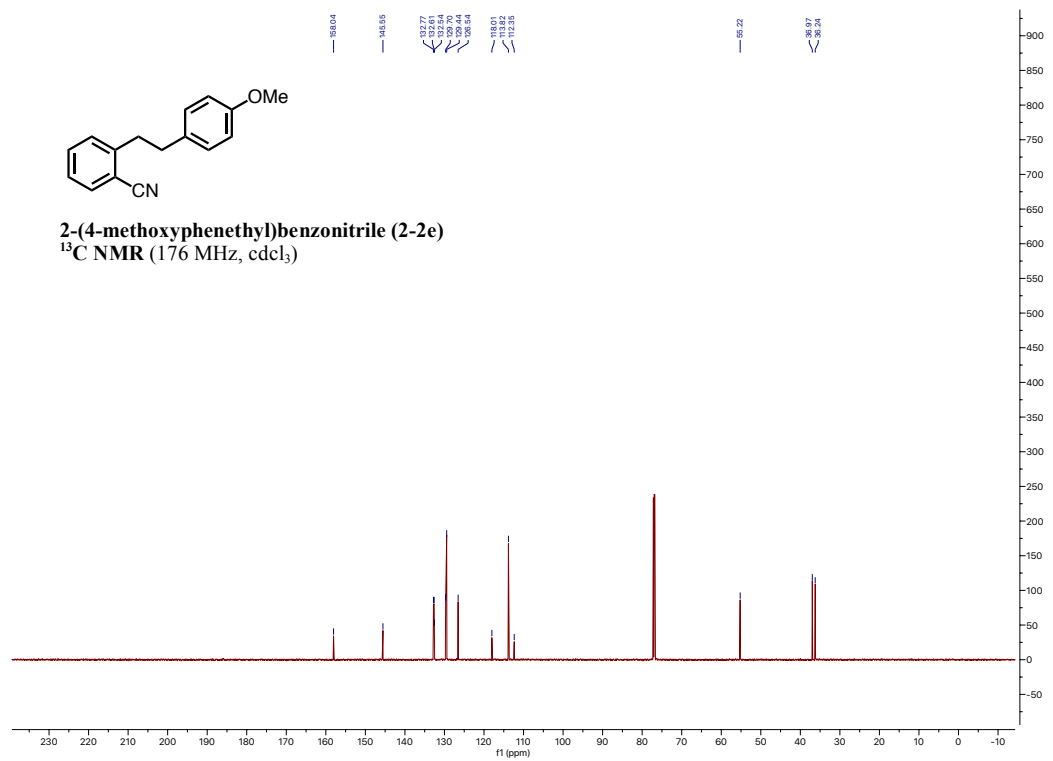
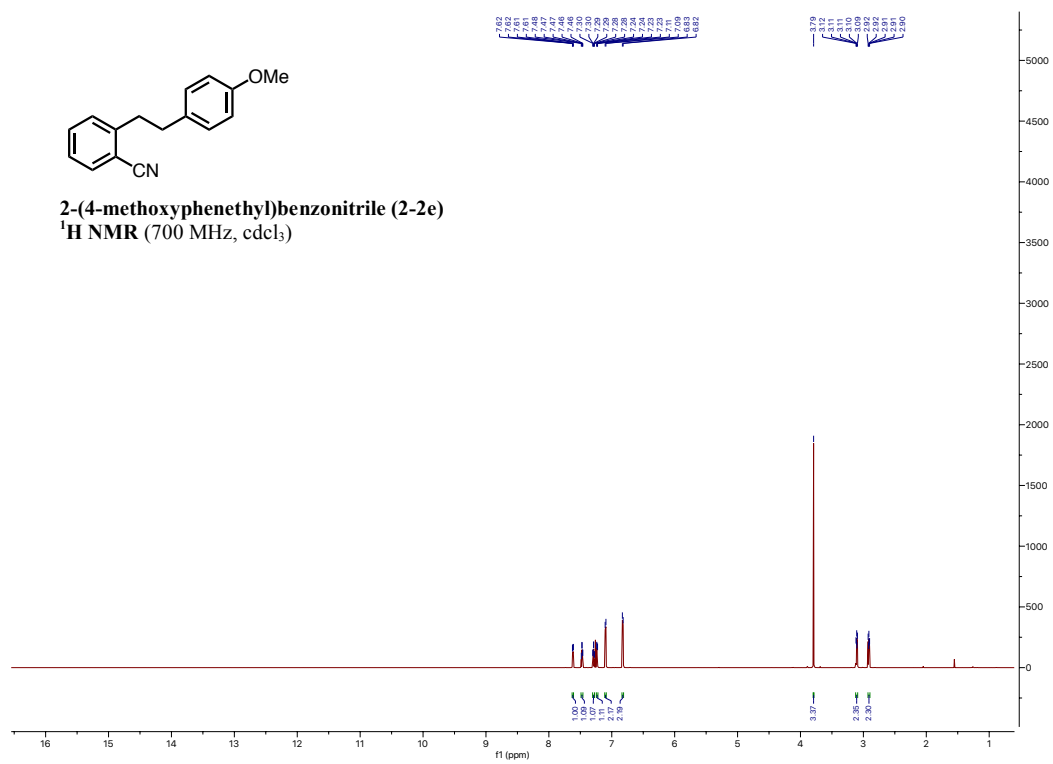


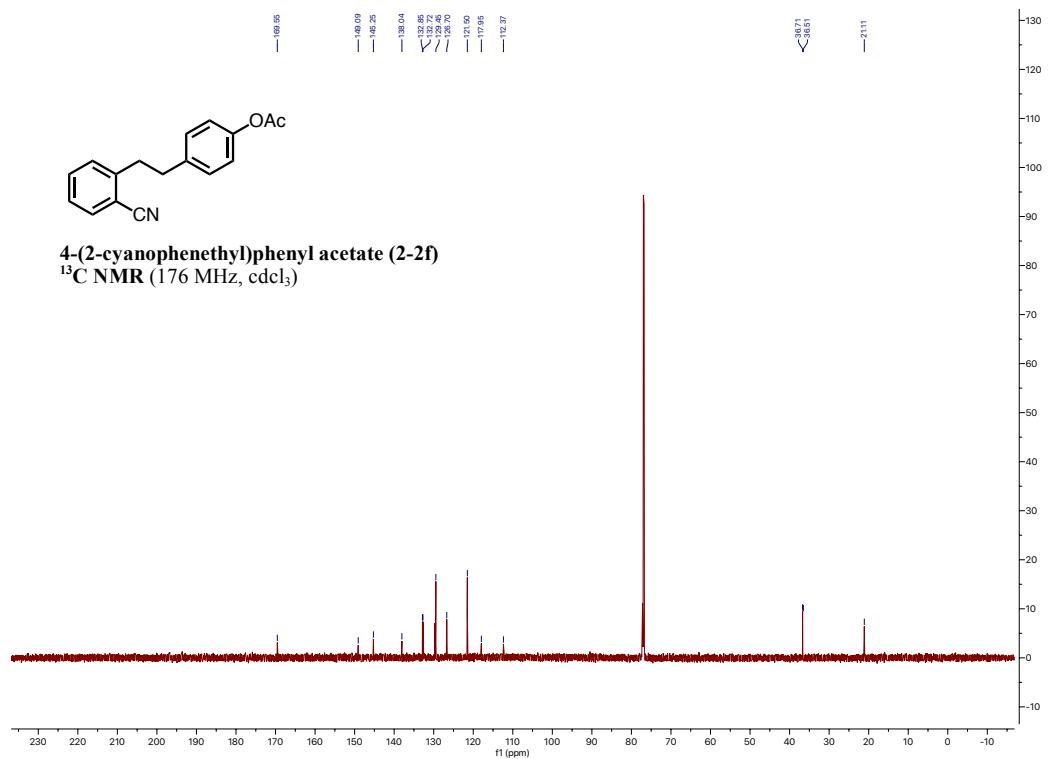
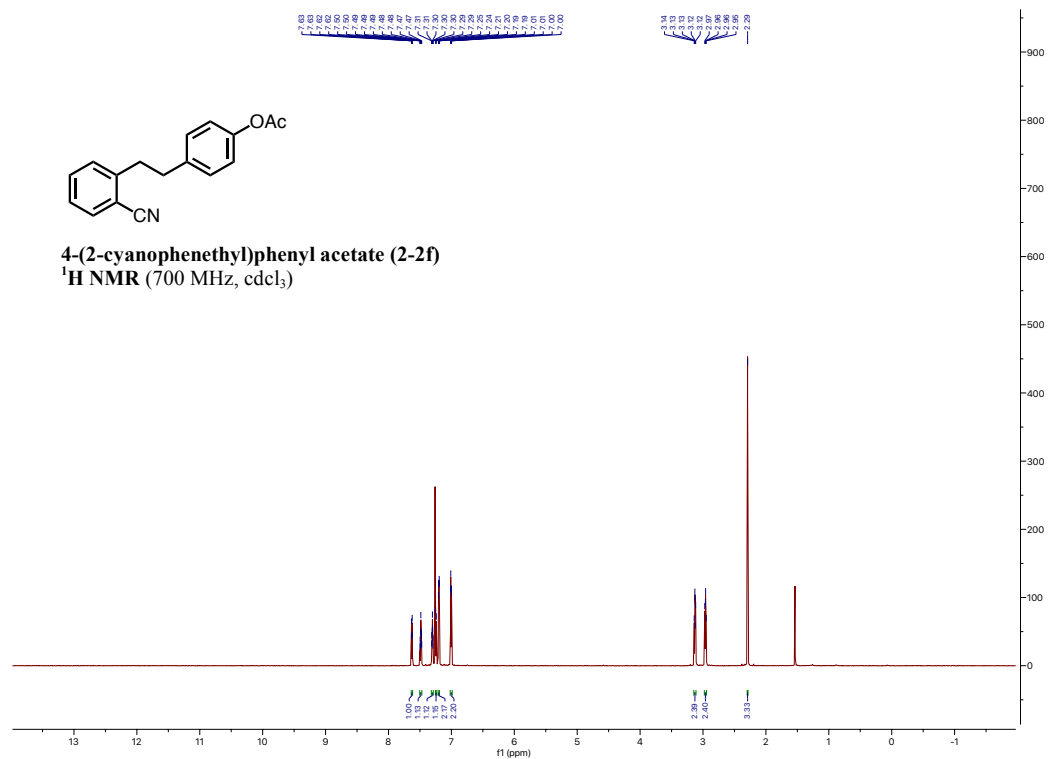




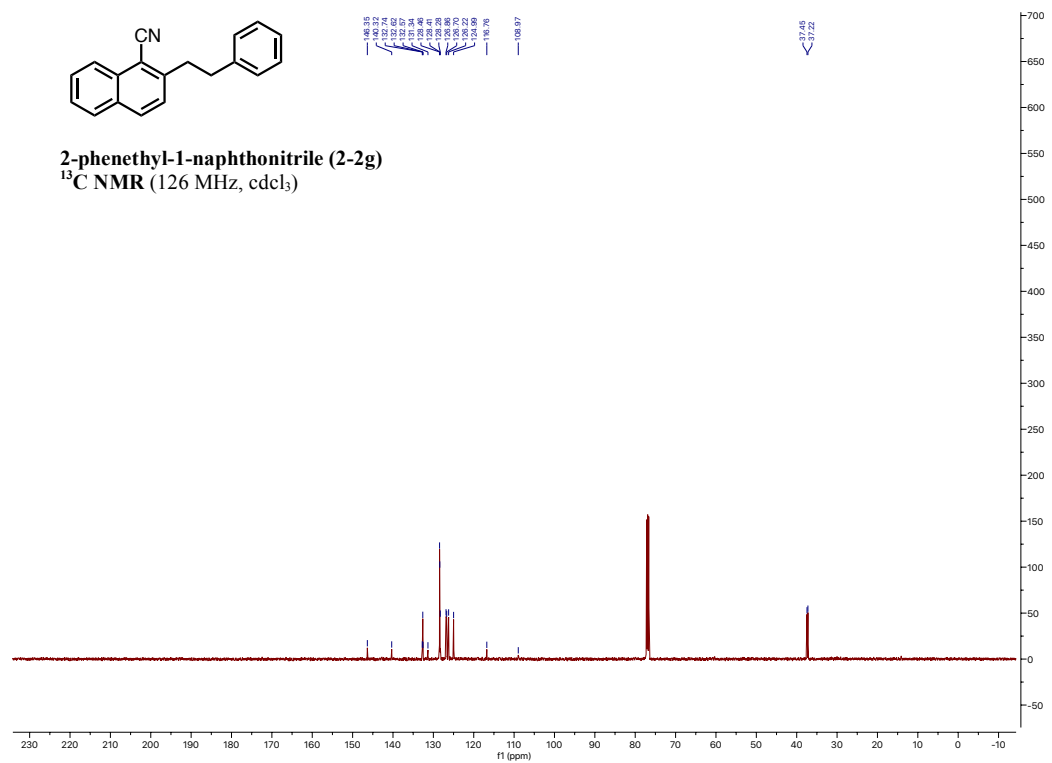
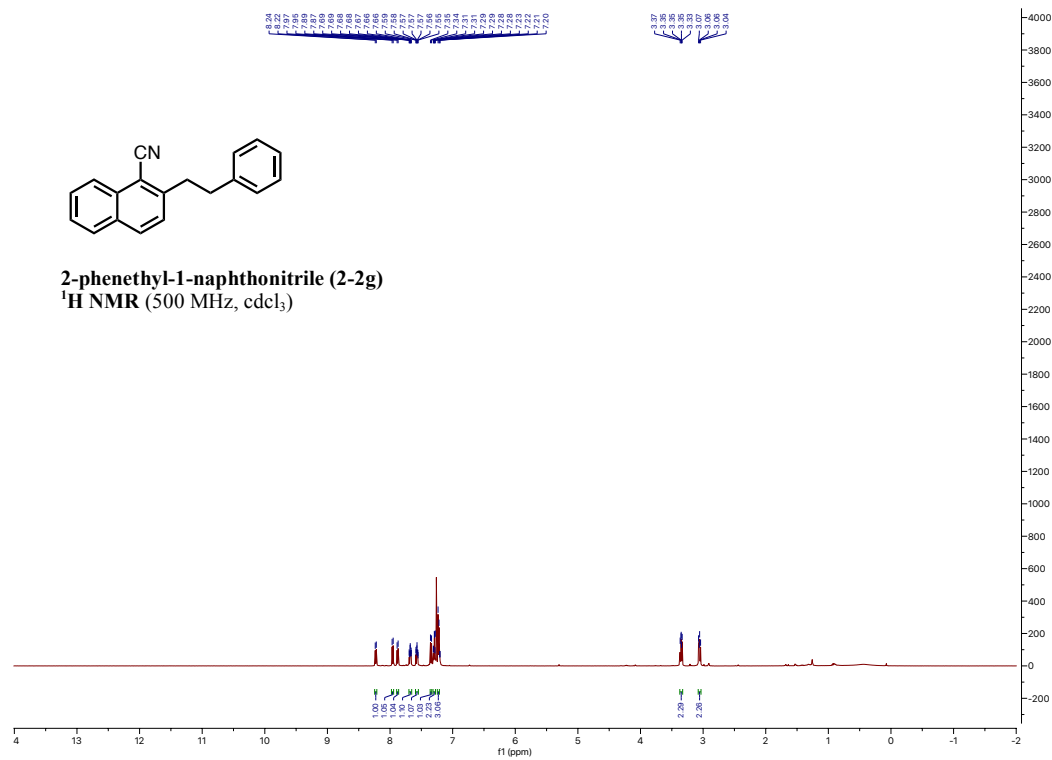


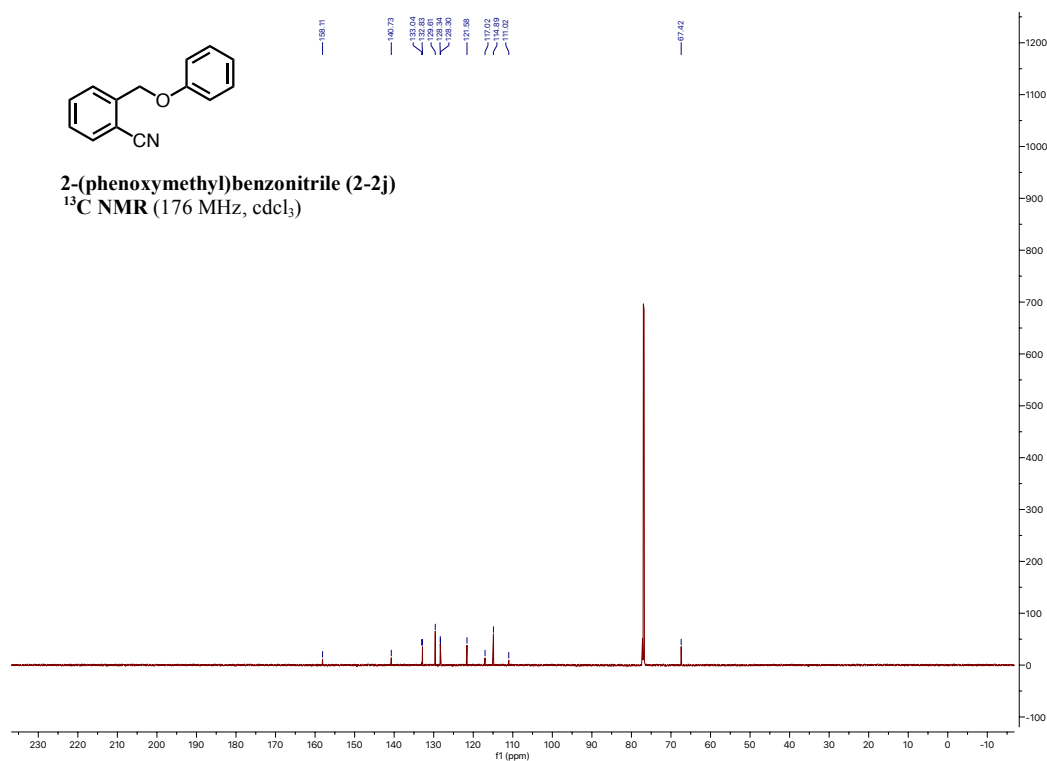
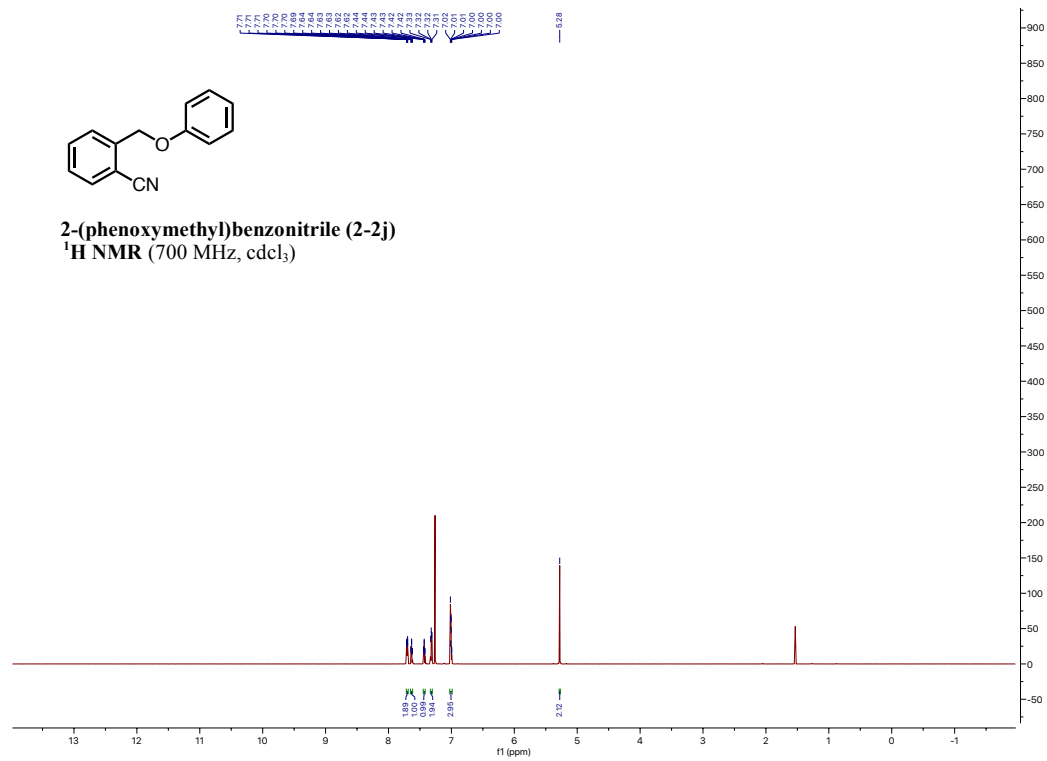


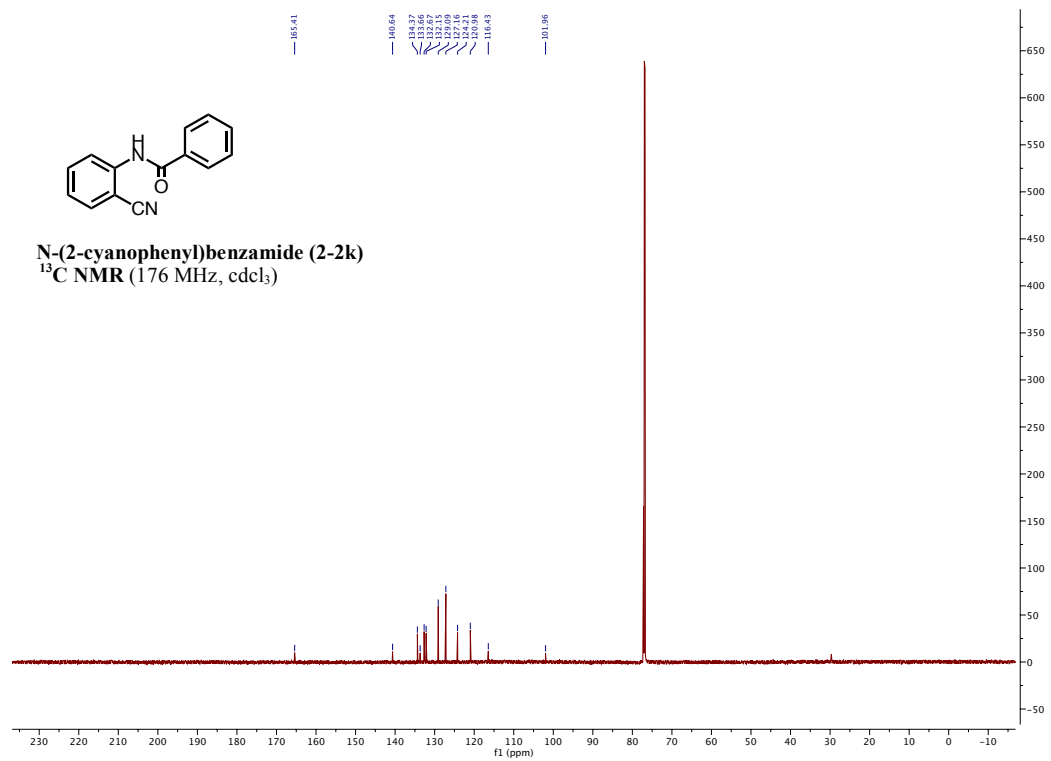
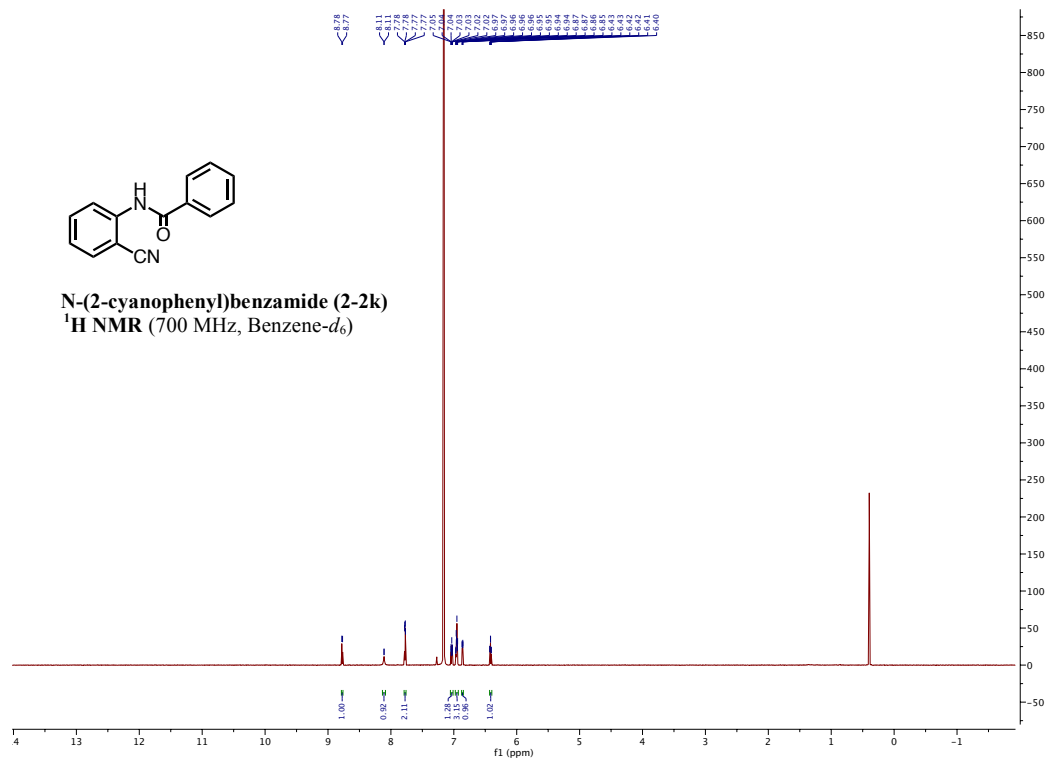


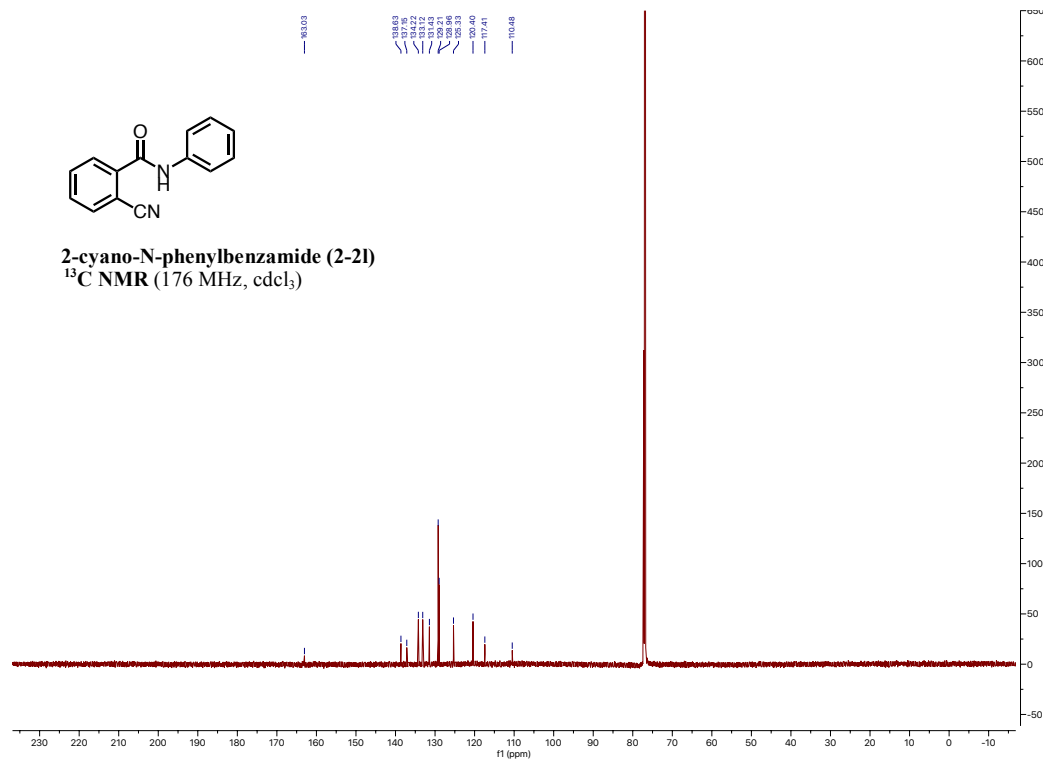
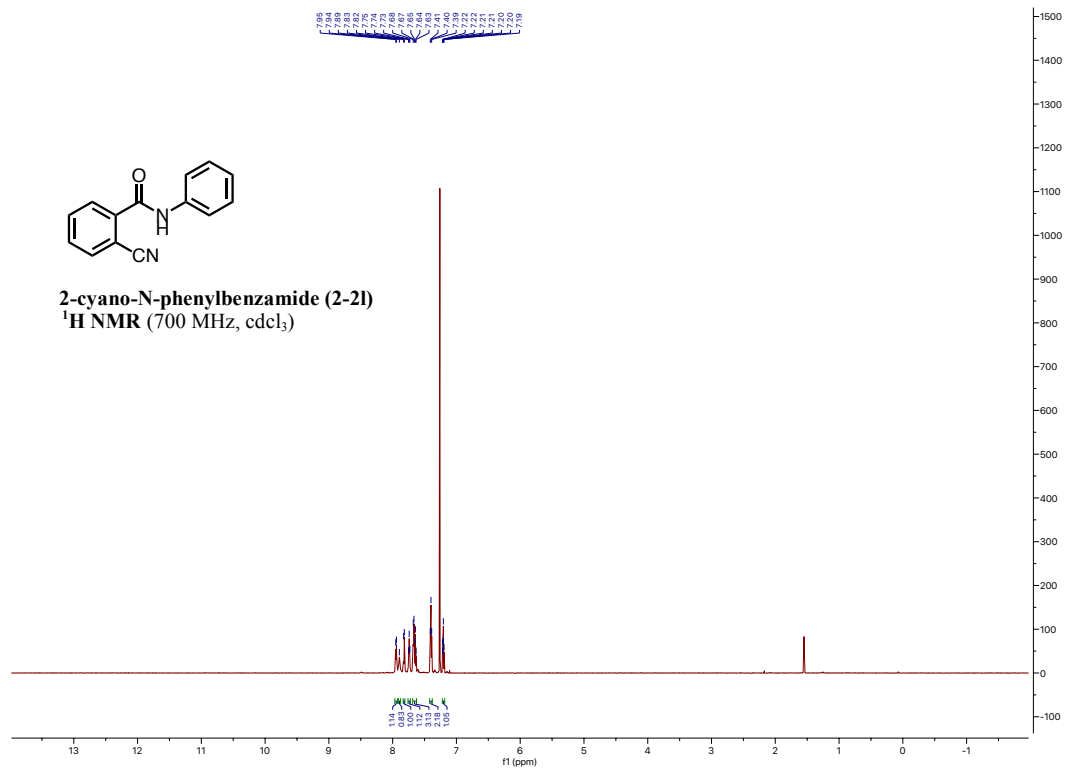


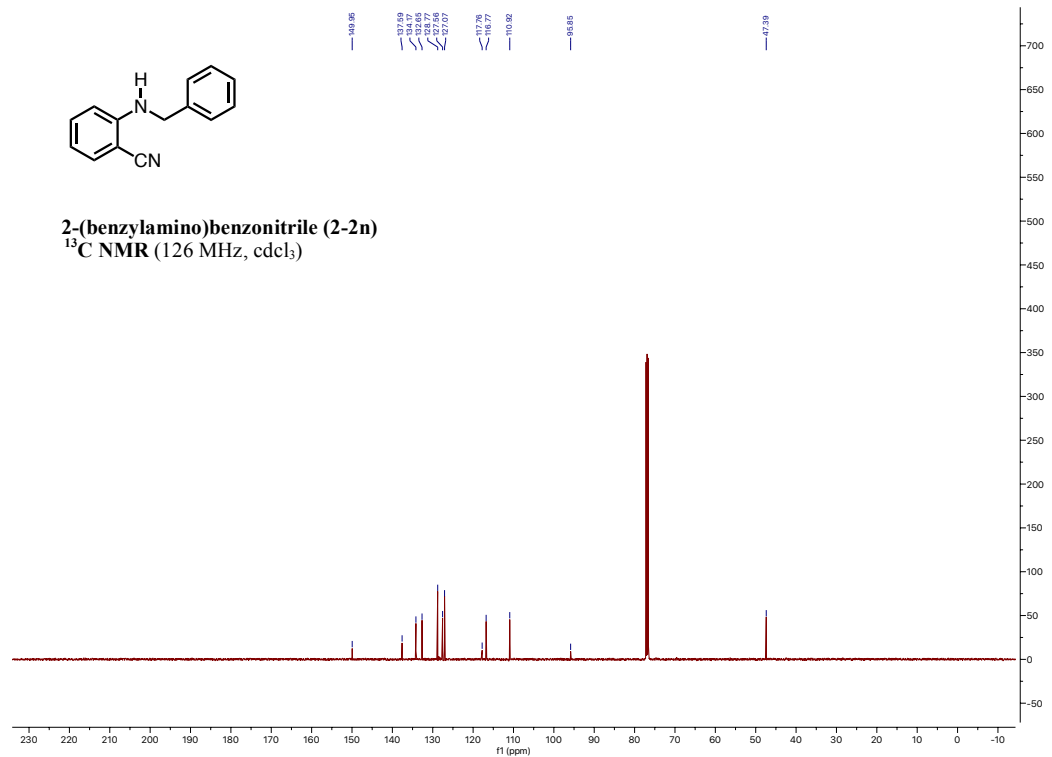
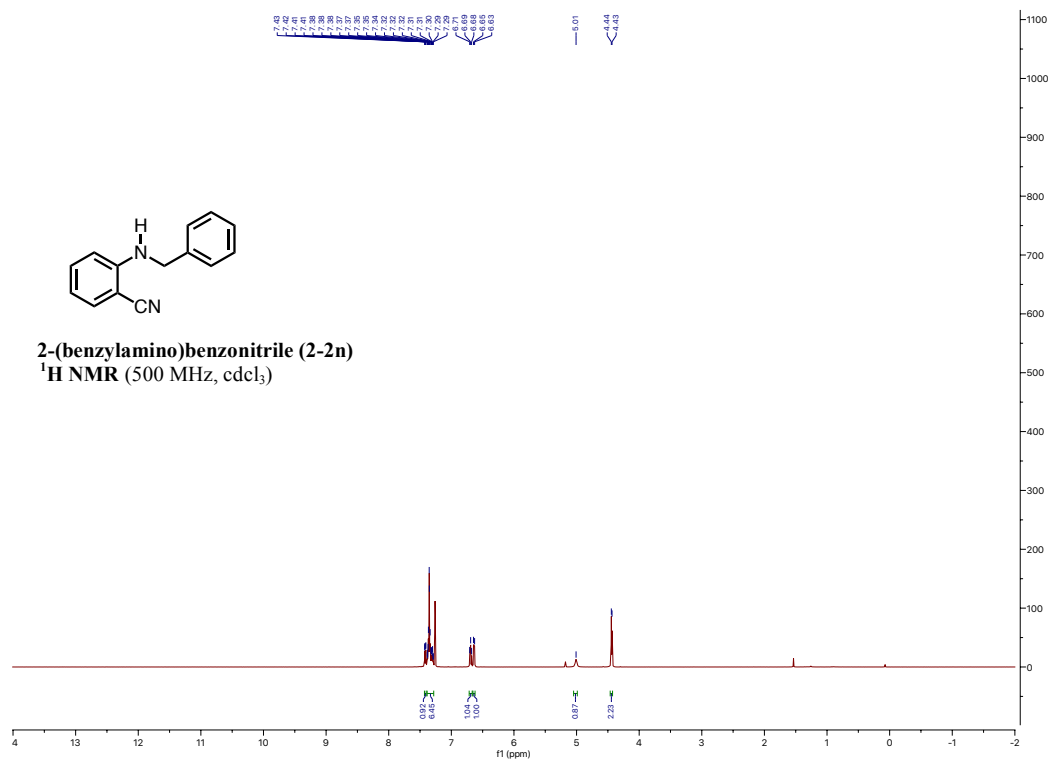
*Same as standard compound 2-5

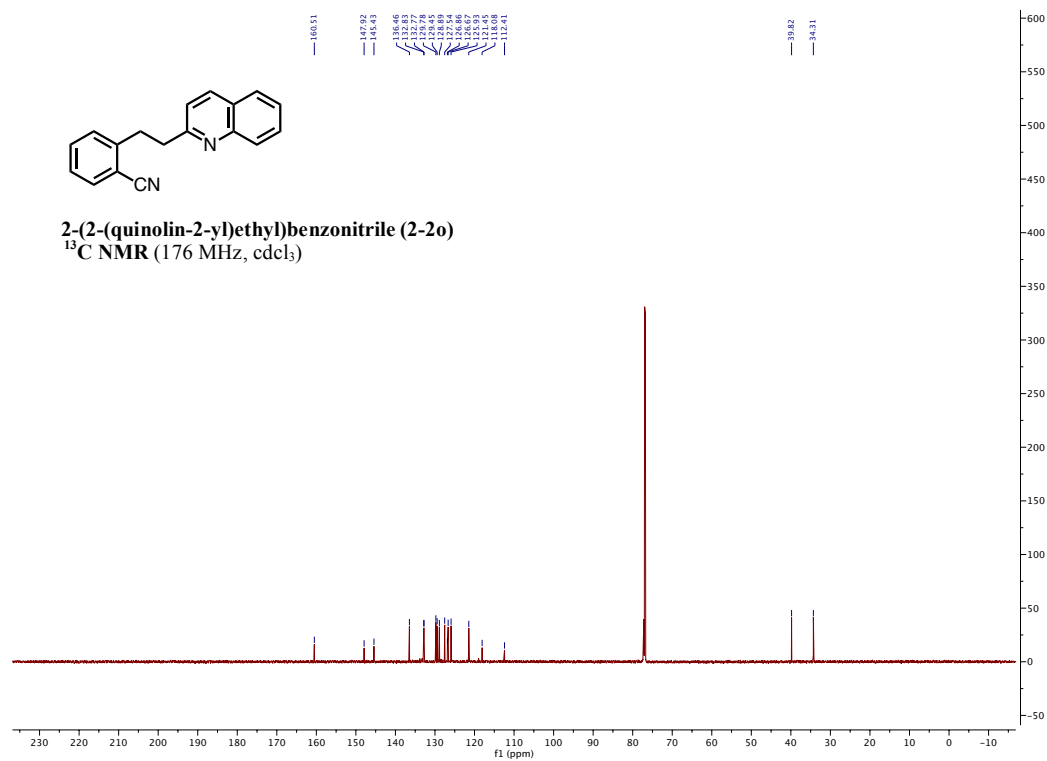
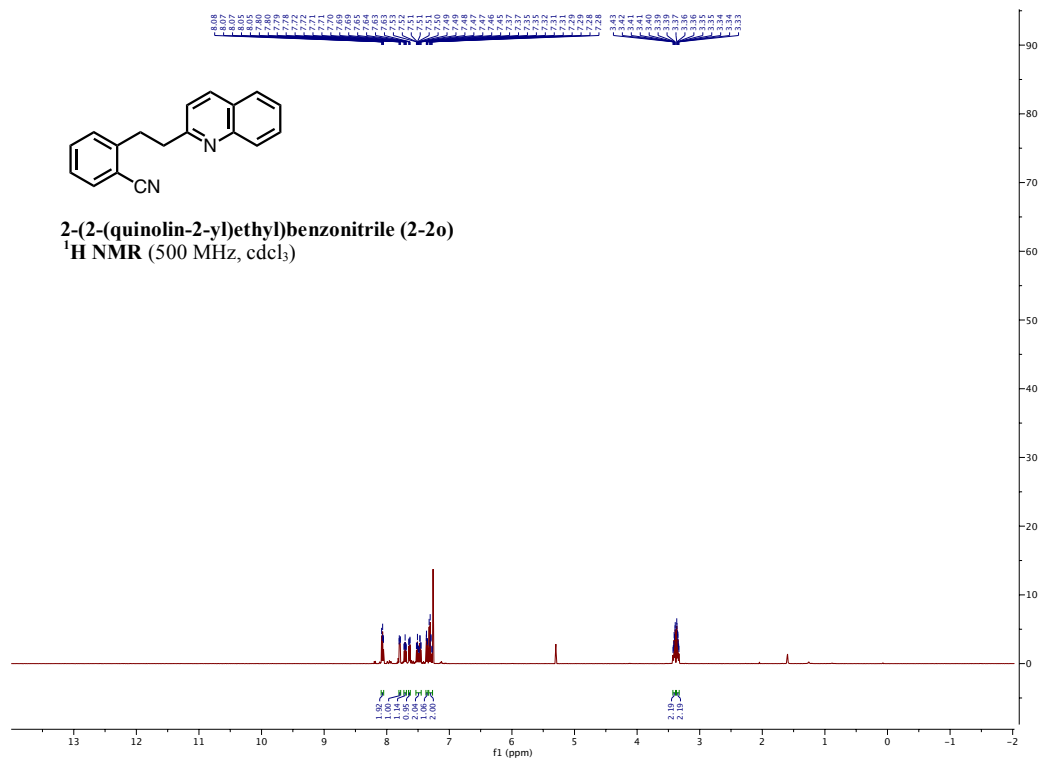


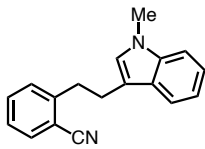




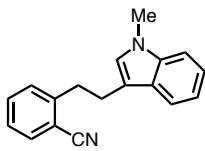
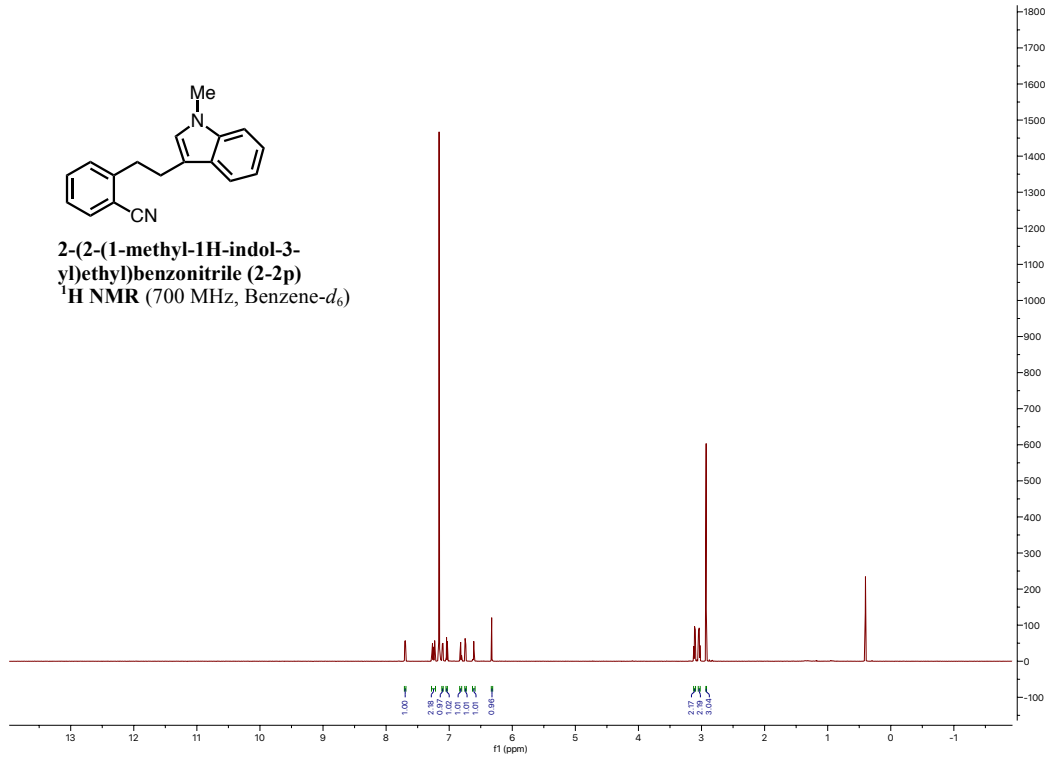




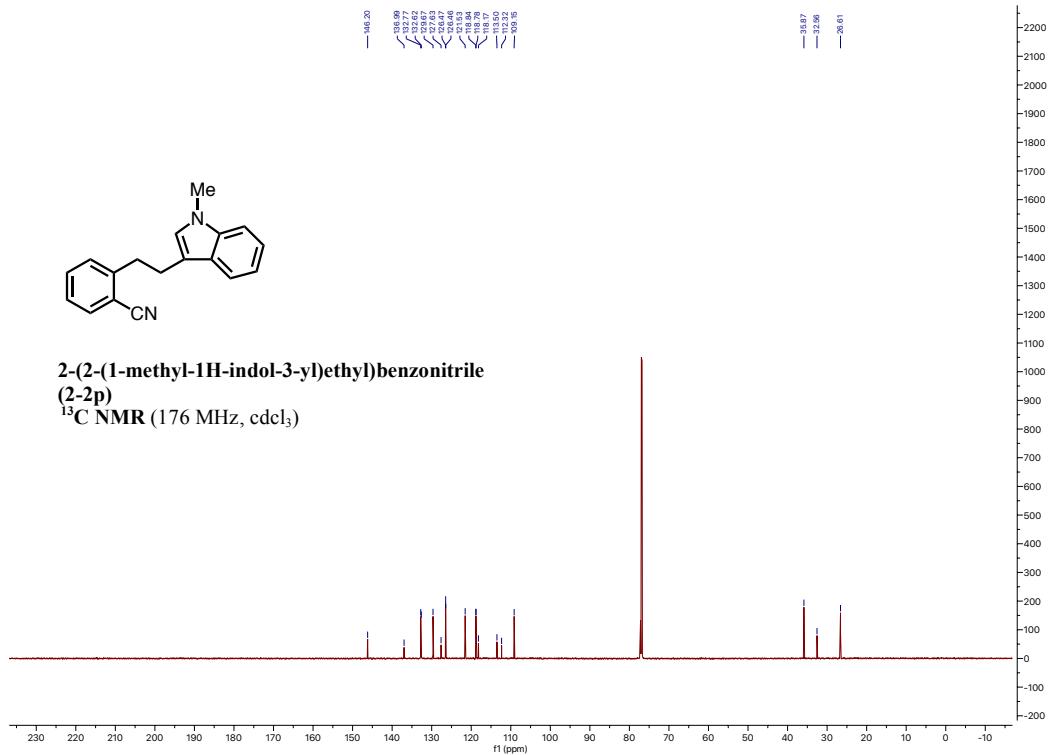


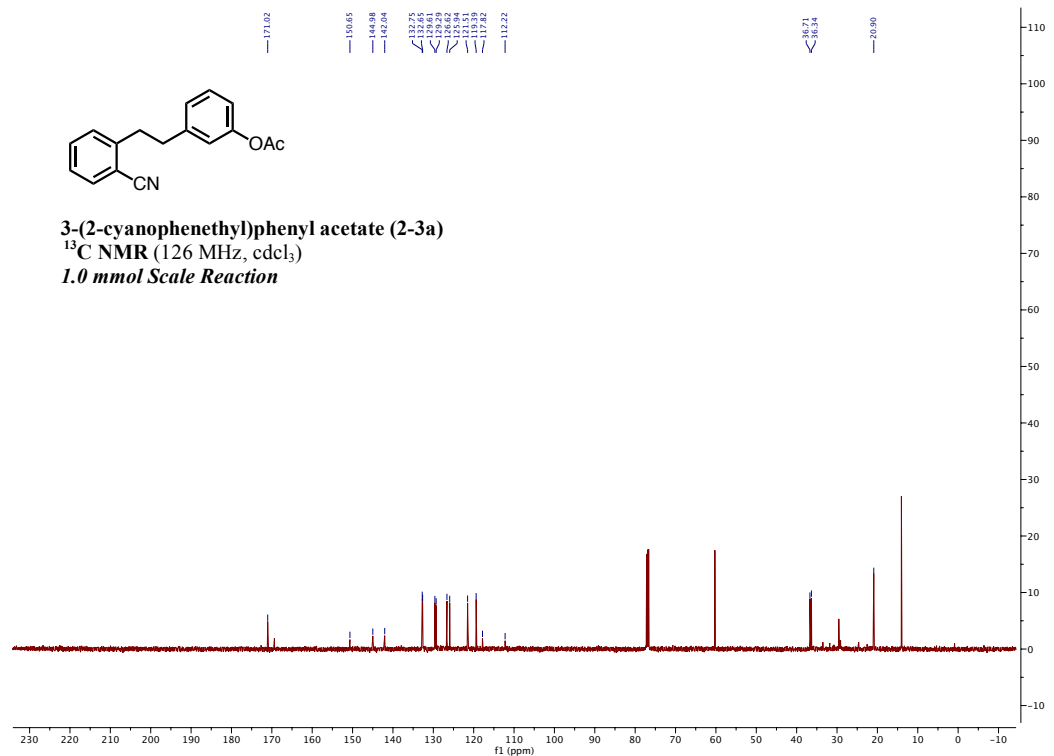
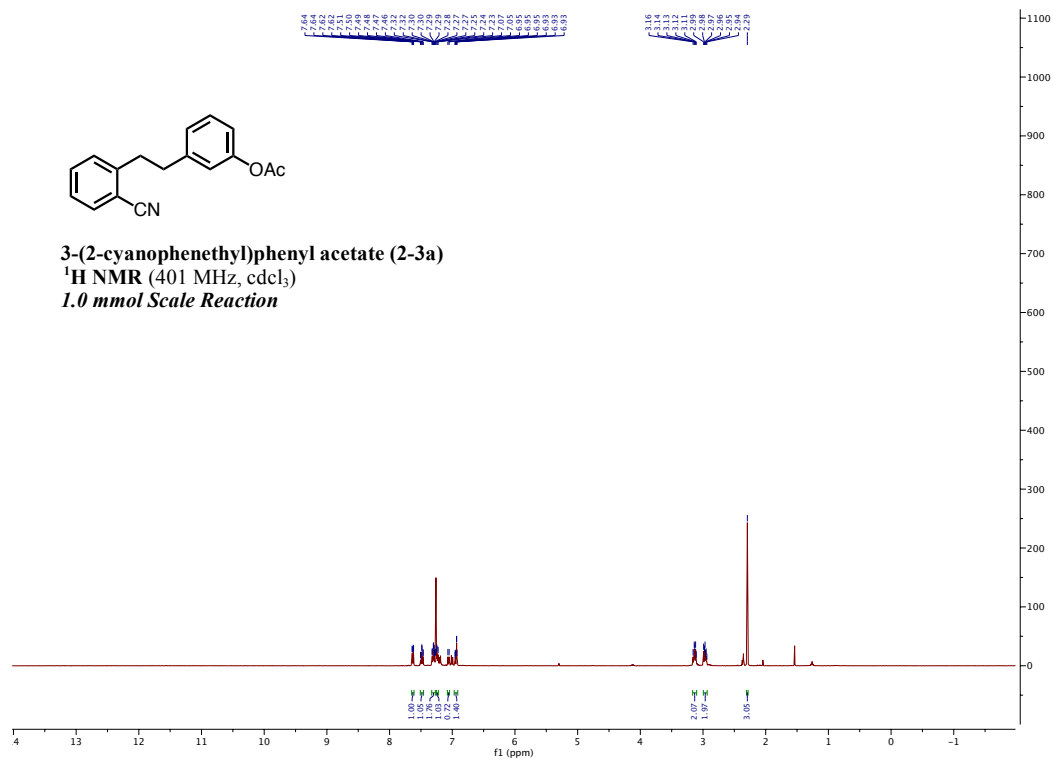


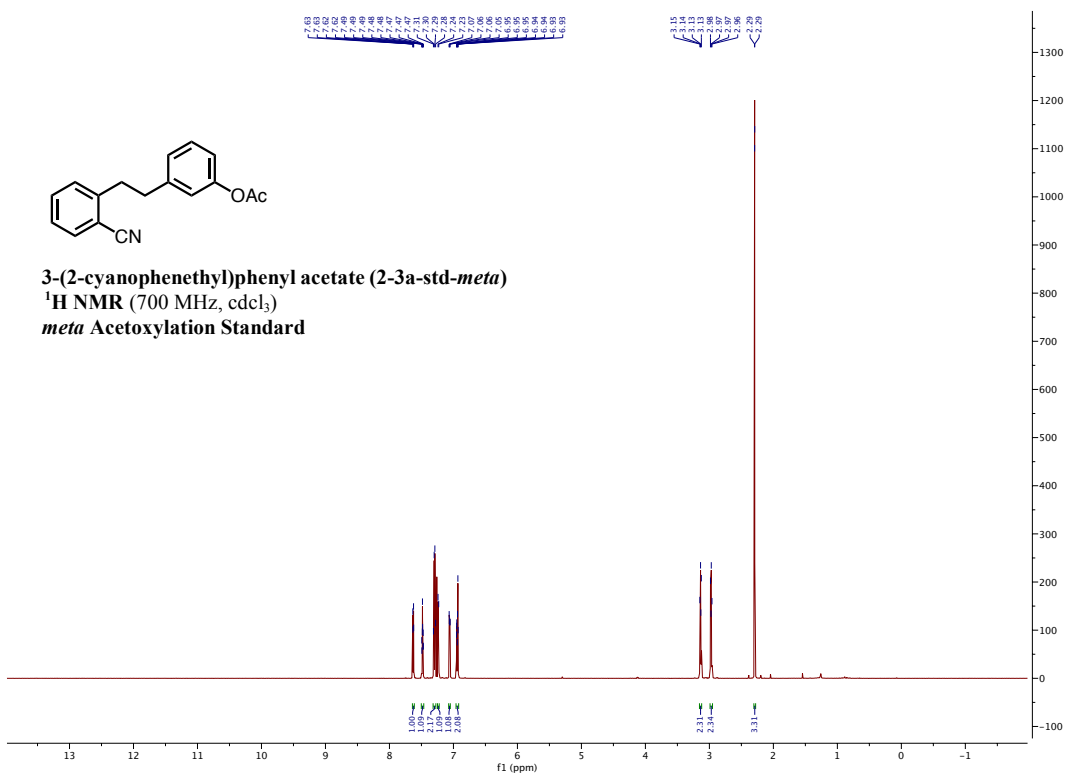
2-(2-(1-methyl-1H-indol-3-yl)ethyl)benzonitrile (2-2p)
¹H NMR (700 MHz, Benzene-*d*₆)

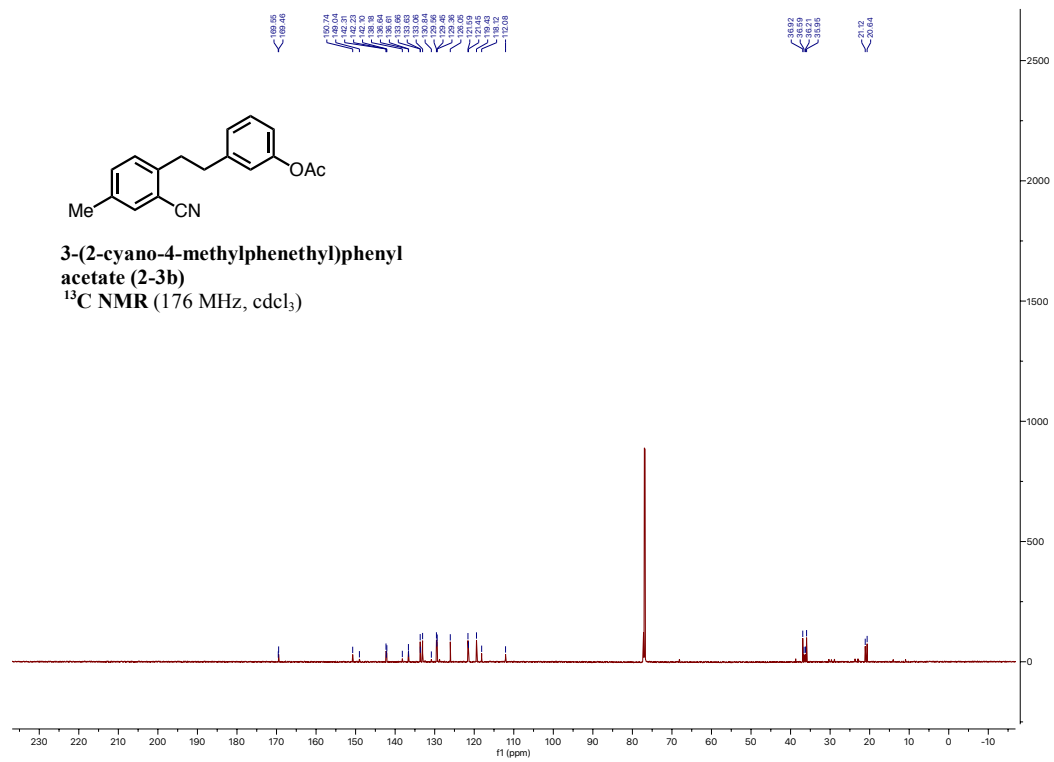
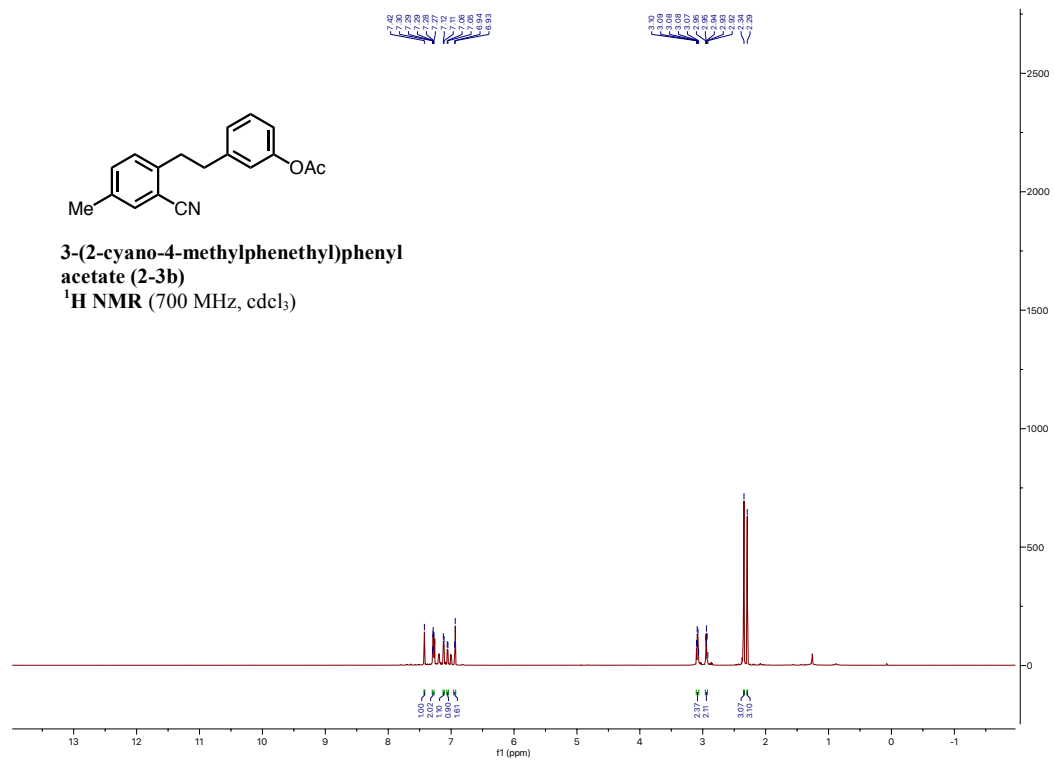


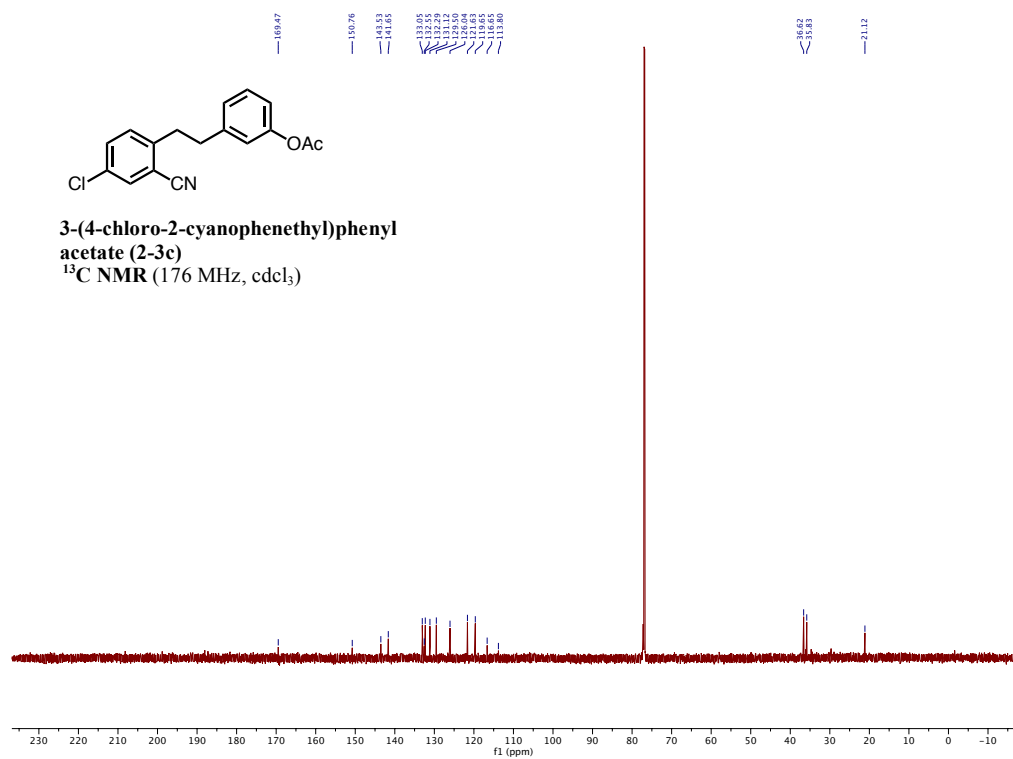
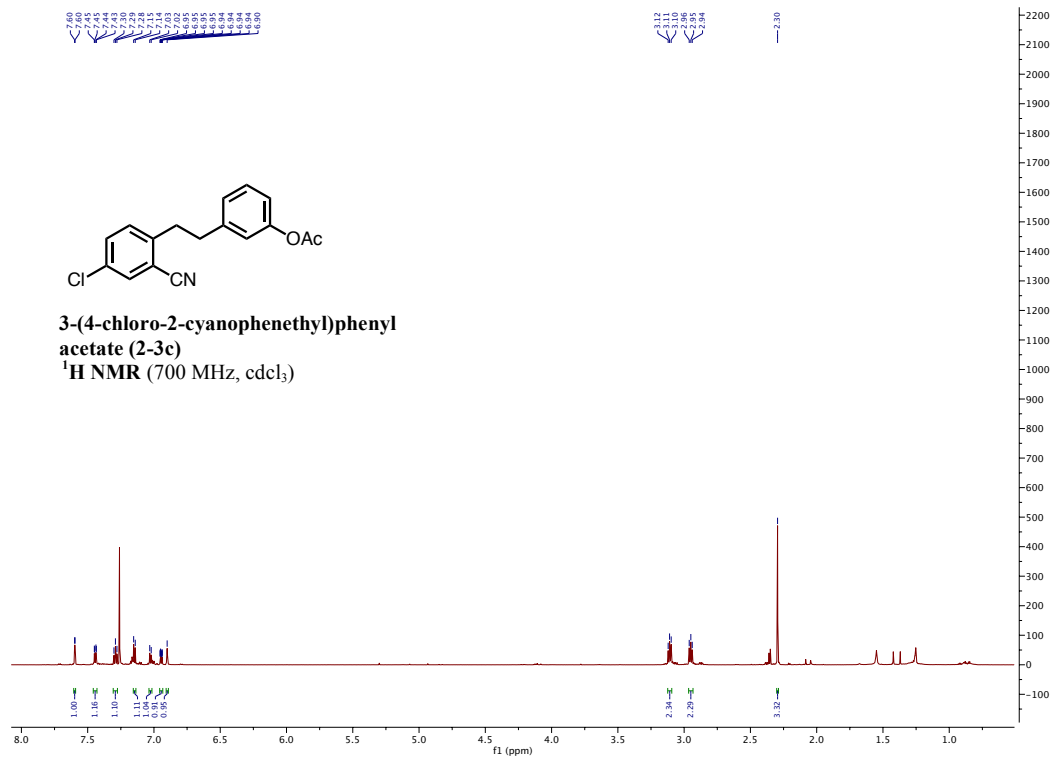
2-(2-(1-methyl-1H-indol-3-yl)ethyl)benzonitrile (2-2p)
¹³C NMR (176 MHz, cdcl₃)

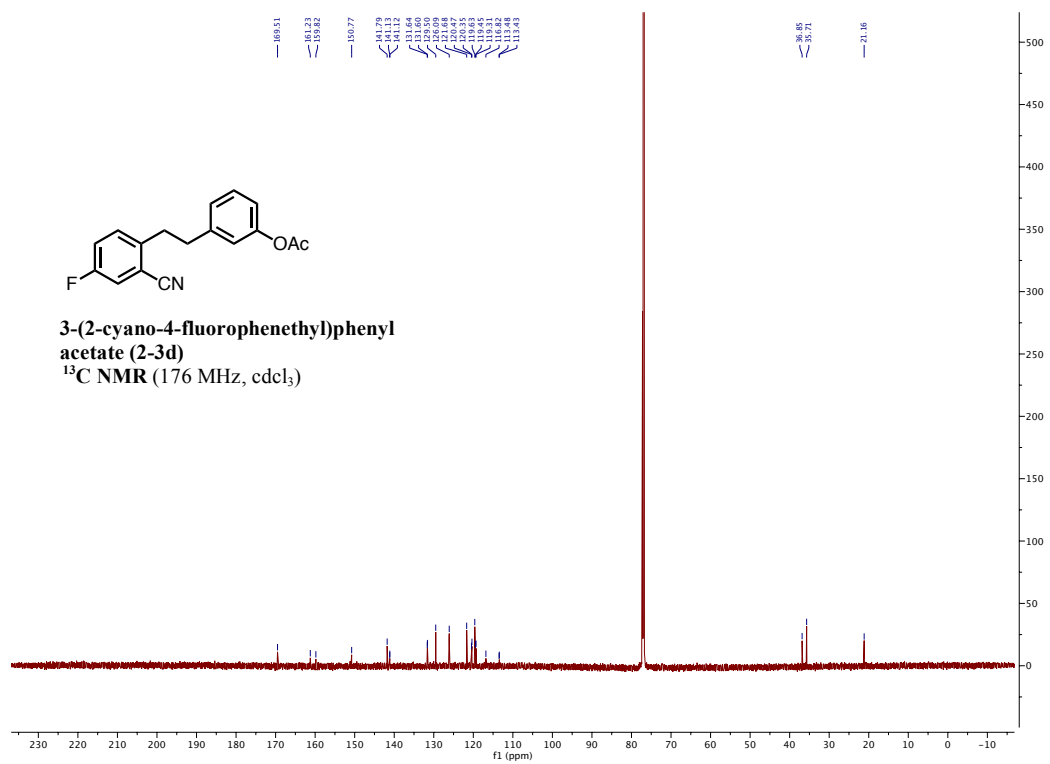
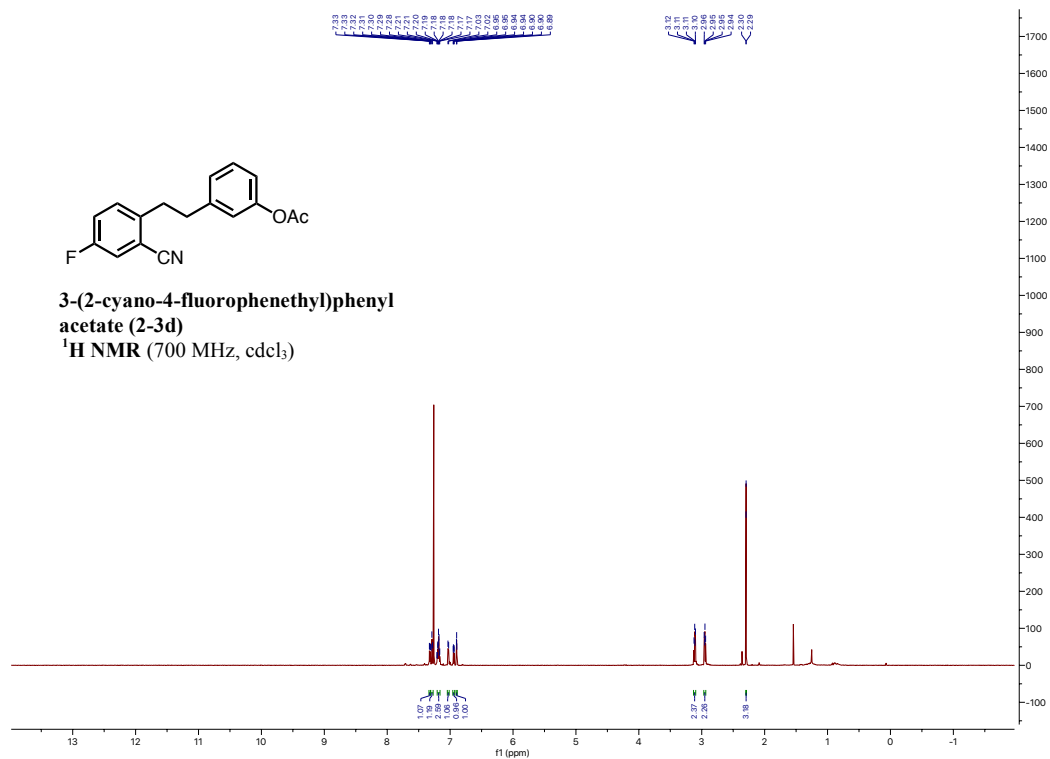


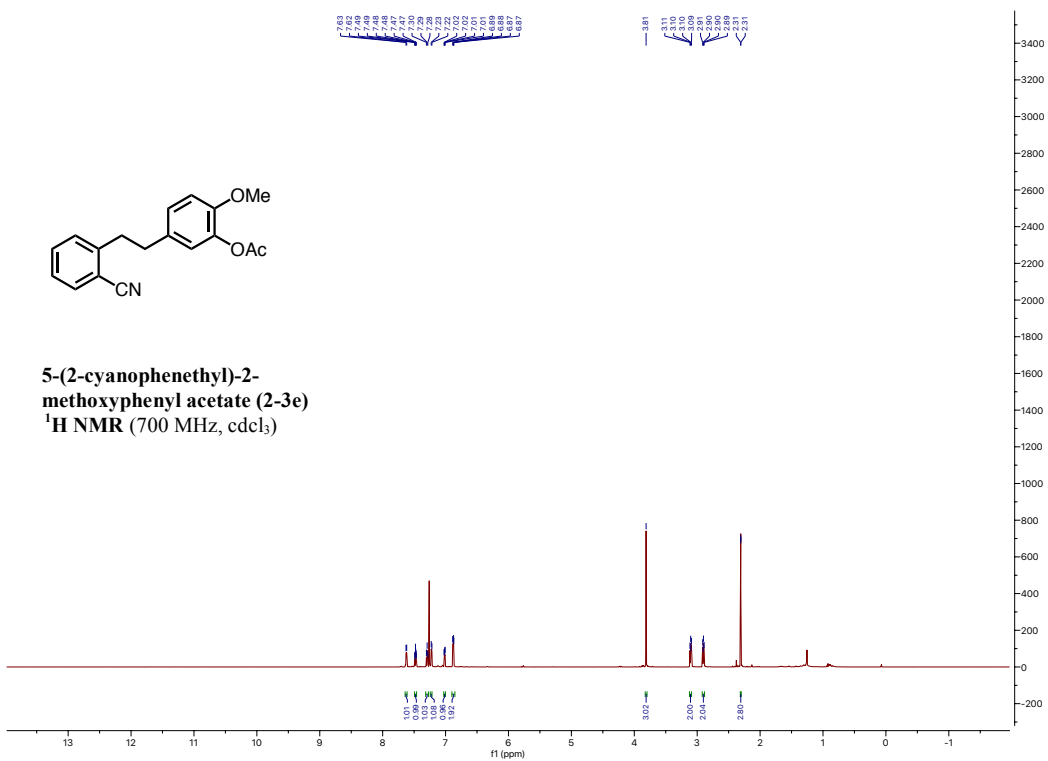


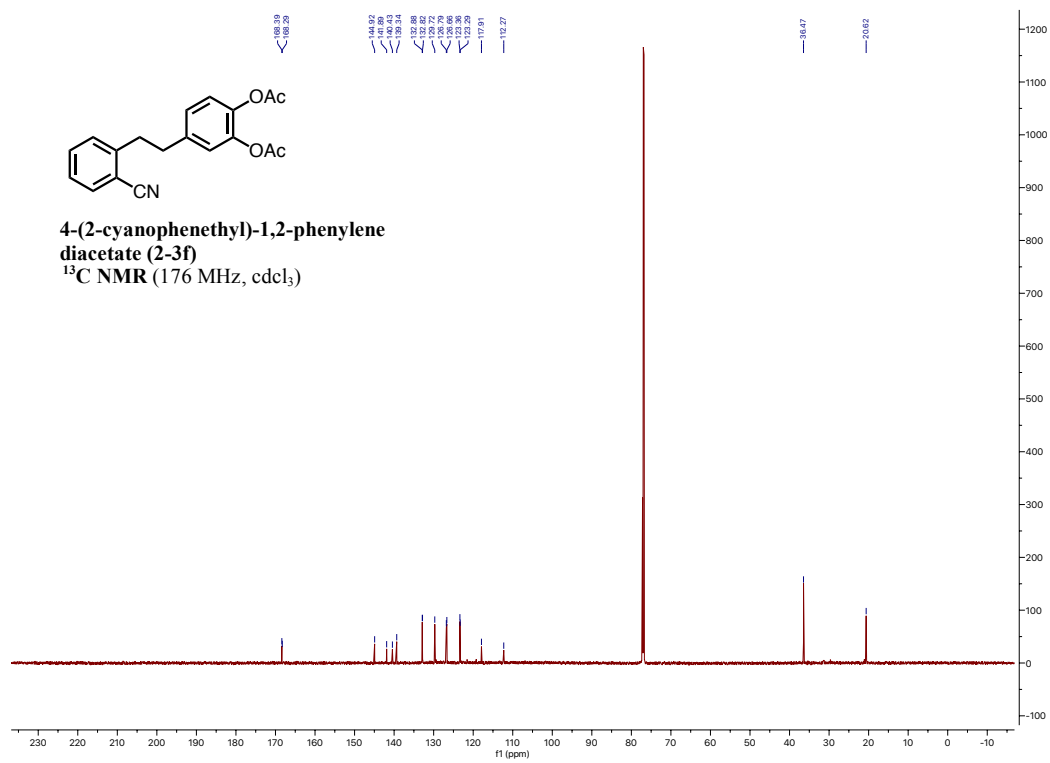
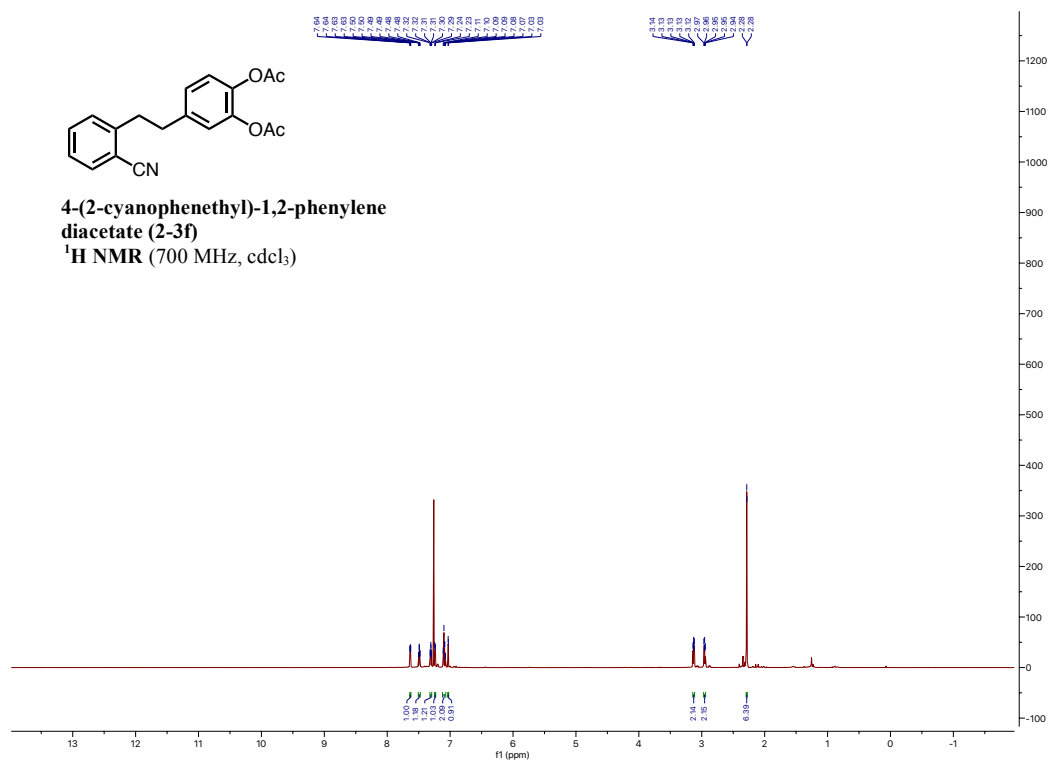


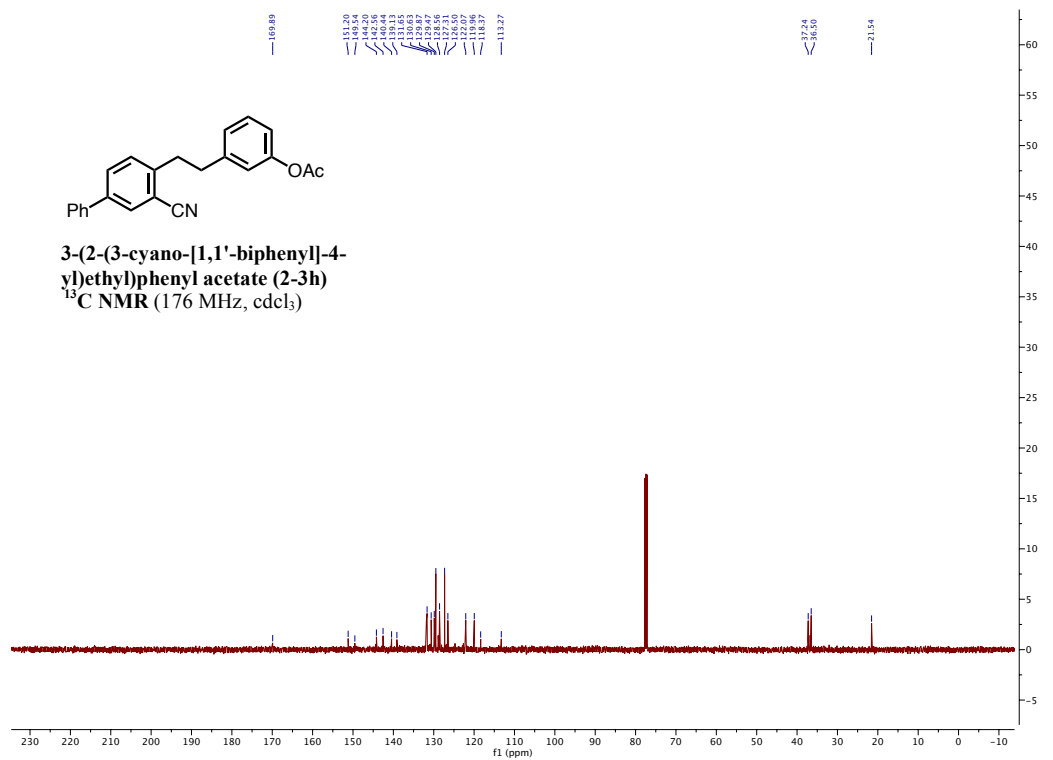
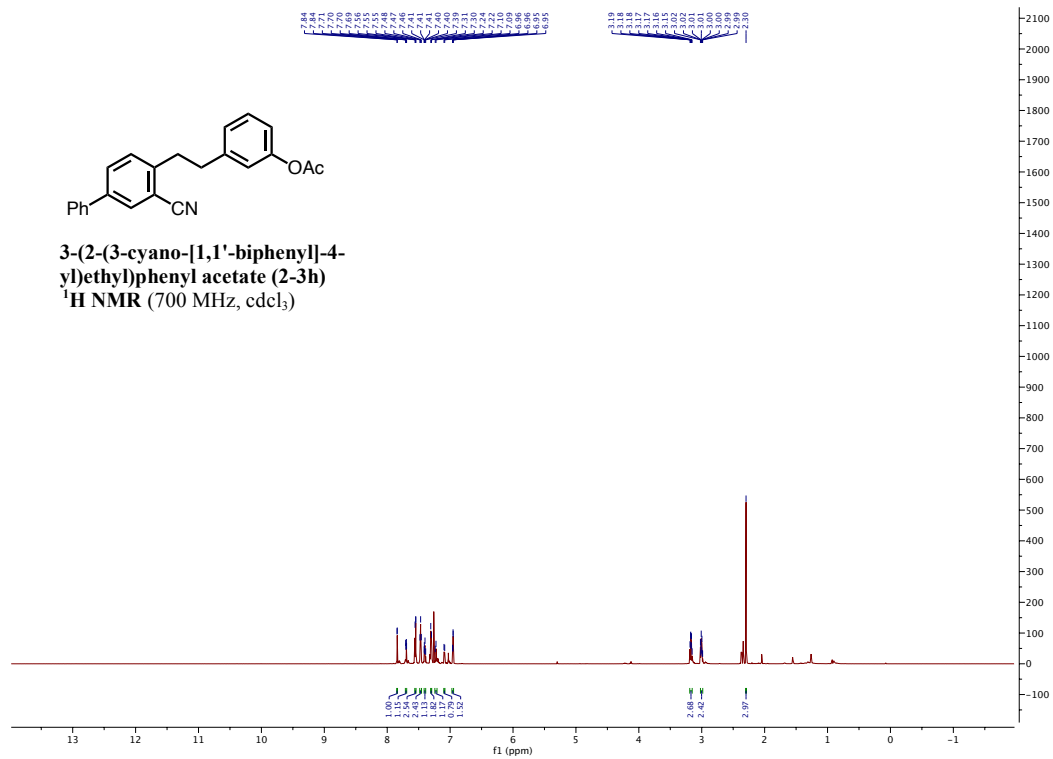


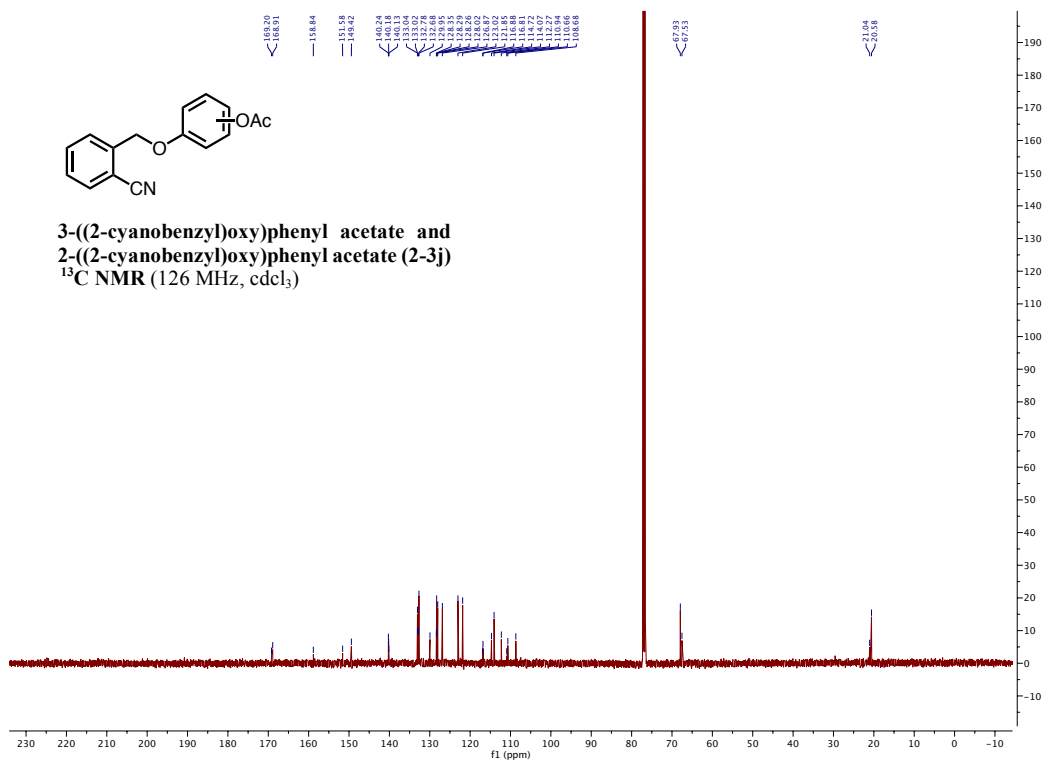
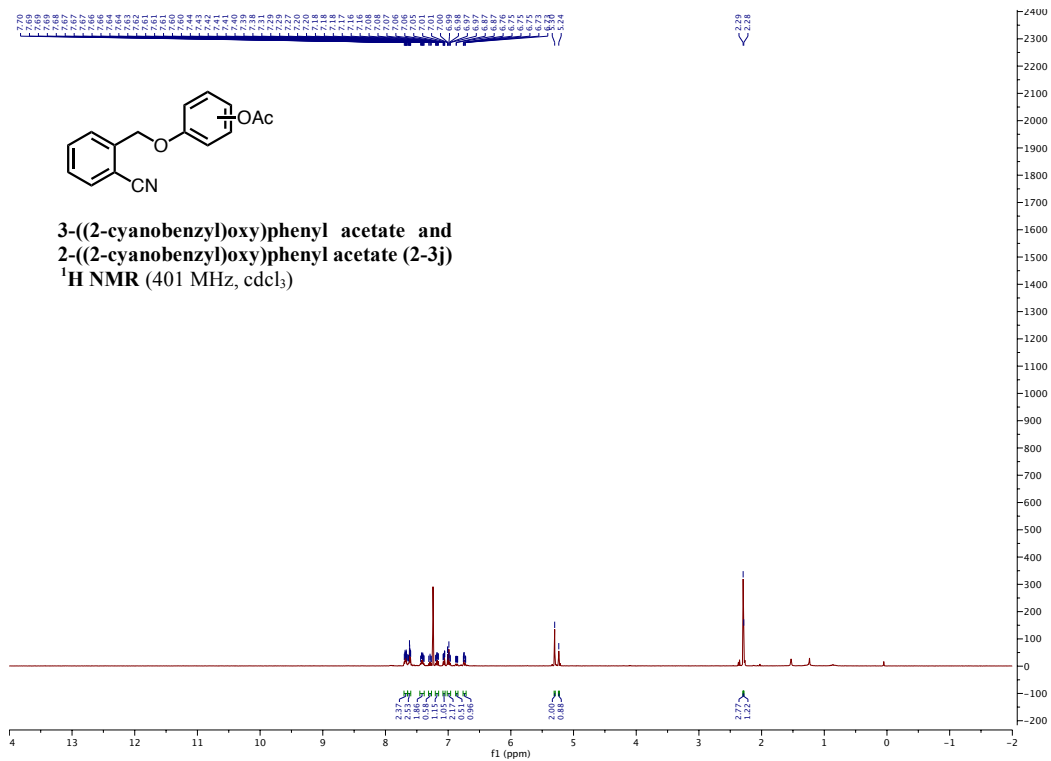


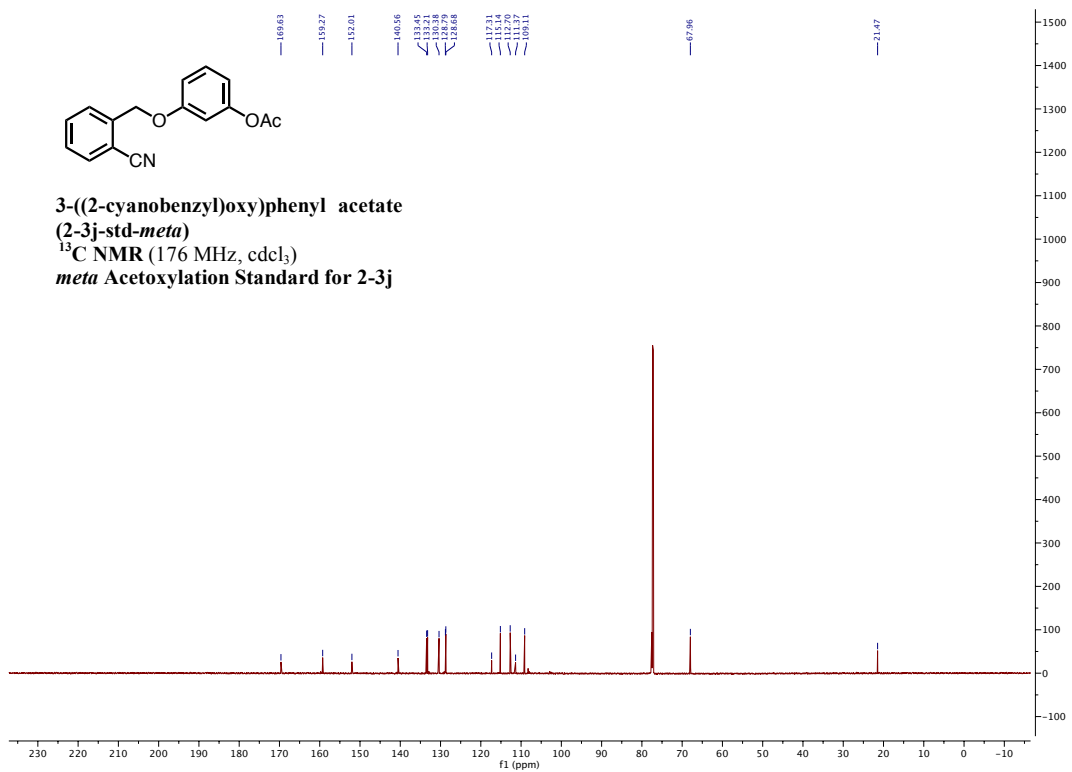
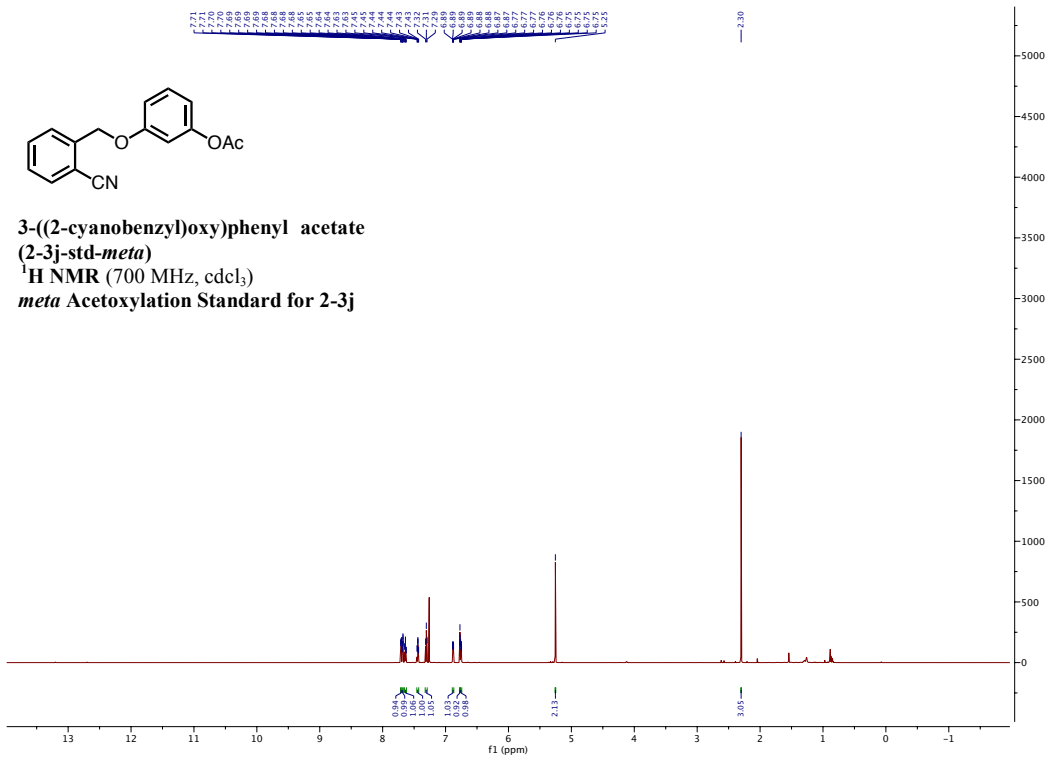


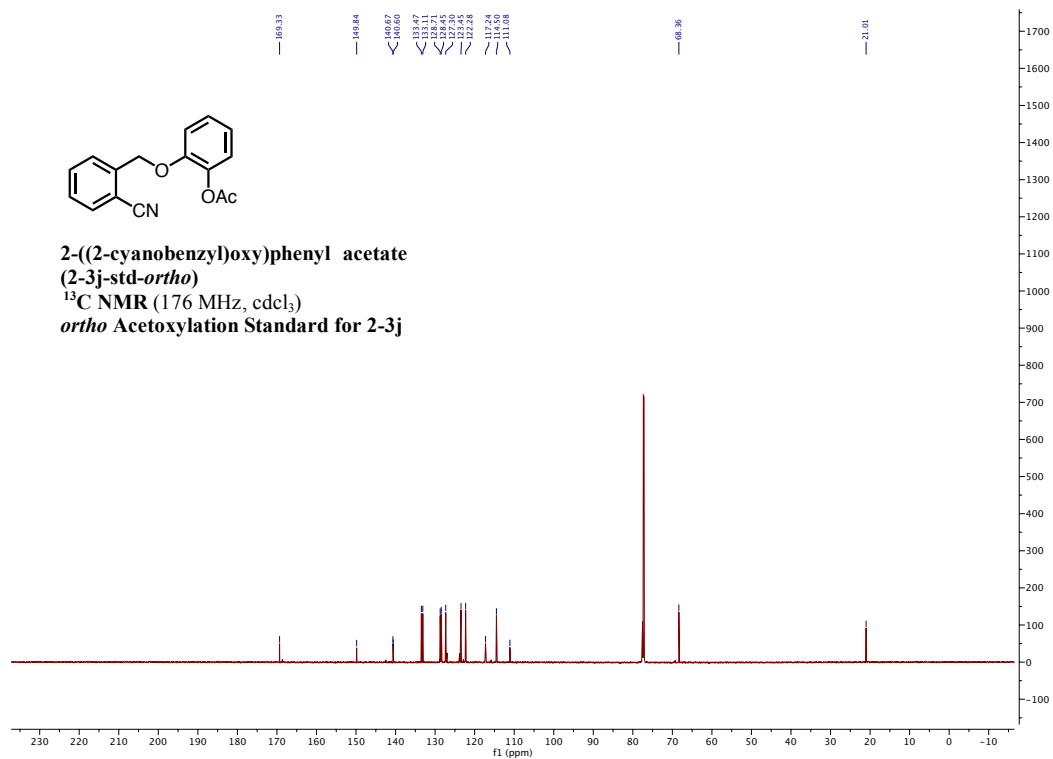
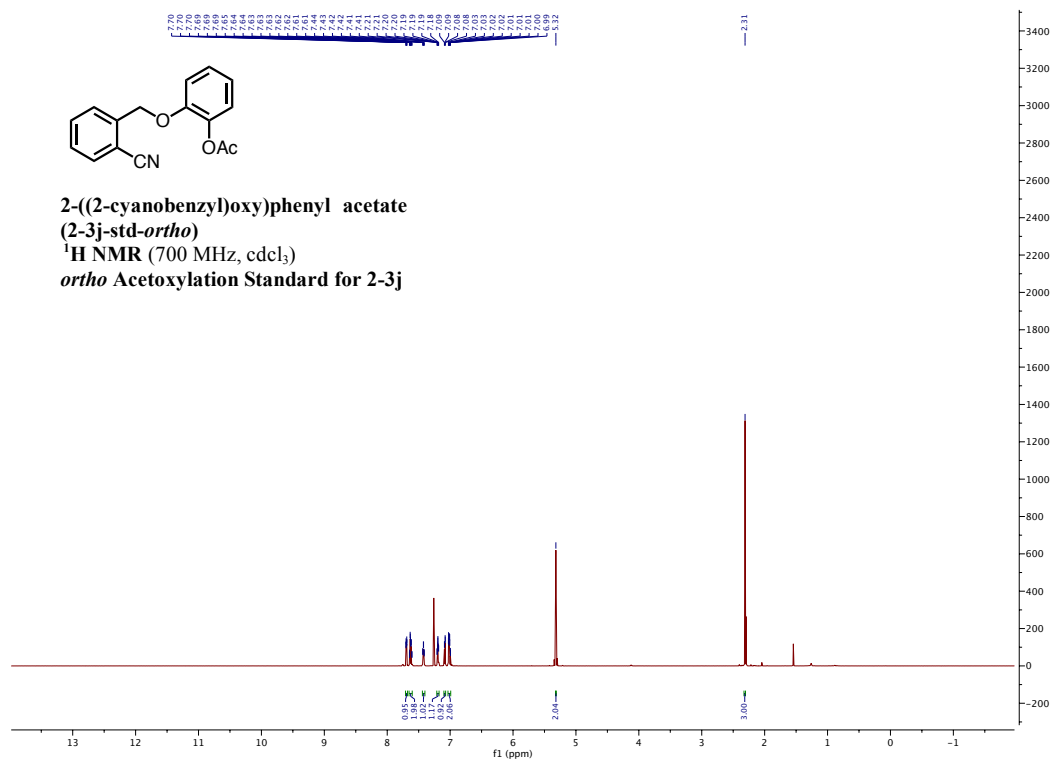


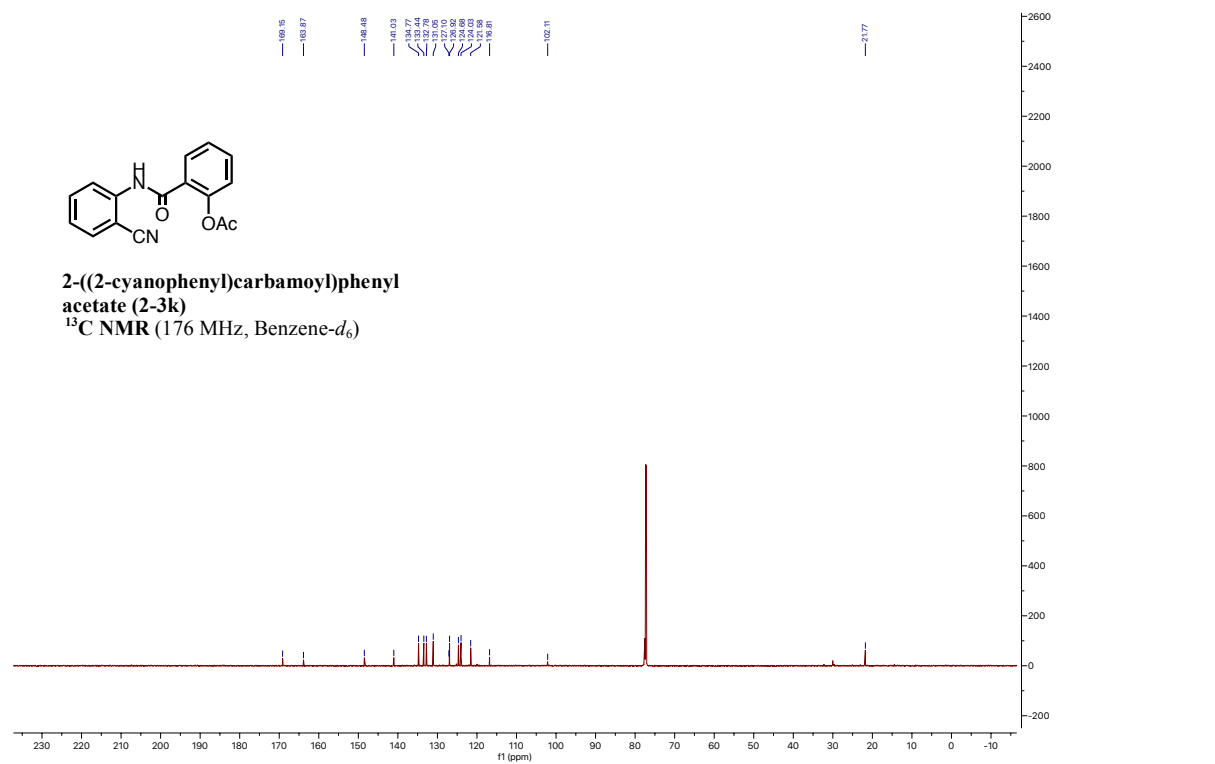
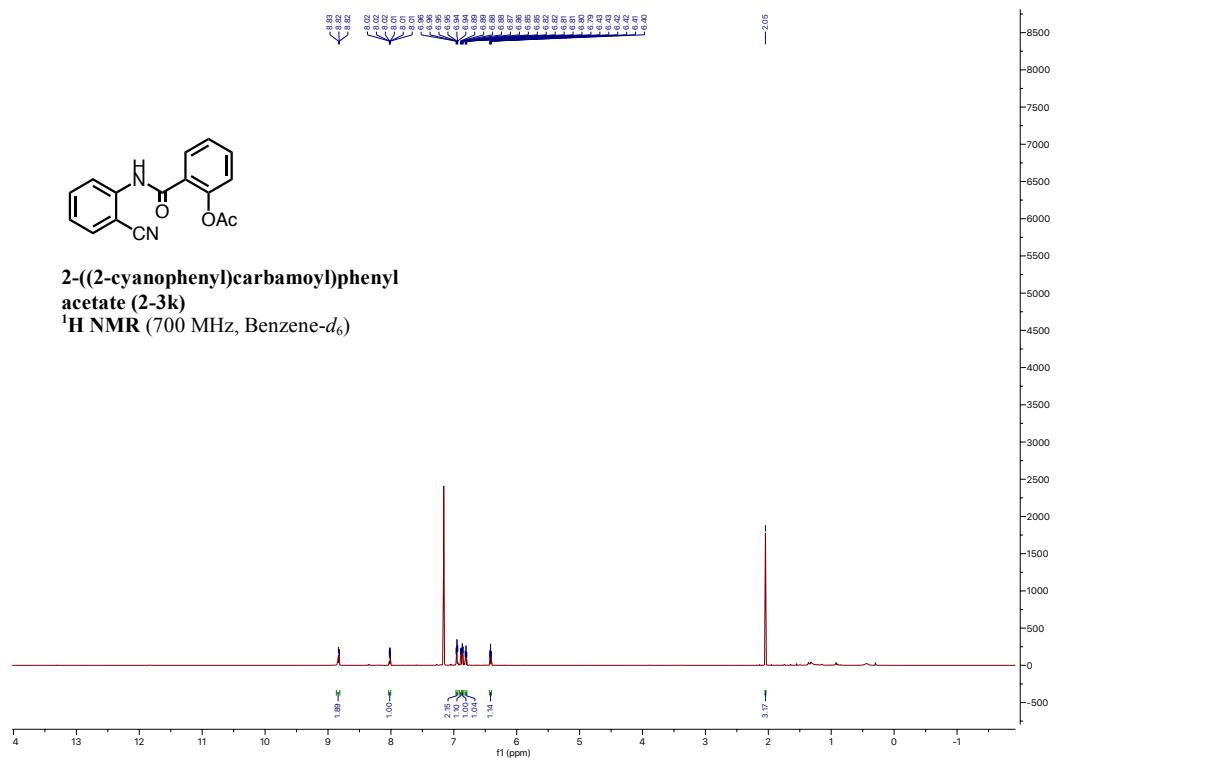


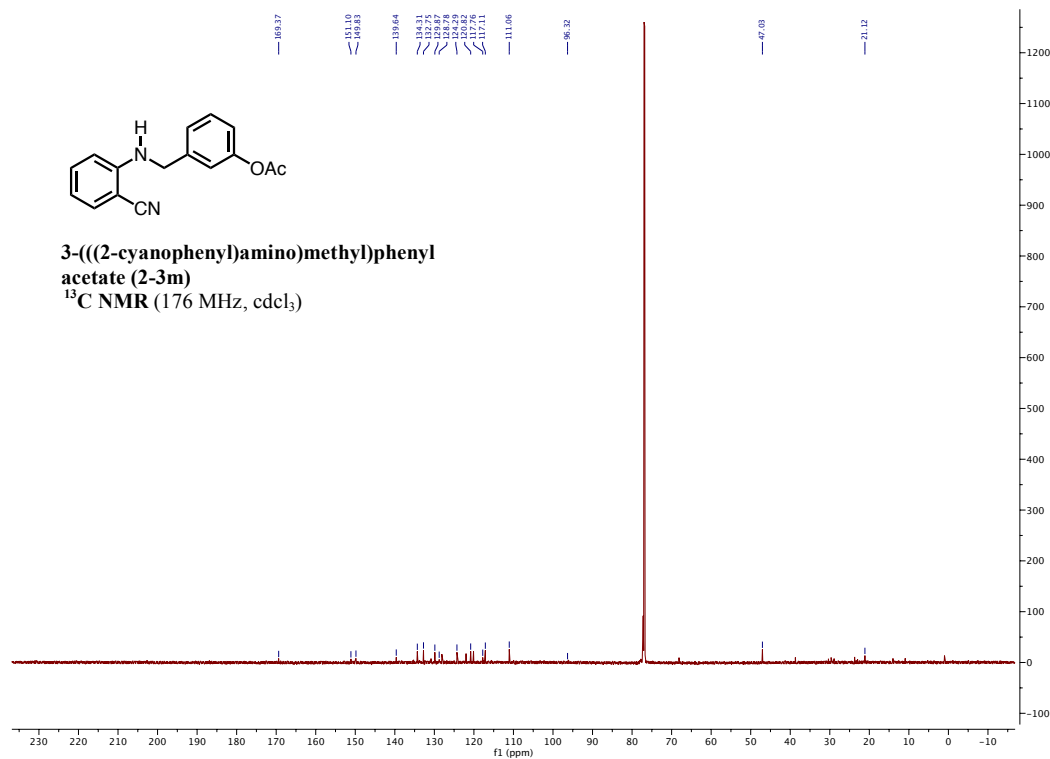
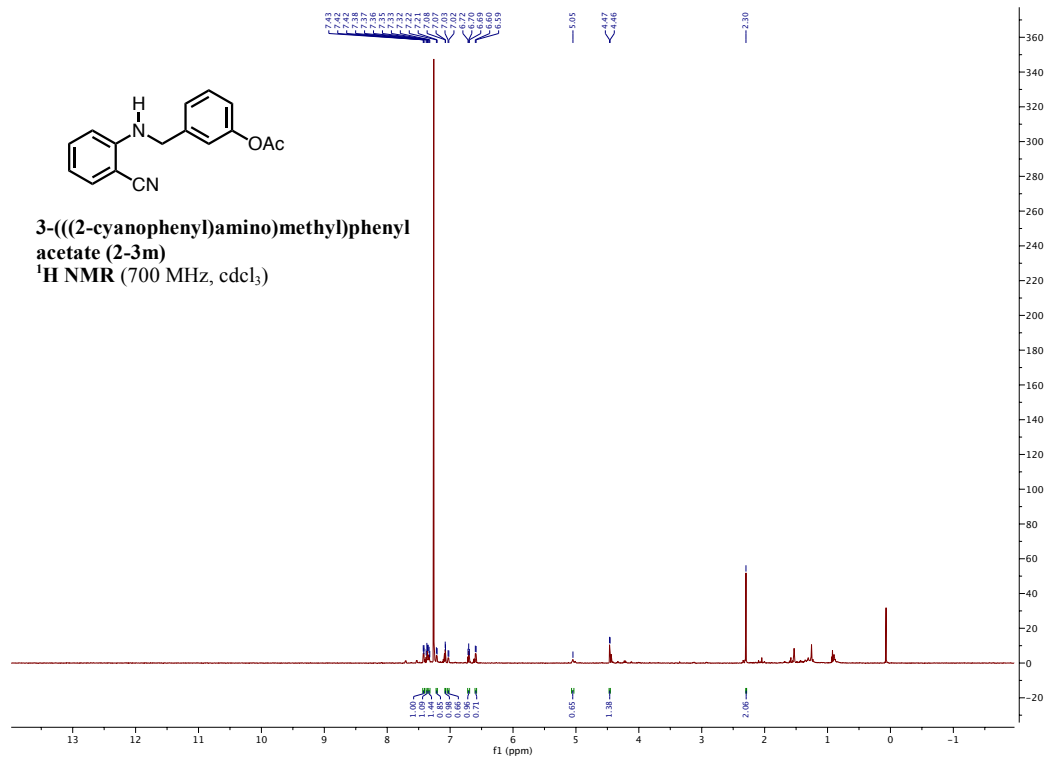


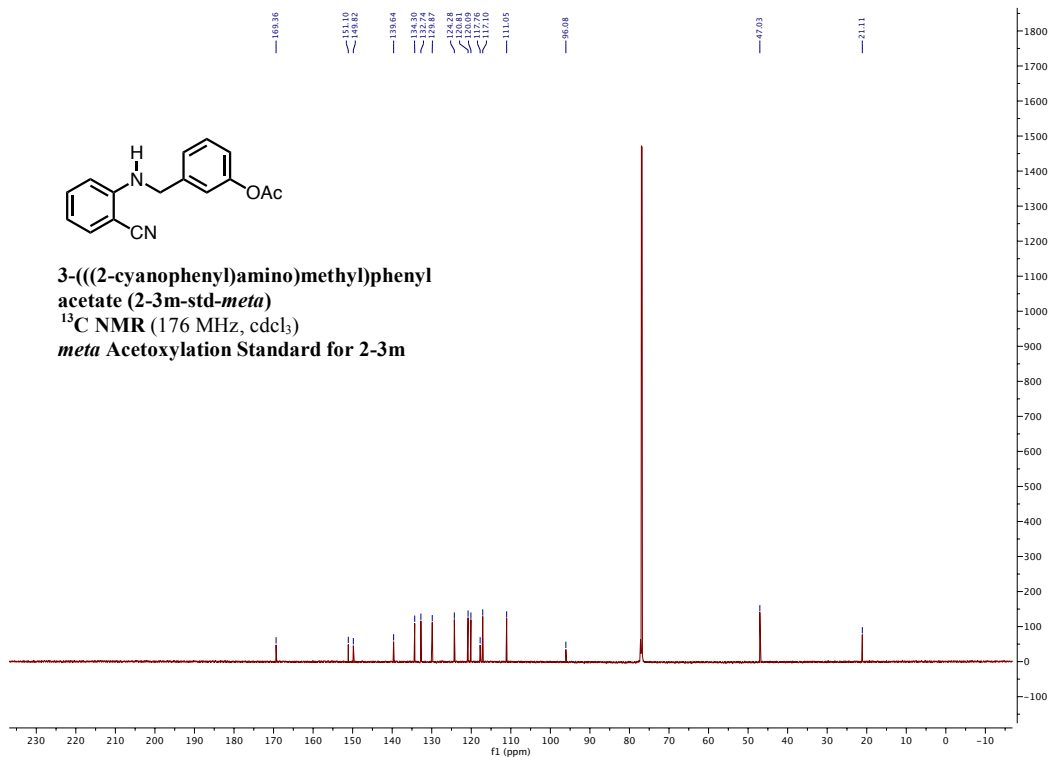
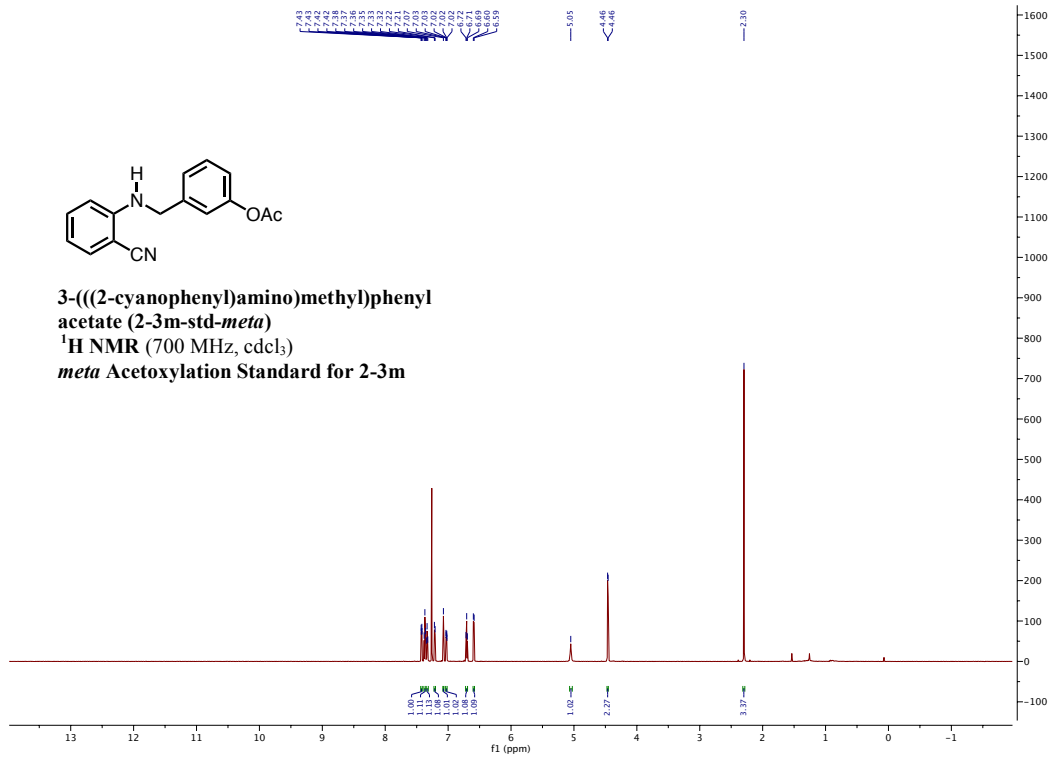


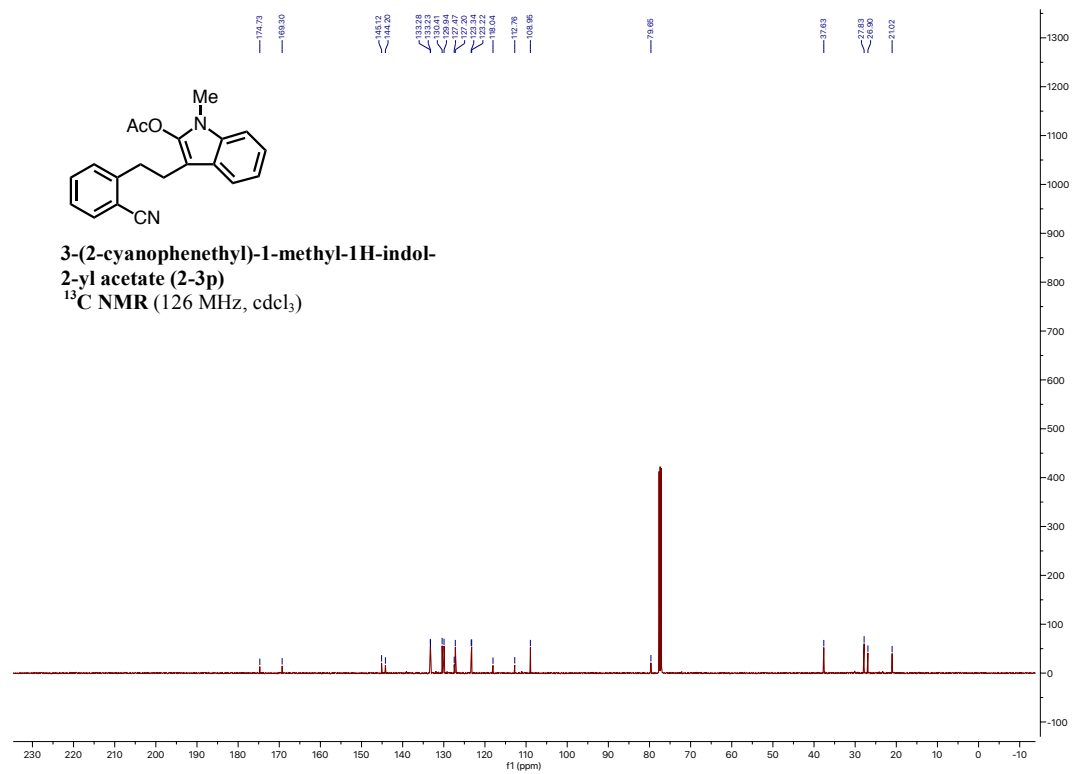
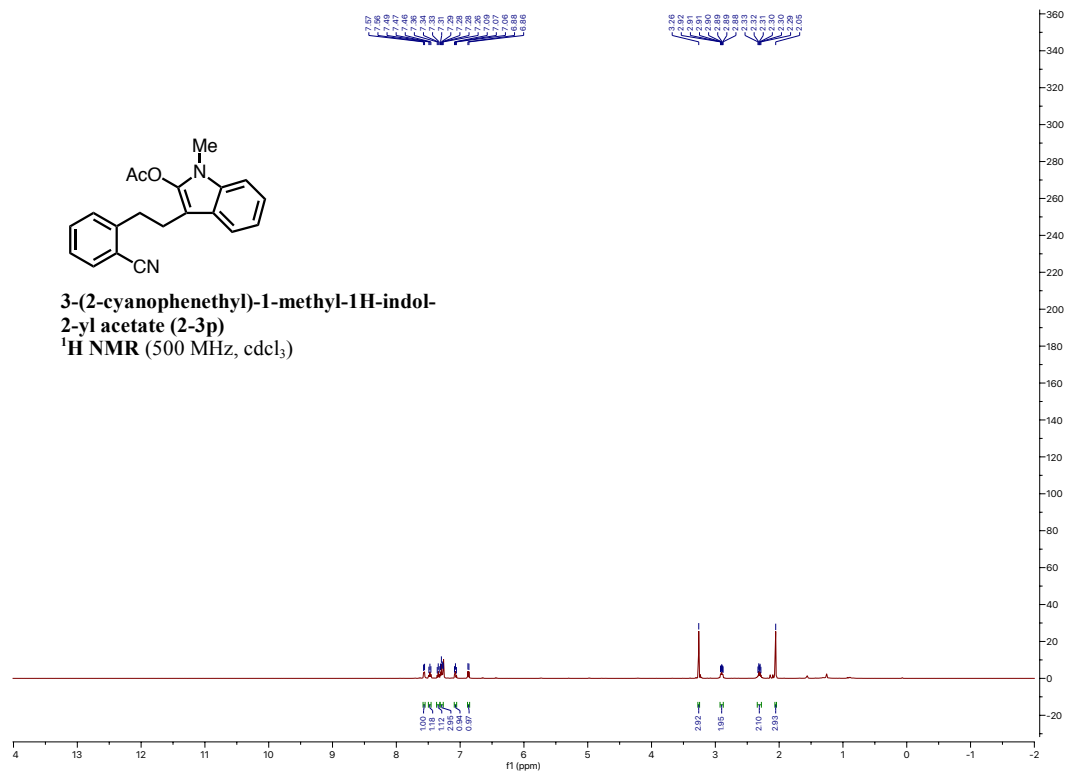


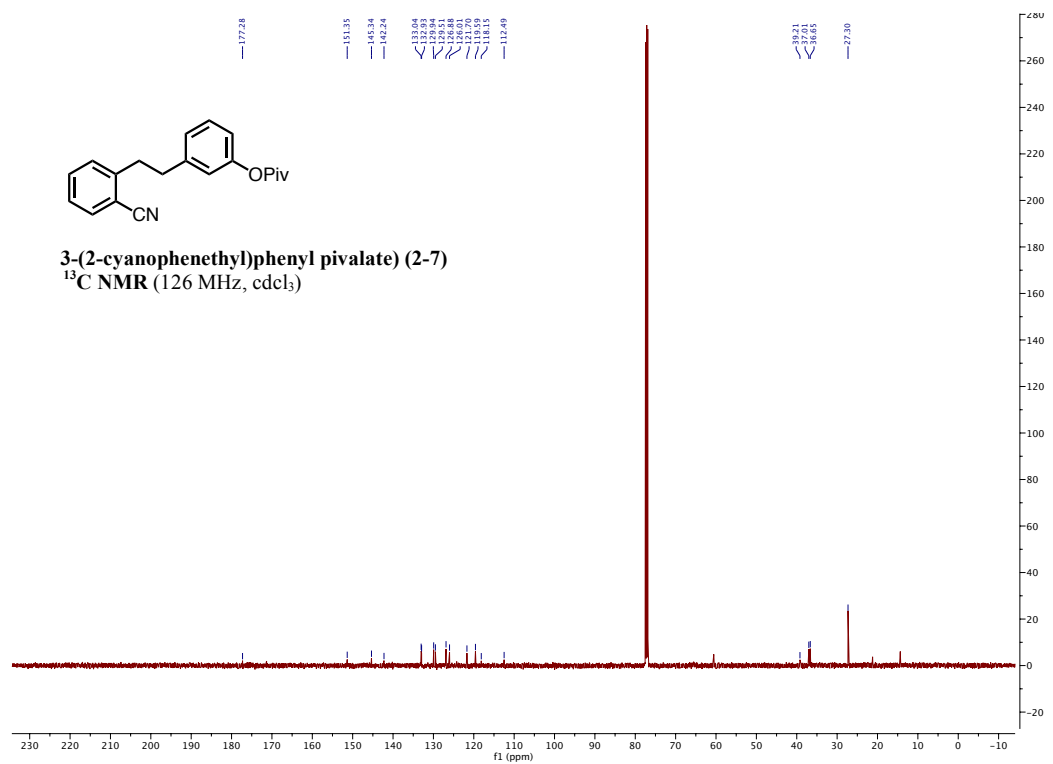
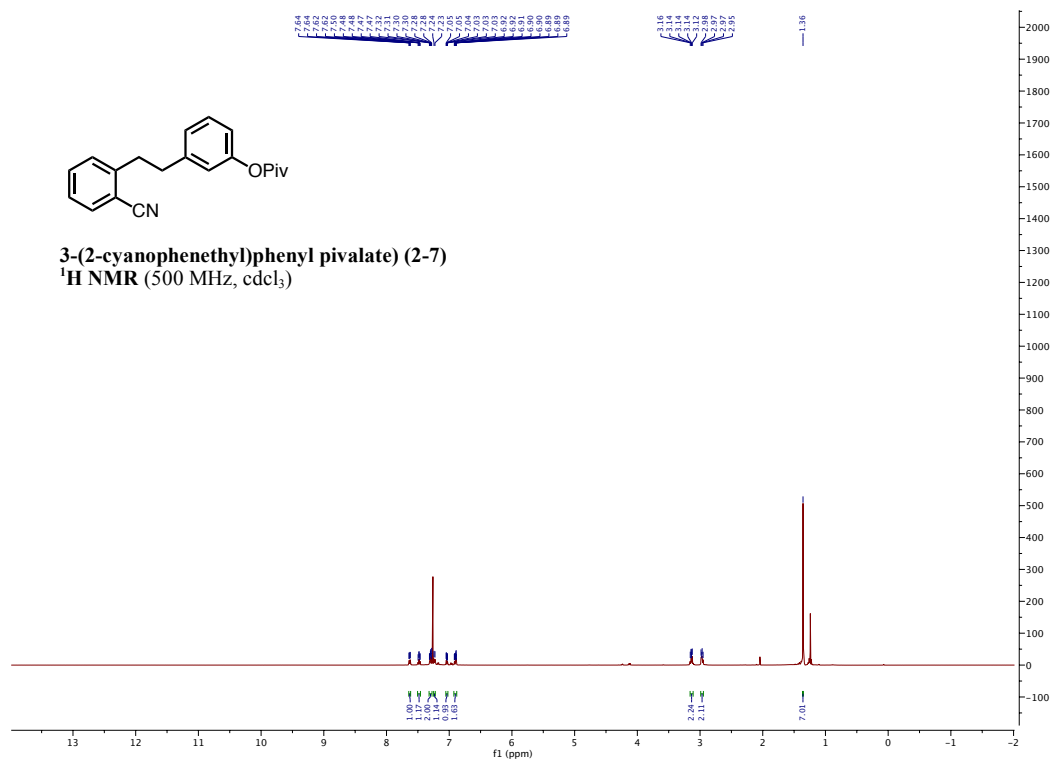


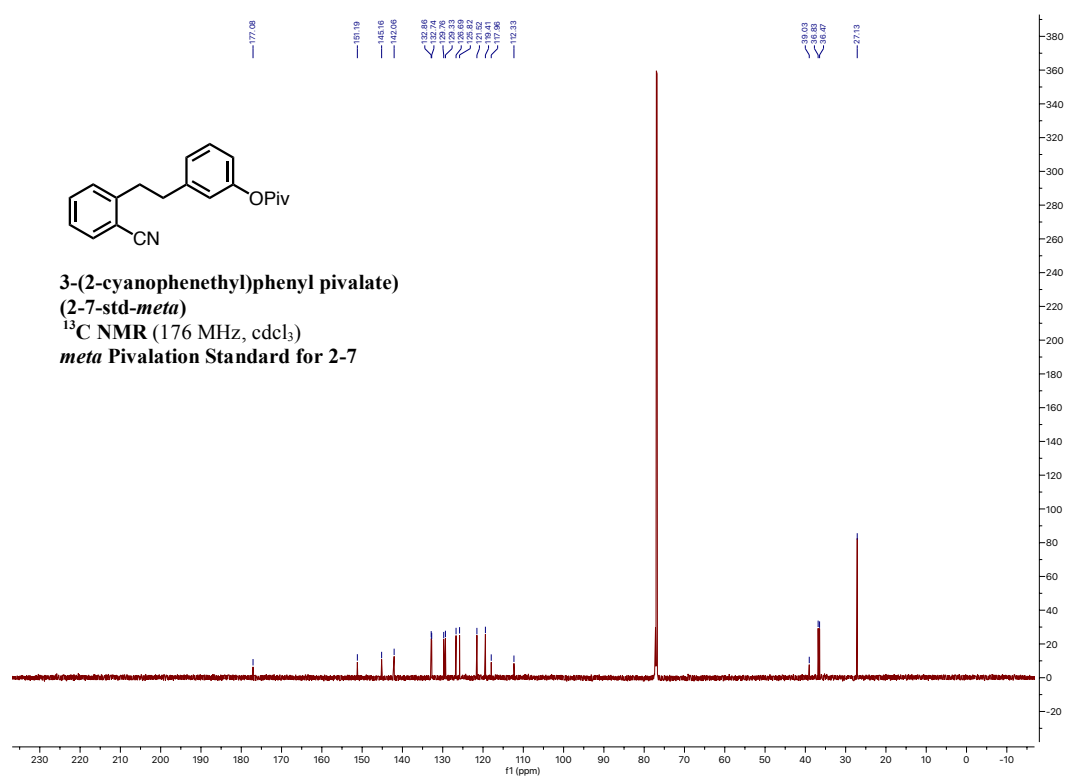
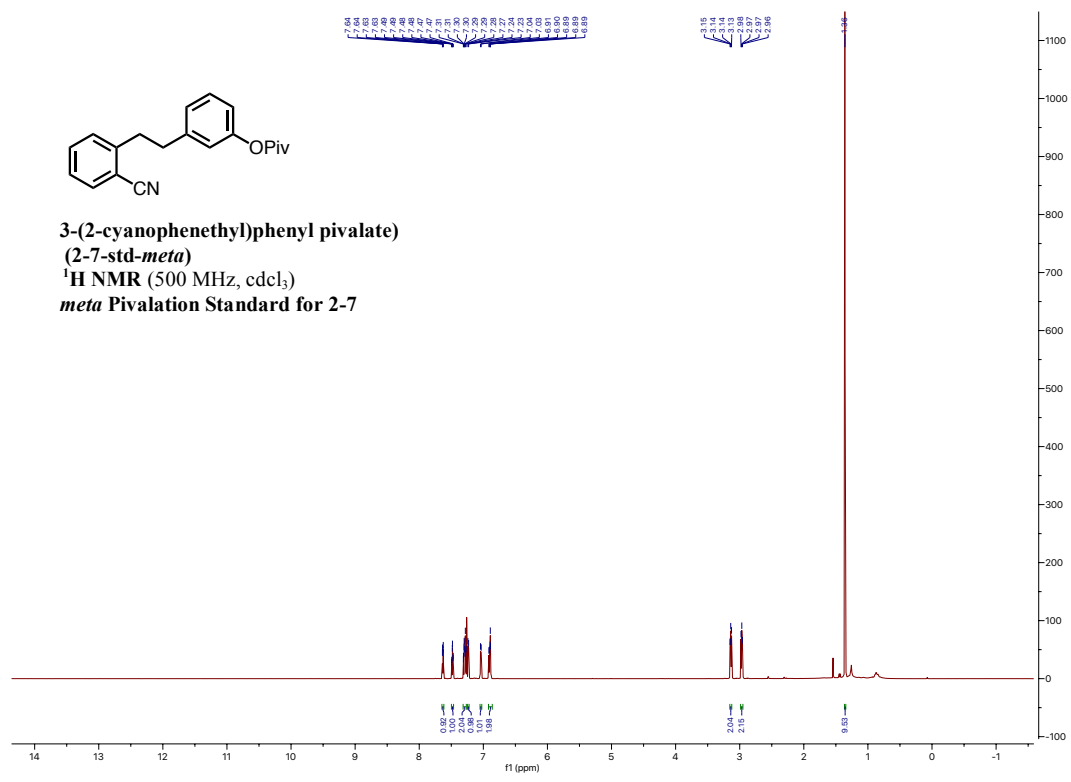


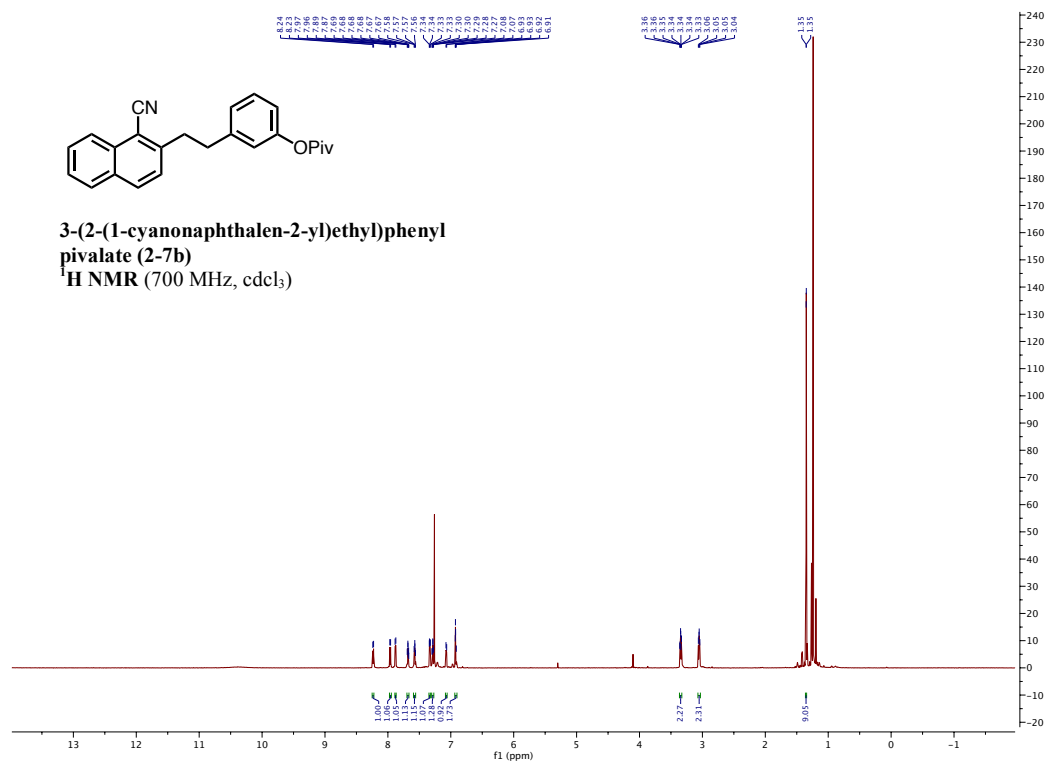


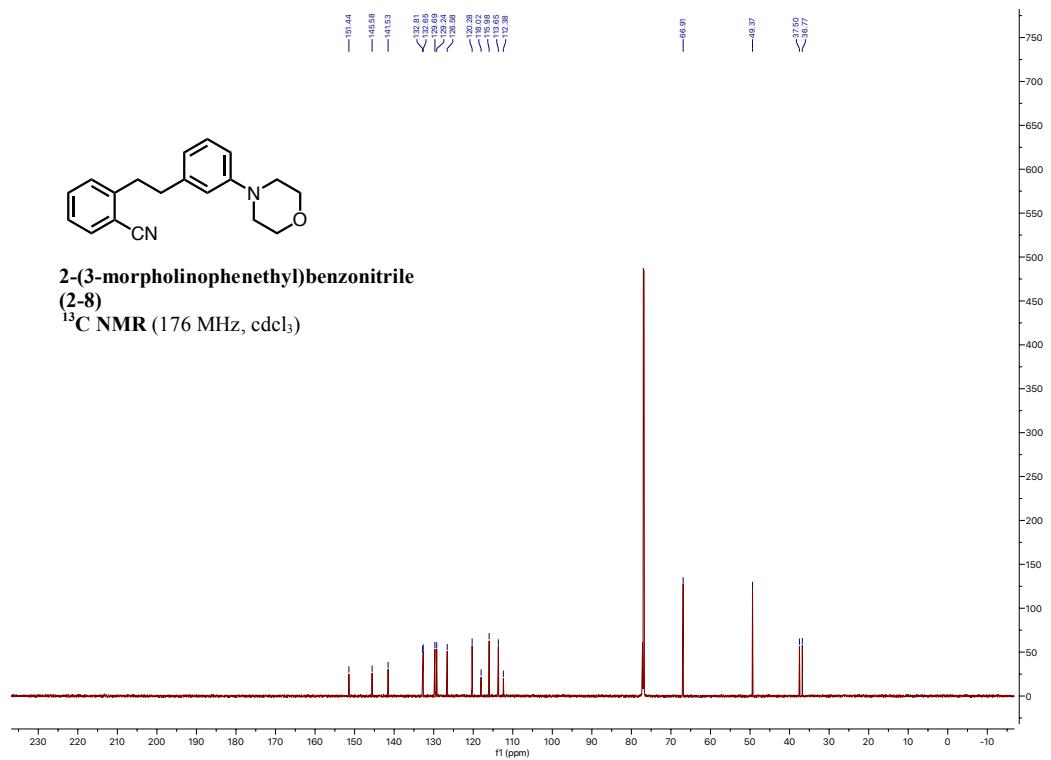
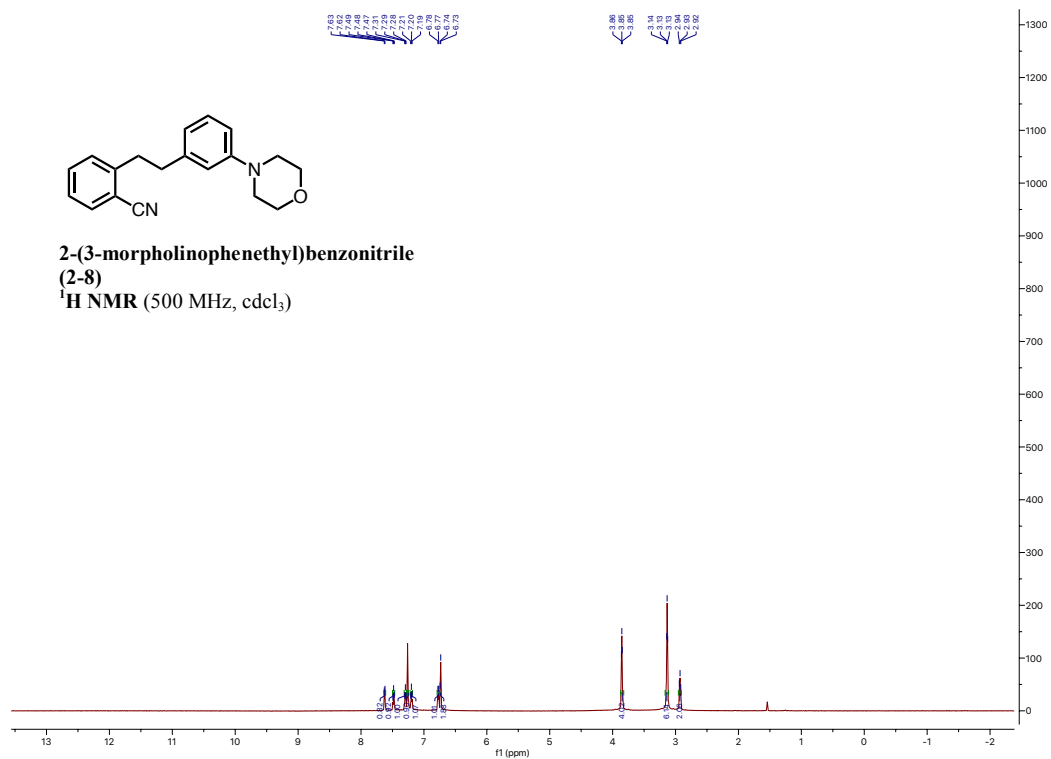


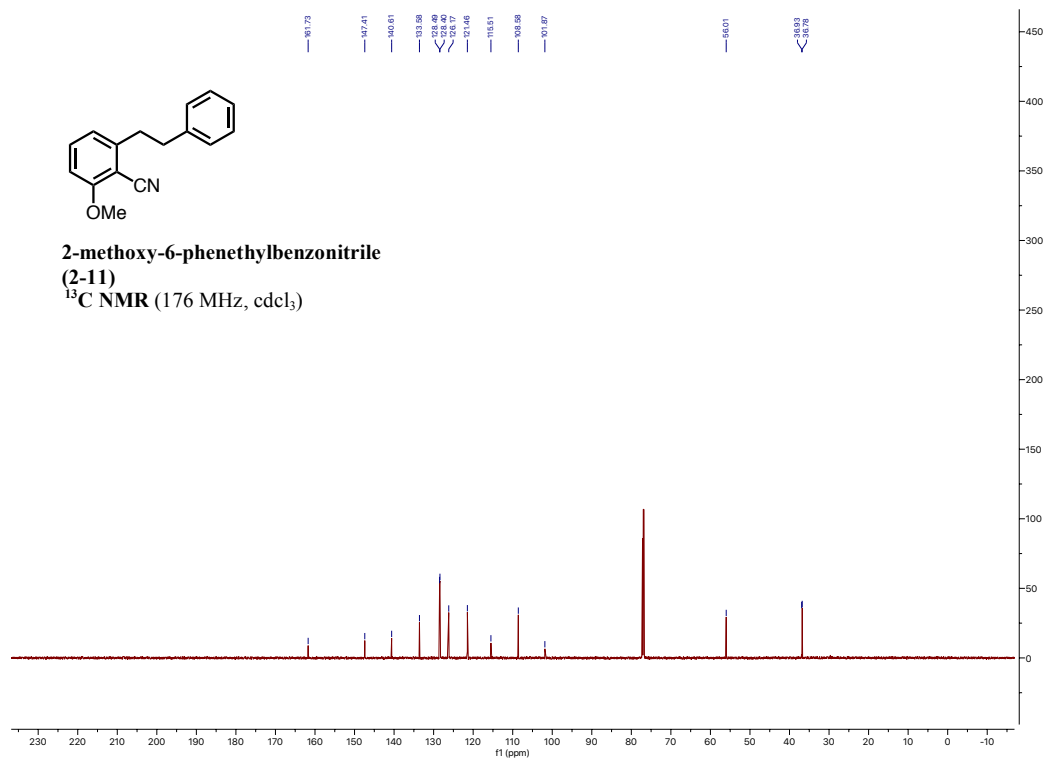
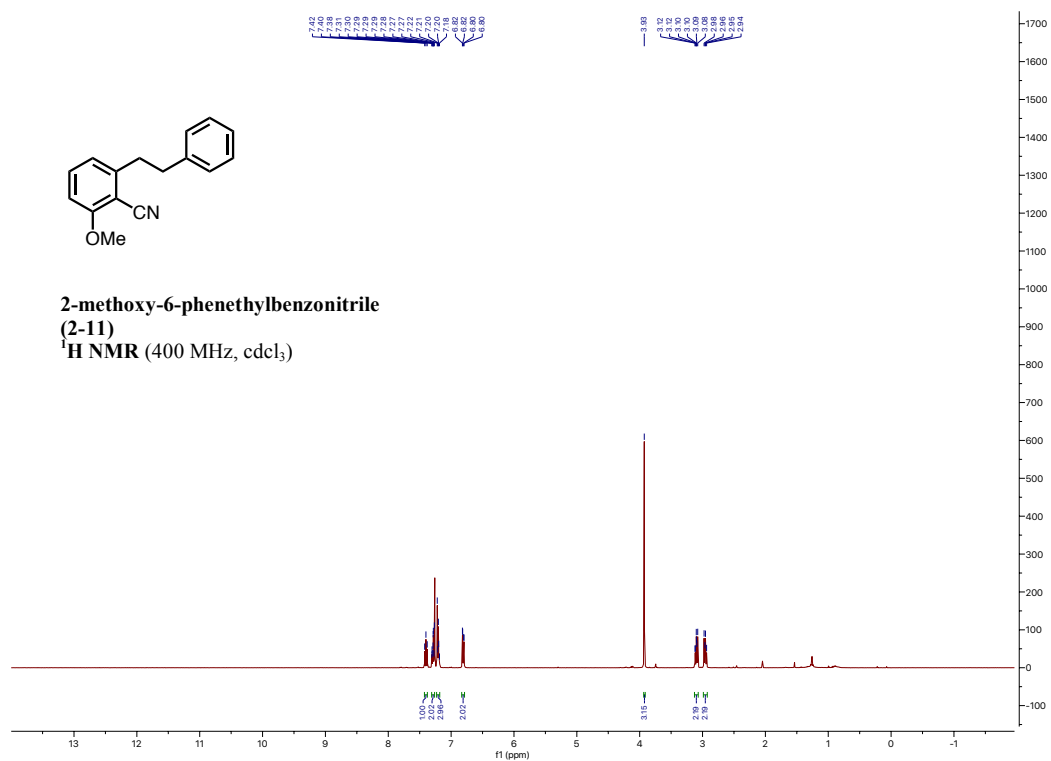


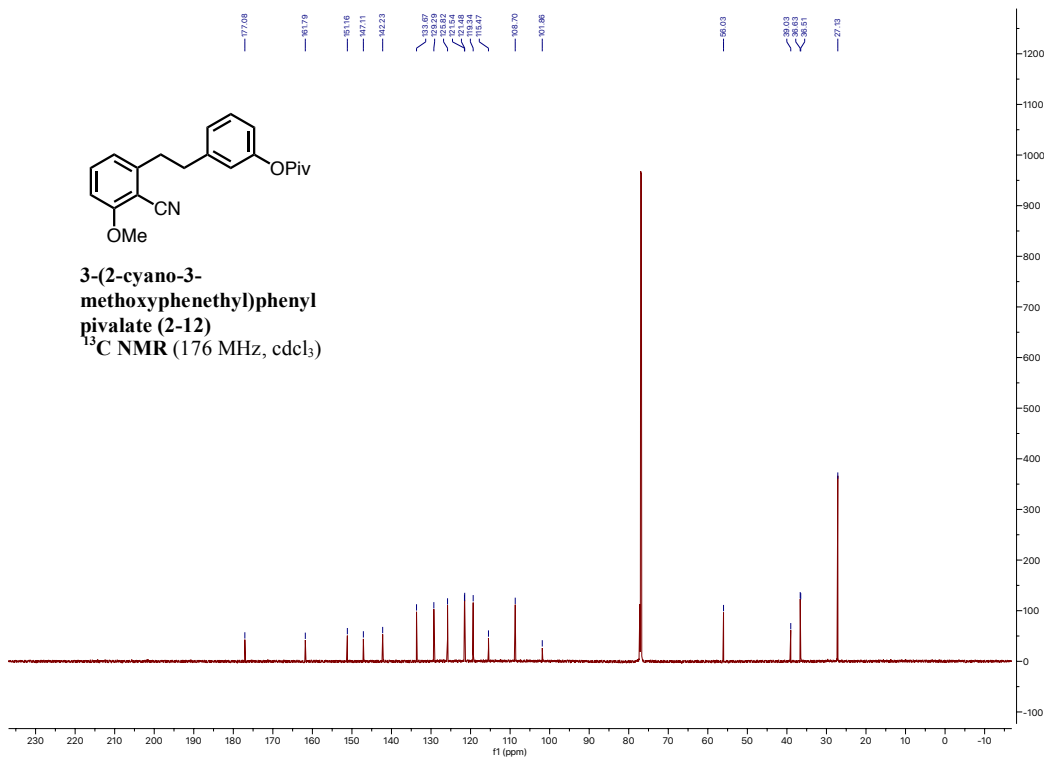
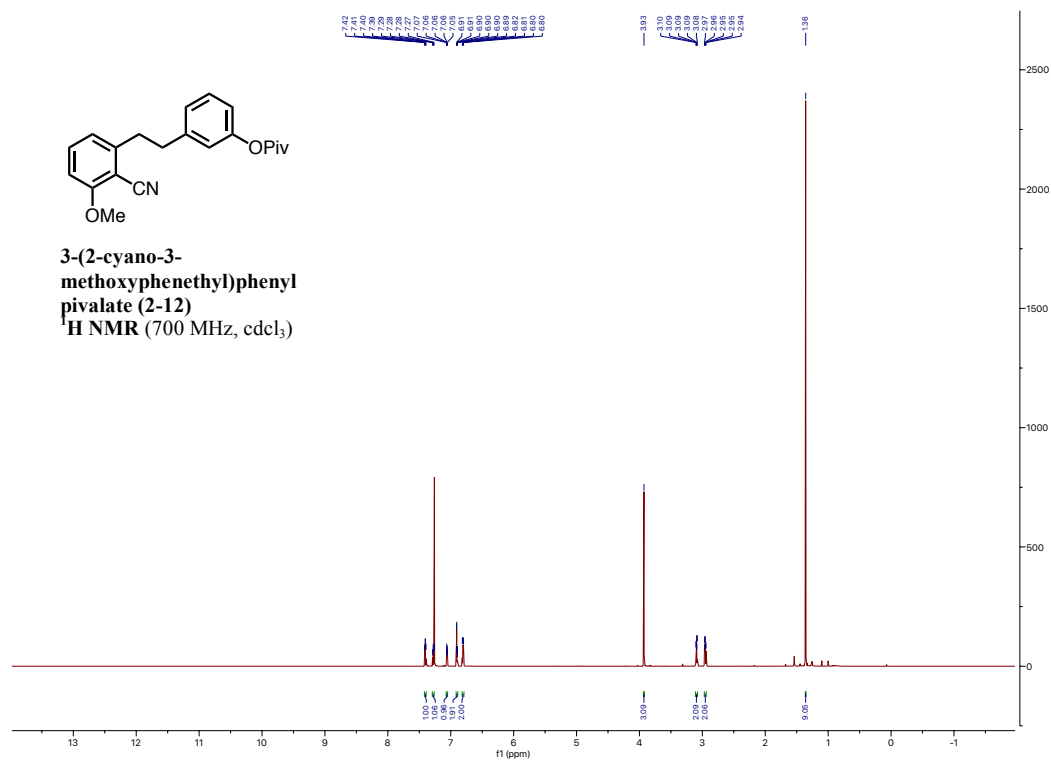


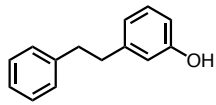




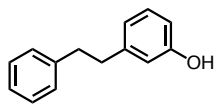
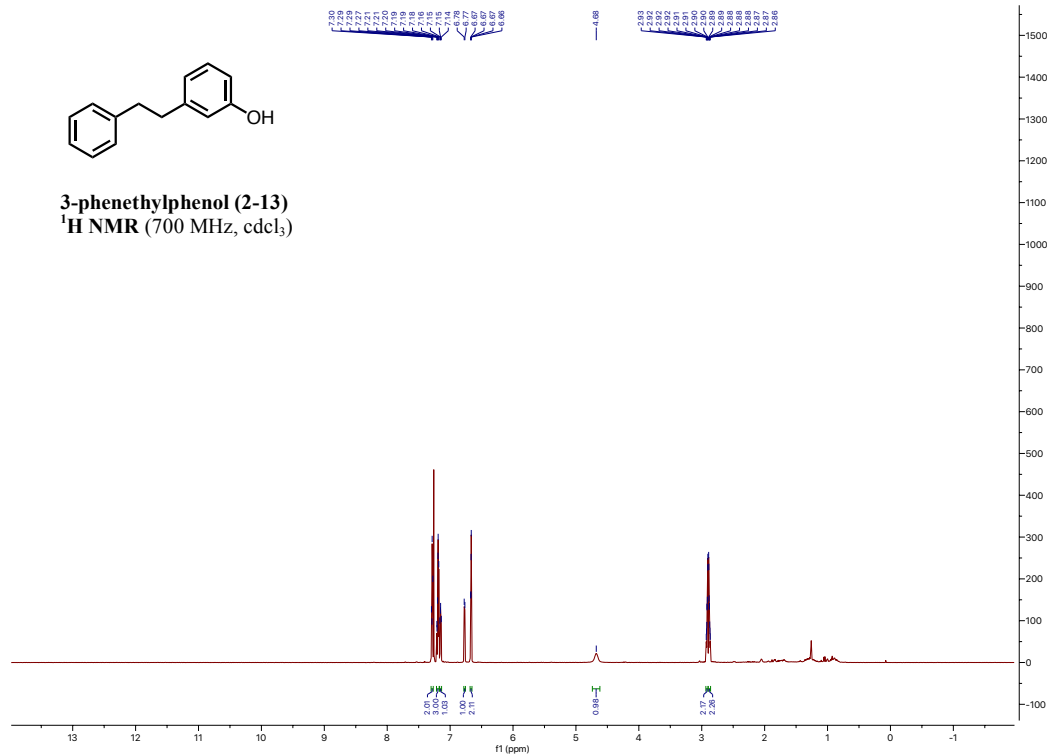




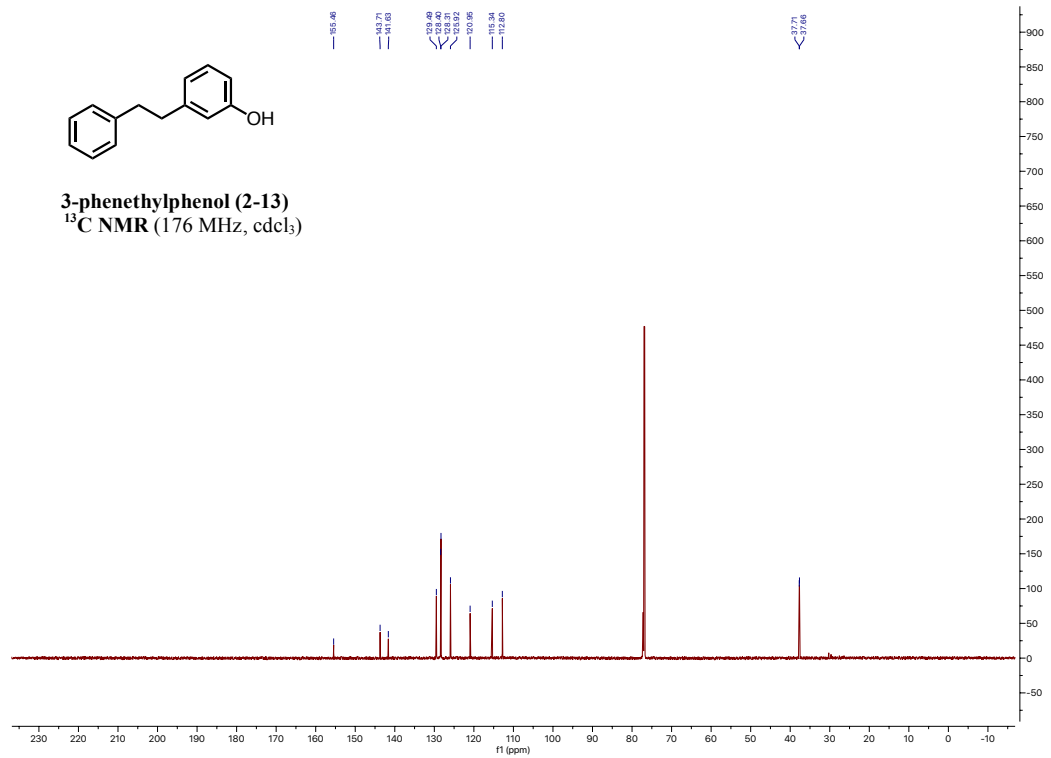


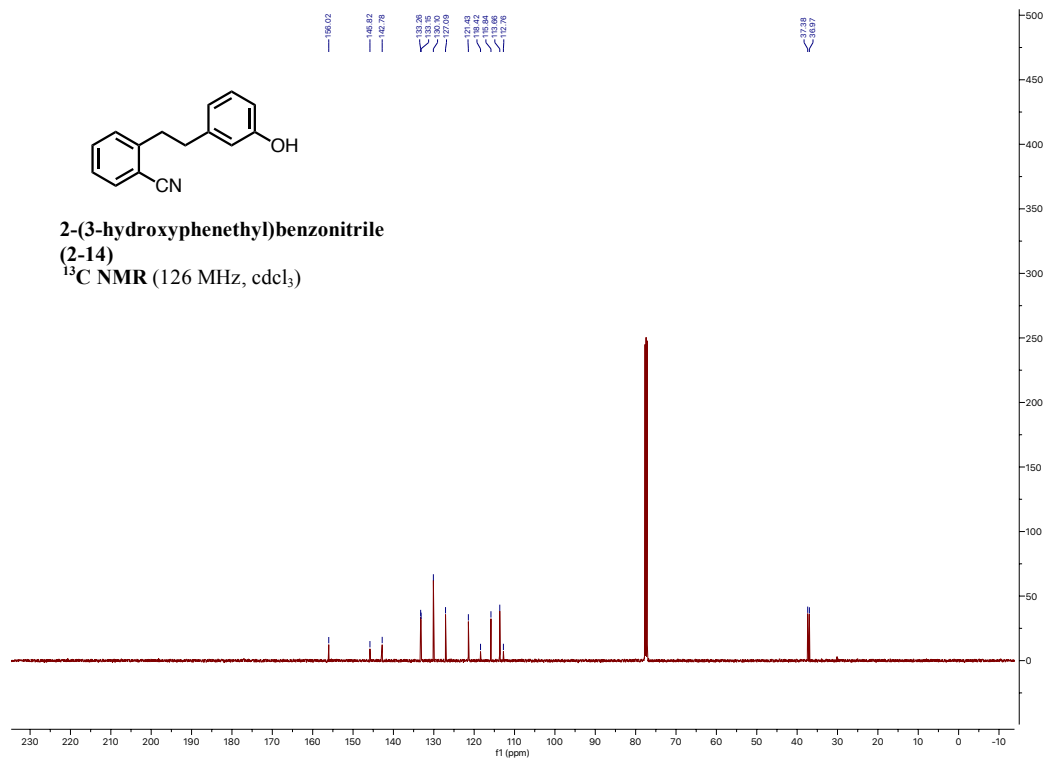
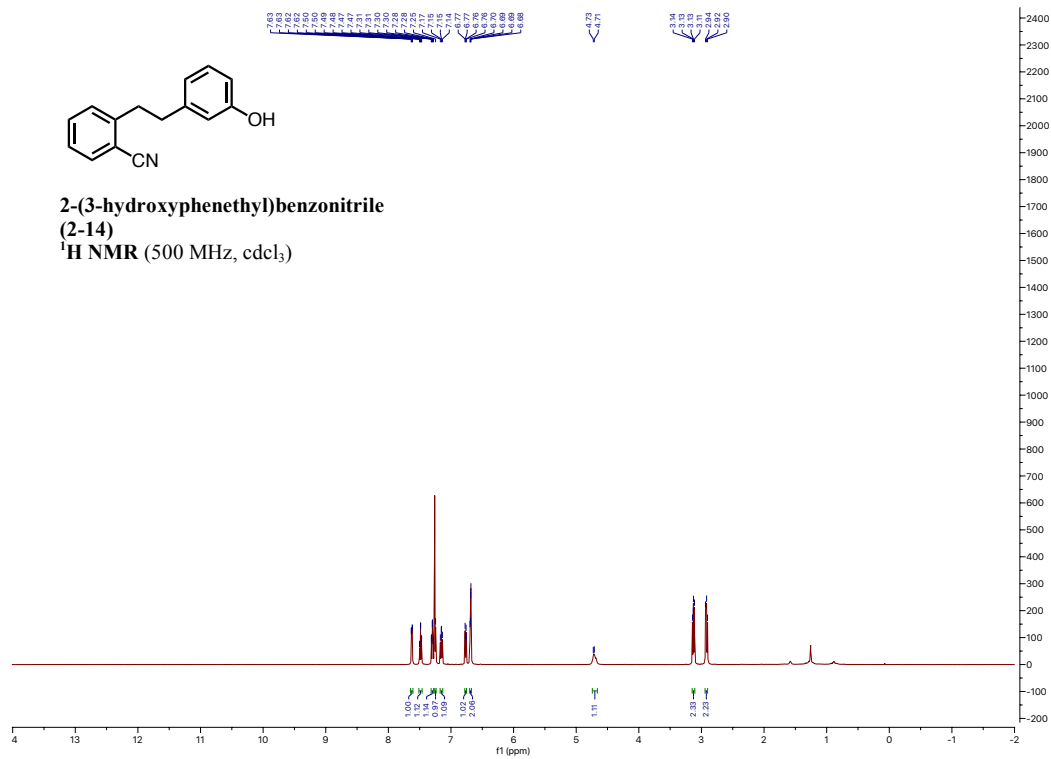


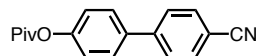
3-phenethylphenol (2-13)
¹H NMR (700 MHz, cdcl₃)



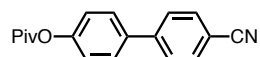
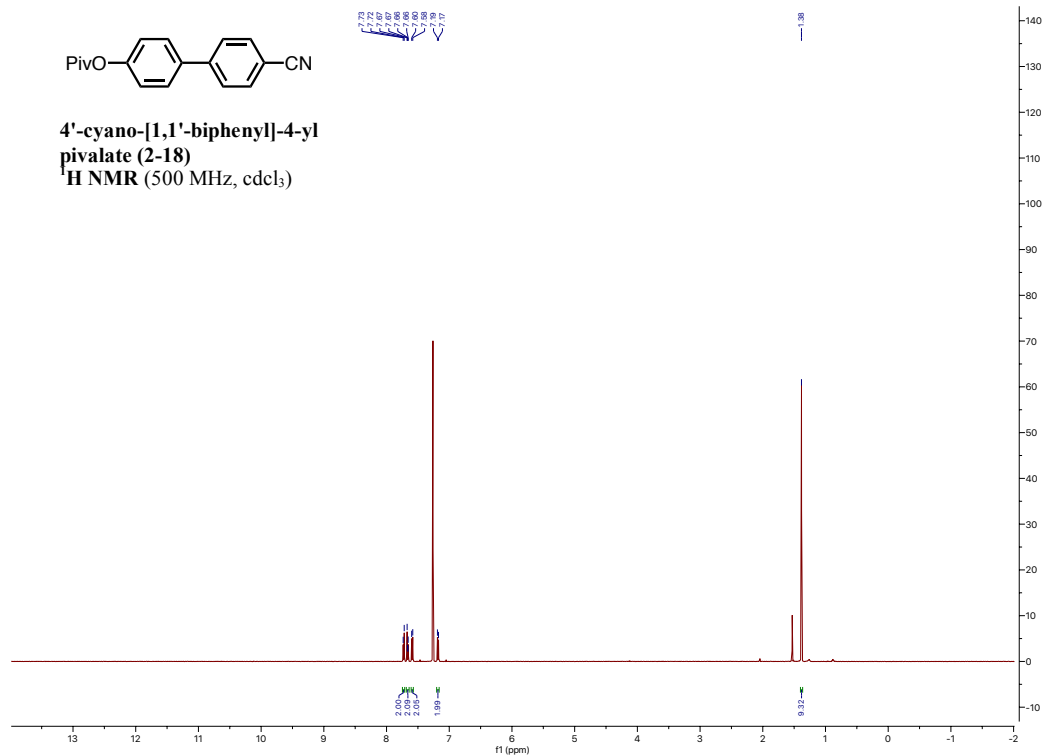
3-phenethylphenol (2-13)
¹³C NMR (176 MHz, cdcl₃)



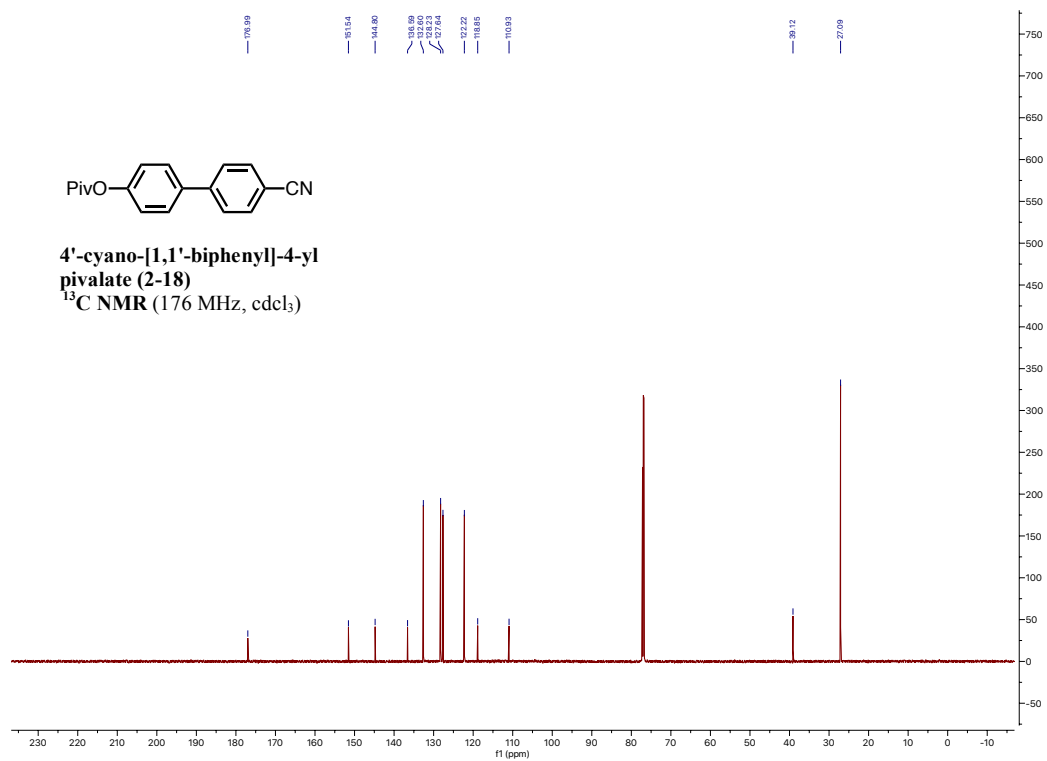


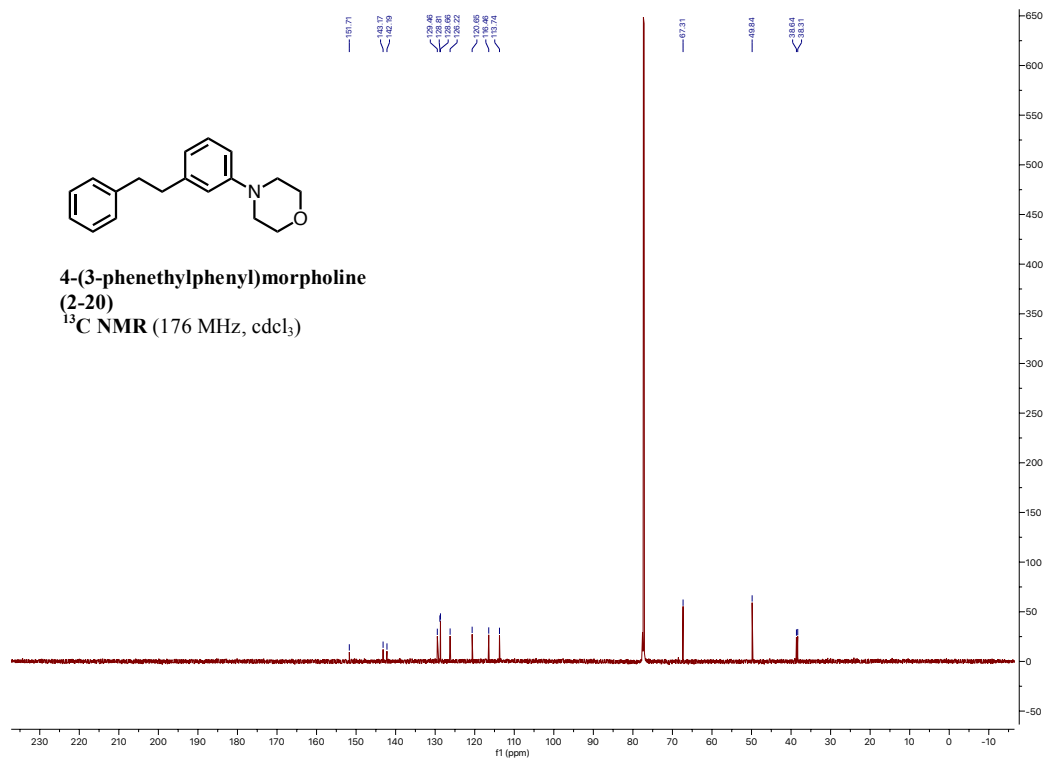
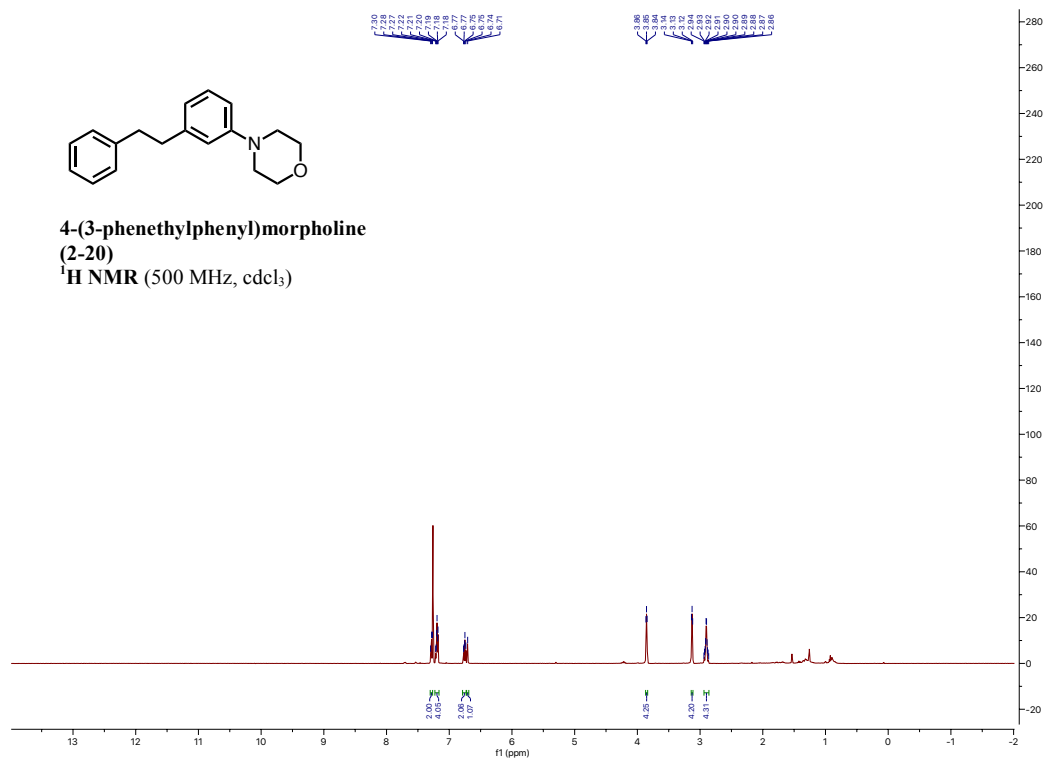


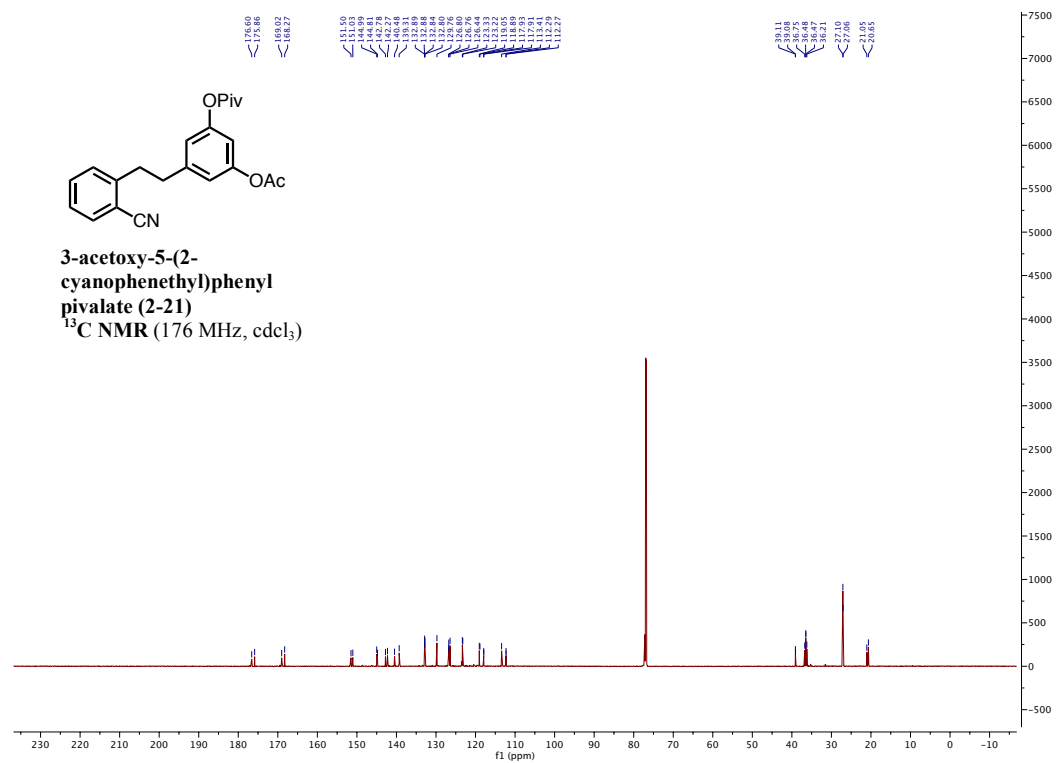
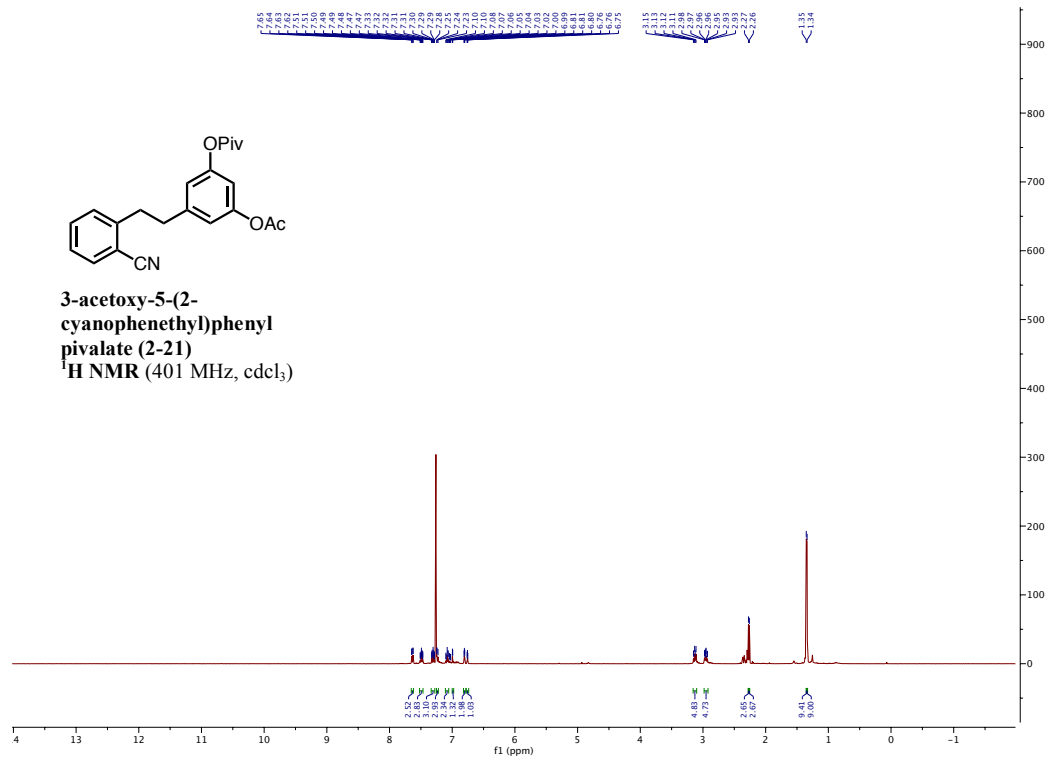
**4'-cyano-[1,1'-biphenyl]-4-yl
pivalate (2-18)**
¹H NMR (500 MHz, cdcl₃)

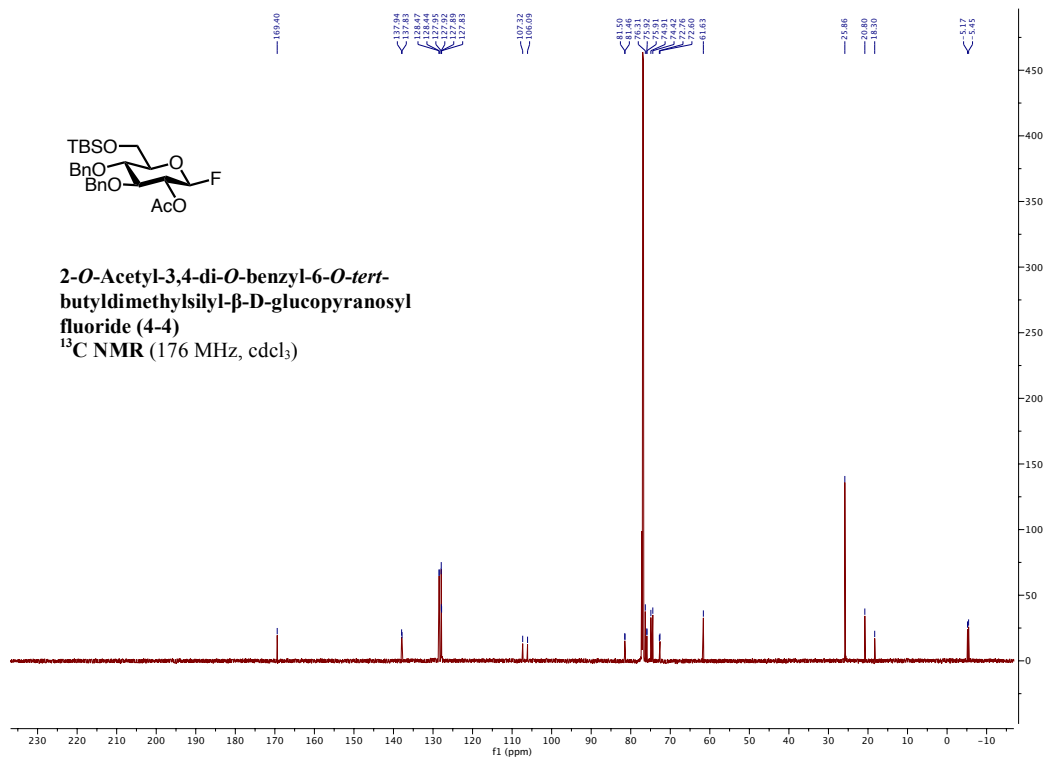
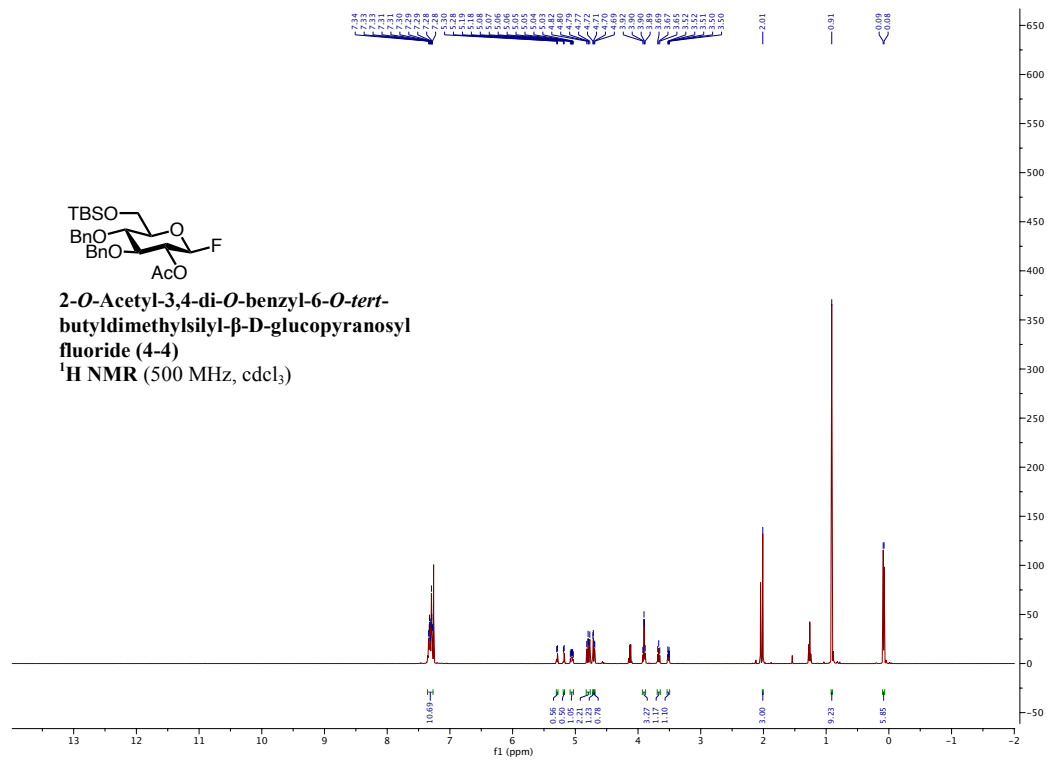


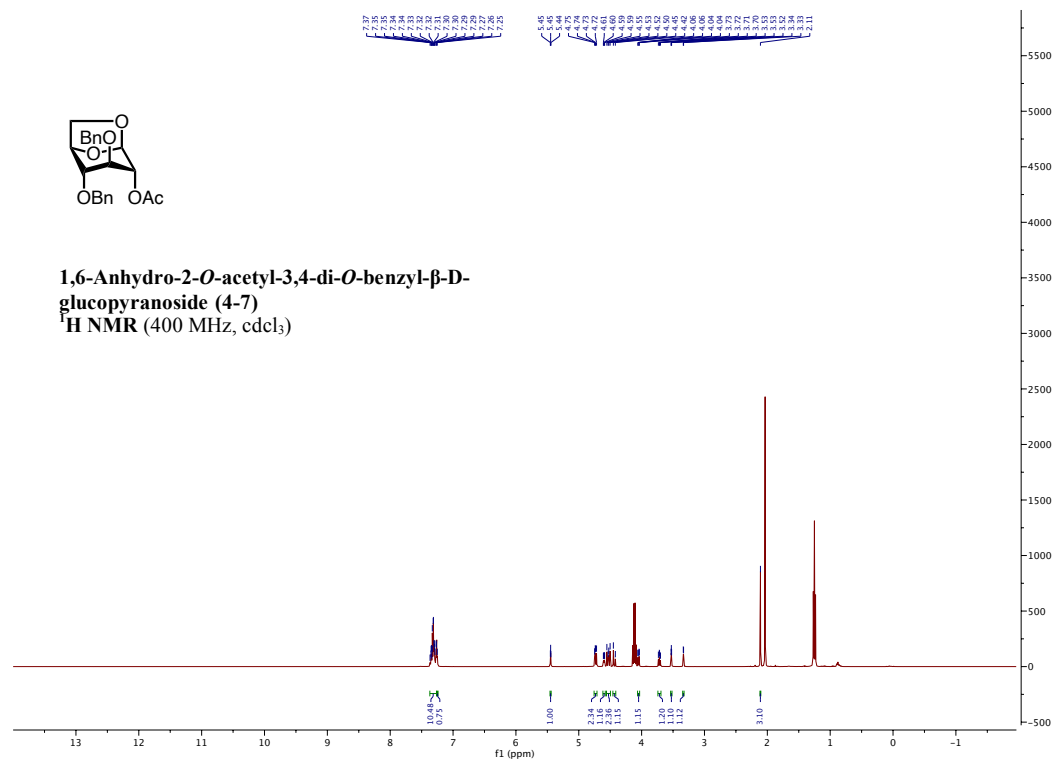
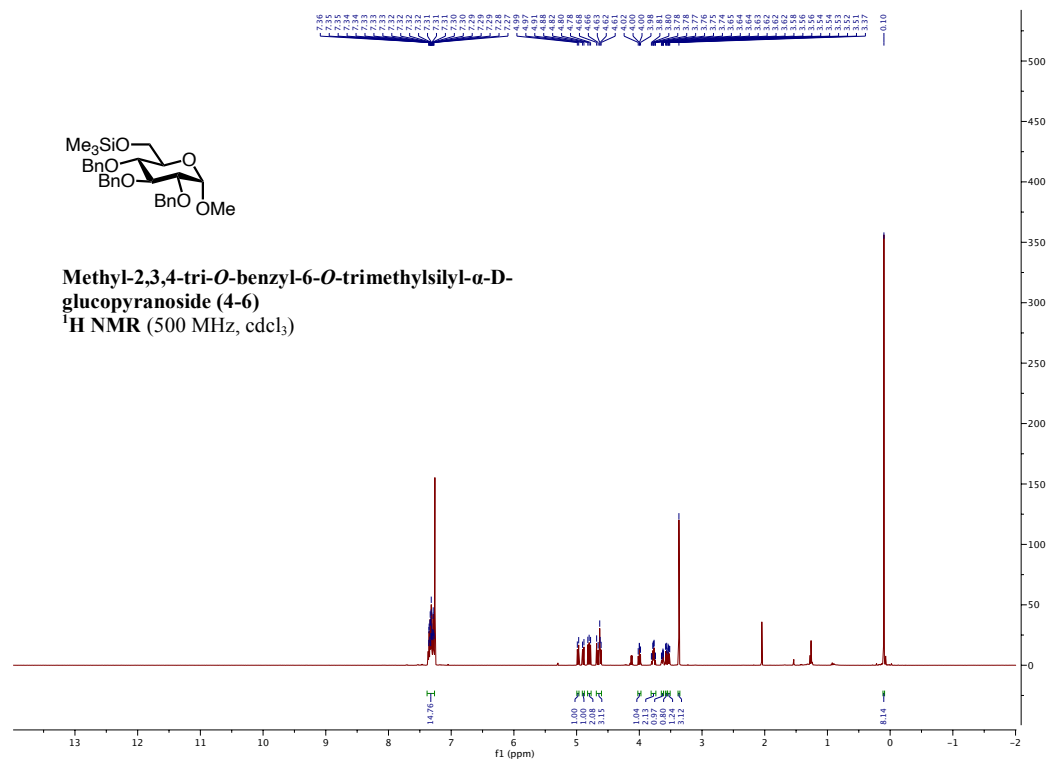
**4'-cyano-[1,1'-biphenyl]-4-yl
pivalate (2-18)**
¹³C NMR (176 MHz, cdcl₃)

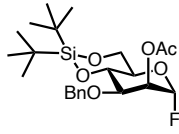




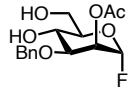
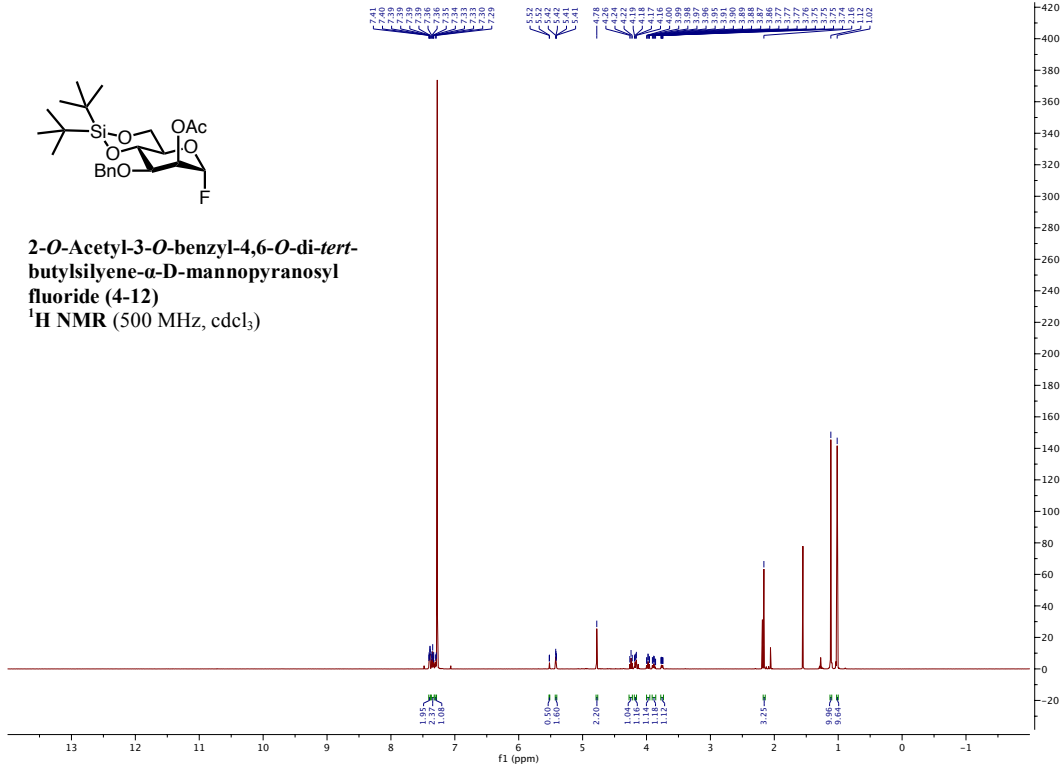








2-O-Acetyl-3-O-benzyl-4,6-O-di-tert-butylsilylene-α-D-mannopyranosyl fluoride (4-12)
¹H NMR (500 MHz, cdCl₃)



2-O-Acetyl-3-O-benzyl-α-D-mannopyranosyl fluoride (4-13)
¹H NMR (500 MHz, cdCl₃)

